

IntechOpen

Supercapacitors

Theoretical and Practical Solutions

Edited by Lionginas Liudvinavičius



SUPERCAPACITORS - THEORETICAL AND PRACTICAL SOLUTIONS

Edited by **Lionginas Liudvinavičius**

Supercapacitors - Theoretical and Practical Solutions

<http://dx.doi.org/10.5772/intechopen.69087>

Edited by Lionginas Liudvinavičius

Contributors

Md Shahrukh Adnan Khan, Yee Wan Wong, Rajprasad Kumar Rajkumar, Anas Syed, Jeeyoung Yoo, Fei Wang, Rajendran Ramachandran, Jonathan Phillips, Steven Lombardo, Xiaowei Teng, Fenghua Guo, Nivedita Gupta, Litty Thekkekara, Guoxin Zhang, Yaqun Wang, Dr Riyaz Ahmad Dar, Cheng Lian, Honglai Liu

© The Editor(s) and the Author(s) 2018

The rights of the editor(s) and the author(s) have been asserted in accordance with the Copyright, Designs and Patents Act 1988. All rights to the book as a whole are reserved by INTECHOPEN LIMITED. The book as a whole (compilation) cannot be reproduced, distributed or used for commercial or non-commercial purposes without INTECHOPEN LIMITED's written permission. Enquiries concerning the use of the book should be directed to INTECHOPEN LIMITED rights and permissions department (permissions@intechopen.com). Violations are liable to prosecution under the governing Copyright Law.



Individual chapters of this publication are distributed under the terms of the Creative Commons Attribution 3.0 Unported License which permits commercial use, distribution and reproduction of the individual chapters, provided the original author(s) and source publication are appropriately acknowledged. If so indicated, certain images may not be included under the Creative Commons license. In such cases users will need to obtain permission from the license holder to reproduce the material. More details and guidelines concerning content reuse and adaptation can be found at <http://www.intechopen.com/copyright-policy.html>.

Notice

Statements and opinions expressed in the chapters are those of the individual contributors and not necessarily those of the editors or publisher. No responsibility is accepted for the accuracy of information contained in the published chapters. The publisher assumes no responsibility for any damage or injury to persons or property arising out of the use of any materials, instructions, methods or ideas contained in the book.

First published in London, United Kingdom, 2018 by IntechOpen

eBook (PDF) Published by IntechOpen, 2019

IntechOpen is the global imprint of INTECHOPEN LIMITED, registered in England and Wales, registration number: 11086078, The Shard, 25th floor, 32 London Bridge Street
London, SE19SG – United Kingdom

Printed in Croatia

British Library Cataloguing-in-Publication Data

A catalogue record for this book is available from the British Library

Additional hard and PDF copies can be obtained from orders@intechopen.com

Supercapacitors - Theoretical and Practical Solutions

Edited by Lionginas Liudvinavičius

p. cm.

Print ISBN 978-1-78923-352-0

Online ISBN 978-1-78923-353-7

eBook (PDF) ISBN 978-1-83881-372-7

We are IntechOpen, the world's leading publisher of Open Access books Built by scientists, for scientists

3,550+

Open access books available

112,000+

International authors and editors

115M+

Downloads

151

Countries delivered to

Our authors are among the
Top 1%

most cited scientists

12.2%

Contributors from top 500 universities



WEB OF SCIENCE™

Selection of our books indexed in the Book Citation Index
in Web of Science™ Core Collection (BKCI)

Interested in publishing with us?
Contact book.department@intechopen.com

Numbers displayed above are based on latest data collected.
For more information visit www.intechopen.com



Meet the editor



Assoc. Prof. Dr. Lionginas Liudvinavičius received qualification of Electrician Engineer in Kaunas University Technology and studied in St. Petersburg Railway Institute (1970-1975). Received Ph.D. degree of Technical Sciences at Vilnius Gediminas Technical University (VGTU) in 2012 and title of Association Professor in 2016. Currently he is working at Department of Railway Transport of VGTU. From 1975 to 2000 he worked as head of various departments of Lithuanian Railways. Transport Minister awarded him “Honored Railwayman Name” (1998) and the second grade awards for contribution to Lithuanian Railways (2010). He is reviewer for IEEE journals. He has authored/coauthored many papers in journals, conference proceedings and he is co-author of study manuals. His research interests are Railway Electrification, Electric Traction, Modern Electric Drive parameters automatic control, Locomotive Traction Converters, Electrical Machinery, Theoretical and Practical Aspects of Use Electrodynamical Braking, Hybrids vehicles, Energy Saving and Storage Systems using Supercapacitors.

Contents

Preface XI

- Chapter 1 **Supercapacitor-Based Hybrid Energy Harvesting for Low-Voltage System 1**
MD Shahrukh Adnan Khan, Rajprasad Kumar Rajkumar, Wong Yee Wan and Anas Syed
- Chapter 2 **Ionic Liquid for High Voltage Supercapacitor 23**
Jeeyoung Yoo
- Chapter 3 **Electrochemical Capacitor Performance: Influence of Aqueous Electrolytes 51**
Rajendran Ramachandran and Fei Wang
- Chapter 4 **Performance of Aqueous Ion Solution/Tube-Super Dielectric Material-Based Capacitors as a Function of Discharge Time 69**
Steven M. Lombardo and Jonathan Phillips
- Chapter 5 **Enhancing Pseudocapacitive Process for Energy Storage Devices: Analyzing the Charge Transport Using Electro-kinetic Study and Numerical Modeling 87**
Fenghua Guo, Nivedita Gupta and Xiaowei Teng
- Chapter 6 **Direct Laser Writing of Supercapacitors 103**
Litty V. Thekkekara
- Chapter 7 **Toward High-Voltage/Energy Symmetric Supercapacitors via Interface Engineering 117**
Yaqun Wang and Guoxin Zhang
- Chapter 8 **Classical Density Functional Theory Insights for Supercapacitors 137**
Cheng Lian and Honglai Liu

Preface

This edited volume is a collection of reviewed and relevant research chapters, concerning the developments within the *Supercapacitors - Theoretical and Practical Solutions* field of study. The book includes scholarly contributions by various authors and is edited by a group of experts pertinent to electronic devices and materials. Each contribution comes as a separate chapter complete in itself but directly related to the book's topics and objectives.

The book contains eight chapters.

The target audience comprises scholars and specialists in the field.

IntechOpen

Supercapacitor-Based Hybrid Energy Harvesting for Low-Voltage System

MD Shahrukh Adnan Khan,
Rajprasad Kumar Rajkumar, Wong Yee Wan and
Anas Syed

Additional information is available at the end of the chapter

<http://dx.doi.org/10.5772/intechopen.71565>

Abstract

This research provides a platform for a novel innovative approach toward an off-grid energy harvesting system for Maglev VAWT. This stand-alone system can make a difference for using small-scale electronic devices. The configuration presents a 200 W 12 V 16 Pole AFPMSG attached to Maglev VAWT of 14.5 cm radius and 60 cm of height. The energy harvesting circuit shows better efficiency in charging battery in all aspects compared to direct charging of battery regardless with or without converter. Based on analysis and results carried out in this research, all feasibility studies and information are provided for the next barrier.

Keywords: supercapacitor, hybrid energy harvesting, low voltage, VAWT, MOSFET switch, PMSG

1. Introduction

Supercapacitors have started to gain attention and are widely used for energy storage in recent years especially in the renewable energy sector. The advantages such as fast charging time, unlimited life cycle, low equivalent series resistance (ESR) and robust and high power density make it attractive and have been used to replace battery in a number of applications [1]. However, supercapacitors are greatly affected by temperature as an increase in temperature will produce negative effects to the electrolyte in the supercapacitor, thus reducing the lifespan. Charge balancing of supercapacitors has always been an issue, and it is important to minimize it in order to improve the performance and reliability. Analysis of few existing

charge balancing circuits along with their pros and cons have been taken into consideration. By placing passive resistors across each capacitor, there is a high power loss from the resistors, which causes the circuit to be inefficient. Another concept of using DC/DC converters across two supercapacitors, on the other hand, results in high efficiency as no other losses occur besides from the converters itself. However, this circuit requires a large amount of components which adds to the cost.

Liyan Qu, Wei Qiao (2011) proposed a novel two-layer constant power control (CPC) scheme for a wind farm equipped with doubly fed induction generator (DFIG) wind turbines [3], where each wind turbine generator (WTG) is equipped with a supercapacitor energy storage system (ESS). The ESS serves as either a source or a sink of active power to control the generated active power of the DFIG wind turbine. Results have shown that the proposed CPC scheme enabled the wind farm to effectively participate in unit commitment and active power and frequency regulations of the grid [2–4]. The proposed system and control scheme provide a solution to help achieve high levels of penetration of wind power into electric power grids. Output power of wind turbine fluctuates constantly, which may cause grid frequency variations, and imposes a high risk on system stability. In order to smoothen power output of wind turbine, the proposed system was used. By using a supercapacitor-based energy storage, the effects of frequency fluctuation and deviation on system during fault condition were minimized. This was one of the early examples of using supercapacitors in wind turbine. However, our research deals with off-grid wind energy harvesting; therefore, Lian Qu's model cannot be used. Moreover, our research aims to charge a DC battery, whereas Lian Qu worked with three-phase grid connection.

Battery and supercapacitors are used together to form a hybrid system. As discussed earlier, battery and supercapacitor have their own advantages and disadvantages. Supercapacitors have high-power density but low energy density, whereas batteries have low power density and high energy density. Besides, battery also has higher ESR which results in high internal loss, thus less efficient compared to supercapacitors. Therefore, both devices are often integrated so that they can complement each other. This system known as hybrid energy storage system (HESS), which is widely used now in order to prolong the lifespan of each device and improve stand-alone systems [5]. For example, Babazadeh et al. [6] implemented an HESS system into a PMSG wind turbine with a large variable wind speed between 6 and 21 m/s. The HESS system helps to smoothen and regulate the output caused by peaks generated due to variation in the wind speed by using a control system to disconnect the battery from wind turbine. This successfully proved that the battery life is able to last longer as the battery experiences lesser stress. The average urban driving patterns that require rapid discharging of battery banks when accelerating and charging of banks when decelerating will reduce the battery banks' lifespan; thus, supercapacitors are beneficial in this case. Since supercapacitors are able to charge and discharge at a fast rate, it is able to provide a boost of power during acceleration and absorbs power during regenerative braking [7, 8].

One of the problems of establishing the hybrid storage system is the different voltage level of the supercapacitor and battery bank. The most common way of coupling the two storage

devices is to connect them in parallel. Although this way of harvesting energy maintains the same voltage in both storage banks, yet it restricts the power delivered by the supercapacitor. The role of an electronic control unit in a 'battery supercapacitor hybrid energy storage system' under different load conditions with the aid of various sensors have been previously studied [9, 10]. Here, the DC/DC converter permits the supercapacitor to supply extra power required by the load. However, in low wind speed, it will not be possible for the turbine to charge a hybrid storage system where both the supercapacitors and battery are connected in parallel. Because at low wind speed the turbine rotates at a very low RPM resulting in a low output voltage at the generator terminal, which is not sufficient to charge the hybrid storage in parallel configuration.

Also areas with low wind do not require a system that includes a generator of mega watt range. Coming back to the energy harvesting circuit, this investigation discovers a novel hybrid circuit with a combination of a battery and supercapacitor bank. In 2010, Worthington proposed a novel circuit that combines the synchronous switched harvesting technique, which was connected to a load capacitor directly to harvest energy [11]. This allowed the capacitor to act as a reservoir that would be disconnected when fully charged and then would discharge to a load. The circuit was connected with a charge pump tire circuit [11]. Experiment results showed that this idea was capable of harvesting three times more the amount of energy compared to the usual bridge rectifier circuit. However, this idea has not yet been implemented into the off-grid wind energy sector. Although Lee [12] implemented a hybrid energy harvesting storage in 2008 for wind power application, it was meant for grid connection and again was of high power range. Hence, it was impossible for the energy storage system to be implemented for the off-grid system. This study brings the supercapacitor-based hybrid energy harvesting for first time into the off-grid low wind power application. A supercapacitor bank is used in this experiment that charges up from the turbine and discharges through the battery with the use of power electronics.

Batteries have relatively high energy density compared to supercapacitors; however, they do not have the characteristics of supercapacitors, that is, instantaneous charging and discharging [13, 14]. Even though batteries can store more energy, it requires longer time to discharge and recharge. Moreover, batteries require constant voltage for charging. If the current exceeds battery rating, it may get heated up and voltage fluctuation reduces life span of the battery. In order to give a constant voltage from the generator, a DC/DC converter has to be used. However, the internal voltage drops in DC/DC converter together with low voltage at generator output does not make a vertical axis wind turbine worthy of charging a battery in low wind speed. Therefore, this research proposes a balancing circuit which introduces the supercapacitor to act as a buffer between the turbine and a battery. The supercapacitor would get charged up from the turbine and discharge through the battery in two separate processes by using MOSFET control switching system. In this research, the proposed hybrid supercapacitor-based battery charging circuit has been implemented into a vertical axis wind turbine in low wind speed and compared with direct charging of battery from the turbine with or without a DC/DC converter. Finally, the proposed system has also been compared with current existing systems of rural Malaysia in terms of cost-effectiveness.

2. Methodology

The novel idea we introduce in this research does not include the conventional DC/DC converter between turbine supercapacitor. Therefore, the converter voltage loss is removed. What had been done is, just after the supercapacitor gets fully charged by the turbine directly, the supercapacitor gets disconnected from the turbine by smart MOSFET switching using Arduino. Then, the fully charged supercapacitor gets connected with the battery by the MOSFET switch, which will charge the battery through a DC/DC converter by self-discharging and the process go on. In this method, voltage as small as 3–4 V can charge up a 6 V/12 V battery.

2.1. System architecture

For harvesting energy from the wind, MagLEV VAWT with PMSG is used, and its specifications are as follows.

From **Table 1**, it can be seen that for low wind speed configuration, voltage ranges from 3.5 to 8 V. As the whole configuration is in low voltage, the battery choice we have is either 6 or 12 V. In low voltage settings, stepping up low input voltage as low as 3–12 V will result in stepping down current by even a smaller amount. Considering the facts stated, 6 V battery was chosen, which was to be charged by the turbine. Between the turbine and battery, a supercapacitor bank is placed which will be charged up by the turbine at first. Then subsequently it will be discharged through the battery. Since a constant voltage is needed for battery to be charged up properly, a DC/DC boost converter is needed between supercapacitor and the battery which will ensure constant stepped-up voltage to the battery when supercapacitor discharges. The field testing was done in the laboratory.

Figure 1 is the schematic diagram of the system architecture. As seen in **Figure 1**, few LED lights along with a 434 Ohm resistor were inserted as loads to discharge the battery.

2.2. Hardware architecture

Initially, supercapacitors are used to store the charges as a part of the hybrid energy harvesting. In this chapter, to construct a supercapacitor bank, four supercapacitors rated 35 F–2.7 V each by Cooper Bussmann are used, which were connected in series. Therefore, a supercapacitor bank rated 8.75 F–10.8 V is formed. Battery choice is a tough one as there are many variations and specifications. For example, for rechargeable or nonrechargeable, different types such as lithium-ion, lead-acid, nickel-metal hybrid, and so on exist, which ultimately lead to confusion. In the research laboratory, there were few good quality batteries but they were rejected due to cost effectiveness and maintenance issues. For instance, Li-ion batteries are omitted because it needs extra circuitry for protection even though it has high efficiency and life cycle. Therefore, considering all these facts lead-acid battery was chosen to be fit for the research for having the optimum characteristics. For this project, a three-cell lead-acid battery manufactured by Yokohama rated 6 V (3.2 AH/20HR) was chosen.

VAWT	Wind speed	5 m/s
	Height	60 cm
	Radius	14.5 cm
	Number of blades	9
PMSG	Phase	3-Phase
	Rated power	200 W
	Rated voltage	12 V
	Diameter	16 cm
	Weight	12.5 kg
	Open circuit voltage	<ul style="list-style-type: none"> • 8 V (wind speed 5 m/s) • 6.5 V (wind speed 4 m/s) • 3.5 V (wind speed 3 m/s)

Table 1. System configuration for energy harvesting circuit.

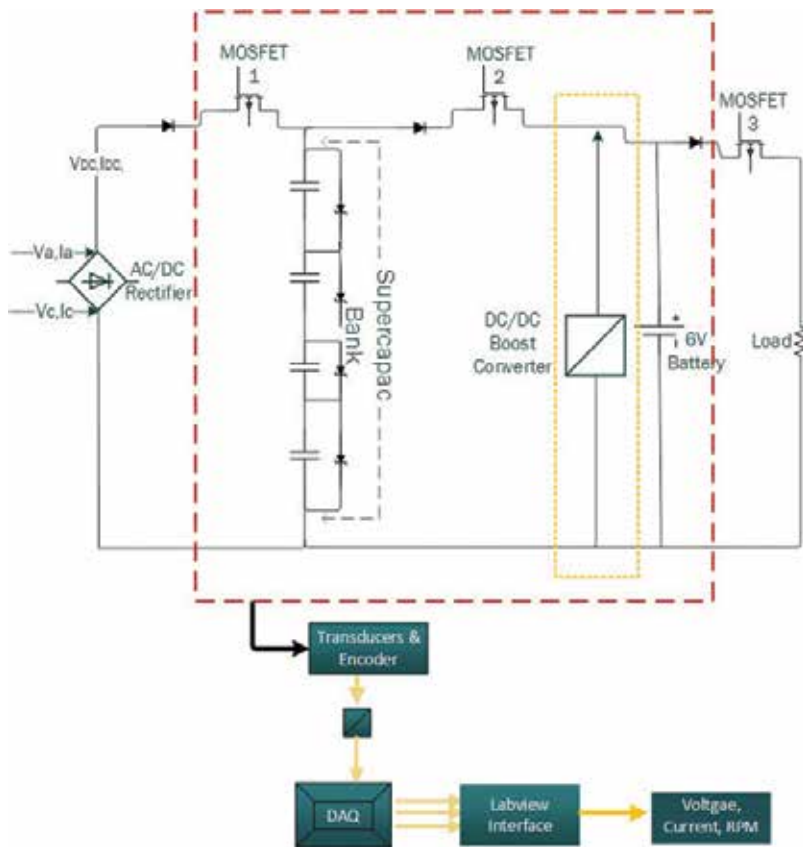


Figure 1. Schematic diagram of system architecture of energy harvesting system.

A DC/DC boost converter was used to give a constant voltage of 7.5 V to the 6 V battery as per the schematic diagram of the hardware architecture. As the setup environment is for small-scale and low voltage system, the “LT1303” micropower step-up high-efficiency DC/DC converter was selected. There is another version of LT1303, that is, LT13035, which has added features like it can supply output voltage up to 25 V and also it is adjustable.

To smartly control the charging and discharging of the supercapacitor bank and the battery, two N-channel MOSFETs were used as a switch, which are controlled by Arduino.

2.2.1. Transducers

Transducers or also known as electrical sensors are a vital part of the system which constantly monitors the physical quantities of the system. The current and voltage transducers used in the system are as follows.

2.2.2. Rotary encoder

A rotary encoder was used to measure the rotational speed of the wind turbine. It was mounted at the base of the turbine. It senses the rotation of the turbine and sends the signal directly to LabView through data acquisition (DAQ). In this case, a simple binary system is used where and whenever the turbine blade cuts through the encoder that sends logic high or otherwise logic low. Counter was used in LabView where it counts the number of logic high sent by the encoder per minute.



Figure 2. Anemometer.

2.2.3. Anemometer

To measure wind speed, an anemometer was used as shown in **Figure 2**. The device gives measurements in miles per hour (mph); therefore, conversion to m/s was required.

2.2.4. Liquid crystal display

To display power and most importantly the current flow through the load in real time, a '16 × 2 LCD' was used as shown in **Figure 3**. LCD screen was controlled by Arduino.

2.2.5. Energy harvesting control system

Switching circuit is the crucial part of this energy harvesting system. Arduino UNO microcontroller is used in this circuit where it controls two N-type MOSFETs namely P36NF06L. For testing, LED was placed in parallel to the gate-source pin of the MOSFET. The system will continue to charge and discharge until the battery reaches up to 6 V. In the stripboard of the energy harvesting circuit, MOSFETs are placed as shown in **Figure 4**. Aligned with the bias voltage, two LEDs are placed to indicate the status of the circuit. When the MOSFET is turned on, the LED will glow and vice versa.



Figure 3. LCD screen of energy harvesting circuit.

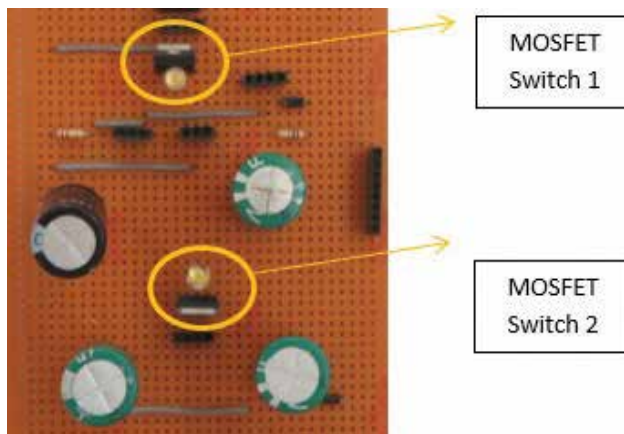


Figure 4. MOSFET configurations in energy harvesting circuit.

The algorithm of the decision-making switching algorithm is illustrated in **Figure 5**. Here MOSFET 3 is usually turned off all the time. However, it is significant to declare that although the MOSFET does not have any role worthy of mention in the system, it is placed there in case the battery has to be discharged manually. Therefore, unless stated otherwise, this MOSFET will be turned off all the time.

As it is seen in **Figure 5**, the control system has mainly two conditions. First one is the supercapacitor charging circuit which occurs when V_{supercap} is less than 4 V. Under this condition, MOSFET 1 is turned on; thus, it will charge the supercapacitor bank. In the meantime,

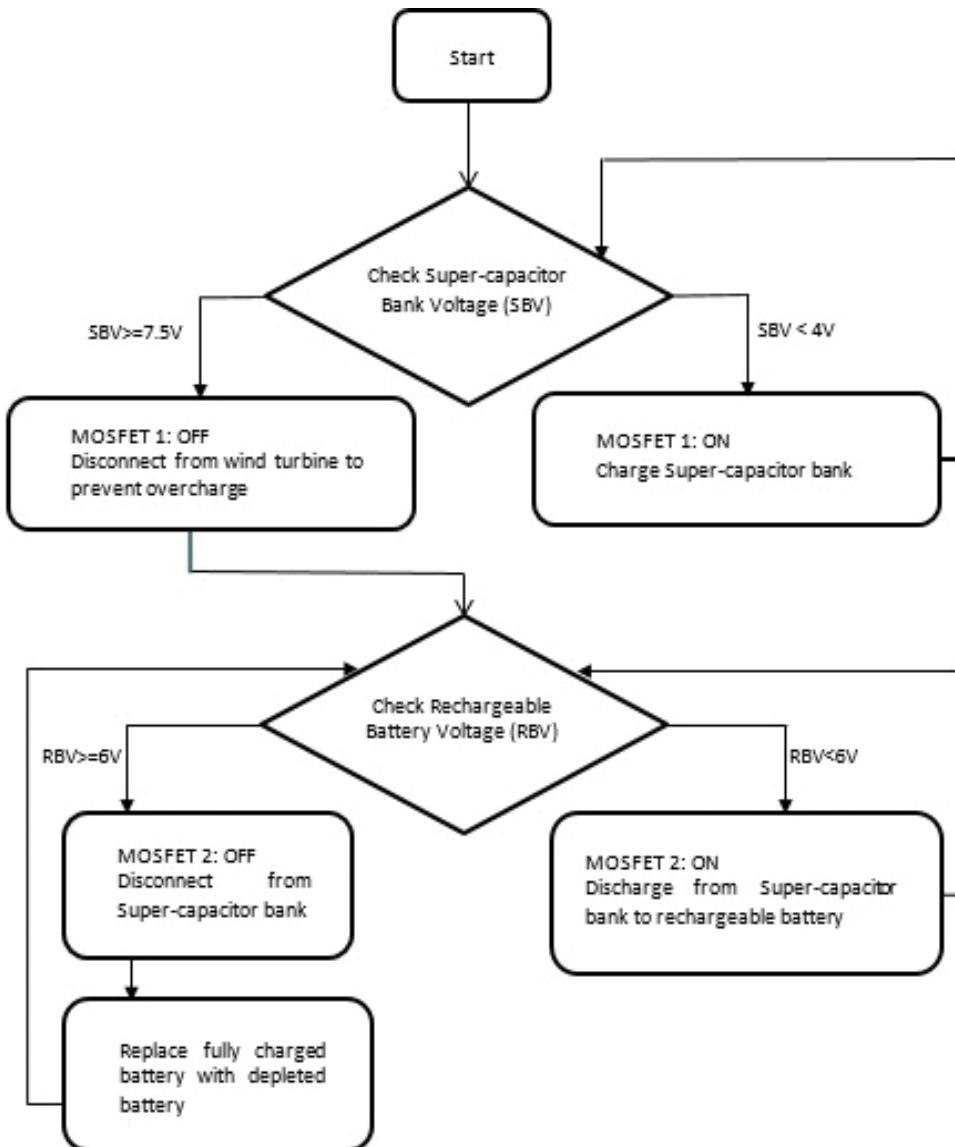


Figure 5. Flowchart of EHC control structure.

MOSFET 2 whose job is to charge the battery from supercapacitor is turned off. When V_{supercap} is greater than or equal to 7.5 V, the second condition triggers which will turn off the MOSFET 1 and turn on MOSFET 2. Thus, overcharging does not occur from the wind turbine. In this time, the rechargeable battery will be charged up to rated voltage 6 V. When the supercapacitors' voltage dropped to 4 V, MOSFET 1 was switched on again. The switching circuit coding in Arduino is given in **Figure 6**.

The basic working principle of this part of the code is very simple. A signal "LOW" corresponding to 0 V was sent to the Arduino digital pin assigned to "MOSFET 1." As soon as the voltage across the supercapacitor bank exceeded 7.5 V, MOSFET 1 was switched off to

```
if (voltage_cap >= 7.5)
{
    digitalWrite(MOSFET1, LOW);
    digitalWrite(MOSFET2, HIGH);
}

else if (voltage_cap < 4)
{
    digitalWrite(MOSFET1, HIGH);
    digitalWrite(MOSFET2, LOW);
}
```

Figure 6. Arduino control coding.



Figure 7. Developed GUI panel of Labview.

prevent overcharging. A signal “HIGH” which equals to 5 V was sent to Arduino digital pin “MOSFET 2” at the same time, and the rechargeable battery then was charged by the supercapacitor bank. Now, a signal “HIGH” was sent to one of the Arduino digital pins assigned “MOSFET 1” as soon as the voltage across supercapacitor bank was lesser than 4 V. A signal “LOW” equivalent to 0 V was sent to Arduino digital pin assigned to “MOSFET 2” at the same time. This charging and discharging of supercapacitor bank algorithm repeated simultaneously until battery was fully charged.

2.2.5.1. DAQ and Labview

With NI-6212 device, data acquisition was implemented. A graphical user interface (GUI) was developed using LabVIEW. This GUI enables the user to easily monitor and analyze data. The LabVIEW interface is shown in Figure 7. This GUI displays supercapacitor and battery’s

	A	B	C	D	E	F	G	H	I	J
1	Time	Supercapacitor 1 Time	Supercapacitor 2 Time	Supercapacitor 3 Time	Supercapacitor 4 Time	Battery				
2	8:00:01 AM	1.7717	8:00:01 AM	1.1286	8:00:01 AM	0.0851	8:00:01 AM	0.0751	8:00:01 AM	4.3092
3	8:00:02 AM	1.7717	8:00:03 AM	1.1311	8:00:03 AM	0.0876	8:00:03 AM	0.0776	8:00:03 AM	4.3167
4	8:00:03 AM	1.7692	8:00:06 AM	1.1361	8:00:06 AM	0.0876	8:00:06 AM	0.0776	8:00:06 AM	4.3167
5	8:00:04 AM	1.7692	8:00:08 AM	1.1386	8:00:08 AM	0.0876	8:00:08 AM	0.0776	8:00:08 AM	4.3167
6	8:00:05 AM	1.7717	8:00:09 AM	1.1386	8:00:09 AM	0.0876	8:00:09 AM	0.0751	8:00:09 AM	4.3167
7	8:00:06 AM	1.7717	8:00:11 AM	1.1436	8:00:11 AM	0.0851	8:00:11 AM	0.0776	8:00:11 AM	4.3167
8	8:00:07 AM	1.7717	8:00:12 AM	1.1411	8:00:12 AM	0.0876	8:00:12 AM	0.0751	8:00:12 AM	4.3167
9	8:00:08 AM	1.7692	8:00:14 AM	1.1461	8:00:14 AM	0.0876	8:00:14 AM	0.0776	8:00:14 AM	4.3167

Figure 8. Data exported to excel spreadsheet from LabVIEW.

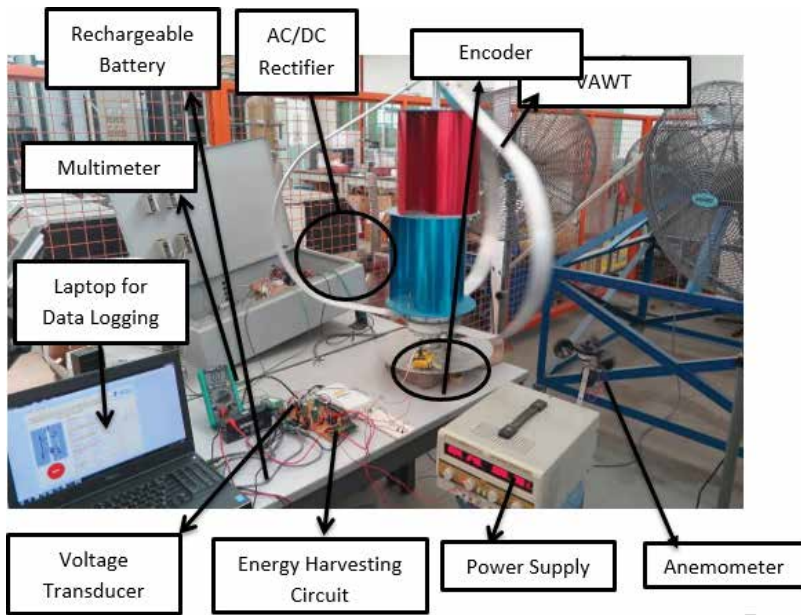


Figure 9. Experimental setup for the integrated system.

voltage, charging current of the supercapacitor, charging current of the battery when supercapacitor discharges and finally the rotational speed of the turbine. The data gathered here can also be easily exported to the spreadsheet software (**Figure 8**). Therefore, this enables the user to keep track of the system in real time of the system 9.

2.2.6. Experimental setup

The energy harvesting circuit built and the experimental setup are shown in **Figure 9**. The field testing was done in the Research Building, Block N, University of Nottingham Malaysia Campus.

3. Results

This section gives a performance analysis of a Supercap (supercapacitor)-based energy harvesting battery charging device operated by the Maglev VAWT adopted to a 200 W PMSG as per the configuration discussed previously which was sent for fabrication. Upon arrival of the turbine, the system was set up in the laboratory, and field testing was performed to tabulate the data.

This subchapter has two parts. First part includes one of the three cases in detail which has been compared for performance analysis. "Case A" showed a battery of 6 V, 3.2 AH, which was charged from 4.2 to 5 V through a DC/DC converter followed by a series of four supercapacitors (2.7 V, 35 F). "Case B" and "Case C" demonstrated the direct charging of the battery where "Case B" was experimented with the converter and "Case C" was without converter. All the three cases were experimented in low wind speed that ranges between 6 and 3 m/s. To keep it short, only results from wind speed 4 m/s will be discussed in detail. The remaining results have been given in a tabularized form to compare and find out the efficiency of the EHC.

3.1. At wind speed = 4 m/s

Case A: Energy harvesting through supercapacitor.

The same procedure from the earlier section was followed, and results were graphically plotted for analysis. Following figures are the details of the charging process. It is noteworthy mentioning that both the Supercap discharge voltage and discharge current were the same as the previous value. This is because while Supercap bank discharged its charge to the battery, the turbine system was isolated through the MOSFET switch. Therefore, wind speed cannot make any impact on the discharging half cycle. Consequently, in all the three cases, the discharge voltage and current amount with respect to time were the same. Here, **Figures 10** and **11** show the charging voltage and current graph with respect to time. For the discharging details, Section 4.5.1 may be reviewed as in both of the cases, the data will be the same.

At this point, 35 min were required to charge up the Supercap bank. Adding the discharging cycle time which was 2 min, the complete cycle duration was then 37 min. The starting current

was 145 mA which took a rapid fall in the next second, bringing the current down to 22 mA. As for the inertia of the turbine, understandably, the charging current at first was very high but that could not be misinterpreted as the actual current. The real current started from 22 mA followed by a gradual decrease that ended up at 2.5 mA. Therefore, the pick current could be considered as 22 mA. **Figure 12** displays the complete cycle process, which basically was the charging and discharging cycle of 37 min.

Again 18 cycles were needed to charge up the Supercap bank from 4.8 to 5 V, but in this time, one cycle consisted of 37 min which in total made the system take 10.4 h of charging time. **Figure 13** represents the battery voltage charging up to 5 V in 10.4 h.

Case B: Energy harvesting without Supercap (with converter).

According to **Figure 14**, it took 18.75 h to reach its maximum value of 4.54 V. After that the increase of the voltage was so less with respect to time, the value was not taken into consideration. Therefore, this charging system was incapable to charge up the device at 4 m/s.

Case C: Energy harvesting without Supercap (without converter).

“Case C” took 15 h to finish the task. **Figure 15** shows the battery charging voltage with respect to time.

Table 2 recapitulates the result of this section in brief.

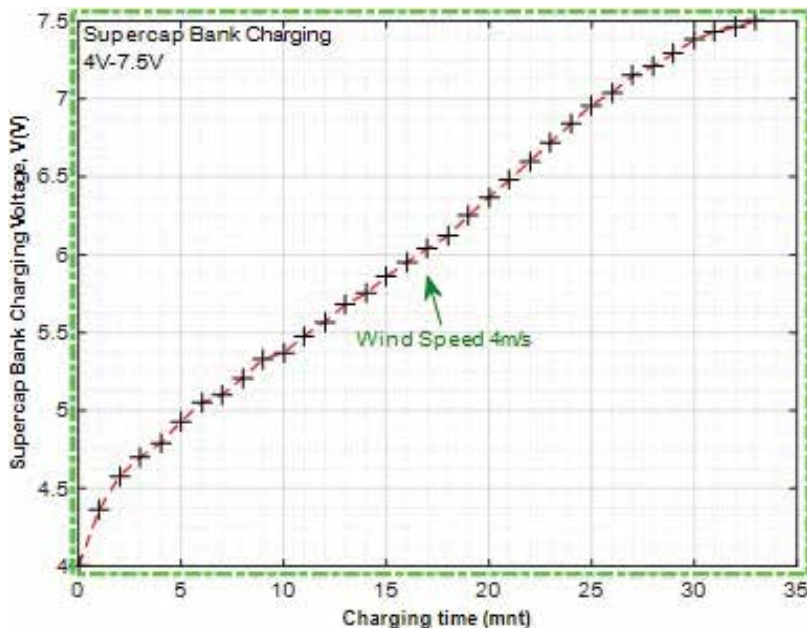


Figure 10. “Supercap charging voltage” vs. “time” at wind speed 4 m/s.

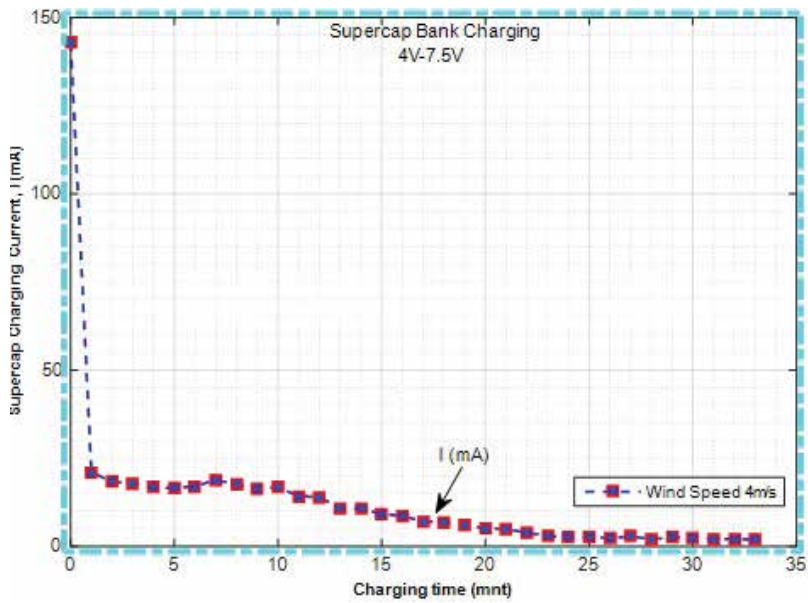


Figure 11. "Supercap charging current" vs. "time" at wind speed 4 m/s.

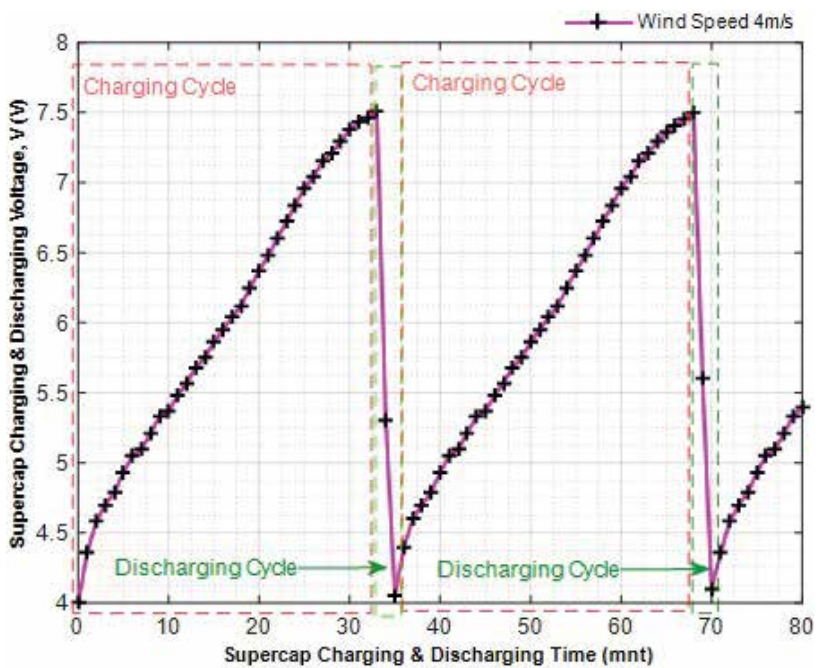


Figure 12. Supercap charging and discharging voltage with respect to time at wind speed 4 m/s.

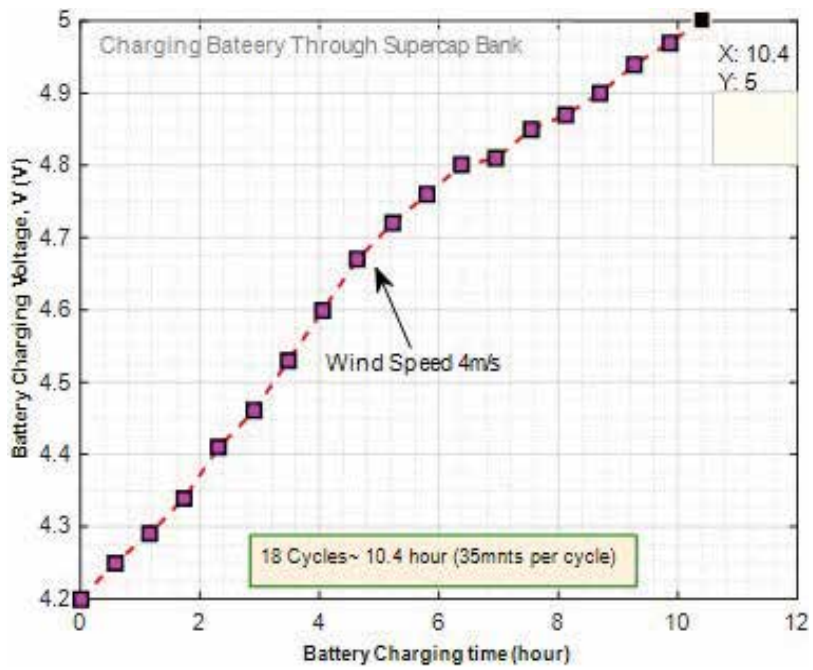


Figure 13. Battery charging voltage with respect to time for 4 m/s wind speed.

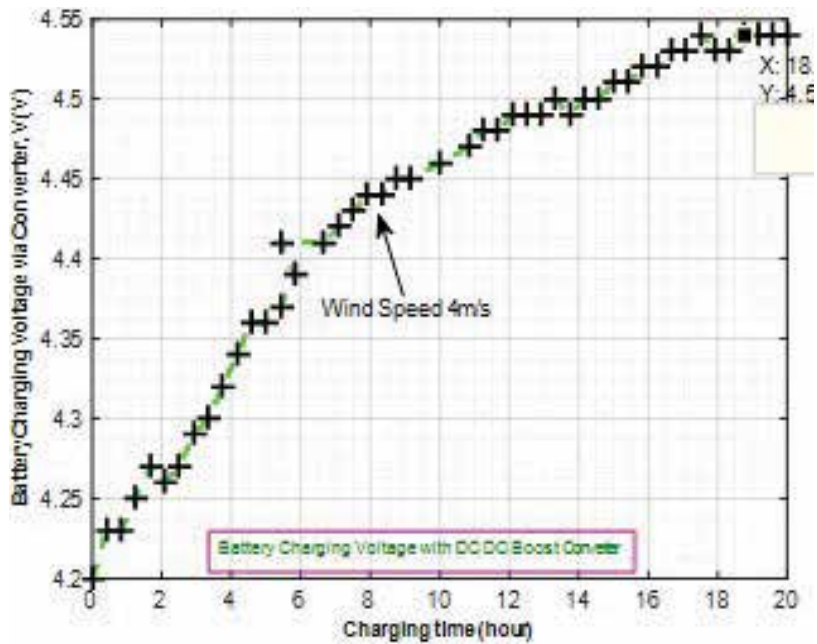


Figure 14. Battery charging voltage with respect to time for 4 m/s wind speed (with converter).

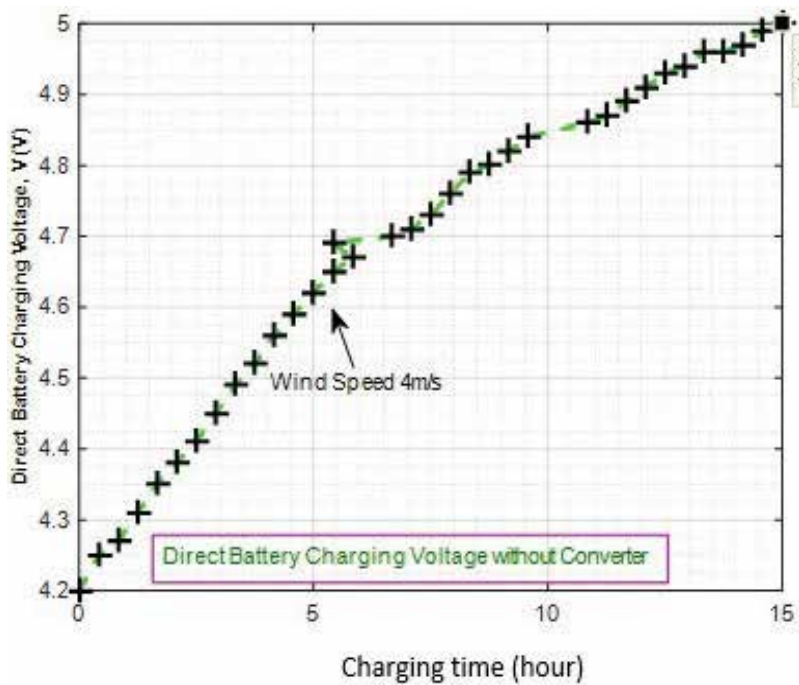


Figure 15. Battery charging voltage with respect to time for 4 m/s wind speed (without converter).

Supercap charging cycle:	35 min
Supercap discharging cycle:	2 min
Number of complete cycle:	18
Maximum Supercap charging current:	22 mA
Maximum Supercap discharging current:	18.5 mA
Time duration:	10.4 h

Efficiency comparison among Case A, Case B and Case C at 4 m/s

Battery charging voltage (4.2–5 V)	Efficiency (%)	Reference point:
Case A (Energy harvesting):	31	Case C – Direct charging without converter
Case B (Charging with converter):	Incompetent	

Table 2. Charging battery (from 4.2 to 5 V) through Supercap at 4 m/s wind speed.

3.2. At wind speed = 3 m/s

Table 3 recapitulates the result of this section in brief.

Supercap charging cycle:	95 min
Supercap discharging cycle:	1 min
Number of complete cycle:	25
Maximum Supercap charging current:	18 mA
Maximum Supercap discharging current:	18.5 mA
Time duration:	38.4 h

Efficiency comparison among 'Case A', 'Case B' and 'Case C' at 3 m/s

Battery charging voltage (4.2–5 V)	Efficiency (%)	Reference point:
Case A (Energy harvesting):	28	Case C – Direct charging without converter
Case B (Charging with converter):	Incompetent	

Table 3. Charging battery (from 4.2 to 5 V) through Supercap at 3 m/s wind speed.

3.3. At wind speed = 5 m/s

Table 4 recapitulates the result of this section in brief.

3.4. Efficiency comparison

As shown in **Table 5**, the energy harvesting circuit data show excellent values for all the results with very good performance overall. Change in the wind speed from 5 to 4 m/s produces better efficiency as it goes to 31% from 19%. For a low speed of 3 m/s, where direct charging displays a poor performance, the energy harvesting circuit, even though it took a long time of 38.4 h to charge up the battery, still maintains its productivity by producing 28% efficiency. Here, the highest amount of efficiency drawn from the system was 31%. Comparing to

Supercap charging cycle:	25 min
Supercap discharging cycle:	2 min
Number of complete cycles:	18
Maximum Supercap charging current:	30 mA
Maximum Supercap discharging current:	18.5 mA
Time duration:	8.1 h

Efficiency comparison among Case A, Case B and Case C at 5 m/s

Battery charging voltage (4.2–5 V)	Efficiency (%)	Reference point:
Case A (Energy harvesting):	19%	Case C – Direct charging without converter
Case B (Charging with converter):	Incompetent	

Table 4. Charging battery (from 4.2 to 5 V) through Supercap at 5 m/s wind speed.

Wind speed (m/s)	Battery charging via Supercap (h)	Direct battery charging time (h)	Efficiency (%)
5	8.1	10	19
4	10.4	15	31
3	38.4	53	28

Table 5. Summary of energy harvesting circuit result for charging a 6 V lead acid battery from 4.2 to 5 V.

Worthington’s work of pulling off 300% more efficiency with hybrid energy harvesting, it is drastically low. However, his storage system was implemented to a pump tire circuit, whereas our circuit was designed for a low wind application. As an off-grid stand-alone low voltage energy harvesting system, the EHC was able to provide, noteworthy, better efficiency in all three low wind speeds.

An important observation had been made in this experiment. At low wind speed, the turbine tends to slow down and stop if there is a heavy load. This is because a permanent magnet synchronous generator has an output frequency, which is proportional to its armature speed. The required torque to rotate the PMSG is proportional to the electrical load. Therefore, at low wind speed, with the increase of the electric load, there is always a tendency to slow down while the mechanical input coming from the VAWT restores it. However, if the load is too much to handle, the mechanical speed from the turbine becomes very slow and eventually the turbine stops.

3.5. Theoretical analysis of battery charging via supercapacitor cycle

For wind speed = 5 m/s.

Theoretical calculation:

$$\text{Energy in supercapacitor bank, } E_{\text{Supercap_Bank}} = \frac{1}{2}CV^2 = \frac{1}{2}8.76 \times 10.8^2 = 511 \text{ J} \quad (1)$$

The peak voltage of Supercap bank cycle = 10.8 V,

However, the boost converter cannot step up voltage less than 4 V. Therefore, usable energy in the supercapacitor bank is

$$\begin{aligned} E_{\text{Supercap_Bank_Effective}} &= \frac{1}{2}CV1^2 - \frac{1}{2}CV2^2 = \frac{1}{2}C(V1^2 - V^2) \\ &= \frac{1}{2}8.76 \times (10.8^2 - 4^2) = 440 \text{ J} \end{aligned} \quad (2)$$

Battery rating, 6 V, 3.2 AH which is equivalent to 19.2 Wh [A 6 V 1 AH can store 12 Wh].

Here, 19.2 Wh ~ (19.2 × 3600 J) ~ 69,120 J.

From one cycle of supercapacitor bank, battery can store energy up to 440 J.

Again, 440 J is stored into a 6 V 3.2 AH battery in one cycle.

Therefore, 69,120 J can be stored into a 6 V 3.2 AH battery in $(69,120/440)$ or 157 cycles.

Note: one charging cycle of supercapacitor bank takes 27 min on average.

Therefore, average time required for battery charging = $[(27 \times 157)/60]h = 70.65 h$.

Experimental observation:

It takes 8.1 h to charge 1 V of the battery [from the previous result section]. Moreover, after 5 V, it takes 18.8 h to charge another 0.5 V.

Therefore, total estimated battery charging hour = $[(8.1 \times 5) + (18.8 \times 2)]h = 78.1 h$.

Percentage of error:

$$\text{Percentage of Error, POE} = \frac{(|70.65 - 78.1|)}{70.65} \times 100\% = 10.54\% \quad (3)$$

The voltage drops in boost converter and MOSFET switch are the main reasons for difference in theoretical and experimental values.

Direct charging without converter:

The battery takes 15 h to charge 1 V from the turbine until 5 V. After 5 V, it takes 24.2 h to charge 0.5 V.

Therefore, average time required for battery charging = $[(15 \times 5) + (24.2 \times 2)]h = 123 h$

$$\text{Efficiency of Supercap – based Battery Charging Circuit} = \frac{(|123 - 78.1|)}{123} \times 100\% = 36\% \quad (4)$$

4. Conclusion

As a conclusion to this research, the achievements are reviewed in terms of research objectives. This consequently facilitates the system, and results are to be analyzed in terms of the percentage and degree of the research objectives that were achieved. Three cases had been compared for performance analysis. “Case A” showed a battery of 6 V, 3.2 AH, being charged from 4.2 to 5 V through a DC/DC converter followed by a series of four Supercaps. “Case B” and “Case C” demonstrated the direct charging of the battery, where “Case B” was experimented with the converter and “Case C” was without converter. Investigation was carried for 3, 4 and 5 m/s wind speed. “Case C” was taken as a reference. For a wind speed of 5 m/s, the result showed an increase of 19% of the charging time for Case A while charging through the Supercap. It took only 8.1 h whereas direct charging without converter took 10 h. Supercap-based charging was also found to be 133% more efficient than direct battery charging with a converter. Keeping in mind, direct charging might not be the appropriate way of charging a device since fluctuation of wind

would result in damaging the battery. As far as wind speed of 4 m/s was concerned, the energy harvesting circuit, taking only 10.4 h to charge up the battery, again showed an excellent performance of 31% efficiency comparing with direct charging that took a straight 15 h lap. For 3 m/s, the energy harvesting circuit still held the top position handsomely with 28% efficiency in comparison with direct charging.

To recapitulate, this research provides an excellent novel idea of a stand-alone Maglev-based VAWT system connected to a PMSG that can harvest energy via Supercap-based battery charging circuit in low wind areas of rural areas. Research contribution is original, and it gives an outstanding foundation for future study in energy harvesting for low wind rural areas.

The entire research had not been absolutely smooth all throughout and naturally it faced few ups and downs.

The limitations of the developed system and technique are listed below:

- i. Firstly, turbine blade design was not taken into consideration in the simulation. As there was no proper mathematical model that relates turbine blade number to output torque or power, the simulation therefore did not account for blade design although it could give better performance if blade number was included in the design. It was not possible to apply finite element analysis (FEA) on turbine blades due to lack of time. Moreover, the position of blade, cut-in angle and vibration analysis of the turbine could be done with FEA. Surely it could have given a wider research scope area on modeling, and blade material could have been brought into the optimization process for a better configuration.
- ii. Moreover, DC/DC boost converter used in this research did not perform well according to the data sheet in its minimum range. As it was stated in the data sheet, the converter can step up voltage from as low as 2.5 V, practically it could not step up voltage less than 4 V. Therefore, the Supercap charging range was made from 4 to 7.5 V, which should have been 3–7.5 V. This had a direct effect on system efficiency.

5. Future work

Conventional DC/DC boost converter is to be replaced with the efficient one, which is specifically designed to work with voltage as low as 2–3 V. This will help Supercap to discharge even more and will play a vital role while dealing with low wind. All these changes will improve the system and should make it capable of performing at 2 m/s. Since most of the electronic devices operate at 12 V, a second DC/DC converter may be placed to charge a 12 V battery from the current 6 V-lead acid battery.

Laptop should be replaced with wireless system in the future. A real-time wireless monitoring interface could be made available. Embedded solutions providing wireless end point connectivity to devices like XBEE modules can be of use in cases like this.

Author details

MD Shahrukh Adnan Khan^{1,2*}, Rajprasad Kumar Rajkumar², Wong Yee Wan² and Anas Syed¹

*Address all correspondence to: shahrukh.adnan@uap-bd.edu

1 University of Asia Pacific, Dhaka, Bangladesh

2 University of Nottingham, UK-Malaysia-China

References

- [1] Caricchi F, Crescimbin F, Honorati O, et al. Performance evaluation of an axial-flux PM generator. In: ...Conference on Electrical..., 1992. pp. 761-765
- [2] MD Shahrukh AK, Rajkumar R, Wong YW, Aravind CV. Feasibility study of a novel 6v supercapacitor based energy harvesting circuit integrated with vertical axis wind turbine for low wind areas. *International Journal of Renewable Energy Research*. 2016. pp. 1167-1177
- [3] MD Shahrukh AK, Rajkumar R, Rajparthiban KR, Aravind CV. Performance analysis of 20 pole 1.5 kW three phase permanent magnet synchronous generator for low speed vertical axis wind turbine. *Energy and Power Engineering*. 2013;5:423
- [4] Xia YY, Fletcher JE, Finney SJ, Ahmed KH, Williams BW. Torque ripple analysis and reduction for wind energy conversion systems using uncontrolled rectifier and boost converter. *IET Renewable Power Generation*. 2011;5(5):377
- [5] Hsiao C-Y, Yeh S-N, Hwang J-C. Design of high performance permanent-magnet synchronous wind generators. *Energies*. Nov. 2014;7(11):7105-7124
- [6] Yin M, Li G, Zhou M, Zhao C. Modeling of the wind turbine with a permanent magnet synchronous generator for integration. In: 2007 IEEE Power Engineering Society General Meeting. 2007. pp. 1-6
- [7] Busca C, Stan A-I, Stanciu T, Stroe DI. Control of permanent magnet synchronous generator for large wind turbines. In: 2010 IEEE International Symposium on Industrial Electronics. 2010. pp. 3871-3876
- [8] Fei W, Luk P. A new technique of cogging torque suppression in direct-drive permanent-magnet brushless machines. *IEEE Transactions on Industry Applications*. Jul. 2010;46(4): 1332-1340
- [9] MD Shahrukh AK, Rajkumar R, Rajparthiban KR, Aravind CV. Optimization of multi-pole permanent magnet synchronous generator based 8 blade magnetically levitated variable pitch low speed vertical axis wind turbine. *Applied Mechanics and Materials*. 2014;492:113-117
- [10] MD Shahrukh AK, Rajkumar R, Rajparthiban KR, Aravind CV. Optimization of multi-pole three phase permanent magnet synchronous generator for low speed vertical axis wind turbine. *Applied Mechanics and Materials*. 2014;446:704-708

- [11] MD Shahrukh AK, Rajprasad KR, Aravind CV, Wong YW. Cost effective design fabrication of a low voltage vertical axis wind turbine. *International Journal of Control Theory and Applications (Serial Publications)*. 2016;**9**:2827-2833
- [12] Baroudi JA, Dinavahi V, Knight AM. A review of power converter topologies for wind generators. *Renewable Energy*. Nov. 2007;**32**(14):2369-2385
- [13] MD Shahrukh AK, Rajkumar R, Rajparthiban KR, Aravind CV. A comparative analysis of three-phase, multi-phase and dual stator axial flux permanent magnet synchronous generator for vertical axis wind turbine. *Applied Mechanics and Materials*. 2014;**446**:709-715
- [14] MD Shahrukh AK, Rajkumar R, Rajparthiban KR, Aravind CV. A novel approach towards introducing supercapacitor based battery charging circuit for off-grid low voltage maglev VAWT. *International Journal of Control Theory and Applications*. 2016;**9**:369-375

Ionic Liquid for High Voltage Supercapacitor

Jeeyoung Yoo

Additional information is available at the end of the chapter

<http://dx.doi.org/10.5772/intechopen.73053>

Abstract

Pure ionic liquids (ILs) and IL mixtures in organic solvents have been investigated for higher operating voltages around 3.0–4.0 V. ILs have design flexibility due to the numerous possible combinations of anions and cations. Current research on ILs as electrolytes has focused on several ILs, including imidazolium and pyrrolidinium. At early stages, various ILs have been studied as salts of electrolyte with organic solvents like acetonitrile and propylene carbonate. Neat ILs have been applied for high-performance electrolyte, and some of them have been used as electrolyte (1-ethyl 3-methylimidazolium tetrafluoroborate). These liquid electrolytes need additional encapsulation; therefore, SCs applied ILs face difficulty in integration and manufacturing flexible devices. These drawbacks can be solved by adopting a polymer electrolyte because the ILs maintain the conductivity even when solidified, unlike a typical organic electrolyte. Common polymer matrixes such as PVdF, PMMA, and PVA have been suggested to embed ILs. Poly(ionic liquid) (PIL) is also studied. PIL is a polymer electrolyte containing a polymer backbone and an IL species in the monomer repeat unit. PIL-based polymer electrolytes have high ionic conductivity, wide electrochemical windows, and high thermal stability.

Keywords: ionic liquid, ion gel, poly (ionic liquid), high voltage supercapacitor, all-solid supercapacitor

1. Introduction

As new markets using energy storage devices increase, various types of energy storage devices are striving to enter the market [1, 2]. In the case of electric vehicles (EVs), Li ion batteries (LIBs), fuel cells (FCs), and supercapacitors (SCs) are in a competitive relationship [3]. LIBs are emerging as the most promising candidates because of their high energy density and technical maturity. However, there is a problem of safety. The unstable supply and price of lithium and cobalt are also serious problems. In addition, FCs still have difficulties in

commercialization due to the disadvantage of obtaining hydrogen from petrochemistry and the reluctance of establishing a hydrogen station. As an alternative to this situation, SCs can be proposed. Up to now, SCs have been applied to an electric bus using regenerative break and electric train powered by pulse power, since the large power density of SCs is suitable for intermittent power supply [4]. However, SCs are facing with critical challenge of low energy density. Therefore, LIBs and SCs are applied together for the complementary purpose. The operating voltage of LIBs is from 3.5 to 4.0 V and that of SCs is approximately under 2.8 V. If SCs achieve the 3.5–4.0 V rated voltage with high energy densities or LIBs achieve high power densities, then the power supply unit can be minimized and integrated [5]. In other words, if SCs archive high energy density without sacrificing power density, SCs can be applied as an alternative energy storage system replacing LIBs and FCs.

There are two ways to increase the energy density of SCs. One is to enhance capacitance, and the other is to increase the operating voltages, since the energy density is proportional to capacitance and operating voltage. At the initial stage, many researchers focused on widening the electrode area for enhancing electric double layer (EDL) capacitance. Various types of activated carbon (AC) are commercialized as a result of these efforts. Carbon nanomaterials like carbon nanotubes (CNTs) and graphene are also highlighted as large capacitance materials [6]. Additionally, redox active electrode materials like metal oxide and conductive polymer are proposed to enlarge capacitance by pseudocapacitance. However, those materials struggle with process abilities, limiting of electrolyte adoption, charging/discharging properties, minimizing high cost, and checking suitability for commercial production lines. Another approach of redox active materials is electrolyte that contains redox active couples. Representative redox couples are halides, vanadium complexes, copper salts, hydroquinone, methylene blue, indigo carmine, p-phenylenediamine, m-phenylenediamine, lignosulfonates, and sulfonated polyaniline [7]. Most of electrolyte adopting redox couple has a problem of solvent selection because such redox couples are effective in aqueous medium. This means that the operating voltage of aqueous electrolyte containing redox active couple is limited under 1.23 V, which is the electrolysis voltage of water. Such boundaries with electrode materials motivate the development of advanced electrolyte with high operating voltages for high energy densities because the operating voltages for SCs depend on the electrochemical stability window of the electrolyte.

At early stages, classical salts and systems are suggested. The solvent is organic solvents such as acetonitrile (AN) and propylene carbonate (PC) [8]. Quaternary ammonium salts and AN are representative electrolyte of SCs, and their operating voltage is about 2.8 V. The electrolytes adopting AN exhibit large specific capacitance due to high ionic conductivity derived from low viscosity of AN. However, SCs applied AN-based electrolyte have to be operated under 80°C due to the boiling point of AN. Otherwise, PC is less toxic and has higher thermal stability than AN. Thus, the electrolyte adopting PC is generally considered a safe electrolyte. Using PC-based electrolytes can achieve slightly higher operating voltages for SCs than those using AN. However, formation of carbonate and evolution of H₂ and CO₂ caused by reaction of carbon electrode and PC have been identified as the main causes of performance degradation at high voltages [9]. To overcome these drawbacks, many electrolytes have been proposed over the past several years as an alternative electrolyte to increase the

operating voltage of SCs. Next alternative organic solvent for high operating voltage is linear sulfones, alkylated cyclic carbonate, and adiponitrile [10–12]. These alternative electrolytes archive 3–3.2 V of operating voltage. Meanwhile they show relatively high viscosity and low ionic conductivity, these characteristic occur decrement of power density. Another type of alternative electrolyte is the LIBs electrolyte system. These electrolytes contain common solvents (cyclic carbonate for high dielectric constant and linear carbonate for low viscosity) and lithium salts like LiPF_6 . These electrolytes exhibit high ionic conductivity and high operating voltage over 3 V. However, they have some issues of moisture sensitivity (formation of HF from LiPF_6), slow intercalation reaction of Li cation, and the presence of a solid electrolyte interphase (SEI). These problems are directly connected to electrical performance and safety of SCs. Also, organic solvent is highly flammable and thermally unstable.

To solve these issues, ionic liquids (ILs) are investigated. ILs are thermally stable because they have negligible vapor pressure and they are nonflammable and relatively high ionic conductivity. More importantly, ILs are very effective for widening the operating voltage due to their wide electrochemical stability window over 3 V. Additionally, ILs are composed of only ions, which means that ILs play a role in both salts and solvents. Therefore, there are no additional salts or solvents. For these reasons, ILs have been widely investigated as an electrolyte material.

2. Ionic liquid as liquid electrolyte for supercapacitors

2.1. Neat ionic liquid as liquid electrolyte for electric double layer

In 1807, Humphry Davy pioneered the study for the electrolysis of molten salts which is referred as ILs later and presented the electrochemical theory of the molten electrolyte, despite the research was concentrated on reactive metal preparation [13]. After that, synthetic method of aluminum with electrolysis of aluminum oxide dissolved in cryolite was suggested by Hall [14]. This method is meaningful that eutectic molten salts were formed at low temperature with electrolysis, and this method is still applied in aluminum industrial production.

ILs have been studied for electrochemical devices such as SCs, FCs, rechargeable batteries, photovoltaic cell, and actuator etc. due to the mobility and flexibility of ions [5, 14–20]. ILs are composed of large and asymmetrical organic cation and charge delocalized inorganic/organic anion by weak interaction [21]. Despite that ILs exist in the cation-anion state, these structures lower the tendency to crystallize, so they provide a fluid phase with reasonable ion conductivity, and they show no decomposition or significant vapor pressure [21, 22]. As mentioned, ILs are composed of organic ions and can be combined to various structures with easy preparation. Thus, various kinds of ILs can be used for the given application with desired properties (**Figure 1**).

Wide tunability of ILs can be combined to satisfy the desired characteristics of SCs such as working voltage, operating temperature range, and internal resistances [23]. For these reasons, ILs have been widely investigated as electrolyte material. As mentioned above, quaternary

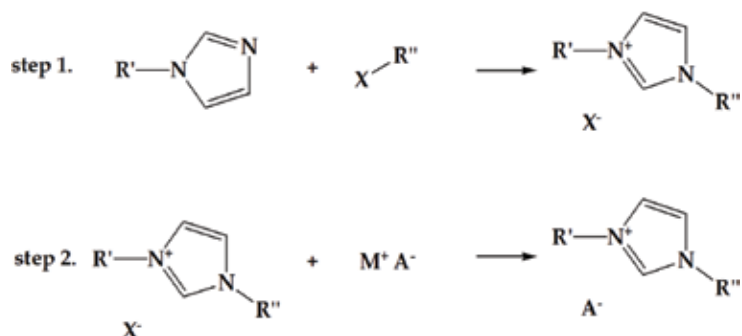


Figure 1. Synthetic mechanism of imidazolium-based ILs.

ammonium salts which is one of ILs are widely investigated with organic solvents, and some of them were already commercialized (1 M of tetraethylammonium tetrafluoroborate ([Et₄N][BF₄]) in AN or PC [24]. Ammonium with different alkyl groups ([Et₄N], tetrapropylene ammonium ([Pr₄N]), and tetrabutyl ammonium ([Bu₄N]) and various anions ([BF₄⁻], hexafluorophosphate ([PF₆]), perchlorate ([ClO₄]), and triplate ([CF₃SO₃⁻]) was applied in organic solvents such as PC, AN, γ -butyrolactone (GBL), and N,N-dimethylformamide (DMF). The ionic conductivities generally decrease in the following order: [Et₄N] > [Pr₄N] > [Bu₄N] > [Me₄N], [BF₄] > [PF₆] > [ClO₄] > [CF₃SO₃]. Similarly, nonaqueous electrolyte with various alkyl imidazolium salts was studied [25]. According to development of organic electrolyte, carbon electrode material which is effective for enhancing EDL capacitance was investigated. These studies were focused about suitability between the ion size of ammonium salts and the pore size of carbon electrode [26].

ILs can be classified as aprotic, protic, and zwitterionic types. Aprotic type ILs have been used for SCs [21]. In the published literature so far, most of ILs used in SCs are based on imidazolium, pyrrolidinium, ammonium, sulfonium, and phosphonium cations. Anions of ILs are [BF₄], [PF₆], bis(trifluoromethanesulfonyl)imide ([TFSI]), bis(fluorosulfonyl)imide ([FSI]), and dicyanamide ([DCA]). Among them, imidazolium and pyrrolidinium based ILs were widely investigated because of relatively lower viscosity and reasonable ionic conductivity [27]. Generally, imidazolium salts were used for high ionic conductivity, and pyrrolidinium salts were applied for wide electrochemical stability window [28, 29] (**Figure 2**). **Table 1** shows representative ILs for electrolyte of SCs.

Most ILs in **Table 1** have several problems, such as high viscosity, low ionic conductivity, and high cost comparison to typical SCs electrolytes. These issues prevent actual application in SCs. (Numerous ILs maintain solid phase at room temperature.) 1-ethyl-3-methyl imidazolium ([EMI][BF₄]) shows high ionic conductivity among ILs; however, the ionic conductivity value of [EMI][BF₄] is 23% level in comparison to 1 M [Et₄N][BF₄] in AN. The viscosity of [EMI][BF₄] is also 130 times higher than common organic electrolyte of SCs [29]. Generally, low ionic conductivity and high viscosity of electrolyte occur increment of internal resistance (equivalent series resistance, ESR) and limit both the energy density and the power density. The energy density is decreased due to Ohmic drop and the power density is also reduced because the power density was oppositely proportional to ESR described as Eq. 1. P is power density, and V is working voltage [30].

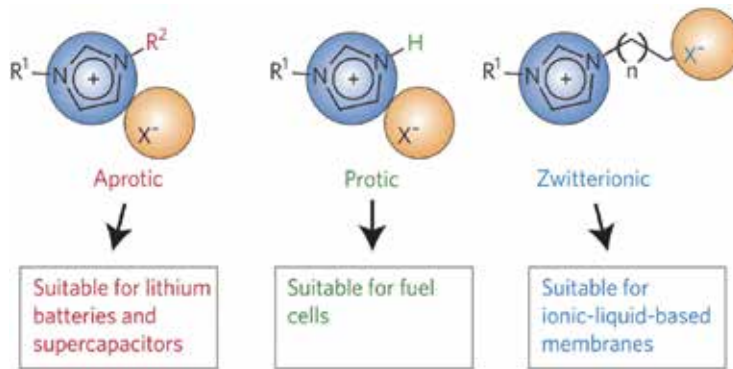


Figure 2. Basic types of ionic liquids: Aprotic, protic, and zwitterionic types [21].

$$P = \frac{V^2}{4 \times ESR} \quad (1)$$

This problem appears to be more severe at room and low temperatures, as evidenced by comparative studies between organic electrolytes and IL electrolytes [22, 28, 31]. These issues are more serious below room temperature. In addition, the EDL capacitance values of ILs adopting SCs can be decreased especially at high scan rates or high charging/discharging rates [32]. Despite these problems, ILs are still attractive materials for electrolytes. ILs show wide stability windows because the ILs are composed of individual ions, which do not participate in any considerable electrochemical reaction over a wide range of potential. Additionally, properties of ILs derived from ionic structure, such as high viscosity, increase the electrochemical decomposition voltage (**Figure 3**).

In terms of the energy density, increment of the operating voltage is advantageous rather than increase the capacitance. The energy density of the SCs is proportional to the square of the voltage as shown in Eq. 2, and E and C are energy density and specific capacitance of SCs, respectively [34].

$$E = \frac{1}{2} C V^2 \quad (2)$$

Figure 4 shows the energy density deference of typical electrolytes of SCs such as KOH aqueous solution, battery electrolyte, and ILs [35]. The hierarchical carbon nanostructure with mesoporous carbon CMK-5 intercalated between reduced graphene oxide (RGO) sheets was proposed as electrode in this research. According to cyclo-voltammograms, capacitive behaviors of applied electrolyte are very similar; however, the differences of stable windows result in significant differences of energy density. When adopting [EMI][BF₄], energy density was increased to 60.7 Wh kg⁻¹, and this value was 11 times higher than energy density of KOH electrolyte (5.2 Wh kg⁻¹).

The electrochemical properties of SCs, especially their capacitances, are highly dependent on the suitability of the electrode material and the electrolyte. ILs are also heavily influenced by the electrode materials. In carbon material including porous activated carbon (AC), the graphitic edges are twisted, which can lead to uneven charge distribution [36]. This effect is

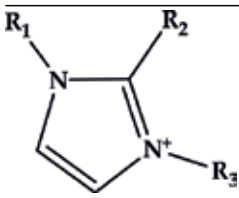
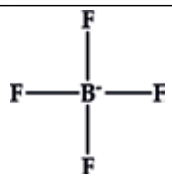
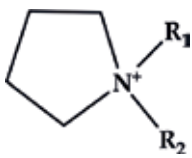
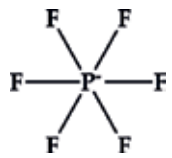
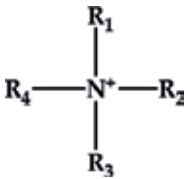
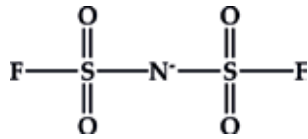
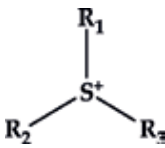
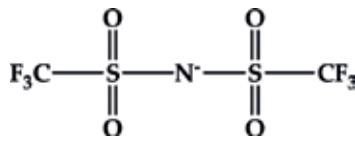
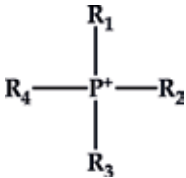
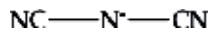
Cation	Anion
 <p>Imidazolium</p>	 <p>Tetrafluoroborate</p>
 <p>Pyrrolidinium</p>	 <p>Hexafluorophosphate</p>
 <p>Ammonium</p>	 <p>Bis(fluorosulfonyl)imide</p>
 <p>Sulfonium</p>	 <p>Bis(trifluoromethylsulfonyl)imide</p>
 <p>Phosphonium</p>	 <p>Dicyanamide</p>

Table 1. Representative cations, anions of ILs for SCs.

more important in ILs because the entire medium is made up of charged ions, so ions interact directly with the localized charge on the electrode surface [37]. Aligned mesoporous carbon provides a good opportunity for diffusion of electroactive species through well-ordered structures, but the chemical composition and degree of graphitization play a decisive role in electrochemical behavior and EDL formation [38]. This effect is more prevalent in ILs, in which the ionic medium is fully interacting. The nature of IL has a profound effect on the capacitive behavior of well-defined mesoporous carbon [39]. Graphene and similar carbonaceous materials are generally covered with various functional groups. Molecular dynamics simulations

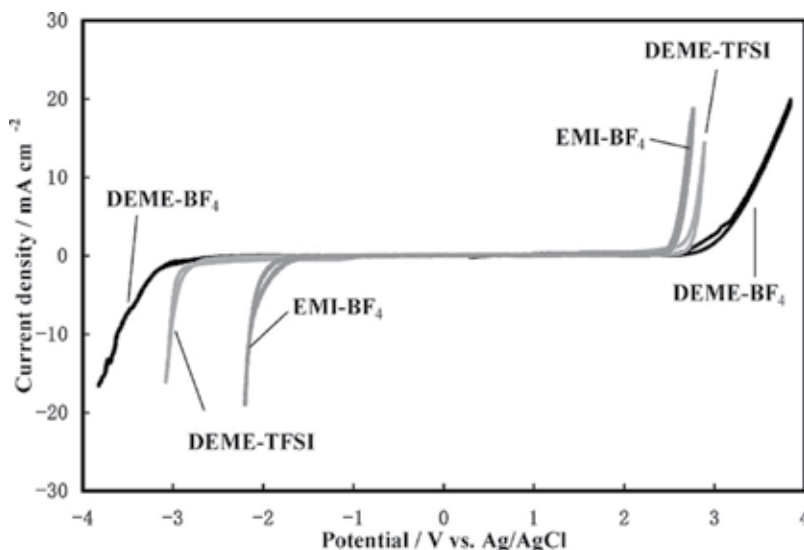


Figure 3. Cyclic voltammogram of the ionic liquids based on the DEME cation and EMI- BF_4 at 25°C . Scan rate: 1 mV s^{-1} , working and counter electrode: Platinum, reference electrode: Ag/AgCl electrode [33]. (DEME: N,N-diethyl-N-methyl-N-(2-methoxyethyl)ammonium, EMI- BF_4 : [EMI][BF_4]).

suggest that functional groups, especially hydroxyl groups, prevent ILs ions from interacting directly with the electrode surface [40]. These phenomena can be occurred polarity and hydrophilic/hydrophobic physical property of functional groups. In case of partially negative functional groups of carbonaceous materials like chlorine treated carbon prevent anion adsorption, or hydrophilic ILs indirectly bonded with the functionalities on surface of porous carbon electrode by hydrogen bonding and ions of ILs cannot be penetrated into narrow micropores. These ions block pores, and consequently, the specific capacitance was reduced especially at the high scan rate [41, 42]. Interestingly, these functional groups of carbonaceous materials are helpful to increase the specific capacitance of SCs in conventional electrolytes especially the aqueous electrolytes due to pseudoreaction. Thus, functional groups of carbonaceous materials have disadvantageous for ILs electrolytes system, while they are not effective with the conventional electrolyte adopted SCs. Pinker et al. controlled the specific capacitance by surface treatment of ordered mesoporous carbon [41]. [EMI][BF_4] was used as the electrolyte. The surface treatment of pristine-ordered mesoporous carbide-derived carbon (OM-CDC) in chlorine gas and oxygen was evaluated. The chlorine gas protects the surface from reoxidation and lowers the surface polarity, thus enhancing the rate capability. The surface treatment of OM-CDC in air introduces oxygen functionalities, which result in a significant decrease of the rate capability. Silicon nanowires coated have attracted attention as a promising candidate for electrolytes for ILs electrolyte-based SCs due to their excellent cycle performance and thermal stability [43, 44]. Since the silicon electrode is not suitable for aqueous electrolytes, the importance of ionic liquid electrolytes has been further emphasized.

Along with the compatibility with the electrodes, the behavior of the ionic liquid at the electrode/electrolyte interface is also important. Without destructive chemical interactions of the IL ion, it is electrochemically stable, but structural changes during cycling are still an important

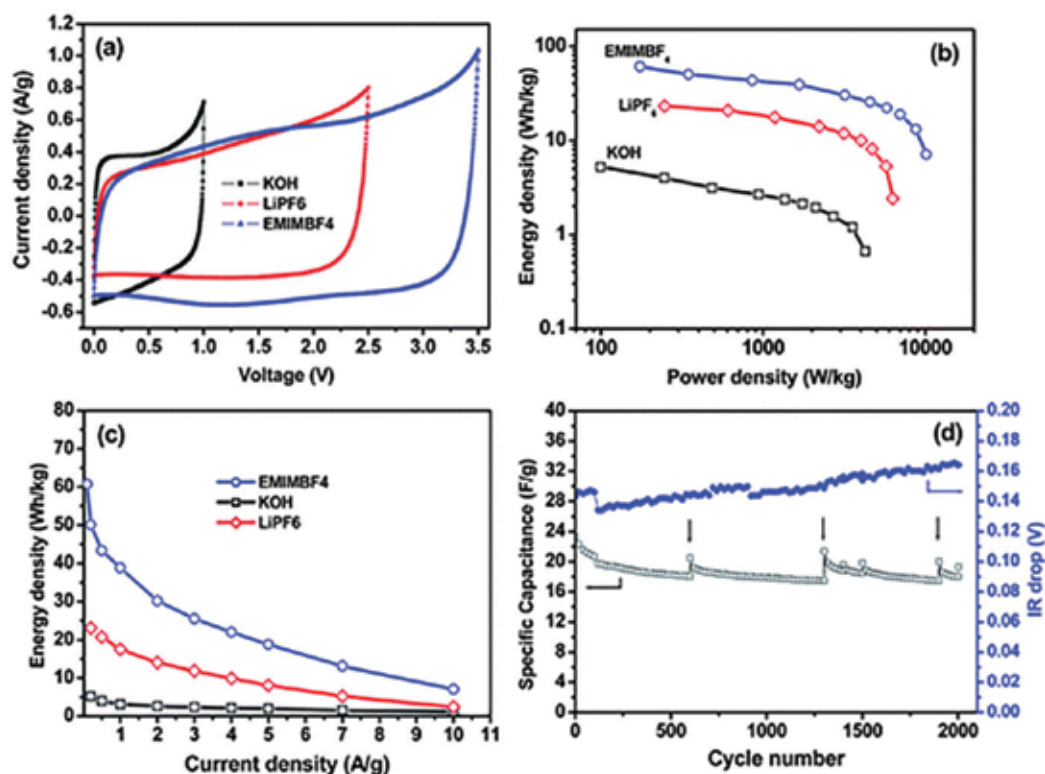


Figure 4. CV behaviors (a), Ragone plots (b), and change of energy density with current density (c) of the RGO-CMK-5 composite electrode measured in different electrolytes. (d) Cycle performance of the RGO-CMK-5 electrode measured in EMIMBF4 electrolyte, with the arrows showing the beginning of a new cycle [35] (CV: cyclic voltammetry, EMIMBF₄:[EMI][BF₄]).

issue and should be carefully considered. To understand the aging or failure mechanism of ILs, electrochemical decomposition of ILs was investigated using in situ techniques (infrared and electrochemical spectroscopy methods and XPS) [45, 46]. These studies were performed to understand the EDL structure of ILs, enhancing electrochemical properties by modifying positive or negative ions or adopting pseudoelectrode material.

As previously mentioned, imidazolium-based ILs are one of the candidates for SCs electrolyte. The electrochemical characteristics of various ILs electrolytes with [EMI] cations and different anions ([BF₄], tetracyanoborate([B(CN)₄]), tris(pentafluoroethyl)trifluorophosphate ([PF₃(C₂F₅)₃]), [TFSI], [FSI], and thiocyanate ([SCN])) was reported using carbon cloth electrodes [47]. Working voltage was changed according to anions, and [EMI][BF₄], [EMI][TFSI], and [EMI][B(CN)₄] were stable up to 3.2 V. The highest energy values at 3.2 V for [EMI][B(CN)₄] were 49 Wh kg⁻¹. Graphene sheet electrode was also evaluated [EMI] cation with various anions, which were categorized representative chemical species. The five anions were [BF₄] as inorganic fluoride, [FSI] as organic fluoride, [DCA] as cyano functionality, ethylsulfate ([EtSO₄]) as ester functionality, and acetate ([OAc]) as acid. The hydrogen-bond-accepting ability of anions was closely related to the viscosity of the ILs. Moreover, [EMI][DCA],

[EMI][BF₄], and [EMI][FSI] showed excellent cycling stability with the same potential window of 2 V. SCs adopting [EMI][BF₄] had the widest potential window of 4 V, which displayed a maximum energy density of 67 Wh kg⁻¹ at a current density of 1 Ag⁻¹ [48] (**Figure 5**).

Other types of imidazolium-based ILs were also investigated. Bettini et al. studied film SCs by adopting ILs electrolytes. The electrolyte was varied out through cation based on [FSI] anion. The applied cations are EMI, 1-butyl-3-methylimidazolium ([BMI]), 1-dodecyl-3-methylimidazolium ([C₁₂MI]), and 1-butyl-1-methylpyrrolidinium ([PYR₁₄]), and electrode was nanostructured carbon (ns-C) [49]. The ionic conductivities were decreased depending on cation size in the order of [EMI] > [BMI] > [PYR₁₄] > [C₁₂MI]. [BMI][FSI] adopted SCs exhibited the highest specific capacitance of 75 F g⁻¹ despite of secondly high ionic conductivity. This means that [BMI][FSI] have chemical affinity with ns-C. Borges et al. use 1-butyl-2,3-dimethylimidazolium [EBDMI] cation and [TFSI] anion as electrolyte of temperature stable SCs [50]. The proposed electrolyte achieved 4.4 V of electrochemical stability window with functionalized double-walled carbon nanotubes (DWCNT).

The pyrrolidinium cations were extensively studied for the wide operating voltage. Most of cases, [PYR₁₄] cation was selected. Largeot et al. introduced high-temperature carbon-carbon SCs working at 100°C with [PYR₁₄][TFSI] electrolyte and microporous carbide-derived carbon electrode [51]. High operating temperature means that ILs are thermally stable, and the viscosity of ILs is not enough to obtain reasonable specific capacitance (Most of pyrrolidinium based ILs exist in quasi solid state at room temperature). The specific capacitance of suggested SCs reached a maximum at 130 F g⁻¹. Mastragostino group also reported several studies using pyrrolidinium cation, [PYR₁₄], [TFSI] was used as anion [52–54]. They tested the ILs electrolytes using hybrid SCs (asymmetric SCs). The AC and the conductive polymer (poly(3-methylthiophene)) were adopted as electrodes. These SCs achieved 3.6 V of the working voltage and 16,000 cycle of the cycle-ability at 60°C. The hybrid supercapacitor delivered 24 Wh kg⁻¹ and 14 kW kg⁻¹ as maximum values. However, low ionic conductivity remains as problems.

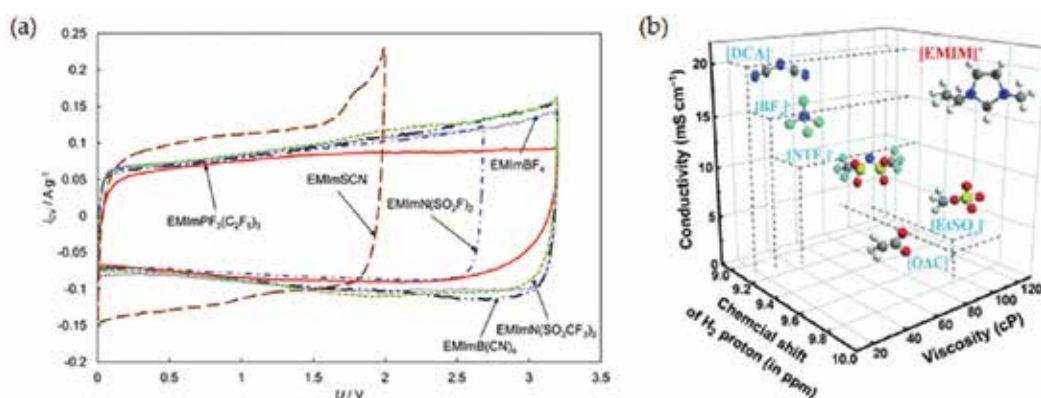


Figure 5. (a) Cyclic voltammograms measured at cell voltage scan rate 1 mV s⁻¹ for SC test cells filled with RTILs. ([EMI][BF₄]; [EMI][PF₃(C₂F₅)₃]; [EMI][B(CN)₄]; [EMI][N(SO₂CF₃)₂]; [EMI][TFSI]; [EMI][N(SO₂F)₂]; [EMI][FSI]; and [EMI][SCN]; [EMI][SCN]) [47], (b) the relationship between the electrical conductivity, viscosity, and ¹H NMR chemical shift of the proton in the 2-position of the imidazole ring of the ILs studied [48].

To overcome the viscosity issue, factionalized electrodes were proposed. Nitrogen-doped reduced graphene oxide aerogel (N-rGO aerogel) was one of them [55]. [PYR₁₄][DCA] was matched with N-rGO aerogel. Reported SCs show excellent electrochemical characteristics of wide working potential of 4.0 V, high specific capacitance of 764.53 F g⁻¹ at 1 A g⁻¹, and a capacity retention of 86% over 3000 charge discharge cycles, and this system provided maximum specific power of 6525.56 W kg⁻¹ and energy of 245.00 Wh kg⁻¹. In addition, ILs with various cations have been studied as electrolytes. The sulfonium and the piperidinium were also investigated to achieve high electrochemical performances [31, 56]. However, these ILs have relatively high melting point about 40–60°C; thus, they applied as electrolytes for high-temperature SCs or as electrolytes with solvents.

2.2. Other approaches of ionic liquid as liquid electrolyte

Approach for reducing the viscosity of ILs is anion eutectic ILs mixture. Several studies were reported to reduce melting transitions and an enhance liquids range, pyrrolidinium- and piperidinium-based ILs which have relatively high viscosity as previously mentioned were selected [57–59]. SC with mixed ILs gave the assurance that the eutectic mixture of ILs could dramatically extend the temperature range of the electrical energy storage device. This is a sufficient result to dispel the recognition that the ILs cannot be used as a low-temperature electrolyte due to the high viscosity of them. SC with mixed ILs showed electrical double layer capacitors able to operate from –50 to 100°C over a wide voltage window (up to 3.7 V) and at very high charge discharge rates of up to 20 V s⁻¹ [59]. **Figure 6** shows the change of specific capacitance versus the temperature according to various electrolytes.

Recently, Lian et al. introduced mixed anion ILs in order to have the same cations but having two types of anions with different sizes and geometries for enhancing the capacitive

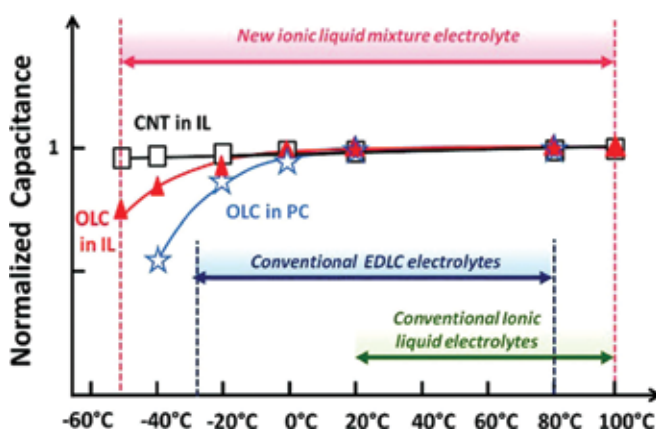


Figure 6. Normalized capacitance ($C/C_{20^\circ\text{C}}$) for the onion like carbon and vertical aligned-CNT electrodes (new ionic liquid mixture electrolyte: $([\text{PIP}_{13}][\text{FSI}]_{0.5}([\text{PYR}_{14}][\text{FSI}])_{0.5})$, conventional EDLC electrolyte: 1 M of $[\text{Et}_4\text{N}][\text{BF}_4]$ in PC, and $[\text{PIP}_{13}]$: N-methyl-N-propylpiperidinium). Capacitances were calculated at 100 mV s⁻¹, except for the –50°C (1 mV s⁻¹) and –40°C (5 mV s⁻¹) experiments. This plot shows that the use of the IL mixture extends the temperature range for supercapacitors into the –50 to 100°C range, while conventional electrolytes using PC as solvent are limited to the –30 to 80°C range. $C_{20^\circ\text{C}}$ was 80 and 4 mF, respectively, for OLC and VA-CNT cells. All cells were cycled from 0 up to 2.8 V [59].

performance [60]. This research provided the capacitive behavior of a planar carbon in two kinds of ILs and their mixture both experimentally and computationally. They selected single cation [EMI] and two different anions of $[BF_4]$ and $[TFSI]$. This study explained that the mixture effect, which makes more counterions pack on and more co-ions leave from the electrode surface, leads to an increase of the counterion density within the EDL and thus a larger capacitance. **Figure 7** compares the distribution of ions at the electrode surface in pure ILs electrolyte and their mixture.

Another approach for ILs is redox active electrolyte. Until recently, SCs using redox reactions have been studied with electrodes. As a result, various electrode materials such as metal oxides and conductive polymers have been proposed [61–63]. These pseudomaterials have been mostly studied using aqueous electrolytes because of the redox mechanism using proton. However, application of ILs has been studied as alternatives due to the limitation of the operating voltage of aqueous electrolyte and the inadequacy of surface functionality of electrode materials. Protic ILs which contain proton were investigated as the electrolyte for pseudo-type electrode. Protic ILs are advantageous over aprotic ILs; however, the high viscosity and slow proton transfer in the ILs electrolyte could limit the charging rate [64, 65]. And their cycle-ability was not enough to actual application. Aprotic ILs were tried as electrolyte for pseudoelectrode in some cases [66]. The pseudomaterial was manganese dioxide (MnO_2), and the IL was $[BMI][DCA]$. The redox mechanisms between ILs and MnO_2 were expressed in Eq. (3). Within a potential range of 3 V, a specific capacitance of 70 F g⁻¹ was obtained.

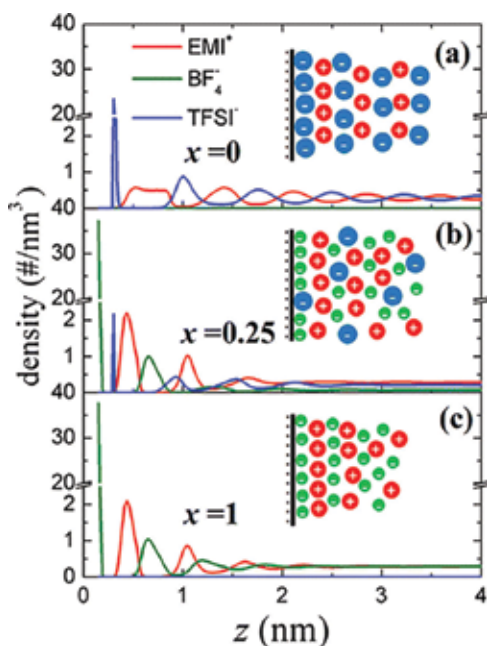
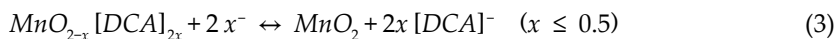


Figure 7. (a) Schematic representation of a ILs mixture near the electrode surface, (b) distributions of cations (red line for [EMI]) and anions (green line for $[BF_4]$ and blue line for $[TFSI]$) in EDL of pure and mixed ILs near a positive surface with positively charged surface = 1.5 V: (a) $x = 0$, (b) $x = 0.25$, and (c) $x = 1$. The inserts are schematics of the EDL structures. (x is the weight fraction of $[EMI][TFSI]$) [61].



A new strategy has been explored to increase the capacitance of SCs by inducing the pseudocapacitive contribution from the redox-active electrolytes [67]. The Faradaic reactions occur in the electrolyte, which can contribute extra capacitance to the SCs. In this case, the pseudocapacitance is not only contributed by the pseudocapacitive electrode materials but can also be contributed from the electrolyte. The introduced redox mediator was halide (mostly iodide), vanadium (IV) oxide sulfate ($VOSO_4$), metal cation (Cu^{2+}), heteropoly acids, fractionalized arene, and quinode-benzoide [67–71]. As mentioned previously, most of redox couple were applied with aqueous medium. However, to achieve higher cell voltage and thus a higher energy density, a number of nonaqueous electrolytes including organic and IL-based electrolytes have been studied and reported. In the case of ILs, halide ion species was used as

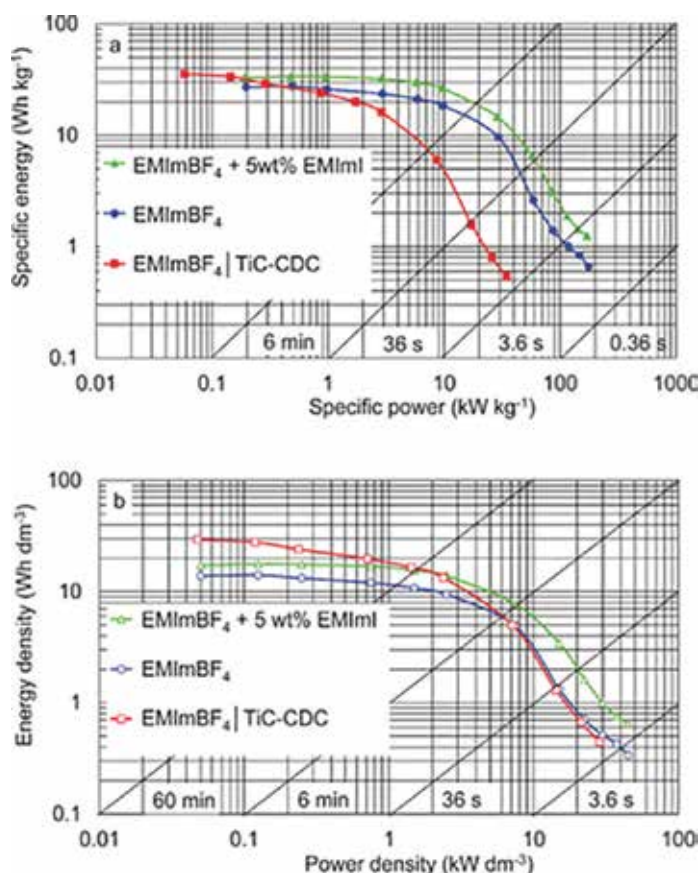


Figure 8. (a) Specific energy vs. specific power and (b) energy density vs. power density plots for EDLCs based on microporous-mesoporous carbon electrodes in EMImBF₄ + 5 wt% EMImI mixture (triangles), in neat EMImBF₄ (circles), obtained from constant power tests within the cell potential range from 2.4 to 0.4 V and for comparison for EDLCs based on TiC-CDC carbon electrodes in EMImBF₄ (squares), and obtained from constant power tests within the cell potential range from 3.0 to 1.5 V. (EMImBF₄: [EMI][BF₄] and EMImI: [EMI][I]) [74].

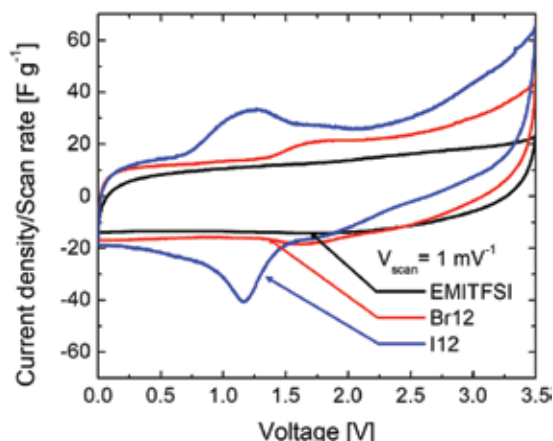


Figure 9. Cyclic-voltammogram of [EMI][TFSI] and [EMI][I] and Br/[EMI][TFSI] mixture at 1 mV s^{-1} .

redox active couple. Taniki et al. reported that the N-ethyl-N-methylpyrrolidinium ([EMPyrr]) fluorohydrogenate ($[(\text{FH})_{2,3}\text{F}]$) could significantly contribute extra specific capacitance to the SCs through the redox reaction of the electrolyte [72]. In the case of charging up to 2.5 V, the EDL capacitance of the positive electrode is 140 F g^{-1} , and the redox capacitance is 150 F g^{-1} , both of which contribute to the total capacitance. Correspondingly, the negative capacitance is the sum of the double-layer capacitance of 130 F g^{-1} and the redox capacitance of 116 F g^{-1} . In 2014, Tooming et al. reported redox active electrolyte using 5 wt% [EMI] iodide into [EMI][BF_4], and they archive a nearly 50% increase in specific capacitance in comparison to bare [EMI][BF_4] [73]. As shown in **Figure 8**, noticeable increase in specific power and power density ($\sim 30\%$ at $P \sim 1 \text{ kW kg}^{-1} / 1 \text{ kW dm}^{-3}$) as well as in specific energy and energy density ($\sim 60\%$ at $P \sim 1 \text{ Wh kg}^{-1} / 1 \text{ Wh dm}^{-3}$) has been achieved by 5 wt% addition of [EMI][I] into [EMI][BF_4].

However, EDL capacitance is proportional to number of the ions (charges). Thus, weight ratio is not appropriate for comparing [EMI][I]/[EMI][BF_4] mixture and neat [EMI][BF_4]. For this reason, our group suggested redox active electrolyte, which have same number of ions. We choose bromide and iodide as redox mediator. The specific capacitances were increased by amount of [EMI] halide (**Figure 9**). The SCs adopting 0.12 mole fraction of [EMI][I] show the highest specific capacity of 176.1 F g^{-1} with 3.5 V of working voltage. The energy density is 231.9 Wh kg^{-1} at 0.5 A g^{-1} , when the power density is 2705.6 W kg^{-1} .

3. Ionic liquid as quasi solid and solid electrolyte

Liquid electrolytes need additional encapsulation. Thus, SCs applied ILs face difficulty in integration and manufacturing flexible devices. These problems can be addressed by solidifying the ILs because the ILs maintain the conductivity even when solidified, unlike a typical organic electrolyte. Generally, polymers are applied for solid state with various devices, and ILs adopted polymer structure are described in **Figure 10**.

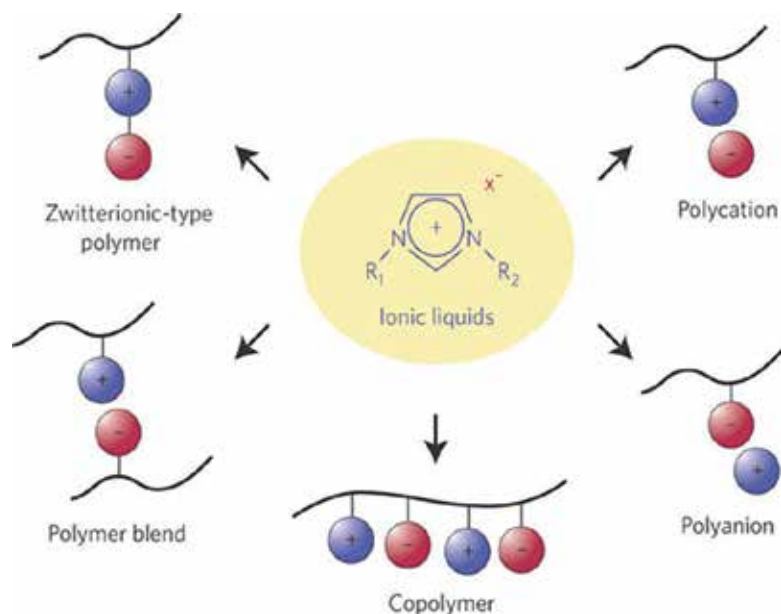


Figure 10. Ionic liquid-polymer electrolyte.

3.1. Ionic liquid-blended polymer electrolyte

ILs blended polymer electrolyte can be referred to ion gel (iongel, ionogel) because most of the ILs blended polymer electrolytes were synthesized in gel polymer type. The initial gel polymer electrolyte consisted of ion conducting salts (ILs), organic solvent, and polymers like gel polymer electrolyte of LIBs. In 1997, Fuller et al. reported iongel that contains ILs, organic solvent, and poly(vinylidene fluoride-co-hexafluoropropylene) (PVdF-HFP) [74]. The iongel which was composed of [EMI][BF₄] and [EMI][CF₃SO₃⁻] and PVdF-HFP achieved the highest ionic conductivity of 5.8 mS cm⁻¹. Various carbon materials were adopted from classical AC to nanostructured carbon such as CNT and graphene [75–77]. Pandey et al. also proposed [EMI][B(CN)₄] and PVdF-HFP-based iongel electrolyte [77]. SCs applied ion gel was tested with multiwall carbon nanotube (MWCNT) electrode. The SCs adopting [EMI][B(CN)₄] based iongel shows good thermal stability up to 310°C, a wider electrochemical window of ~3.8 V, and a high ionic conductivity of $\sim 9 \times 10^{-3}$ S cm⁻¹ at room temperature. The SCs also show a specific energy of ~ 3.5 W h kg⁻¹ and a specific power of ~ 4.2 kW kg⁻¹. Lu et al. also studied ion gel with PVdF-HFP and [EMI][FSI] [78]. They compared different polymer composites. The ion gels were flexible and mechanically strong and show 28 Wh kg⁻¹ of the energy density with 2317 W kg⁻¹ of the power density. The features of iongel and the structure of the SCs using the iongel are shown in **Figure 11**.

Each carbon electrode was attached on a polypropylene plate on the aluminum foil side. ([EMIM][Tf₂N]: [EMI][FSI] and PTFE: Poly(tetrafluoroethylene)) [78]. Other type of polymers and ILs has been tried as ion gel electrolyte. Tamilarasan et al. reported ion gel as stretchable electrolyte. The synthesized [BMI][TFSI] incorporated stretchable poly(methyl methacrylate)(PMMA) electrolyte [79]. The device has specific capacitance of 83 F g⁻¹,

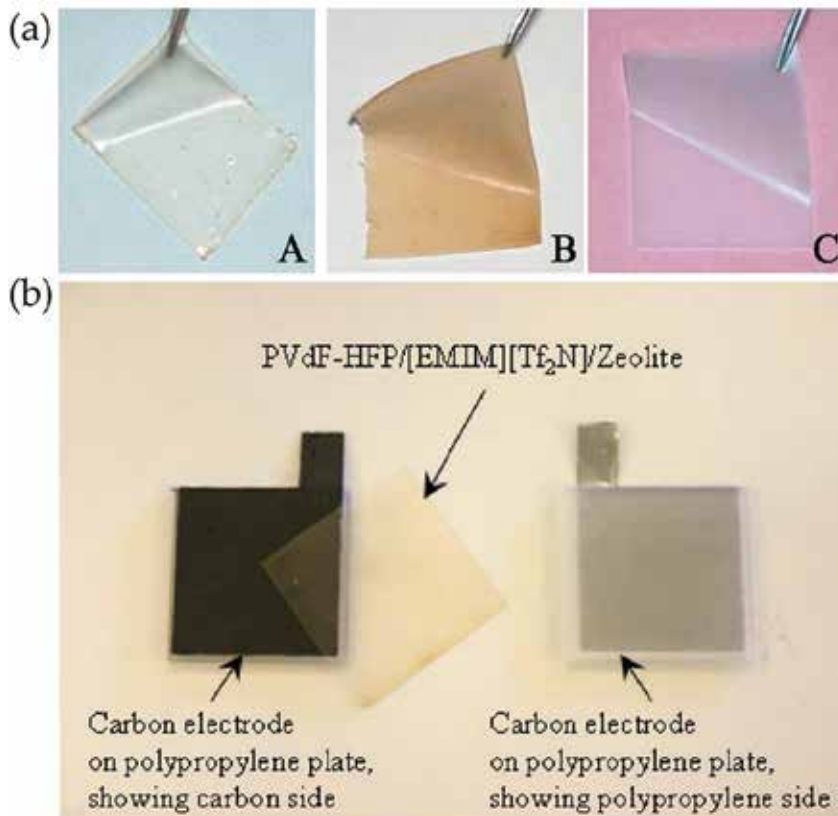


Figure 11. (a) Photographs of ILGPEs prepared by different methods: (A) PVdF-HFP/EMIM][Tf₂N] by ionic-liquid-polymer gelation method, (B) PVdF-HFP/[EMIM][Tf₂N]/zeolite by ionic-liquid-inorganicpolymer composite method, and (C) PTFE/[EMIM][Tf₂N] by ionic-liquid-polymer membrane method. (b) Photograph of a capacitor before assembly from two carbon electrodes and a PVdF-HFP/[EMIM][Tf₂N]/zeolite ILGPE.

specific current of 2.67 A g⁻¹, and energy density and power density of 25.7 Wh kg⁻¹ and 35.2 kW kg⁻¹, respectively. The ion gel stretched up to 150%. Other polymeric matrixes such as poly(acrylonitrile), polyvinylidene fluoride/polyvinyl acetate, poly(ethylene oxide), poly(vinylalcohol), poly(methylmethacrylate), poly(tetrafluoroethylene), and chitosan were investigated [80–83].

Most of the introduced ILs and iongel operated at 2.0–3.5 V. These operating voltages were not enough to overcome intrinsic limitation of ILs because ILs have low ionic conductivity and high viscosity, such properties cause decrement of specific capacity. To overcome relatively low specific capacity, operating voltage have to be enhanced at 3.5–4.0 V. Additionally, high operating voltage is helpful to manage power supply. SCs are regarded as excellent energy storage devices due to their high power density and permanent life cycles. However, SCs face with critical challenge of low energy density. Therefore, LIBs and SCs are applied together for the complementary purpose. The typical case is a wireless detection system that needs two kinds of power supply units. One is a continuous power supply for operation, and the other is a pulse power to transmit data to the control system. Continuous power systems require

high-energy densities, while pulse power systems need high-power densities. Consequently, LIBs are responsible for device operation, while SCs are used for data transmission. A critical issue in this system is voltage leveling between the LIBs and SCs. The operating voltage of LIBs is from 3.5 to 4.0 V. Thus two or more SCs in series are needed for a wireless detection system. If SCs achieve the 3.5–4.0 V rated voltage with high energy densities or LIBs achieve high power densities, then the power supply unit can be minimized and integrated. LIBs have intrinsic limitations in power densities due to their energy storage mechanisms. Hence, SCs that show high energy densities and wide operating voltages have been researched extensively. Thus, new approaches were reported to enhance working voltage of SCs. Pandey et al. adopted zeolite as additives for enhancing operating voltage, and the zeolite added SCs were stable up to 4.1 V [78]. Cross-linked polymer matrix was suggested as solid electrolyte for high-voltage SCs. Choi et al. suggested all printable SCs using UV curable materials. [BMI][BF₄] and UV-cured ethoxylated trimethylolpropane triacrylate (ETPTA)-based gel polymer electrolytes are incorporated to produce the solid-state SCs. They showed various shapes of inkjet-printed SCs described in **Figure 12**. Interestingly, proposed UV-cured ion gel was water proof despite of adopting [BMI][BF₄] [84].

Our team proposed a quasi-solid polymer electrolyte based on a composite cross-linked poly-4-vinylphenol (c-P₄VPh) embedded [EMI][TFSI] [5]. [EMI][TFSI] was selected for its high ionic conductivity, and c-P₄VPh was used for its ability to enhance electrochemical stability by hydrogen bonding between [EMI][TFSI] and c-P₄VPh in addition to maintaining a quasi-solid state. Also, cross-linked polymers can keep a larger amount of ILs than other polymer by swelling. The composite electrolytes are highly ionic conductive solid state due to the rigid framework of c-P₄VPh and high ionic conductivity from large contents of [EMI][TFSI] over 60 wt%. The IL-CPs are thermally stable over 300°C and electrochemically stable over 7.0 V, since there are hydrogen bonds between c-P₄VPh and [EMI][TFSI]. We also introduced all-solid state SCs that operate at 4.0 V and have high energy density without sacrificing power density. SCs showed the best electrochemical performances and had capacitance of 172.5 F g⁻¹ and energy density of 72.3 Wh kg⁻¹. Their structure and electrochemical characteristics are displayed in **Figure 13**.

3.2. Poly ionic liquid as solid electrolyte

A poly IL (PIL) or polymeric ionic liquid is a polymer electrolyte containing a polymer backbone and an IL species in the monomer repeat unit. Certain characteristics of IL such as negligible vapor pressure, thermal stability, nonflammability, relatively high ionic conductivity, and broad electrochemical stability window are transferred to the polymer chain (from oligomers to high molecular weight polymers) [85]. Various PIL structures and properties are required for various applications of polymer electrolytes, electrochemical devices, smart materials, catalyst supports, porous polymer structures, and antibacterial PILs. The standard synthetic pathway for PILs relies on a basic strategy: (1) direct chain growth polymerization of IL with or without nonionic monomers; (2) step-growth polymerization of IL monomers; and (3) post-modification of polymer chains with IL monomers.

Properties required as solid electrolytes include ionic conductivity, thermal stability, and electrochemical stability. The ionic conductivity of PILs is an important property when applied as

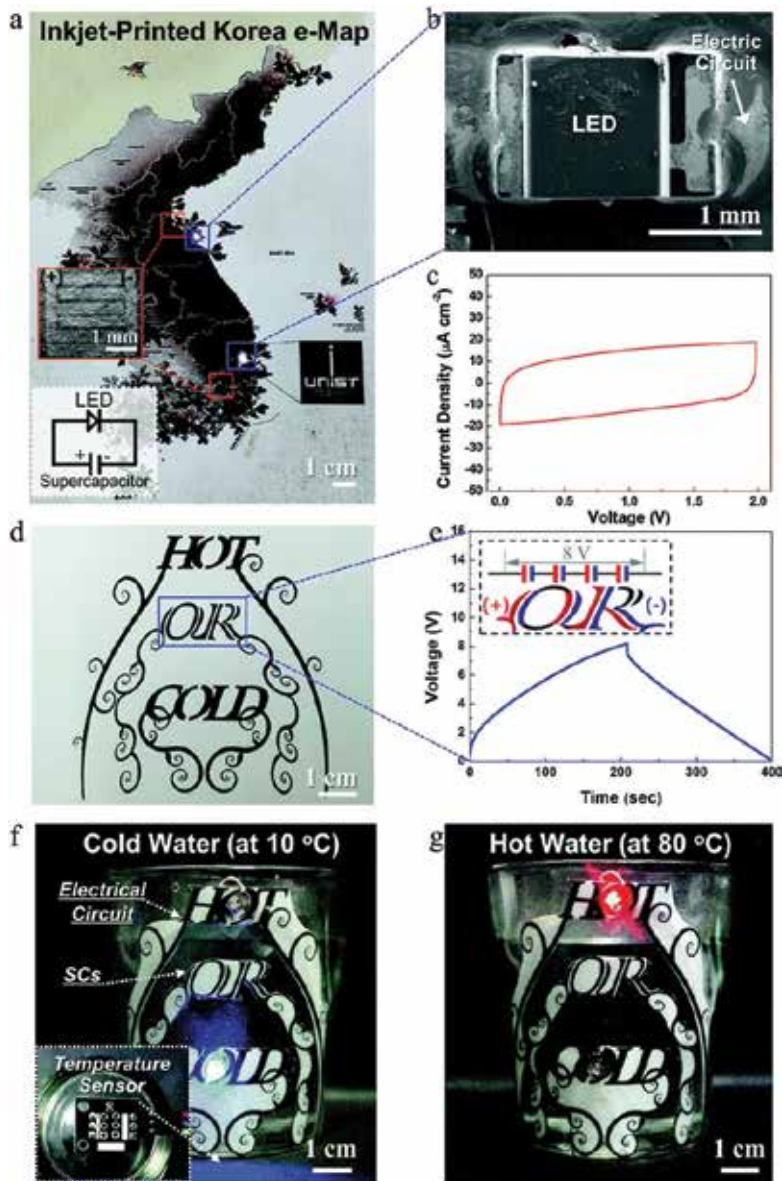


Figure 12. Esthetic versatility and IoT applications of the inkjet-printed SCs as object-tailored/monolithically integrated power sources. (a) Photograph of the inkjet-printed Korea map, wherein the inkjet-printed SCs (marked by red boxes) were seamlessly connected to LED lamps (marked by blue boxes) via the inkjet-printed electric circuits. (b) SEM image of the LED lamp connected to the inkjet-printed electric circuits. (c) CV profile (scan rate = 1.0 mV s⁻¹) of the inkjet-printed SC in the map. (d) Photograph of the inkjet-printed, letter (“OR”) shaped SCs that were seamlessly connected to the letter (“HOT” and “COLD”) shaped electric circuits onto A4 paper. (e) Galvanostatic charge/discharge profile (current density = 1.0 mA cm⁻²) of the inkjet-printed, letter (“OR”) shaped SCs that were composed of 4 cells connected in series. (f) Photograph depicting the operation of the blue LED lamp in the smart cup (for cold water (~10°C)), wherein the inset is a photograph of a temperature sensor assembled with an Arduino board. (g) Photograph depicting the operation of the red LED lamp in the smart cup (for hot water (~80°C)) [84].

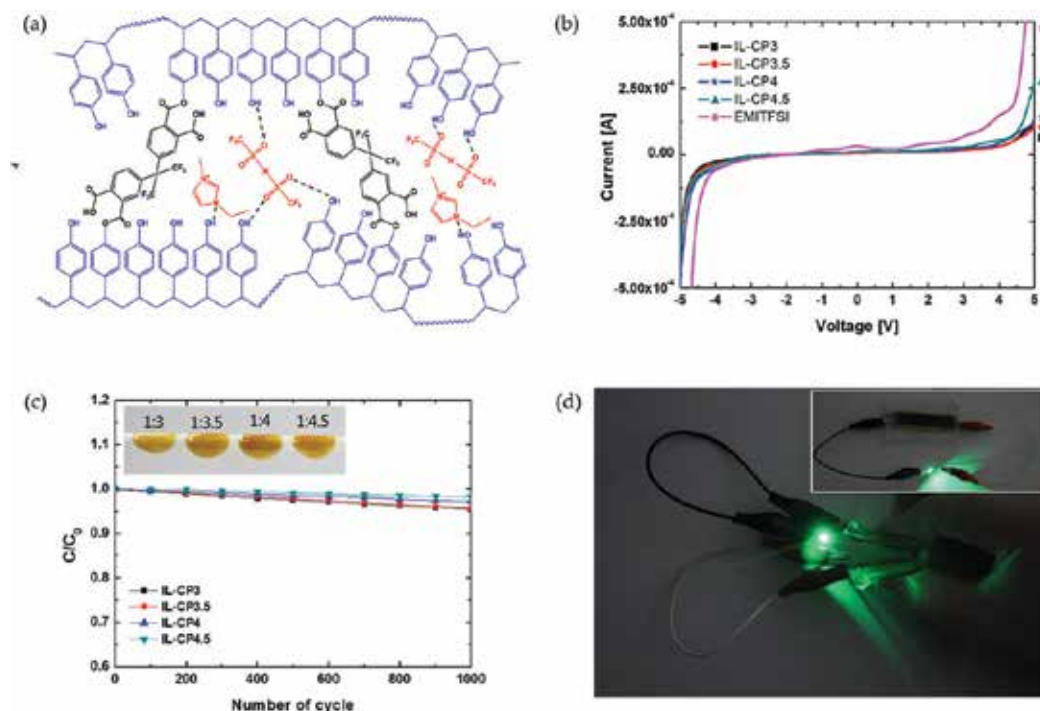


Figure 13. (a) Chemical structure of IL-CPs, (b) LSV for EMITFSI and IL-CPs in the SUS/SUS cell (CR 2032), (c) flexibility of IL-CPs and bending performance of SCs with IL-CPs for 1000 cycles, and (d) photograph of a green light-emitting-diode (LED) powered by a single SC with IL-CP3.5. (IL-CPs: [EMI][TFSI]/c-P_iVPh composite, and IL-CPx: x = weight ratio of [EMI][TFSI]) [5].

a solid electrolyte. Unlike ILs and ion gels in which both anions and cations can move, PILs are typically single-ion conductors. In this case, anions or cations are structurally constrained as part of the polymer skeleton [86]. Therefore, the ionic conductivity of PIL is generally lower than that of monomeric ILs ionic conductivity. This phenomenon is due to the significant increment of glass transition temperature (T_g) and depletion of mobile ions after covalent or ionic bonding [85]. The ionic conductivity of PIL is affected by polymer architecture, molecular weight, and chemical nature of polymer chains.

Particularly, the ionic conductivity of PIL is related to the glass transition temperature, and the ionic conductivity is usually increased when the T_g is low. PIL has weak binding ions and can exhibit low T_g despite having very high charge densities due to weak electrostatic ion pair interactions. Counter ions affect the T_g of these polymers. Therefore, a method of lowering the T_g using a different kind of anion has been proposed. Tang et al. found that anion tendency with poly 1-(p-Vinylbenzyl)-3-methyl-imidazolium cation, the T_g also changes in order [FSI] (3°C) < o-benzoic sulphimide (40°C) < $[\text{BF}_4]$ (78°C) < $[\text{PF}_6]$ (85°C) [87]. For PILs with the same anion $[\text{BF}_4]$, the T_g varied according to the backbone and Poly[(1-butylimidazolium-3)methyl-ethylene oxide (33°C) < 1-[2-(Methacryloyloxy)ethyl]-3-butyl-imidazolium (54°C) < Poly[1-(p-Vinylbenzyl)-3-butyl-imidazolium (78°C) < poly 1-(p-Vinylbenzyl)-3-methyl-imidazolium

(110°C). Flexible backbones yield lower T_g values. Similarly, Hu et al. directly grafted TFSI anions onto the polyethylene oxide backbone via anionic ring-opening polymerization [88]. The resulting PIL exhibits a low T_g value (up to -14°C) and an average conductivity of 10^{-5} S cm⁻¹ at 30°C and $\sim 10^{-3}$ S cm⁻¹ at 90°C.

The thermal stability of the PILs is directly related to the lifetime and stability of the capacitor and chemical and electrochemical stability. In thermogravimetric analysis (TGA) experiments, the decomposition starting temperature (T_{onset}) is usually controlled through the nature of the PIL backbone chemical structure. Imidazolium-based PILs have improved thermal stability due to conjugate structure and steric hindrance. They have higher T_{onset} values than pyrrolidinium-based PILs. The thermal stability of PILs increases with the length of the substituent of the cation. The chemical structure of anions also affects the T_{onset} value of PILs. Poly (1-vinyl-3-ethyl-imidazolium) X-PIL was studied by comparing the effects of counter anions on PIL thermal stability [89]. $[\text{CF}_3\text{SO}_3^-] > [\text{TFSI}] > [\text{C}_{12}\text{H}_{25}\text{C}_6\text{H}_4\text{SO}_3^-] > [\text{PF}_6] > \text{bromide} > [\text{C}_{16}\text{H}_{34}\text{PO}_4^-]$.

PIL-based polymer electrolytes have high ionic conductivity (up to 10^{-3} S cm⁻¹ at 25°C), wide electrochemical windows (up to 5 V), and high thermal stability (up to 350°C) [86]. Pyrrolidinium-based PILs have been reported to have better electrochemical stability than imidazolium-based PILs. The pyrrolidinium cations also exhibit a much larger cathodic electrolysis potential than the quaternary ammonium cations of the noncyclic and unsaturated rings [90]. Because of excellent electrochemical stability and reasonable ionic conductivity in solid phase, PIL electrolytes have been considered as an ideal electrolyte for supercapacitors. However, only a few studies have been reported in this area by Marcilla group, and (Diallyldimethylammonium) bis (trifluoromethanesulfonyl) imide dissolved in $[\text{PYR}_{14}]$ was prepared and applied as a solid state electrolyte [91, 92]. Impregnating the electrode with the electrolyte before assembling the SCs is an important process for improving the carbon-electrolyte contact. However, these manufactured SCs high ESR values due to poor electrode/electrolyte interface performance. Further studies using pyrrolidinium-based PIL electrolytes with high ionic conductivity have greatly improved relative dielectric constant. **Figure 14** shows the PILs structure and electrochemical characteristics.

In conclusion, ILs have tremendous potential in electrochemical systems with combination of cations and anion. However, their applicability has been limited by the general perception that they are ionic electrolytes for replacing conventional electrolytes. However, due to its high viscosity, low ionic conductivity, and high price, it is difficult to replace conventional electrolytes directly. In other words, ILs should not be chosen as an alternative to organic solvents. Therefore, it is considered that the ILs-based liquid electrolyte are used to enhance the energy density by increasing the high operating voltage of the SCs. They are also helpful to secure the stability and safety of SCs. In addition, since IL is stable at high temperatures, it can be applied to SCs that must be used under extreme conditions. In the same way, IL is more attractive as a solid electrolyte instead of a conventional electrolyte. In particular, IL-based solid polymer electrolytes appear to be one of the most promising choices for flexible SCs. However, current research on ILs as electrolytes has focused on several ILs, including imidazolium and pyrrolidinium cation. As mentioned, ILs have design flexibility due to the

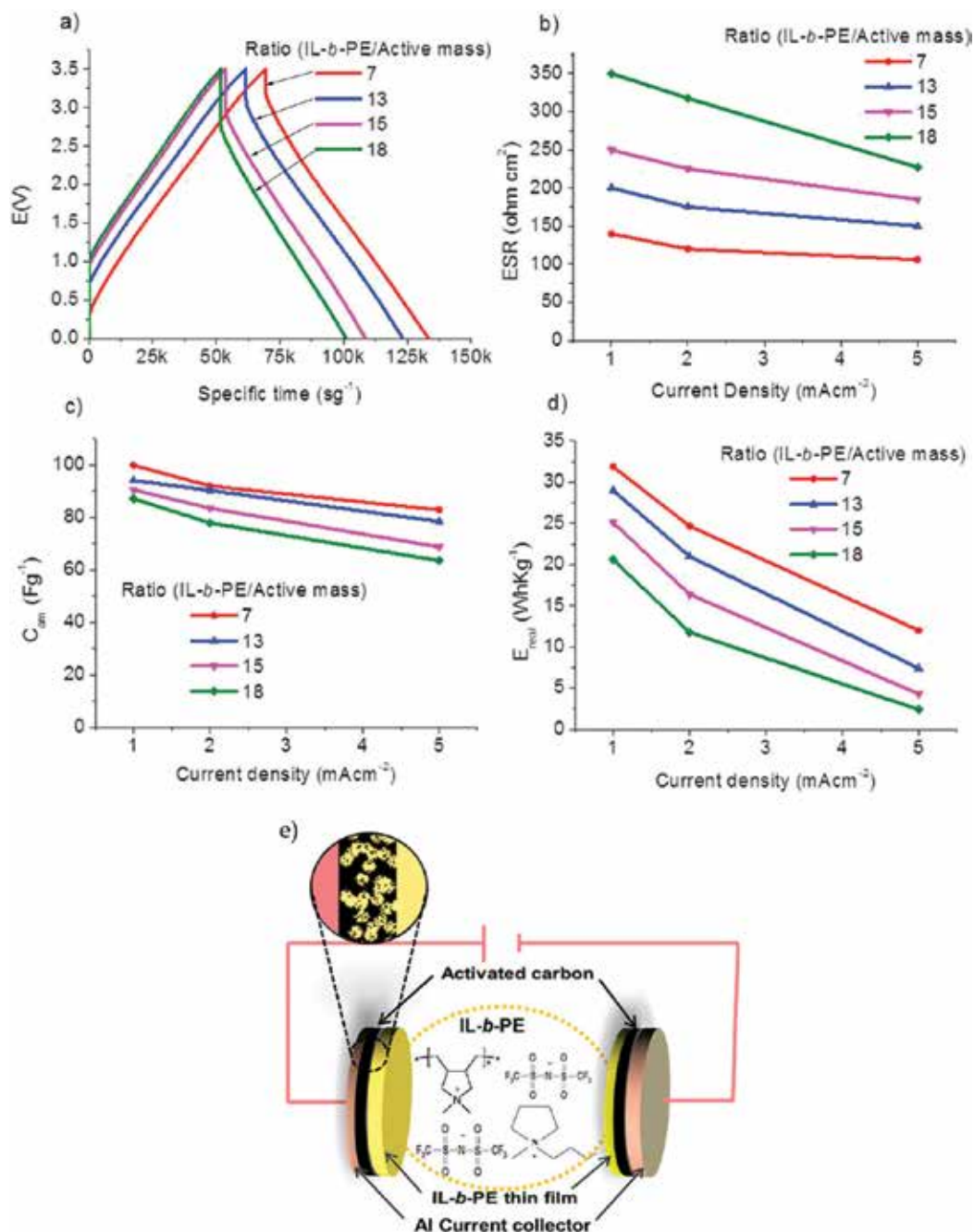


Figure 14. Charge–discharge characterization of all-solid state supercapacitors with different impregnation ratios. (a) Charge–discharge profiles from 0 to 3.5 V at 1 mAcm⁻², (b) equivalent series resistance (ESR), (c) specific capacitance (C_{am}), (d) specific real energy (E_{real}) from charge–discharge profiles at different current densities and (e) schematic representation of all-solid state supercapacitors. (IL-b-PE: Ionic liquid based polymer electrolyte).

numerous possible combinations of anions and cations. We believe this flexibility should be achieved by designing a new type of supercapacitor by thinking outside the box beyond what is available.

Author details

Jeeyoung Yoo

Address all correspondence to: [jyoo78@snu.ac.kr](mailto: jyoo78@snu.ac.kr)

Program in Nano Science and Technology, Graduate School of Convergence Science and Technology, Seoul National University, Seoul, Republic of Korea

References

- [1] Zhang F, Zhang T, Yang X, Zhang L, Leng K, Huang Y, Chen Y. A high-performance supercapacitor-battery hybrid energy storage device based on graphene-enhanced electrode materials with ultrahigh energy density. *Energy & Environmental Science*. 2013; **6**:1623-1632. DOI: 10.1039/C3EE40509E
- [2] Mahlia TMI, Saktisahdan TJ, Jannifar A, Hasan MH, Matseelar HSC. A review of available methods and development on energy storage; technology update. *Renewable and Sustainable Energy Reviews*. 2014;**33**:532-545. DOI: 10.1016/j.rser.2014.01.068
- [3] Hannan MA, Hoque MM, Mohamed A, Ayob A. Review of energy storage systems for electric vehicle applications: Issues and challenges. *Renewable and Sustainable Energy Reviews*. 2017;**69**:771-789. DOI: 10.1016/j.rser.2016.11.171
- [4] Zhang Z, Zhang X, Chen W, Rasim Y, Salman W, Pan H, Yuan Y, Wang C. A high-efficiency energy regenerative shock absorber using supercapacitors for renewable energy applications in range extended electric vehicle. *Applied Energy*. 2016;**178**:177-188. DOI: 10.1016/j.apenergy.2016.06.054
- [5] Ahn Y, Kim B, Ko J, You D, Yin Z, Kim H, Shin D, Cho S, Yoo J, Kim YS. All solid state flexible supercapacitors operating at 4 V with a cross-linked polymer-ionic liquid electrolyte. *Journal of Materials Chemistry A*. 2016;**4**:4386-4391. DOI: 10.1039/C6TA00643D
- [6] Béguin F, Presser V, Balducci A, Frackowiak E. Carbons and electrolytes for advanced supercapacitors. *Advanced Materials*. 2014;**26**:2219-2251. DOI: 10.1002/adma.201304137
- [7] Senthilkumar ST, Selvan RK, Melo JS. Redox additive/active electrolytes: A novel approach to enhance the performance of supercapacitors. *Journal of Materials Chemistry A*. 2013;**1**:12386-12394. DOI: 10.1039/C3TA11959A

- [8] Ue M. Chemical capacitors and quaternary ammonium salts. *Electrochemistry*. 2007; **8**:565-572. DOI: 10.5796/electrochemistry.75.565
- [9] Naoi K, Ishimoto S, Miyamoto J, Naoi W. Second generation 'nanohybrid supercapacitor': Evolution of capacitive energy storage devices. *Energy & Environmental Science*. 2012;**5**:9363-9373. DOI: 10.1039/C2EE21675B
- [10] Chiba K, Ueda T, Yamaguchi Y, Oki Y, Shimodate F, Naoi K. Electrolyte systems for high withstand voltage and durability I. Linear sulfones for electric double-layer capacitors. *Journal of The Electrochemical Society*. 2011;**158**(8):A872-A882. DOI: 10.1149/1.3593001
- [11] Chiba K, Ueda T, Yamaguchi Y, Oki Y, Saiki F, Naoi K. Electrolyte systems for high withstand voltage and durability. *Journal of The Electrochemical Society*. 2011;**158**(12):A1320-A1327. DOI: 10.1149/2.038112jes
- [12] Brandt A, Isken P, Lex-Balducci A, Balducci A. Adiponitrile-based electrochemical double layer capacitor. *Journal of Power Sources*. 2012;**204**:213-219. DOI: 10.1016/j.jpowsour.2011.12.025
- [13] Davy H. *Philosophical Transactions of the Royal Society*. 1807;**97**:1-56. DOI: 10.1098/rstl.1807.0001
- [14] Hall CM. Aluminium From Its Fluoride Salts By Electrolysis. US Patent 400664; 1889
- [15] Matsumoto H, Yanagida M, Tanimoto K, Nomura M, Kitagawa Y, Miyazaki Y. Highly conductive room temperature molten salts based on small trimethylalkylammonium cations and bis(trifluoromethylsulfonyl)imide. *Chemistry Letters*. 2000;**29**(8):922-923. DOI: 10.1246/cl.2000.922
- [16] Nohira T, Ishibashi T, Hagiwara R. Properties of an intermediate temperature ionic liquid NaTFSA-CsTFSA and charge-discharge properties of NaCrO₂ positive electrode at 423 K for a sodium secondary battery. *Journal of Power Sources*. 2012;**205**:506-509. DOI: 10.1016/j.jpowsour.2011.11.086
- [17] Forsyth M, Howlett PC, Tan SK, MacFarlane DR, Birbilis N. An ionic liquid surface treatment for corrosion protection of magnesium alloy AZ31. *Electrochemical and Solid-State Letters*. 2006;**9**(11):B52-B55. DOI: 10.1149/1.2344826
- [18] Khoo T, Howlett PC, Tsagouria M, MacFarlane DR, Forsyth M. The potential for ionic liquid electrolytes to stabilise the magnesium interface for magnesium/air batteries. *Electrochimica Acta*. 2011;**58**:583-588. DOI: 10.1016/j.electacta.2011.10.006
- [19] Noda A, Susan MABH, Kudo K, Mitsushim S, Hayamizu K, Watanabe M. Brønsted acid-base ionic liquids as proton-conducting nonaqueous electrolytes. *The Journal of Physical Chemistry B*. 2003;**107**:4024-4033. DOI: 10.1021/jp022347p
- [20] Bai Y, Cao Y, Zhang J, Wang M, Li R, Wang P, Zakeeruddin SM, Grätzel M. High-performance dye-sensitized solar cells based on solvent-free electrolytes produced from eutectic melts. *Nature Materials*. 2008;**7**:626-630. DOI: 10.1038/nmat2224

- [21] Armand M, Endres F, MacFarlan DR, Ohno H, Scrosati B. Ionic-liquid materials for the electrochemical challenges of the future. *Nature Materials*. 2009;**8**:621-629. DOI: 10.1038/nmat2448
- [22] Brandt A, Pohlmann S, Varzi A, Balducci A, Passerini S. Ionic liquids in supercapacitors. *MRS Bulletin*. 2013;**38**(7):554-559. DOI: 10.1557/mrs.2013.151
- [23] Freemantle M. Designer solvents-ionic liquids may boost clean technology development. *Chemical and Engineering News*. 1998;**76**(13):32-37. DOI: 10.1021/cen-v076n013.p032
- [24] Ue M, Ida K, Mori S. Electrochemical properties of organic liquid electrolytes based on quaternary onium salts for electrical double-layer capacitors. *Journal of The Electrochemical Society*. 1994;**141**(11):2989-2996. DOI: 10.1149/1.2059270
- [25] Yoo J, Kim K, Kim S, Yeu T. The preparation of ionic liquids based on alkylimidazolium salts for the electrolyte of EDLC. 210th Meeting Abstract of The Electrochemical Society. 2006;**3**:135
- [26] Chmiola J, Yushin G, Gogotsi Y, Portet C, Simon P, Taberna PL. Anomalous increase in carbon capacitance at pore sizes less than 1 nanometre. *Science*. 2006;**313**(5794):1760-1763. DOI: 10.1126/science.1132195
- [27] Galinski M, Lewandowski A, Stepniak I. Ionic liquids as electrolytes. *Electrochimica Acta*. 2006;**51**:5567-5580. DOI: 10.1016/j.electacta.2006.03.016
- [28] Lewandowski A, Galinski M. Practical and theoretical limits for electrochemical double-layer capacitors. *Journal of Power Sources*. 2007;**137**:822-828. DOI: 10.1016/j.jpowsour.2007.05.062
- [29] Fuller J, Carlin RT, Osteryoung RA. The room temperature ionic liquid 1-Ethyl-3-methylimidazolium tetrafluoroborate: Electrochemical couples and physical properties. *Journal of The Electrochemical Society*. 1997;**144**(11). DOI: 10.1149/1.1838106
- [30] Burke. Ultracapacitors: Why, how, and where is the technology. *Journal of Power Sources*. 2000;**91**(1):37-50. DOI: 10.1016/S0378-7753(00)00485-7
- [31] Lewandowski A, Olejniczak A, Galinski M, Stepniak I. Performance of carbon-carbon supercapacitors based on organic, aqueous and ionic liquid electrolytes. *Journal of Power Sources*. 2010;**195**:5814-5819. DOI: 10.1016/j.jpowsour.2010.03.082
- [32] Chen Y, Zhang X, Zhang D, Yu P, Ma Y. High performance supercapacitors based on reduced graphene oxide in aqueous and ionic liquid electrolytes. *Carbon*. 2011;**49**(2):573-580. DOI: 10.1016/j.carbon.2010.09.060
- [33] Sato T, Masuda G, Takagi K. Electrochemical properties of novel ionic liquids for electric double layer capacitor applications. *Electrochimica Acta*. 2004;**49**(21):3603-3611. DOI: 10.1016/j.electacta.2004.03.030
- [34] Zhang LL, Zhao XS. Carbon-based materials as supercapacitor electrodes. *Chemical Society Reviews*. 2009;**38**:2520-2531. DOI: 10.1039/B813846J

- [35] Lei Z, Liu Z, Wang H, Sun X, Lu L, Zhao XS. A high-energy-density supercapacitor with graphene-CMK-5 as the electrode and ionic liquid as the electrolyte. *Journal of Materials Chemistry A*. 2013;**1**:2313-2321. DOI: 10.1039/C2TA01040B
- [36] Eftekhari A, Garcia H. The necessity of structural irregularities for the chemical applications of graphene. *Materials Today Chemistry*. 2017;**4**:1-16. DOI: 10.1016/j.mtchem.2017.02.003
- [37] Fedorov MV, Kornyshev AA. Ionic liquids at electrified interfaces. *Chemical Reviews*. 2014;**114**(5):2978-3036. DOI: 10.1021/cr400374x
- [38] Shen G, Sun X, Zhang H, Liu Y, Zhang J, Meka A, Zhou L, Yu C. Nitrogen-doped ordered mesoporous carbon single crystals: Aqueous organic-organic self-assembly and superior supercapacitor performance. *Journal of Materials Chemistry A*. 2015;**3**:24041-24048. DOI: 10.1039/C5TA06129F
- [39] Rennie AJR, Sanchez-Ramirez N, Torresi RM, Hall PJ. Ether-bond-containing ionic liquids as supercapacitor electrolytes. *The Journal of Physical Chemistry Letters*. 2013;**4**:2970-2974. DOI: 10.1021/jz4016553
- [40] Eftekhari A. Supercapacitors utilising ionic liquids. *Energy Storage Materials*. 2017;**9**:47-69. DOI: 10.1016/j.ensm.2017.06.009
- [41] Pinkert K, Oschatz M, Borchardt L, Klose M, Zier M, Nickel W, Giebeler L, Oswald S, Kaskel S, Eckert J. Role of surface functional groups in ordered mesoporous carbide-derived carbon/ionic liquid electrolyte double-layer capacitor interfaces. *ACS Applied Materials & Interfaces*. 2016;**6**(4):2922-2928. DOI: 10.1021/am4055029
- [42] Jaramillo MM, Mendoza A, Vaquero S, Anderson M, Palma J, Marcilla R. Role of textural properties and surface functionalities of selected carbons on the electrochemical behaviour of ionic liquid based-supercapacitors. *RSC Advances*. 2012;**2**:8439-8446. DOI: 10.1039/C2RA21035E
- [43] Aradilla D, Gentile P, Bidan G, Ruiz V, Gómez-Romero P, Schubert TJS, Sahin H, Frackowiak E, Sadki S. High performance of symmetric micro-supercapacitors based on silicon nanowires using N-methyl-N-propylpyrrolidinium bis(trifluoromethylsulfonyl) imide as electrolyte. *Nano Energy*. 2014;**9**:273-281. DOI: 10.1016/j.nanoen.2014.07.001
- [44] Alper JP, Wang S, Rossi F, Salviati G, Yiu N, Carraro C, Maboudian R. Selective ultrathin carbon sheath on porous silicon nanowires: Materials for extremely high energy density planar micro-supercapacitors. *Nano Letters*. 2014;**14**(4):1843-1847. DOI: 10.1021/nl404609a
- [45] Romann T, Oll O, Pikma P, Tamme H, Lust E. Surface chemistry of carbon electrodes in 1-ethyl-3-methylimidazolium tetrafluoroborate ionic liquid – An in situ infrared study. *Electrochimica Acta*. 2014;**125**(10):183-190. DOI: 10.1016/j.electacta.2014.01.077
- [46] Kruusma J, Tõnisoo A, Pärna R, Nõmmiste E, Lust E. In situ XPS studies of electrochemically positively polarized molybdenum carbide derived carbon double layer capacitor electrode. *Journal of The Electrochemical Society*. 2014;**161**(9):A1266-A1277. DOI: 10.1149/2.0641409jes

- [47] Kurig H, Vestli M, Tönurist K, Jänes A, Lust E. Influence of room temperature ionic liquid anion chemical composition and electrical charge delocalization on the supercapacitor properties. *Journal of The Electrochemical Society*. 2012;**159**(7):A944-A951. DOI: 10.1149/2.022207jes
- [48] Shi M, Kou S, YAn X. Engineering the electrochemical capacitive properties of Graphene sheets in ionic-liquid electrolytes by CorrectSelection of anions. *ChemSusChem*. 2014;**7**:3053-3062. DOI: 10.1002/cssc.201402275
- [49] Bettini LG, Galluzzi M, Podestà A, Milani P, Piseri P. Planar thin film supercapacitor based on cluster-assembled nanostructured carbon and ionic liquid electrolyte. *Carbon*. 2013;**59**:212-220. DOI: 10.1016/j.carbon.2013.03.011
- [50] Borges RS, Ribeiro H, Lavall RL, Silva GG. Temperature stable supercapacitors based on ionic liquid and mixed functionalized carbon nanomaterials. *Journal of Solid State Electrochemistry*. 2012;**16**(11):3573-3580. DOI: 10.1007/s10008-012-1785-5
- [51] Largeot C, Taberna PL, Gogotsi Y, Simon P. Microporous carbon-based electrical double layer capacitor operating at high temperature in ionic liquid electrolyte. *Journal of The Electrochemical Society*. 2011;**14**(12):A174-A176. DOI: 10.1149/2.013112esl
- [52] Balducci A, Henderson WA, Mastragostino M, Passerini S, Simon P, Soavi F. Cycling stability of a hybrid activated carbon//poly(3-methylthiophene) supercapacitor with N-butyl-N-methylpyrrolidinium bis(trifluoromethanesulfonyl)imide ionic liquid as electrolyte. *Electrochimica Acta*. 2005;**50**(11):2233-2237. DOI: 10.1016/j.electacta.2004.10.006
- [53] Balducci A, Soavi F, Mastragostino M. The use of ionic liquids as solvent-free green electrolytes for hybrid supercapacitors. *Applied Physics A*. 2006;**82**(4):627-632. DOI: 10.1007/s00339-005-3402-2
- [54] Balducci A, Dugas R, Taberna PL, Simon P, Plée D, Mastragostino M, Passerini S. High temperature carbon-carbon supercapacitor using ionic liquid as electrolyte. *Journal of Power Sources*. 2004;**6**(6):566-570. DOI: 10.1016/j.elecom.2004.04.005
- [55] Iamprasertkun P, Krittayavathananon A, Sawangphruk M. N-doped reduced graphene oxide aerogel coated on carboxylmodified. *Carbon*. 2016;**102**:455-461. DOI: 10.1016/j.carbon.2015.12.092
- [56] Anouti M, Timperman L, Mostafa el hilali, Boisset A, Galiano H. Sulfonium bis(trifluoro-sulfonimide) plastic crystal ionic liquid as an electrolyte at elevated temperature for high-energy Supercapacitors. *The Journal of Physical Chemistry C* 2012;**116**(17):9412-9418. DOI: 10.1021/jp3012987
- [57] Kunze M, Jeong S, Paillard E, Winter M, Passerini S. Melting behavior of pyrrolidinium-based ionic liquids and their binary mixtures. *The Journal of Physical Chemistry C*. 2010;**114**(28):12364-12369. DOI: 10.1021/jp103746k
- [58] Kunze M, Montanino M, Appetecchi GB, Jeong S, Schönhoff M, Winter M, Passerini S. Melting behavior and ionic conductivity in hydrophobic ionic liquids. *The Journal of Physical Chemistry. A*. 2010;**114**(4):1776-1782. DOI: 10.1021/jp9099418

- [59] Lin R, Taberna P, Fantini S, Presser V, Pérez CR, Malbosc F, Rupesinghe NL, Teo KBK, Gogotsi Y, Simon P. Capacitive energy storage from -50 to 100°C using an ionic liquid electrolyte. *Journal of Physical Chemistry Letters*. 2011;**2**(19):2396-2401. DOI: 10.1021/jz201065t
- [60] Lian C, Liu K, Aken KLV, Gogotsi Y, Wesolowski DJ, Liu HL, Jiang DE, Wu JZ. Enhancing the capacitive performance of electric double-layer capacitors with ionic liquid mixtures. *ACS Energy Letter*. 2016;**1**(1):21-26. DOI: 10.1021/acsenerylett.6b00010
- [61] Zhi M, Xiang C, Li J, Li M, Wu N. Nanostructured carbon-metal oxide composite electrodes for supercapacitors: A review. *Nanoscale*. 2013;**5**:72-88. DOI: 10.1039/C2NR32040A
- [62] Wang G, Zhang L, Zhang J. A review of electrode materials for electrochemical supercapacitors. *Chemical Society Reviews*. 2012;**41**:797-828. DOI: 10.1039/C1CS15060J
- [63] Snook GA, Kao P, Best AS. Conducting-polymer-based supercapacitor devices and electrodes. *Journal of Power Sources*. 2011;**196**(1):1-12. DOI: 10.1016/j.jpowsour.2010.06.084
- [64] Rochefort D, Pont A. Pseudocapacitive behaviour of RuO₂ in a proton exchange ionic liquid. *Electrochemistry Communications*. 2006;**8**(9):1539-1543. DOI: 10.1016/j.elecom.2006.06.032
- [65] Mayrand-Provencher L, Lin S, Lazzerini D, Rochefort D. Pyridinium-based protic ionic liquids as electrolytes for RuO₂ electrochemical capacitors. *Journal of Power Sources*. 2010;**195**(15):5114-5121. DOI: 10.1016/j.jpowsour.2010.02.073
- [66] Chang J, Lee M, Tsai W, Deng M, Sun I. X-ray photoelectron spectroscopy and in situ X-ray absorption spectroscopy studies on reversible insertion/desertion of dicyanamide anions into/from manganese oxide in ionic liquid. *Chemistry of Materials*. 2009;**21**(13):2688-2695. DOI: 10.1021/cm9000569
- [67] Lota G, Frackowiak E. Striking capacitance of carbon/iodide interface. *Electrochemistry Communications*. 2009;**11**(1):87-90. DOI: 10.1016/j.elecom.2008.10.026
- [68] Suárez-Guevara J, Ruiz V, Gomez-Romero P. Hybrid energy storage: High voltage aqueous supercapacitors based on activated carbon-phosphotungstate hybrid materials. *Journal of Materials Chemistry A*. 2014;**2**:1014-1021. DOI: 10.1039/C3TA14455K
- [69] Frackowiak E, Fic K, Meller M, Lota G. Electrochemistry serving people and nature: High-energy ecocapacitors based on redox-active electrolytes. *ChemSusChem*. 2012;**5**(7):1181-1185. DOI: 10.1002/cssc.201200227
- [70] Roldán S, Granda M, Menéndez R, Santamaría R, Blanco C. Mechanisms of energy storage in carbon-based supercapacitors modified with a quinoid redox-active electrolyte. *Journal of Physical Chemistry C*. 2011;**115**(35):17606-17611. DOI: 10.1021/jp205100v
- [71] Mai L, Minhas-Khan A, Tian X, Hercule KM, Zhao Y, Lin X, Xu X. Synergistic interaction between redox-active electrolyte and binder-free functionalized carbon for ultrahigh supercapacitor performance. *Nature Communications*. 2013;**4**(1-7):2923. DOI: 10.1038/ncomms3923

- [72] Taniki R, Matsumoto K, Nohira T, Hagiwara R. Evaluation of double-layer and redox capacitances of activated carbon electrodes in n-ethyl-n-methylpyrrolidinium fluorohydrogenate ionic liquid. *Journal of The Electrochemical Society*. 2013;**160**(4):A734-A738. DOI: 10.1149/2.022306jes
- [73] Tooming T, Thomberg T, Siinor L, Tõnurist K, Jänes A, Lust EA. Type high capacitance supercapacitor based on mixed room temperature ionic liquids containing specifically adsorbed iodide anions. *Journal of The Electrochemical Society*. 2014;**161**(3):A222-A227. DOI: 10.1149/2.014403jes
- [74] Fuller J, Breda AC, Carlin RT. Ionic liquid-polymer gel electrolytes. *Journal of The Electrochemical Society*. 1997;**144**(4):L67-L70. DOI: 10.1149/1.1837555
- [75] Pandey GP, Liu T, Hancoc C, Li Y, Sun XS, Li X. Thermostable gel polymer electrolyte based on succinonitrile and ionic liquid for high-performance solid-state supercapacitors. *Journal of Power Sources*. 2016;**328**:510-519. DOI: 10.1016/j.jpowsour.2016.08.032
- [76] Tiruye GA, Muñoz-Torrero D, Palma J, Anderson M, Marcilla R. Performance of solid state supercapacitors based on polymer electrolytes containing different ionic liquids. *Journal of Power Sources*. 2016;**15**:560-568. DOI: 10.1016/j.jpowsour.2016.03.044
- [77] Pandey GP, Hashmi SA. Ionic liquid 1-ethyl-3-methylimidazolium tetracyanoborate-based gel polymer electrolyte for electrochemical capacitors. *Journal of Materials Chemistry A*. 2013;**1**:3372-3378. DOI: 10.1039/C2TA01347A
- [78] Lu W, Henry K, Turchi C, Pellegrino J. Incorporating ionic liquid electrolytes into polymer gels for solid-state ultracapacitors. *Journal of The Electrochemical Society*. 2008;**155**(5):A361-A367. DOI: 10.1149/1.2869202
- [79] Tamilarasan P, Ramaprabhu S. Stretchable supercapacitors based on highly stretchable ionic liquid incorporated polymer electrolyte. *Materials Chemistry and Physics*. 2014;**148**:48-56. DOI: 10.1016/j.matchemphys.2014.07.010
- [80] Lewandowski A. Electrochemical capacitors with polymer electrolytes based on ionic liquids. *Solid State Ionics*. 2003;**161**:243-249. DOI: 10.1016/S0167-2738(03)00275-3
- [81] Yang L, Hu J, Lei G, Liu H. Ionic liquid-gelled polyvinylidene fluoride/polyvinyl acetate polymer electrolyte for solid supercapacitor. *Chemical Engineering Journal*. 2014;**258**:320-326. DOI: 10.1016/j.cej.2014.05.149
- [82] Lewandowski A, Świdarska A. Solvent-free double-layer capacitors with polymer electrolytes based on 1-ethyl-3-methylimidazolium triflate ionic liquid. *Applied Physics A*. 2005;**82**:579-584. DOI: 10.1007/s00339-005-3396-9
- [83] Yamagata M, Soeda K, Ikebe S, Yamazaki S, Ishikawa M. Chitosan-based gel electrolyte containing an ionic liquid for high-performance nonaqueous supercapacitors. *Electrochimica Acta*. 2013;**100**:275-280. DOI: 10.1016/j.electacta.2012.05.073
- [84] Choi K, Yoo J, Lee CK, Lee S. All-inkjet-printed, solid-state flexible supercapacitors on paper. *Energy & Environmental Science*. 2016;**9**:2812-2821. DOI: 10.1039/C6EE00966

- [85] Döbbelin M, Azcune I, Bedu M, Ruiz de Luzuriaga A, Genua A, Jovanovski V, Cabañero G, Odriozola I. Synthesis of pyrrolidinium-based poly(ionic liquid) electrolytes with poly(ethylene glycol) side chains. *Chemistry of Materials*. 2012;**24**(9). DOI: 10.1021/cm203790z
- [86] Qian W, Texter J, Yan F. *Frontiers in poly(ionic liquid)s: Syntheses and applications*. *Chemical Society Reviews*. 2017;**46**:1124-1159. DOI: 10.1039/C6CS00620E
- [87] Tang J, Tang H, Sun W, Radosz M, Shen Y. Poly(ionic liquid)s as new materials for CO₂ absorption. *Journal of Polymer Science Part A: Polymer Chemistry*. 2005;**45**(22):5477-5489. DOI: 10.1002/pola.21031
- [88] Hu H, Yua W, Lu L, Zhao H, Jia Z, Baker GL. Low glass transition temperature polymer electrolyte prepared from ionic liquid grafted polyethylene oxide. *Journal of Polymer Science Part A: Polymer Chemistry*. 2014;**52**(15):2104-2110. DOI: 10.1002/pola.27217
- [89] Marcilla R, Blazquez JA, Fernandez R, Grande H, Pomposo JA, Mecerreyes D. Synthesis of novel polycations using the chemistry of ionic liquids. *Macromolecular Chemistry and Physics*. 2005;**206**(2):299-304. DOI: 10.1002/macp.200400411
- [90] Appetecchi GB, Kim G, Montanino M, Carewska M, Marcilla R, Mecerreyes D, De Meazza I. Ternary polymer electrolytes containing pyrrolidinium-based polymeric ionic liquids for lithium batteries. *Journal of Power Sources*. 2010;**195**(11):3668-3675. DOI: 10.1016/j.jpowsour.2009.11.146
- [91] Tiruye GA, Muñoz-Torrero D, Palma J, Anderson M, Marcilla R. All-solid state supercapacitors operating at 3.5 V by using ionic liquid based polymer electrolytes. *Journal of Power Sources*. 2015;**279**:472-480. DOI: 10.1016/j.jpowsour.2015.01.039
- [92] Tiruye GA, Munoz-Torrero D, Palma J, Anderson M, Marcilla R. Performance of solid state supercapacitors based on polymer. *Journal of Power Sources*. 2016;**326**:560-568. DOI: 10.1016/j.jpowsour.2016.03.044

Electrochemical Capacitor Performance: Influence of Aqueous Electrolytes

Rajendran Ramachandran and Fei Wang

Additional information is available at the end of the chapter

<http://dx.doi.org/10.5772/intechopen.70694>

Abstract

Due to low energy characteristics such as energy density and cyclic life, it is mandatory to enhance the energy characteristics of the supercapacitors (ESs). Electrolytes have been recognized as the most prominent ingredients in electrochemical supercapacitor performance. Most commercially available ESs use organic electrolytes and have some advantage like wide operating voltage. However, compared with aqueous alternatives, organic electrolytes are expensive, flammable, and, in some cases, toxic. It is reliable to assert that even though aqueous electrolytes examined by a cramped working voltage, the ions present in them are yet capable of incredibly faster carrier rates than organic electrolytes and can achieve better performance of ESs. Thus, efforts turned toward enlarging the working voltage window of aqueous electrolytes to increase overall operating potential and energy density of supercapacitor devices. This book chapter comprises the latest accomplishments in this area and provides an insight into the aqueous electrolyte advancement.

Keywords: supercapacitors, energy density, aqueous electrolyte, operating voltage, electrolyte

1. Introduction

The dramatic global warming and the accessibility to fossil fuels in the earth require society to shift in the direction of renewable and sustainable resources. Due to this, the growth and ramp-up of sustainable, clean energy sources, as well as their associated technologies, are taken into account worldwide as a critical problem. The majority of the renewable and clean energy sources depend on the countrywide weather conditions. Among different energy storage systems, the electrochemical energy storage (EES) systems including batteries, fuel cells, as well as electrochemical capacitors or supercapacitors (ESs) are most efficient and frequently used in several applications [1]. The most common characteristic of these three

devices is that the energy-producing processes perform at electrode/electrolyte interfaces. In both academia and industry, supercapacitors have drawn much importance due to benefits of high power density and long cyclic life compared with batteries and fuel cells [2]. By their charge storage process, ES is divided into three categories: (1) electric double layer capacitors (EDLC), (2) pseudocapacitors, and (3) hybrid capacitors [3]. Due to the technical maturity of EDLCs, almost all of the commercially available supercapacitors are made up by using EDLC electrode materials such as activated carbon. The low energy density ($\sim 10 \text{ Wh kg}^{-1}$ for commercial supercapacitors) is truly the most significant challenge for supercapacitors in comparison to rechargeable batteries and fuel cells [4]. For that reason, enormous research attempts were carried out aiming to enhance the energy density of supercapacitors [5]. The important characteristic to get extraordinary energy density of supercapacitors is shown in **Figure 1**. As seen from the figure, the energy density of supercapacitors is directly proportional to the capacitance and square of the working voltage. Therefore, enhancing the capacitance and improving the working potential are considered as promising approaches to further improve high energy density supercapacitors. The high energy density can be attained by choosing appropriate electrode material with a high specific capacitance and electrolyte with a large operating voltage. Considering that the energy density is directly proportional to the square of the voltage, increasing the working potential window could be a more efficient way to improve the energy density rather than to improve the specific capacitance. Therefore, developing a new electrolyte with a large potential window is the top priority effort in comparison to seeking new electrode materials.

1.1. Effect of the electrolyte on supercapacitor performance

It is well recognized that the working potential of the supercapacitors is highly relying on the electrochemical stability of the electrolytes. For example, organic electrolytes and ionic liquid (IL)-derived supercapacitors can easily be handled at a large potential window of 2.5–2.7 and 3.5–4.0 V, respectively [6]. However, the electrodes are steady in aqueous electrolytes within the potential choice of 1.0–1.3 V due to H_2/O_2 evaluation reactions [7]. Since the interaction involving the electrode and electrolyte acts an essential function in the overall supercapacitor



Figure 1. Important characteristic of high energy density supercapacitors.

performance, aside from the operating voltage, the electrolytes have substantially influenced on the other parameters such as power density, cycling stability, operating temperature, equivalent series resistance, life time, and self-discharge rate of the capacitors [8]. The electrolyte ionic conductivity performs a serious role in the internal resistance of supercapacitors. It is highly crucial that the electrolyte ion size should be equal or less than that of the pore size of electrode material to possess a high capacitance and a high power density [9]. For a few cases, the freezing point and viscosity of electrolytes also affect the thermal stability of supercapacitor performance, and hence the working voltage range would be shifted [10, 11].

An ideal electrolyte of supercapacitor needs to have some fundamental requirements: (1) broad potential window, (2) a wide range of working temperature, (3) high ionic conductivity, (4) low viscosity, (5) high electrochemical stability, (6) environmentally friendly, (7) low cost, and (8) low flammability. Each electrolyte has its merits and drawbacks, and it is feasible to meet all the above specifications with one electrolyte. Nonstop and tremendous research efforts have been made in the present and will also keep going in the future for the electrolyte development investigation.

2. Types of electrolyte

Following the nature of electrolyte like the ion type, ion size, ion concentration, and the interplay among the ion and solvent, various electrolytes have been developed and examined currently. The electrolyte can be divided into three groups such as liquid, solid or semisolid, and redox-additive as shown in **Figure 2**. The liquid electrolyte can be further classified into aqueous electrolyte, nonaqueous electrolyte, and organic electrolyte [12].

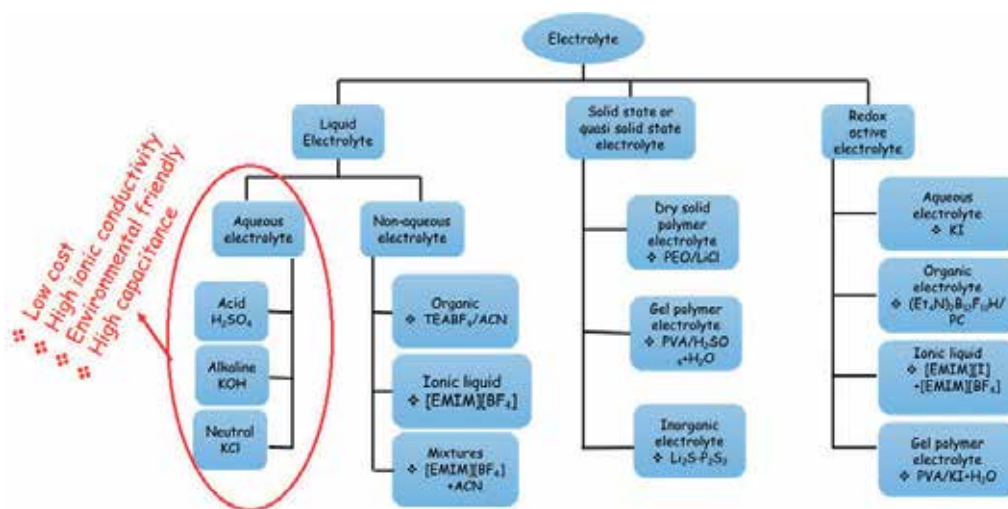


Figure 2. Classification of supercapacitor electrolytes.

As mentioned previously, no single electrolyte can meet all the requirements. For example, both high capacitance and ionic conductivity can be achieved by aqueous electrolytes, but the narrow decomposition voltage made the lower operating voltage of aqueous electrolytes. Though organic and ionic liquid electrolytes provide a wide operating voltage, they normally suffered from the low conductivity (large internal resistance), high cost, and high flammability which cause continual trouble during application in supercapacitor device. In this regard, extensive efforts are committed to the successful development of the overall performance of electrolytes. Some strategies have already been strived to enhance the electrolyte performance, including “(1) developing an entirely new electrolyte as well as improving its efficiency concerning a wide range of functioning voltage, high ionic conductivity, large working temperature range, and so on [13]; (2) investigation of the effect of electrolytes on capacitance, energy and power densities, thermal stability, and self-discharge rate of supercapacitors [14]; and (3) initiate and becoming familiar with a fundamental concept of the electrolyte on supercapacitor performance over sophisticated characterization, modeling, and simulation utilities [15].”

3. Aqueous electrolytes

Usually, regarding the energy density study, the aqueous electrolytes really are a poor selection for technical supercapacitor products because of their small voltage window. This could be the reason for why nearly all the commercial supercapacitors use organic electrolyte rather than aqueous electrolytes. Though aqueous electrolytes possess an insufficient cell voltage, they were considerably employed in the literature from 1997 onward because of that aqueous electrolytes seem to be cheaper and can be quite easily taken care of in the laboratory without having a special circumstance. However, ionic liquid and organic electrolytes generally call for complex purification treatments under a rigidly controlled environment to stay clear of moisture. All of these features of aqueous electrolytes tremendously explain the design and assembling of supercapacitors. Generally, aqueous electrolytes exhibit extremely high conductivity (**Table 1**) which is at least one magnitude larger than that of organic or IL electrolytes.

Electrolyte	Conductivity (mS cm ⁻¹)	Potential window (V)
Aqueous KOH	540	0–1
Aqueous KCl	210	0–1
Aqueous H ₂ SO ₄	750	0–1
Aqueous K ₂ SO ₄	88.6	0–1
Aqueous Na ₂ SO ₄	91.1	0–1
Organic TEABF ₄ /PC	14.5	2.5–3
Organic TEABF ₄ /ACN	59.9	2.5–3
IL, [Et ₂ MEIM] ⁺ [BF ₄] ⁻	8	4

Table 1. Electrolytic conductivity and operating voltage of various electrolytes at room temperature.

The high conductivity of the aqueous electrolyte is propitious for reducing equivalent series resistance (ESR) which leads to significantly high power density supercapacitors.

To evaluate the overall performance of aqueous electrolytes, some typical criteria should be taken into consideration such as the dimensions of hydrated and bare ions (**Table 2**), the flow of ions which alters the ionic conductivity, as well as the specific capacitance.

The aqueous electrolytes can be categorized into three groups such as alkaline, acid, and neutral solutions. The most commonly used aqueous electrolytes are KOH, H₂SO₄, and Na₂SO₄, respectively.

3.1. Acid electrolytes

Sulfuric acid (H₂SO₄) is the most frequently used aqueous acid electrolyte in supercapacitor simply because of its extremely high conductivity (~0.8 cm⁻¹ at 25°C for 1 M H₂SO₄) [16]. Since the electrolyte ionic conductivity is dependent on the concentrations, optimum molar concentrations have already been investigated to attain the highest possible ionic conductivities of a given electrolyte at particular temperature. So far, the electrolyte ionic conductivity can be quickly dropped when the concentration becomes extremely low or excessively high. So, the greater number of research studies uses 1 M H₂SO₄ solution, especially for carbon-based supercapacitors.

Type of ion	Size of bare ion (Å)	Size of hydrated ions (Å)	Gibbs energy (kcal mol ⁻¹)	Ion conductivity (S cm ² mol ⁻¹)
H ⁺	1.15	2.80		350.1
Li ⁺	0.60	3.82	138.4	38.69
Na ⁺	0.95	3.58	162.3	50.11
K ⁺	1.33	3.31	179.9	73.5
NH ₄ ⁺	1.48	3.31	–	73.7
Mg ₂ ⁺	0.72	4.28	–	106.12
Ca ₂ ⁺	1.00	4.12	–	119
Ba ₂ ⁺	1.35	4.04	–	127.8
Cl ⁻	1.81	3.32	–	76.31
NO ₃ ⁻	2.64	3.35	–	71.42
SO ₄ ²⁻	2.90	3.79	–	160.0
OH ⁻	1.76	3.00	–	198
ClO ₄ ⁻	2.92	3.38	–	67.3
PO ₄ ³⁻	2.23	3.39	–	207
CO ₃ ²⁻	2.66	3.94	–	138.6

Table 2. Size of electrolytic bare and hydrated ions and their conductivity [10].

3.1.1. H_2SO_4 electrolyte-based EDLC and pseudocapacitors

Recently, several researchers discovered that for the carbon-based capacitors (EDLCs), specific capacitance obtained in the H_2SO_4 electrolyte is much higher than the specific capacitance in a neutral electrolyte. Moreover, due to the high value of H_2SO_4 ionic conductivity, the ESR value of supercapacitors is much lower in comparison to the neutral electrolyte. Torchala et al. have examined the EDLC behavior of activated carbon in the H_2SO_4 electrolyte, and they ascertained that the specific capacitance could be raised with increased electrolyte conductivity [17]. In past several years, many literatures have reported that the carbon-based materials had provided the specific capacitance within the range between 100 and 300 F g⁻¹. Certain reported values are usually higher compared to those acquired in the commercial electrolytes. The changes in specific capacitance might replicate the diverse interplays among the electrode materials and the electrolyte ions caused by various electrolytes. As pointed out above, because of the small potential window of aqueous electrolyte, the energy density of EDLCs turns considerably lower. Thus, enormous attempts have been performed to raise the ES energy density by investigating other methods which can include utilizing pseudocapacitive behavior in electrodes.

In addition to the EDLC capacitance, it was discovered that the H_2SO_4 electrolyte also induced pseudocapacitance contribution due to the active redox reactions of carbon material surface functionalities. Introducing some heteroatoms that include nitrogen, oxygen, and boron to the carbon materials surface could enhance the pseudocapacitance contributions [18]. The doping of heteroatoms not only increases the specific capacitance but also improves the cycle life of the electrode materials even at a larger potential in the aqueous electrolytes. The pseudocapacitance materials including metal oxides, metal sulfides, and conducting polymers have much higher theoretical capacitance value compared to carbon-based electrodes in aqueous electrolyte [19]. Since the metal oxides and sulfide materials are highly sensitive to nature and pH of the electrolyte, these electrodes typically are not steady in the acidic electrolyte which restricts use in commercial products. As well known, ruthenium oxide (RuO_2) is one of the potential electrodes that has been extensively examined for its pseudocapacitance in the H_2SO_4 electrolyte. Amorphous RuO_2 can deliver a very high value of ~ 1000 F g⁻¹ in acidic electrolyte resulting from easy insertion of the proton in the amorphous structure. Sadly, the expensive and limited Ru sources have restricted their practical usage.

3.1.2. H_2SO_4 electrolyte-based hybrid supercapacitors

To increase the energy densities of supercapacitors in aqueous electrolytes, designing a hybrid supercapacitor is the most potentially promising way. As a result of the gas evolution reactions, the maximum cell voltage is limited for a symmetric supercapacitor by using the same electrode materials in aqueous electrolyte. The combinations of two alternative electrodes (asymmetric supercapacitors) can be performed in different working potentials, leading to a larger functioning potential window in aqueous electrolyte. Currently, several types of asymmetric-based supercapacitors such as carbon// PbO , carbon// RuO_2 , and carbon with various mass and properties in cathode and anode electrodes have already been examined in strong acidic electrolytes. An energy density of 25–30 Whkg⁻¹ has been delivered by carbon// PbO_2 asymmetric supercapacitor, which was considerably higher than that of the symmetric

carbon-based EDLCs ($3\text{--}6 \text{ Whkg}^{-1}$) in the acidic electrolyte. Similar to metal oxide, conducting polymer and carbon-based asymmetric supercapacitor have delivered enough energy density for commercial applications. It was found that the energy density could reach up to 11.46 Whkg^{-1} when polyaniline (PANI) was used as a positive electrode and carbon as a negative electrode at a wider potential range (-1 V to $+1 \text{ V}$) [20]. Though the energy density has reached higher than symmetric carbon capacitors, PANI is limited in the commercial product due to its poor stability. The stability can be improved through the use of liquid H_2SO_4 electrolyte for conducting polymer-based electrodes. When compared to solid-state polymer aqueous electrolytes, the thermal stability of liquid H_2SO_4 is high. Thus, the stability and the energy density of supercapacitors could possibly be improved in liquid-based electrolytes. For example, $0.5 \text{ M H}_2\text{SO}_4$ liquid electrolyte has delivered the energy density about $\sim 20 \text{ Wh kg}^{-1}$ for $\text{RuO}_2/\text{carbon}$ nano-onion symmetric ESs, which is twofold higher than that of polymer gel acidic electrolyte (Figure 3) [21].

3.2. Alkaline electrolytes

Since acidic electrolytes are commonly not suitable for some cost-effective metal materials and metal oxides (Ni, Co, Eu, etc.), alkaline electrolytes have been utilized extensively in the literatures. Potassium hydroxide (KOH) is most commonly used alkaline aqueous electrolyte, simply because of its significantly better ionic conductivity (0.6 S cm^{-1}).

3.2.1. Alkaline electrolyte-based EDLC and pseudocapacitors

The energy density of EDLC-based supercapacitors in aqueous KOH is similar to that reported with H_2SO_4 electrolyte. So, massive efforts have been given to raise the EDLC material

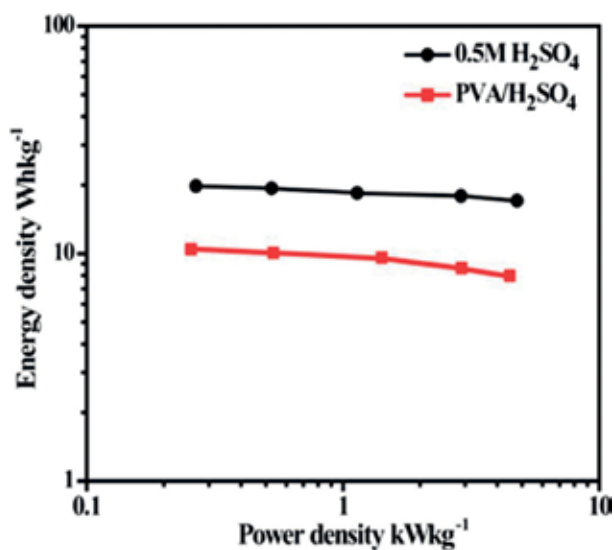
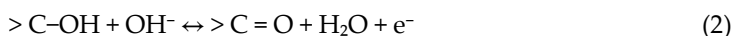
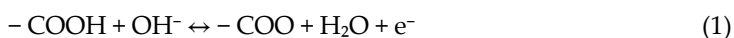


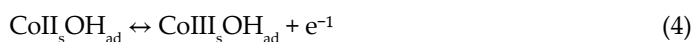
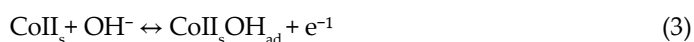
Figure 3. Ragone plot of $\text{RuO}_2/\text{carbon}$ nano-onion symmetric ESs. (Reproduced from [21] with permission from ACS).

energy density in the alkaline electrolyte by increasing the capacitance and enhancing the operating voltage. Some of the efforts were made as follows: (1) increasing carbon materials' specific capacitance by doping some pseudocapacitance functional groups, (2) discovering some pseudocapacitance materials with large specific capacitance, (3) establishing new composite materials (EDLC material + pseudocapacitance material), and (4) developing asymmetric supercapacitors with a wider potential window.

As pointed out previously, the functional groups of carbon materials undergo the faradic redox reactions which are due to the interaction involving the electrolyte ions and the attached functional groups. It has been confirmed in literatures that the KOH electrolyte was favorable for the functioning/doping carbon materials to further increase their pseudocapacitance. The existence of oxygen functional groups in carbon material (graphene) can increase the pseudocapacitance contribution in KOH electrolyte, and hence overall capacitance of the electrode can be improved [22]. The redox reaction of those functional groups in KOH electrolyte can be expressed as follows:



From this, it is well known that the electrode and electrolyte ion interaction performs a serious role for pseudocapacitance contribution. Since the theoretical capacitance of some metal oxides, sulfides, and hydroxides such as Co_3O_4 , NiO , MnO_2 , NiCo_2O_4 , $\text{Ni}(\text{OH})_2$, CoS , etc. have extremely high values, these electrode materials have also been examined for supercapacitor applications in aqueous KOH electrolyte. For example, the specific capacitance has reached extremely high ($\sim 1400 \text{ F g}^{-1}$) for Co_3O_4 nanofilm in 2 M KOH electrolyte [23]. The conversation of different oxidation states like Co^{II} to Co^{III} and then Co^{IV} in KOH aqueous electrolyte enhanced the capacitance of the electrode and described as follows:



Similarly, though metal sulfides (CoS , MnS , NiS , etc.) have poor pseudocapacitance performance in KOH electrolyte, the electrochemical transformation of sulfides into some different electroactive forms ($\text{Co}(\text{OH})_2$, $\text{Ni}(\text{OH})_2$) might improve the pseudocapacitance of the electrodes. Some characteristics of the electrolyte including ion type, size, and concentrations can affect the working temperature and ES performance. Since the pH of KOH electrolyte seems to be high, the corrosion of electrode surface might be possible when using more concentrated electrolyte. Thus, optimization of the electrolyte concentration is a mandatory task to avoid the corrosion behavior of current collector. In addition to the concentration, the electrolyte ion type and size also impact the total efficiency of ESs. The rate of intercalation/de-intercalation of the ions in the electrolyte can determine the quantity of pseudocapacitance of materials.

Mison et al. [24] have achieved a higher specific capacitance of MnO_2 electrode in LiOH electrolyte than that in KOH, resulting from the miniature-sized ionic radius of Li^+ ions. The smaller radius can be favorable to the relatively easy intercalation/de-intercalation of ions into electrode material and improved the redox reactions. In addition, the effects of the different aqueous electrolytes on NiCo_2O_4 nanostructures at a wider range of temperature have been investigated, and the highest energy density from KOH electrolyte has been achieved in comparison with NaOH as well as LiOH electrolytes (**Figure 4**). Because of the smaller size of K^+ , the ion mobility in KOH turned into much higher which enhances the fast redox reactions between electrode and electrolyte [25]. Barzegar also reported that for activated carbon electrode, 6 M KOH could demonstrate significantly better electrochemical performance than Na_2SO_4 and LiCl electrolytes [26]. Besides of the cations, electrolyte anions also play a crucial role in ES performance. Ramachandran et al. performed extensive research toward the effect of anions on the specific capacitance behavior in potassium-based alkaline and neutral electrolytes (KOH and KCl) [27]. They have reported that the small size of OH^- ions can enhance the redox reaction of cobalt sulfide/graphene materials in KOH electrolyte. Due to the smaller ionic size of OH^- , only a limited number of literatures are available for comparative studies of different alkaline aqueous electrolyte behaviors, and still the electrolyte phenomenon and mechanisms are unclear.

It is well known that the cyclic stability of pseudocapacitive materials is generally poor in the alkaline electrolyte when compared to EDLC materials, which could be associated with the repeated redox reactions in the electrolyte. An existing research was focused on enhancing the cyclic life of pseudocapacitive materials with carbon materials (composite materials). The composite materials not only improved the electrode stability but also increased the working potential range of alkaline electrolytes. For example, Fe_2O_3 nanodots/N-doped graphene composite material showed the ultralong cyclic stability of 75.3% even after 100,000 cycles in KOH electrolyte [28], and this might be due to the fact that the pyrolic N atoms in graphene can promote the electron transfer reactions of the composite.

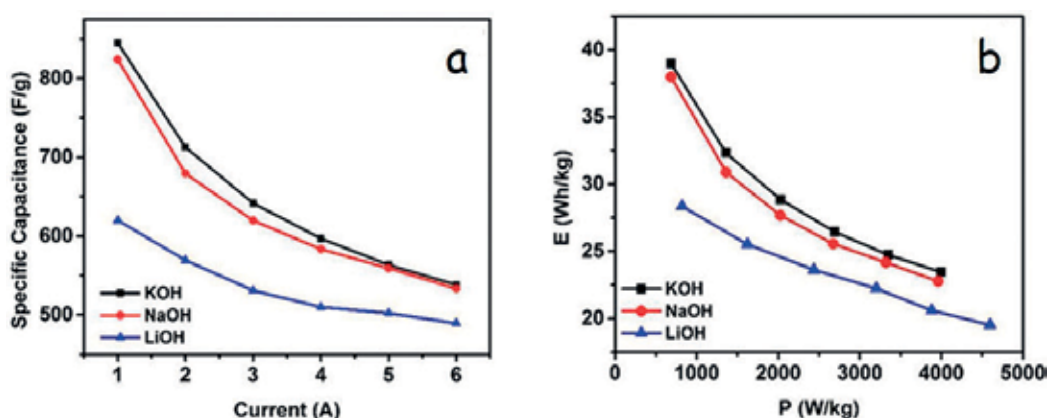


Figure 4. (a) Specific capacitance plot and (b) Ragone plot of NiCo_2O_4 at various alkaline aqueous electrolytes. (Reproduced from [25] with permission from Nature).

3.2.2. Alkaline electrolyte-based hybrid supercapacitors

A sequence of alkaline electrolytes has been studied for hybrid supercapacitors to increase their energy density with a wide range of the potential. The working voltage of the KOH electrolyte can be improved up to ~ 1.7 V when asymmetric electrodes are used. For example, carbon//metal hydroxides (carbon//Ni(OH)₂ -1.7 V and carbon//Co(OH)₂ -1.6 V) and carbon//RuO₂ (~ 1.4 V) asymmetric devices have been delivered high energy densities in KOH electrolyte. As a result of their wider potential window and high faradic reactions, most of the hybrid devices could deliver higher energy densities between 20 and 40 W h kg⁻¹, which has been similar to rechargeable lithium-ion batteries. Recently, Chen and Xue [29] have demonstrated that the vanadium-based colloids/activated carbon-based hybrids could provide a high energy density of ~ 50.4 W h kg⁻¹ with potential range of 0–1.8 V in 2 M KOH electrolyte. In situ formation of electroactive vanadium-based colloids with high utilization of cations in asymmetric device enhanced the performance and the operating voltage. Thus, developing asymmetric hybrid supercapacitor is an efficient way to increase the operating voltage and could be used in practical applications in KOH electrolyte.

3.3. Neutral electrolyte

When compared with alkaline and acid electrolytes, neutral electrolytes have also been studied extensively due to their larger working potential and less corrosive feature. Up to date, there are many types of neutral electrolytes such as LiCl, Li₂SO₄, Na₂SO₄, NaCl, KCl, K₂SO₄, etc. used in supercapacitor studies. Among them, Na₂SO₄ neutral electrolyte has shown promising electrochemical reactions for electrodes especially pseudocapacitance materials.

3.3.1. Neutral electrolyte-based EDLC and pseudocapacitors

Since the lower H⁺ and OH⁻ concentrations of the neutral electrolyte, the potential of hydrogen and oxygen evolution reaction can be shifted into the higher potential window and the electrolyte-stable potential windows (ESPW) can be increased in comparison to the alkaline electrolyte. Demarconnay et al. reported an excellent cyclic stability even after 10,000 charge-discharge cycles for the symmetric-activated carbon-based device at a high cell potential of 1.6 V in 0.5 M Na₂SO₄ neutral electrolyte [30]. The cell voltage can be extended up to 2.2 V for carbon-based electrodes in the Li₂SO₄ electrolyte as a consequence of its miniature size of bare ions (**Table 2**). The small size of Li⁺ ions can enhance the charge accumulation process in carbon electrode/electrolyte interfaces and avoid the evolution of gases such as oxygen and hydrogen at higher potential. The reported operating voltage of neutral electrolyte for carbon materials is relatively higher and less corrosive than H₂SO₄ and KOH electrolytes. Symmetric carbon ESs in neutral electrolyte have been identified as a potential candidate for higher energy density and lower environmental impact devices. A few comparable studies of the neutral electrolyte with various salts (Li⁺, K⁺, Na⁺) based on carbon ESs have been reported to experience the impact of ions on capacitive performance. Several studies reported the electrochemical performance of carbon materials shown in neutral electrolytes following the order Li₂SO₄ > Na₂SO₄ > K₂SO₄ [31, 32]. As mentioned above, the performance of ESs not only relies

on the type of electrolyte but also depends on the electrode preparation and analysis circumstances, which include voltage, scan rate, and temperature. With this view, the additional research work may be required to interpret the effect of salts on the ES performance.

Some of the pseudocapacitive materials like RuO_2 , MnO_2 , and V_2O_5 have shown excellent ES performance in neutral electrolytes. MnO_2 is the most common pseudocapacitive material, and it has been studied widely in the neutral electrolyte. Li et al. [33] have confirmed that the order of energy density and specific capacitance of mesoporous MnO_2 electrode is obtained in neutral electrolytes as follows: $\text{Li}_2\text{SO}_4 > \text{Na}_2\text{SO}_4 > \text{K}_2\text{SO}_4$. This behavior appears to be associated with the magnitude of these alkali metal bare and hydrated ion size, i.e., $\text{Li}^+ < \text{Na}^+ < \text{K}^+$, suggesting that the smaller ion size is advantageous for improving the performance. The same phenomenon was also confirmed from Fic et al., for a RuO_2 electrode in different neutral electrolytes. They observed that the mobility of alkali metal ions rises in the order of $\text{Li}^+ < \text{Na}^+ < \text{K}^+$. In accordance with the ion shape and dimensions (obtained by modeling) [31], which is shown in **Figure 5**, the high mobility of Li^+ ions is more favorable for increasing the overall performance of the pseudocapacitive materials.

3.3.2. Neutral electrolyte-based hybrid supercapacitors

Like EDLC and pseudocapacitive ESs, neutral electrolytes were also utilized for asymmetric supercapacitor devices, which provided a wider range of potential window to achieve high energy density. Though MnO_2 -based symmetric ESs delivered enough specific capacitance, the operating voltage is limited and so is its overall energy density. The cell working voltage of approximately 1 V was applied for MnO_2 symmetric devices in many cases. By substituting some carbon materials (CNT and activated carbon) as the negative electrode, the cell voltage of MnO_2 can be significantly increased [34]. In contrast, manganese phosphate ($\text{Mn}_3(\text{PO}_4)_2$)-based symmetric ESs can be performed at an extremely high voltage in the Na_2SO_4 electrolyte (~1.8 V); therefore, it reached a maximum energy density of 19.09 Wh kg^{-1} [35]. From **Figure 6**, it is noticeable that both symmetric and asymmetric ESs have delivered high energy density in neutral electrolyte rather than the alkaline electrolyte. The reason for this enhanced performance and

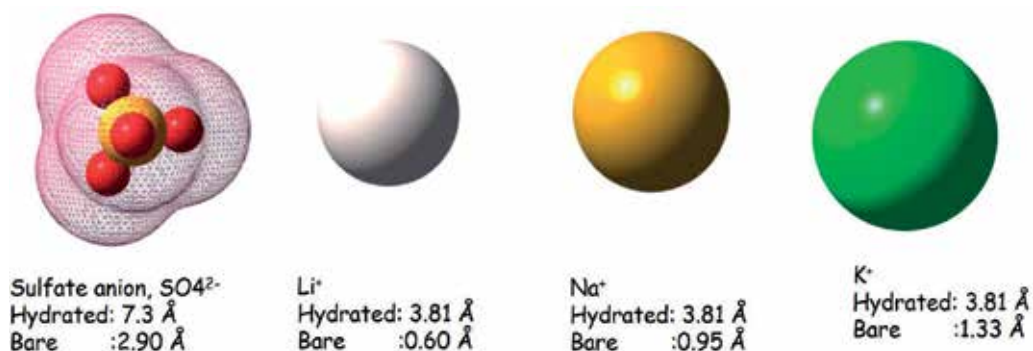


Figure 5. Ion size and dimensions in aqueous electrolyte obtained by modeling. (Reproduced from [31] with permission from RSC).

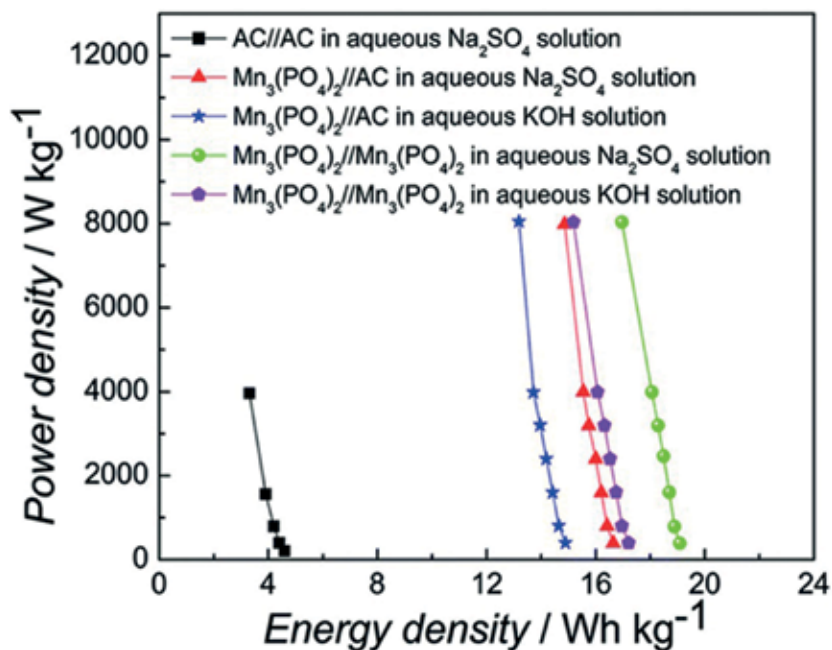


Figure 6. Ragone plot of $\text{Mn}_3(\text{PO}_4)_2$ -based symmetric and asymmetric ESs in different neutral electrolytes. (Reproduced from [35] with permission from RSC).

Aqueous electrolyte/ concentration	Electrode material	Cs (F/g)	E (Wh kg ⁻¹)	Potential window (V)	Ref
H ₂ SO ₄ /0.5 M	RuO ₂ -graphene	479	20.28	1.2	[36]
H ₂ SO ₄ /1 M	Graphene- mesoporous PANI	510	133	1	[37]
H ₂ SO ₄ /1 M	RuO ₂ -carbon nano-onion	570	10.62	1	[21]
KOH/6 M	Graphene	303	6.5	1	[38]
KOH/2 M	NiCo ₂ O ₄	1647.6	38	0.41	[39]
KOH/1 M	Ni(OH) ₂ /graphene	160	48	1.5	[40]
KOH/6 M	Iron nanosheets/ graphene	720	140	1.2	[41]
KCl/3 M	Ni(OH) ₂	718	–	0.5	[42]
NaOH/1 M	Fe ₂ O ₃	178	–	0.5	[43]
Na ₂ SO ₄ /1 M	CNT/V ₂ O ₅ nanocomposite// MnO ₂ /C	–	16	1.6	[44]
Li ₂ SO ₄ /1 M	Activated carbon	180	–	2.2	[31]
Na ₂ SO ₄ /1 M	Hydrous RuO ₂	56.66	18.77	1.6	[45]

Table 3. Some important aqueous-based electrolyte supercapacitors and their performance.

high cyclic stability of $\text{Mn}_3(\text{PO}_4)_2$ is still unclear in neutral electrolyte. To date, several positive and negative electrodes have been investigated for asymmetric supercapacitors in neutral electrolytes, and some of them are given in **Table 3**. The potential window of these asymmetric devices in the series of $\sim 1.5\text{--}2.0\text{ V}$ is larger than those described in alkaline and acidic electrolytes.

The advantage of the neutral aqueous electrolytes is not solely solving the corrosion problems of the ESs but also affording a low cost and environmentally friendly choice to enhance the performance of ESs with larger operating voltage and energy density. There are still some challenges to develop the cycle stability of ESs in neutral aqueous electrolytes.

4. Summary and future research directions

In summary, this chapter contributes comprehensive review of the development and modern trends concerning aqueous electrolyte for ESs. The effect of aqueous electrolyte properties including ionic conductivity, ion size, ESPW, etc. on the ES performance like specific capacitance, cyclic stability, energy density, and temperature performance have been reviewed in details. In particular, the effect of interaction among the electrodes and electrolytes has been discussed. This argument shows that the current explored ESs relying on neutral aqueous electrolytes provide numerous benefits such as low cost, environmentally friendly, and safe, over the other electrolyte systems. Despite of considerable accomplishments in this field, still, some difficulties exist such as lower energy density and operating voltage in aqueous electrolytes. To overcome these problems, several research directions can be considered in the future as follows:

1. *Increasing the ESPW values of electrolyte:* In aqueous electrolytes, the ESPW values are dependent on the cations and anions of a given conducting salts. Therefore, the enhancement of the ESPW values could be achieved by finding a new aqueous electrolyte salt and by optimization of the suitable electrolytes.
2. *Enhancing surface area of the pseudocapacitive materials:* As the energy density mainly depends on the capacitance, the performance of ESs could be enhanced by improving charge capacity of the electrode material. Compared to EDLC, the pseudocapacitive material-based symmetric and asymmetric ESs provide higher energy density in aqueous electrolyte. Thus, improving the specific surface area of the pseudocapacitive materials is the promising strategy to enhance the efficiency of ESs.
3. *Building the purity of the aqueous electrolyte:* In some cases, the contamination in electrolyte causes the negative effect on ESPW and also leads to high self-discharge rate. So, it is highly considered to develop the purity of the electrolyte to improve the ES performance.

Acknowledgements

This work was supported by National Natural Science Foundation of China (Project No. 51505209) and Shenzhen Science and Technology Innovation Committee (Projects No.

JCYJ20170412154426330). Fei Wang is also supported by Guangdong Natural Science Funds (Project Nos. 2015A030313812 and 2016A030306042). This chapter is partly supported by the State Key Laboratories of Transducer Technology, Shanghai, China.

Author details

Rajendran Ramachandran^{1,2} and Fei Wang^{1,2,3*}

*Address all correspondence to: wangf@sustc.edu.cn

1 Department of Electronic and Electrical Engineering, Southern University of Science and Technology, Shenzhen, China

2 Shenzhen Key Laboratory of 3rd Generation Semiconductor Devices, Shenzhen, China

3 State Key Laboratories of Transducer Technology, Shenzhen, China

References

- [1] Ramachandran R, Saranya M, Grace AN, Wang F. MnS nanocomposites based on doped graphene: Simple synthesis by a wet chemical route and improved electrochemical properties as an electrode material for supercapacitors. *RSC Advances*. 2017;**7**:2249-2257. DOI: 10.1039/C6RA25457H
- [2] Yu G, Xie X, Pan L, Bao Z, Cui Y. Hybrid nanostructured materials for high-performance electrochemical capacitors. *Nano Energy*. 2013;**2**:213-234. DOI: <https://doi.org/10.1016/j.nanoen.2012.10.006>
- [3] Ramachandran R, Saranya M, Kollu P, Ragupathy BPC, Jeong SK, Grace AN. Solvothermal synthesis of zinc sulfide decorated graphene (ZnS/G) nanocomposites for novel supercapacitor electrodes. *Electrochimica Acta*. 2005;**178**:647-657. DOI: <https://doi.org/10.1016/j.electacta.2015.08.010>
- [4] Conway BE. *Electrochemical Supercapacitors: Scientific Fundamentals and Technological Applications*. New York: Kluwer Academic/Plenum; 1999
- [5] Xia L, Yu L, Chen GZ. Electrolytes for electrochemical energy storage. *Materials Chemistry Frontiers*. 2017;**1**:584-618. DOI: 10.1039/C6QM00169F
- [6] Jiang DE, Jin Z, Henderson D, Wu J. Solvent effect on the pore-size dependence of an organic electrolyte supercapacitor. *The Journal of Physical Chemistry Letters*. 2012;**3**:1727-1731. DOI: 10.1021/jz3004624
- [7] Vindt ST, Skou EM. The buffer effect in neutral electrolyte supercapacitors. *Applied Physics*. 2016;**122**:64-69. DOI: 10.1007/s00339-015-9563-8

- [8] Yan J, Wang Q, Wei T, Fan Z. Recent advances in design and fabrication of electrochemical supercapacitors with high energy densities. *Advanced Energy Materials*. 2014; **4**:1300816. DOI: 10.1002/aenm.201300816/full
- [9] Simon P, Gogotsi Y. Materials for electrochemical capacitors. *Nature Materials*. 2008; **7**:845-854. DOI: 10.1038/nmat2297
- [10] Zheng H, Zhang H, Fu Y, Abe T, Ogumi Z. Temperature effects on the electrochemical behavior of spinel LiMn_2O_4 in quaternary ammonium-based ionic liquid electrolyte. *The Journal of Physical Chemistry*. 2005; **109**:13676-13684. DOI: 10.1021/jp051238i
- [11] Girard GMA, Hilder M, Zhu H, Nucciarone D, Whitbread K, Zavorine S, Moser M, Forsyth M, MacFarlane DR, Howlett PC. Electrochemical and physicochemical properties of small phosphonium cation ionic liquid electrolytes with high lithium salt content. *Physical Chemistry Chemical Physics*. 2015; **17**:8706-8713. DOI: 10.1039/C5CP00205B
- [12] Zhong C, Deng Y, Hu W, Qiao J, Zhang L, Zhang J. A review of electrolyte materials and composites for electrochemical supercapacitors. *Chemical Society Reviews*. 2015; **44**:7484-7539. DOI: 10.1039/C5CS00303B
- [13] Peng X, Liu H, Yin Q, Wu J, Chen P, Zhang G, Liu G. A zwitterionic gel electrolyte for efficient solid-state supercapacitors. *Nature Communications*. 2016; **7**:11782-11789. DOI: 10.1038/ncomms11782
- [14] Zhao Y, Hao M, Wang Y, Sha Y, Su L. Effect of electrolyte concentration on the capacitive properties of NiO electrode for supercapacitors. *Journal of Solid State Electrochemistry*. 2016; **20**(1):81-85. DOI: 10.1007/s10008-015-3009-2
- [15] Lehtimäki S, Railanmaa, Keskinen, Kujala M, Tuukkanen S, Lupo D. Performance, stability and operation voltage optimization of screen-printed aqueous supercapacitors. *Scientific Reports*. 2017; **7**:46001. DOI: 10.1038/srep46001
- [16] Galinski M, Lewandowski A, Pniak IS. Ionic liquids as electrolytes. *Electrochimica Acta*. 2006; **51**:5567-5580. DOI: <https://doi.org/10.1016/j.electacta.2006.03.016>
- [17] Torchala K, Kierzek K, Machnikowski J. Capacitance behavior of KOH activated meso-carbon microbeads in different aqueous electrolytes. *Electrochimica Acta*. 2012; **86**:260-267. DOI: <https://doi.org/10.1016/j.electacta.2012.07.062>
- [18] Pognon G, Brousse T, Demarconnay L, Belanger D. Performance and stability of electrochemical capacitor based on anthraquinone modified activated carbon. *Journal of Power Sources*. 2011; **196**:4117-4122. DOI: <https://doi.org/10.1016/j.jpowsour.2010.09.097>
- [19] Augustyn V, Simon P, Dunn B. Pseudocapacitive oxide materials for high-rate electrochemical energy storage. *Energy & Environmental Science*. 2014; **7**:1597-1614. DOI: 10.1039/C3EE44164D
- [20] Khomenko V, Pinero ER, Frackowiak E, Beguin F. High-voltage asymmetric supercapacitors operating in aqueous electrolyte. *Applied Physics A*. 2006; **82**:567-573. DOI: 10.1007/s00339-005-3397-8

- [21] Muniraj VKA, Kamaja CK, Shelke MV. RuO₂·nHO nanoparticles anchored on carbon nano-onions: An efficient electrode for solid state flexible electrochemical supercapacitor. *ACS Sustainable Chemistry & Engineering*. 2016;4:2528-2534. DOI: 10.1021/acssuschemeng.5b01627
- [22] Ramachandran R, Saranya M, Velmurugan V, Ragupathy BPC, Jeong SK, Grace AN. Effect of reducing agent on graphene synthesis and its influence on charge storage towards supercapacitor applications. *Applied Energy*. 2015;153:22-31. DOI: <https://doi.org/10.1016/j.apenergy.2015.02.091>
- [23] Feng C, Zhang JF, He Y, Zhong C, Hu WB, Liu L, Deng YD. Sub-3 nm Co₃O₄ nanofilms with enhanced supercapacitor properties. *ACS Nano*. 2015;9:1730-1739. DOI: 10.1021/nn506548d
- [24] Misnon II, Aziz RA, Zain NK, Vidhyadharan B, Krishnan SK, Jose R. High performance MnO₂ nanoflower electrode and the relationship between solvated ion size and specific capacitance in highly conductive electrolytes. *Materials Research Bulletin*. 2014;57:221-230. DOI: <https://doi.org/10.1016/j.materresbull.2014.05.044>
- [25] Gupta RK, Candler J, Palchoudhury S, Ramasamy K, Gupta BK. Flexible and high performance supercapacitors based on NiCo₂O₄ for wide temperature range applications. *Scientific Reports*. 2015;5:15265. DOI: 10.1038/srep15265
- [26] Barzegar F, Momodu DF, Fashedemi OO, Bello A, Dangbegnon JK, Manyala N. Investigation of different aqueous electrolytes on the electrochemical performance of activated carbon-based supercapacitors. *RSC Advances*. 2015;5:107482-107487. DOI: 10.1039/C5RA21962K
- [27] Ramachandran R, Grace AN, Subramaniam CK. Cobalt sulfide-graphene (CoSG) composite based electrochemical double layer capacitors. *MRS Proceedings*. 2015;1786:19-30. DOI: <https://doi.org/10.1557/opl.2015.784>
- [28] Liu L, Lang J, Zhang P, Hu B, Yan X. Facile synthesis of Fe₂O₃ nano-dots@nitrogen-doped graphene for supercapacitor electrode with ultralong cycle life in KOH electrolyte. *ACS Applied Materials & Interfaces*. 2016;8:9335-9344. DOI: 10.1021/acsami.6b00225
- [29] Chen K, Xue D. High energy density hybrid supercapacitor: In-situ functionalization of vanadium-based colloidal cathode. *ACS Applied Materials & Interfaces*. 2016;8:29522-29528. DOI: 10.1021/acsami.6b10638
- [30] Demarconnay L, Pinero ER, Beguin F. A symmetric carbon/carbon supercapacitor operating at 1.6 V by using a neutral aqueous solution. *Electrochemistry Communications*. 2010;12:1275-1278
- [31] Fic K, Lota G, Meller M, Frackowiak E. Novel insight into neutral medium as electrolyte for high-voltage supercapacitors. *Energy & Environmental Science*. 2012;5:5842-5850. DOI: 10.1039/C1EE02262H

- [32] Chae JH, Chen GH. Influences of ions and temperature on performance of carbon nano-particulates in supercapacitors with neutral aqueous electrolytes. *Particuology*. 2014;**15**:9-17. DOI: <https://doi.org/10.1016/j.partic.2013.02.008>
- [33] Li S, Qi L, Lu L, Wang H. Facile preparation and performance of mesoporous manganese oxide for supercapacitors utilizing neutral aqueous electrolytes. *RSC Advances*. 2012;**2**:3298-3308. DOI: 10.1039/C2RA00991A
- [34] Long JW, Belanger D, Brousse T, Sugimoto W, Sassin MB, Crosnier O. Asymmetric electrochemical capacitors—Stretching the limits of aqueous electrolytes. *MRS Bulletin*. 2011;**36**:513-522. DOI: <https://doi.org/10.1557/mrs.2011.137>
- [35] Ma XJ, Zhang WB, Kong LB, Luo YC, Kang L. Electrochemical performance in alkaline and neutral electrolytes of a manganese phosphate material possessing a broad potential window. *RSC Advances*. 2016;**6**:40077-40085. DOI: 10.1039/C6RA02217K
- [36] Deng LJ, Wang JF, Zhu G, Kang LP, Hao ZP, Lei ZB, Yang ZP, Liu ZH. RuO₂/graphene hybrid material for high performance electrochemical capacitor. *Journal of Power Sources*. 2014;**248**:407-415. DOI: <https://doi.org/10.1016/j.jpowsour.2013.09.081>
- [37] Wang Q, Yan J, Fan ZJ, Wei T, Zhang ML, Jing XY. Mesoporous polyaniline film on ultrathin graphene sheets for high performance supercapacitors. *Journal of Power Sources*. 2014;**247**:197-203. DOI: <https://doi.org/10.1016/j.jpowsour.2013.08.076>
- [38] Wang HJ, Sun XX, Liu ZH, Lei ZB. Creation of nanopores on graphene planes with MgO template for preparing high-performance supercapacitor electrodes. *Nanoscale*. 2014;**6**:6577-6584. DOI: 10.1039/C4NR00538D
- [39] Li L, Peng S, Cheah Y, Teh P, Wang J, Wee G, Ko Y, Woung C, Srinivasan M. Electrospun porous NiCo₂O₄ nanotubes as advanced electrodes for electrochemical capacitors. *Chemistry: A European Journal*. 2013;**19**:5892-5898. DOI: 10.1002/chem.201204153
- [40] Wang H, Liang Y, Mirfakhrai T, Chen Z, Casalomgue HS, Dai H. Advanced asymmetrical supercapacitors based on graphene hybrid materials. *Nano Research*. 2011;**4**(8):729-736. DOI: 10.1007/s12274-011-0129-6
- [41] Long C, Wei T, Yan J, Jiang L, Fan Z. Supercapacitors based on graphene-supported iron nanosheets as negative electrode materials. *ACS Nano*. 2013;**7**(12):11325-11332. DOI: 10.1021/nn405192s
- [42] Lee JW, Ahn T, Kim JH, Ko JM, Kim JD. Nanosheets based mesoporous NiO microspherical structures via facile and template-free method for high performance supercapacitors. *Electrochimica Acta*. 2011;**56**:4849-4857. DOI: 10.1016/j.electacta.2011.02.116
- [43] Kulal PM, Dubal DP, Lokhande CD, Fulari VJ. Chemical synthesis of Fe₂O₃ thin films for supercapacitor application. *Journal of Alloys and Compounds*. 2011;**509**:2567-2571. DOI: 10.1016/j.jallcom.2010.11.091

- [44] QT Q, Shi Y, Li LL, Guo WL, Wu YP, Zhang HP, Guan SY, Holze R. $V_2O_5 \cdot 0.6H_2O$ nanoribbons as cathode material for asymmetric supercapacitor in K_2SO_4 solution. *Electrochemistry Communications*. 2009;**11**:1325-1328. DOI: 10.1016/j.elecom.2009.05.003
- [45] Xia H, Meng YS, Yuan G, Cui C, Lu L. A symmetric RuO_2/RuO_2 supercapacitor operating at 1.6 V by using a neutral aqueous electrolyte. *Electrochemical and Solid-State Letters*. 2012;**15**:A60-A63. DOI: 10.1149/2.023204esl

Performance of Aqueous Ion Solution/Tube-Super Dielectric Material-Based Capacitors as a Function of Discharge Time

Steven M. Lombardo and Jonathan Phillips

Additional information is available at the end of the chapter

<http://dx.doi.org/10.5772/intechopen.71003>

Abstract

The discharge time dependence of key parameters of electrostatic capacitors employing a dielectric composed of the oxide film formed on titanium via anodization, saturated with various aqueous ion solutions, that is tube-super dielectric materials (T-SDM), was thoroughly documented for the first time. The capacitance, dielectric constant, and energy density of novel paradigm supercapacitors (NPS) based on T-SDM saturated with various concentrations of NaNO_3 , NH_4Cl , or KOH were all found to roll-off with decreasing discharge time in a fashion well described by simple power law relations. In contrast, power density, also well described by a simple power law, was found to increase with decreasing discharge time, in fact nearly reaching 100 W/cm^3 for both 30 wt% KOH and NaNO_3 solution-based capacitors at 0.01 s, excellent performance for pulsed power. For all capacitors, the dielectric constant was tested, which was greater than 10^5 for discharge times >0.01 s, confirming the materials are in fact T-SDM. The energy density for most of the capacitors was greater than 80 J/cm^3 of dielectric at a discharge time of 100 s, once again demonstrating that these capacitors are competitive for energy storage not only with existing commercial supercapacitors but also with the best prototype carbon-based supercapacitors.

Keywords: supercapacitor, superdielectric material, anodized titania, electric energy storage

1. Introduction

High-pulsed electrical power is required for lasers, flash photography, spark ignition, spot welders, fusion reactors, kinetic weapon systems, rapid acceleration of electric vehicles, etc. Capacitors, generally electric double layer capacitors (EDLC), also known as supercapacitors,

are preferred for pulse power applications, because they provide far higher power electric pulses, per weight/volume, than batteries [1, 2]. Moreover, unlike batteries, capacitors are not damaged by providing pulsed power. This robust feature leads to their employment as power load levelers to extend battery life. For example, in satellites, systems designed to transfer high power demand from batteries to a parallel capacitor system can significantly increase battery and satellite, lifetime.

Most research into increasing capacitor energy density is focused on developing graphene, the conductive material with the highest surface area ($\sim 2600 \text{ m}^2/\text{g}$), electrodes for the next generation EDLC [3–7]. The theory suggests that capacitors with graphene electrodes could have an ultimate energy density of $\sim 800 \text{ J}/\text{cm}^3$, a value far less than the current generation commercial lithium ion battery ($\sim 2200 \text{ J}/\text{cm}^3$). Notably, current commercial supercapacitors have an energy storage rating of $< 50 \text{ J}/\text{cm}^3$.

Recently, a new type of ‘supercapacitor’ was invented, NP supercapacitors (NPS) with energy density rivaling the best prototype EDLC, but based on an entirely different paradigm [8–14]. Unlike EDLC that gain energy density through the use of high surface area electrodes with low dielectric value, NPS use low surface area electrodes and dielectrics with remarkably high dielectric constants, specifically super dielectric materials (SDM), that is materials with dielectric values greater than 10^5 , although values $> 10^{11}$ are reported. SDM are composed of an ‘active phase’, such as salt dissolved in a liquid, and an ‘inactive’ mechanical phase such as anodized titania, T-SDM [8, 9], high surface area porous refractory oxides, Powder-SDM [10–12], or even simple fabrics, Fabric-SDM [13], that hold the active phase in place. The theoretical basis of SDM [8, 9] is that in an electric field the ions in solution travel to create dipoles, which are far longer (ca. $1 \mu\text{m}$) than those found in solid dielectrics (ca. $10^{-4} \mu\text{m}$). It is the ‘field canceling’ effect of dipoles, proportional to length, which leads to increased capacitance, as per the classic model of dielectric behavior [15–17].

It is reasonable to label NPS, a new type of supercapacitor based on the energy storage values achieved, approx. $400 \text{ J}/\text{cm}^3$ for T-SDM with aqueous NaCl solutions at very slow discharge rates, rivaling, perhaps surpassing, the best graphene-based EDLC prototypes [18–20]. One unresolved issue: NPS performance as a function of frequency. Given the theory of NPS requires micron scale ionic migration in a liquid to form giant dipoles, there should be significant performance degradation (‘roll-off’) with increasing frequency. That is, if not enough time is available in a charge cycle for dipoles to fully form via ion travel, the dielectric value, energy density, etc. will be reduced. Thus, it is important to directly test the performance of NPS as a function of frequency. Given the most likely application, power release over very short times, ca. 0.05 s, special attention should be paid to discharge rate dependence of power and energy.

The one study of NPS performance as a function of discharge time was on F-SDM, a variety not found to have particularly high energy density. Significant roll-off of all parameters with decreasing discharge period (roughly equivalent to increasing frequency) was documented. The roll-offs, all parameters, were well fit by simple power law relations over orders of magnitude of discharge time. In the present study, we employed the same method used in the earlier study to characterize performance as a function of discharge period of a variety of high energy density NPS, those employing anodized titania saturated with various aqueous free ion solutions. Once again, significant roll-off was observed as expected and the power

law relation was found. Still, even with the noted degradation, the performance at the time periods of interest (e.g. 0.05 s discharge) was better than any commercial supercapacitor and possibly any EDLC prototype. Notably, comparison with EDLC prototype performance was difficult as fitted data on time response of these capacitors are apparently nonexistent.

2. Experimental

The NP supercapacitors were constructed of anodized titania foils filled with various aqueous salt solutions. The remaining metal of the original titania was one electrode and a graphitic material served as the other electrode. The performance of these capacitors was characterized using standard galvanostat constant current protocols. All procedures are described below.

Anodization process—Titanium foil anodes (99.99% Sigma Aldrich), approx. 0.05 mm thick, were anodized, as described elsewhere [8, 9, 21–23], in an ethylene glycol solution containing small quantities of ammonium fluoride (0.25% w/w) and water (2.75% w/w), using a titanium cathode (2 cm distant from the anode) at a constant DC voltage of 40 V for 46 min. This process created a layer of cylindrical hollow titania tubes on the parent titanium, average length measured to be $7.7\pm 0.4\ \mu\text{m}$ [24], but for purposes of conservative computation of energy density and all other parameters, assumed to be 8 μm in length. The tube diameter was found to be approximately 90 nm, but that figure does not enter the computations. In prior studies employing a nearly identical protocol, but using different anodization time periods, the intent was to create anodized layers/tubes of various lengths in order to test the impact of tube length on dielectric value and energy density. In this study, the intent was to focus only on the impact of the liquid phase composition, thus all the matrix material, that is the anodized titania, was produced using a single protocol and produced nearly identical anodized layers. Typical tubes formed from this process are very regular in structure and densely packed together [8, 9, 23, 24]. They are all oriented with the long axis perpendicular to the surface of the parent foil. No effort was made to crystallize the tubes via a thermal treatment.

Assembly of capacitors—All the capacitors employed were a standard parallel plate construction, consisting of an electrode composed of the unanodized section of the original titania foil, the dielectric consisting of the anodized section ($2 \times 1\ \text{cm}$) filled with an free ion containing aqueous solution, and a positive electrode of Grafoil, a form of compressed graphite. The tubes in the anodized layer were filled with solution simply by placing them in a beaker filled with the solution for 50 min at room temperature. Three different ion precursors were used: sodium nitrate (NaNO_3), ammonia chloride (NH_4Cl), and potassium hydroxide (KOH). Capacitors were constructed from aqueous solutions of the three salts, specifically three weight percent concentrations of each salt, 10, 20, and 30%, for a total of nine capacitors. A 'control study' employing distilled water was run as well.

After the salt solution saturation, the capacitor had one electrode, the metallic component of the anodized titanium foil, and a compound dielectric in the form of the titania tubes filled with aqueous solution. Placing a Grafoil sheet ($2 \times 1\ \text{cm}$) on top of the open tube end of the anodized film completed the capacitor. Specifically, a rectangle of Grafoil (compressed natural graphite, 99.99% carbon [25, 26]) 0.3 mm thick was placed on top. The metallic part of the

anodized foil was connected to the negative terminal of the galvanostat, and the Grafoil sheet connected to the positive terminal. The final volume used in subsequent calculations was that of the dielectric section, $8 \mu\text{m} \times 2 \text{ cm} \times 1 \text{ cm}$. Greater detail is given elsewhere [24].

2.1. Electrical measurement

All parameters, including energy density, power density, capacitance, and dielectric values, were derived from 'constant current' galvanostat data (BioLogic Model SP 300 Galvanostat, Bio-Logic Science Instruments SAS, Claix, France). Operated in constant current charge/discharge mode over a selected voltage range (2.3–0.1 V), the data can be employed directly to determine capacitance as a function of voltage from the slope of voltage as a function of time, that is, for constant current:

$$C = \frac{dq}{dV} / \frac{dV}{dt} = I / \frac{dV}{dt}$$

Clearly for capacitance which is not a function of voltage, this equation predicts a perfect saw tooth voltage vs. time pattern. In fact, in this and earlier studies, it was found that the capacitance is a function of voltage, leading to 'irregular wave forms' [8–13]. As discussed in earlier work, this indicates that the capacitance is voltage dependent, specifically decreasing as voltage increases. For this reason, the capacitance reported herein is for the voltage region between 0.1 and ~ 0.8 V. In this voltage regime, the voltage vs. time relationship was always found to be nearly linear for all discharge times greater than 0.001 s indicating constant capacitance over this voltage region. In all cases, it was found that capacitance decreases with increasing voltage as a function of discharge time. The shorter the discharge time the more pronounced the departure from constant capacitance (**Figure 1**).

Given the variability of capacitance with voltage, energy cannot be computed directly from 'capacitance', but it can be determined directly from the constant current data. Specifically, energy was determined from the integrated area under the total discharge curve (volt seconds) multiplied by the constant current. Power was determined by dividing the directly determined energy, by the time required, during discharge, for the voltage to go from the maximum to the minimum value. Energy and power density were then determined by dividing energy or power by the volume of the dielectric.

Methods to determine energy and power density that require the use of data 'extrapolated' beyond the voltage range actual measured can lead to severe errors, generally overestimates. For example, impedance spectroscopy measures the dielectric constant over a narrow voltage range, generally 0 ± 15 mV [27, 28], and provides little reliable information about energy storage characteristics. Determining the energy storage/power production of most capacitors requires a collection of data over the full voltage operating range [29–31].

Galvanostats operated in the constant current mode do not permit selection of frequency. In order to obtain capacitance as a function of frequency, the current is changed. In essence increasing the current decreases the period required to charge/discharge. Hence, each capacitor was tested over

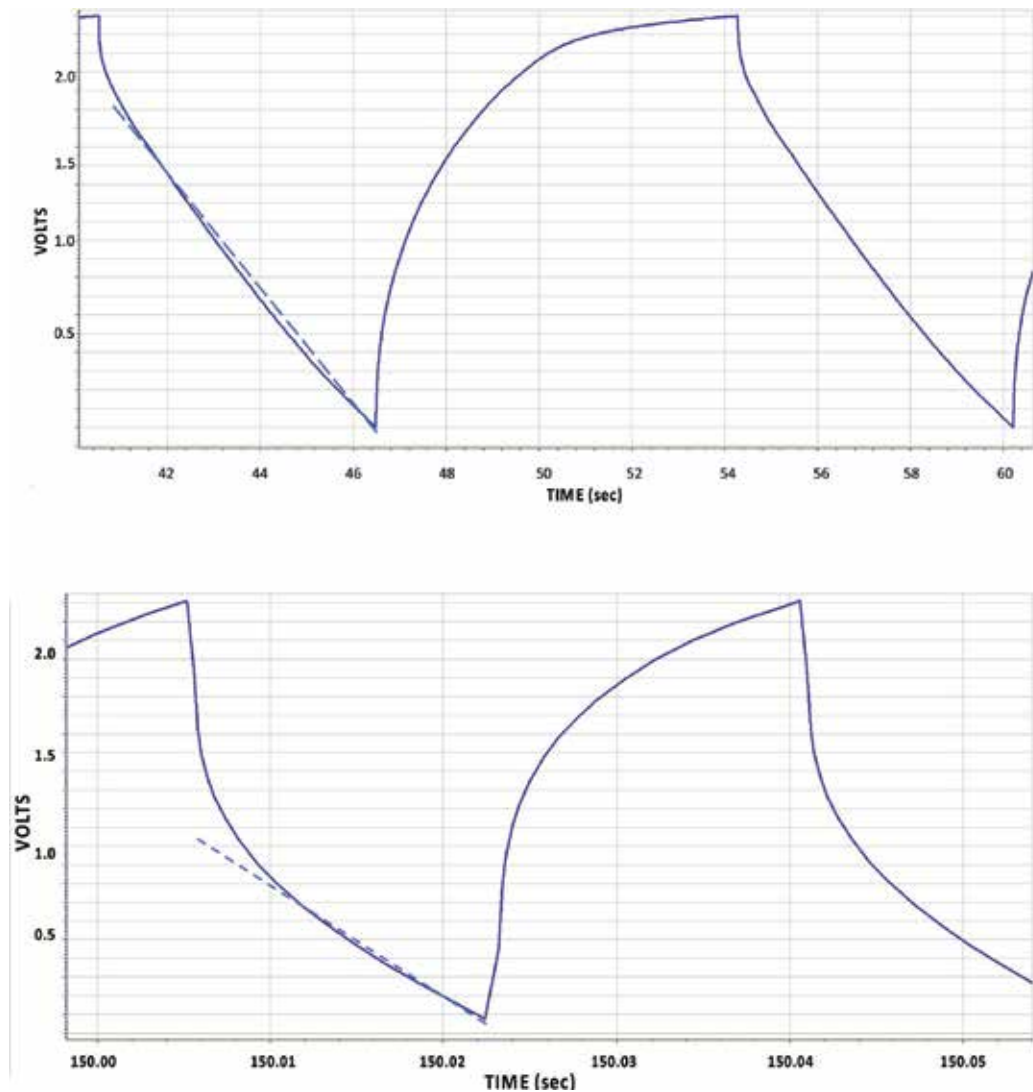


Figure 1. Deviation from voltage independent capacitance. (Top) For relatively long discharge times (>1 s), the capacitance is nearly independent of voltage to nearly 2 V, as illustrated by the dashed line nearly matching data over a broad voltage range. (sample: NH_4Cl 30%; charge rate: 10 mA). (Bottom) As the discharge time decreases, the deviation from ideal behavior, capacitance independent of voltage, becomes more pronounced (sample: NH_4Cl 30%; charge rate: 100 mA). For all discharge times studied, the capacitance was nearly constant below 0.8 V.

a wide range of current values over the range 5–250 mA. In all cases, the charging current was the same magnitude as the discharge current, but of opposite sign. For each capacitor studied nine different currents in this range were used to determine capacitive behavior over approximately four orders of magnitude of the discharge time. At each selected constant current at least 10 complete cycles were recorded and generally 20. Averaged data from these cycles are reported. As noted, in all cases, the voltage was in the range 2.3–0.1 V. The finding that linear power law data

could fit the data collected in this fashion (see Results) demonstrates the efficacy of this method for determination of frequency response. An error analysis of this approach available elsewhere [13] suggests that all data for energy and power density is accurate to within 10% absolute.

3. Results

In brief, experiments were interpreted to yield information regarding the frequency dependence of these parameters: capacitance and dielectric values below 0.8 V, energy density, and power density over the range of 0.1–2.3 V. For all nine capacitors containing aqueous solutions with dissolved ions, but not the control using distilled water, the data permitted excellent power law fits to all parameters.

3.1. Control

A capacitor employing distilled water as the electrolyte had such low values of relevant parameters that it was difficult to determine any parameters with precision, given the small capacitor size and the parameter ranges chosen for this study. A reliable power law 'roll-off' function was not obtained for any parameter as the absolute values were so small that the signal/noise ratio was large; however, it can be stated with certainty that the highest measured energy density was less than 0.03 J/cm^3 clearly demonstrating that anodized titania-based T-SDM containing distilled water are not SDM.

3.2. KOH

In order to illustrate general trends for all three solutes, the data on all three capacitors created with KOH-based SDM are presented in detail. The trends of energy and power density as well as dielectric and capacitance values determined below 0.8 V are shown on log-log plots, and in each case, it is clear that the data are well represented by simple power law relations over a wide range of discharge times.

Energy and power values are derived directly from data over the entire discharge voltage, thus may be considered as the most reliable. As shown in **Figure 2**, all the energy density data for KOH are well fit by simple power law relationships over four orders of magnitude of discharge time, that is from 20 to 0.002 s. Moreover, the curve fit is clearly of a quality that permits reasonable extrapolation to the energy density anticipated even for a 1000 s discharge. This value of energy density at this very slow discharge rate is suggested herein as a reasonable comparison point with battery energy densities (**Table 1**). It is notable that energy density is not a linear function of KOH concentration, but the 30 wt% sample was clearly superior.

Power density, following a trend observed previously for capacitors constructed with fabric-SDM (13), increases as the discharge time decreases. The data for the KOH SDM-based capacitors are shown in **Figure 3**. The trend shown was also found for SDM based on NaNO_3 and NH_4Cl aqueous solutions. The absolute values are also very informative. For example, the capacitors can provide of the order 100 W/cm^3 for discharges of 0.01 s, a remarkably high value appropriate

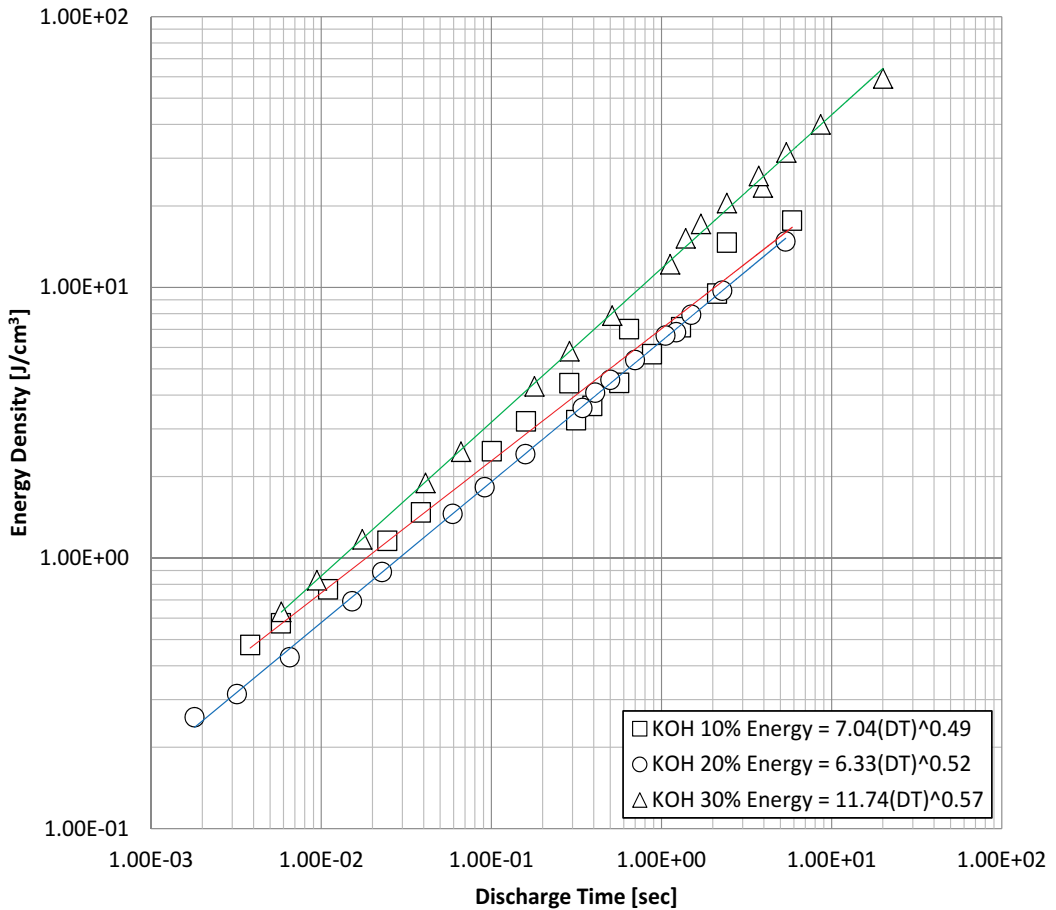


Figure 2. Energy density vs. discharge time for KOH-based capacitors. At all three KOH concentrations, the energy density ‘rolls off’ as a very specific function of discharge time. This allows determination of energy density with high precision over a broad discharge time range. Note the curve slope increases, and the energy density at all concentrations increases with increasing solute concentration. Employing the linear fitting equations with DT, in seconds, yields energy in J/cm³.

for many pulsed power applications. The data for NaNO₃ and NH₄Cl are only shown in a figure representing a summary of all nine capacitors. Greater detail is available elsewhere [24].

Capacitance as a function of discharge time for all three KOH-based systems is shown in **Figure 4**. These values were computed directly from the slope of the curves below ~0.8 V (**Figure 1**) and hence are only valid below this value. Despite this limitation, the data are of interest as it shows remarkably high values for very small volume systems.

It is notable that none of the parameters, including capacitance, show a clear pattern with salt concentration. The fact that key parameters do not track with salt concentration has been noted with all other SDM-based capacitors [9–13].

The final parameter of interest is the dielectric constant, generally an excellent engineering value as it permits the selection of capacitors, based on this single number, with a high degree

Solute (wt%)	Dielectric constant<0.8V		Energy density (J/cm ³)		Power density (Watt/cm ³)
	10 s	1000 s	10 s	1000 s	0.01 s
KOH (10)	1.1 E+8	7.3 E+8	22	208	74
KOH (20)	1.2 E+8	1.0 E+9	21	230	58
KOH (30)	2.1 E+8	1.8 E+9	44	602	85
NH ₄ Cl (10)	2.7 E+8	4.1 E+9	35	556	56
NH ₄ Cl (20)	2.2 E+8	2.9 E+9	30	356	72
NH ₄ Cl (30)	2.1 E+8	1.9 E+9	34	363	98
NaNO ₃ (10)	1.3 E+7	9.8 E+7	4	23	26
NaNO ₃ (20)	3.1 E+7	3.0 E+8	12	125	37
NaNO ₃ (30)	3.0 E+7	2.8 E+8	12	142	36

The values at 10 s (discharge time) are in the measured range. The values at 1000 s are extrapolated values based on using the power law fits.

Table 1. Select parameters.

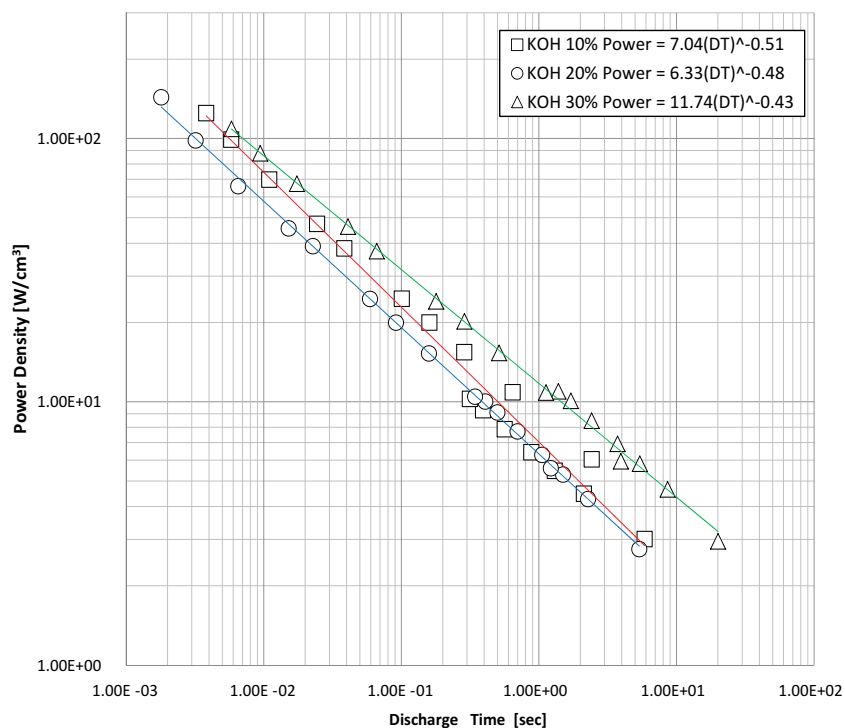


Figure 3. Power density vs. discharge time for KOH-based capacitors. At all three KOH concentrations, the power density increases with decreasing discharge time. The data clearly follow a simple power law in all cases, permitting determination of power density with high precision over a broad discharge time range. Employing the linear fitting equations, with DT, in s, yields power in W/cm³.

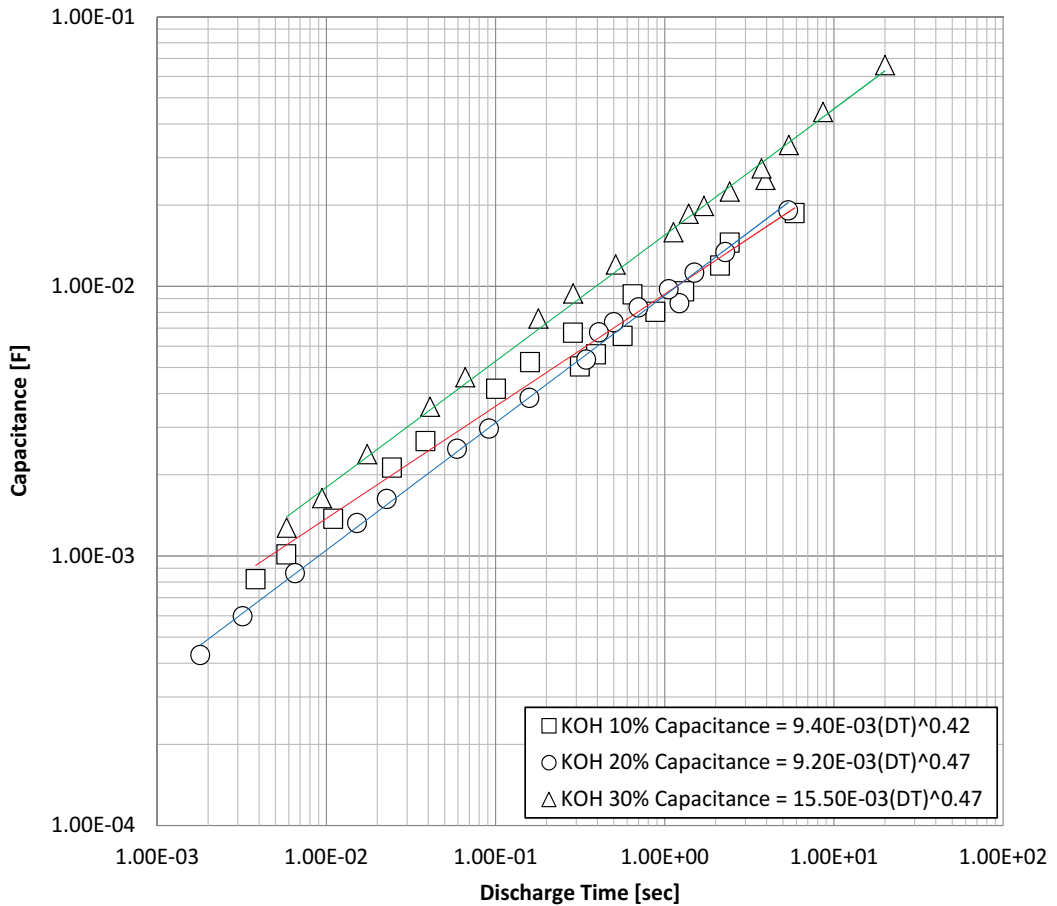


Figure 4. Capacitance vs. discharge time for KOH-based capacitors. At all three KOH concentrations, the capacitance clearly follows a simple power law in all cases, permitting determination of its value with high precision over a broad discharge time range.

of certainty they will perform as anticipated. However, for SDM-based capacitors employed for energy storage, for which dielectric constant is not a constant of voltage or frequency, it is not a quantitative predictor of performance. Notably, the dielectric constant also does not serve any role in rating EDLC for which dielectric constants in the traditional sense cannot really be measured. In fact, for EDLC a dielectric constant with units, F/cm² is the only 'dielectric' value cited [31–34]. Still, there are two good reasons for measuring and reporting this value. First, it provides a qualitative predictor of energy and power density. Second, the values (Figure 5) permit a quantitative comparison with the historic database of dielectric materials, including other super dielectric materials. For example, the far greater values of dielectric constants for SDM below ~1 V, generally more than 10⁵ greater than any solid dielectric, show them to be a distinct class of materials.

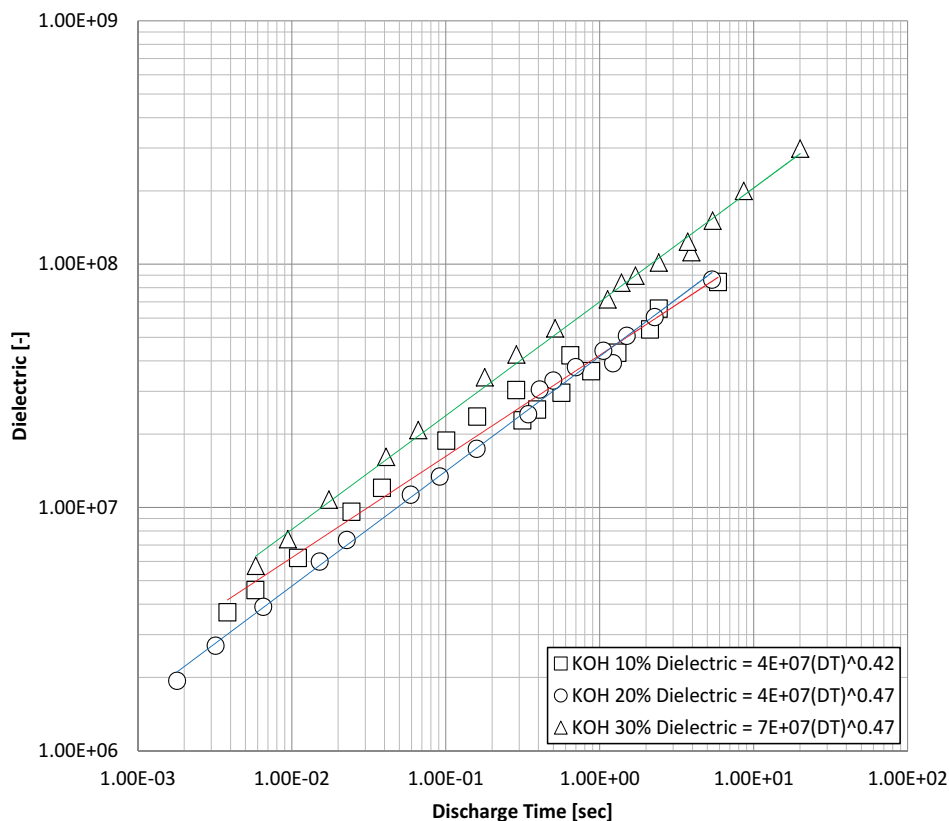


Figure 5. Dielectric constant vs. discharge time for KOH-based capacitors. At all three KOH concentrations, the dielectric constant follows, below ~ 0.8 V, a simple power law, permitting determination of its value with high precision over a broad discharge time range. The absolute values of the dielectric constant are greater than 10^6 even at a discharge time of order 10^{-3} s, indicating these materials were super dielectric materials over the full range tested.

3.3. NH_4Cl

The only complete data set shown for the aqueous NH_4Cl -based dielectric is the dielectric constant as a function of discharge time (**Figure 6**). The values of this parameter are similar to those of the aqueous KOH-based dielectrics and the other values are as well. Only dielectric constant is displayed as this parameter is most easily compared to the historic data set of dielectric materials. It is also notable that the data derived from aqueous NH_4Cl solutions show greater variability than data from capacitors made with either of the other solutions.

3.4. NaNO_3

For the aqueous NaNO_3 -based dielectric, the only complete data set provided is the dielectric constant as a function of discharge time (**Figure 7**). The values of this parameter are distinctly less, on the order of a factor of five at any given discharge time, than those

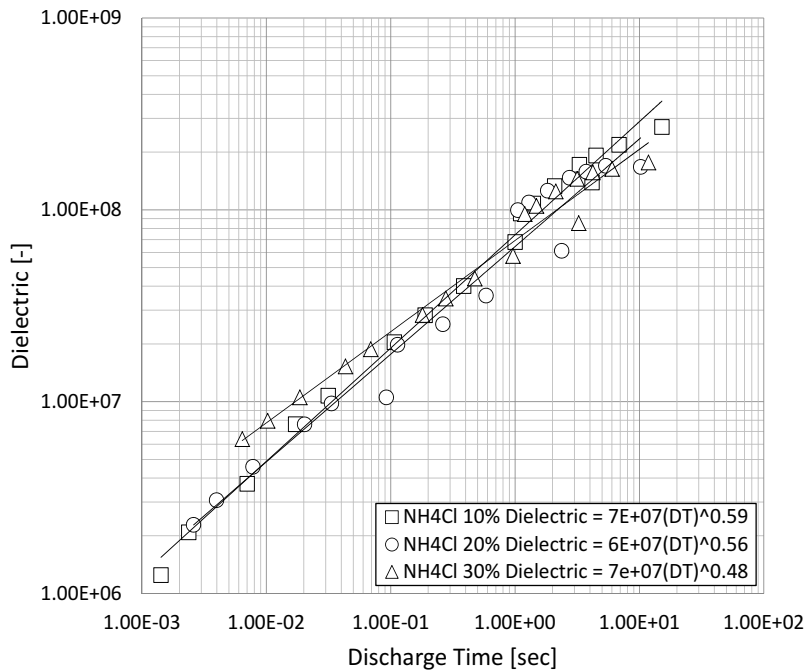


Figure 6. Dielectric constant vs. discharge time for NH_4Cl -based capacitors. At all three NH_4Cl concentrations, the dielectric constant follows, below ~ 0.8 V, a simple power law. The absolute values of the dielectric constant are similar to those of KOH at all discharge times, and greater than 10^6 even at a discharge time of order 10^{-3} s, indicating these materials were super dielectrics over the full range tested.

observed for both the aqueous KOH- and NH_4Cl -based dielectrics. This is a qualitative indicator that the energy and power density of capacitors built T-SDM employing this solution will not perform as well for storing energy and providing power. This is shown to be true in the next section.

3.5. Energy and power

The energy density for all three aqueous salt solutions with 30 wt% concentration is shown in **Figure 8**. The energy density for two of these solutions, KOH and NH_4Cl , are very similar across the entire range of discharge times collected. This is consistent with the observations that they have very similar dielectric values over the same tested time range. The energy density of the capacitors employing NaNO_3 is less than a third the value of capacitors built using either of the other two solutions at any given frequency and also qualitatively consistent with the relatively low dielectric value of this solution. Also notable is the clear indication that the method does not provide reliable data for discharge times less than approximately 0.001 s. At this high rate of discharge, the method does not capture a sufficient number of data points to provide a reliable integrated energy density.

A comparison of the power density for the three capacitors built with 30 wt% salt solutions is shown in **Figure 9**. Once again, the KOH and NH_4Cl behavior is very similar, as anticipated

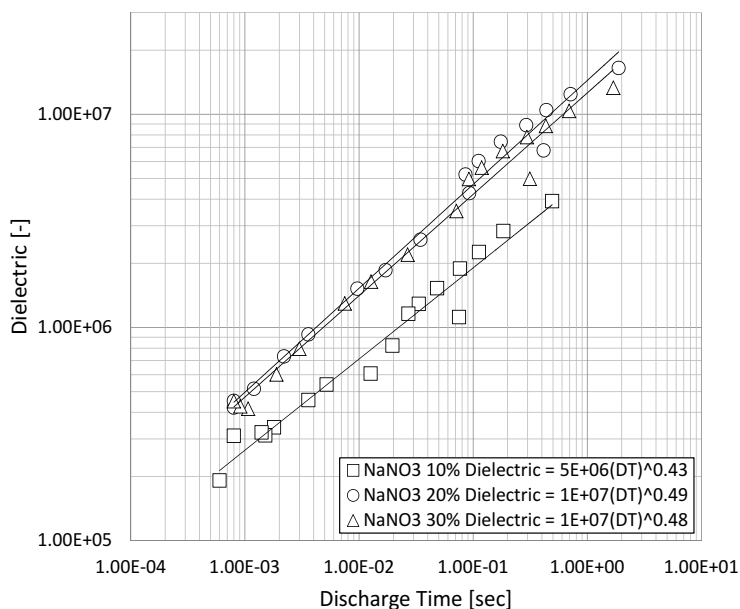


Figure 7. Dielectric constant vs. discharge time for NaNO_3 -based capacitors. At all three concentrations, the dielectric constant follows, below ~ 0.8 V, a simple power law. The absolute values of the dielectric constant are about an order of magnitude less than the KOH and NH_4Cl -based capacitors at any given discharge time. Still, at all discharge times tested the dielectric constant was greater than 10^5 , indicating these materials were super dielectrics over the full range tested.

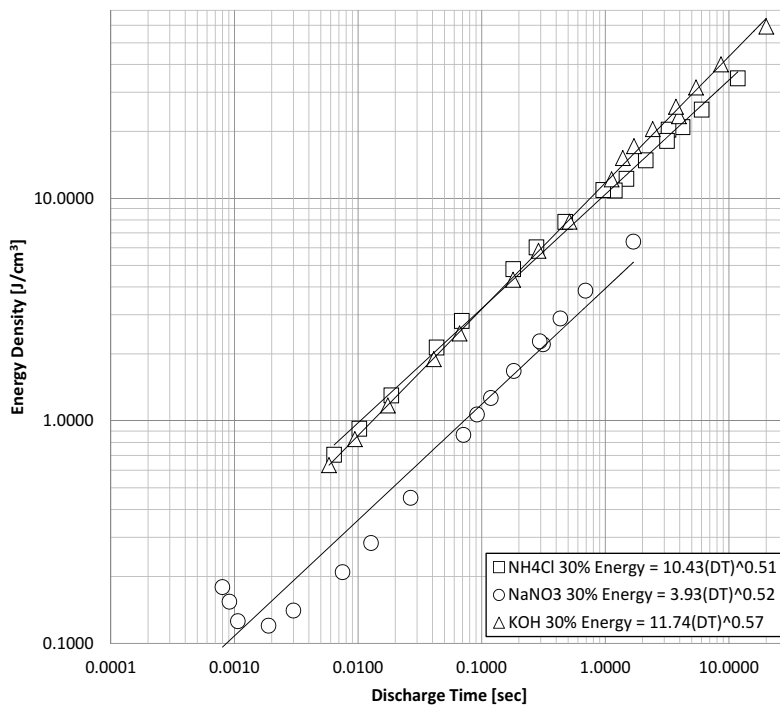


Figure 8. Energy density comparisons. The energy density for capacitors built with three different 30 wt% salt solutions is shown over more than three orders of magnitude of discharge time. The data below 0.001 s discharge time are considered inaccurate due to insufficient data collection times.

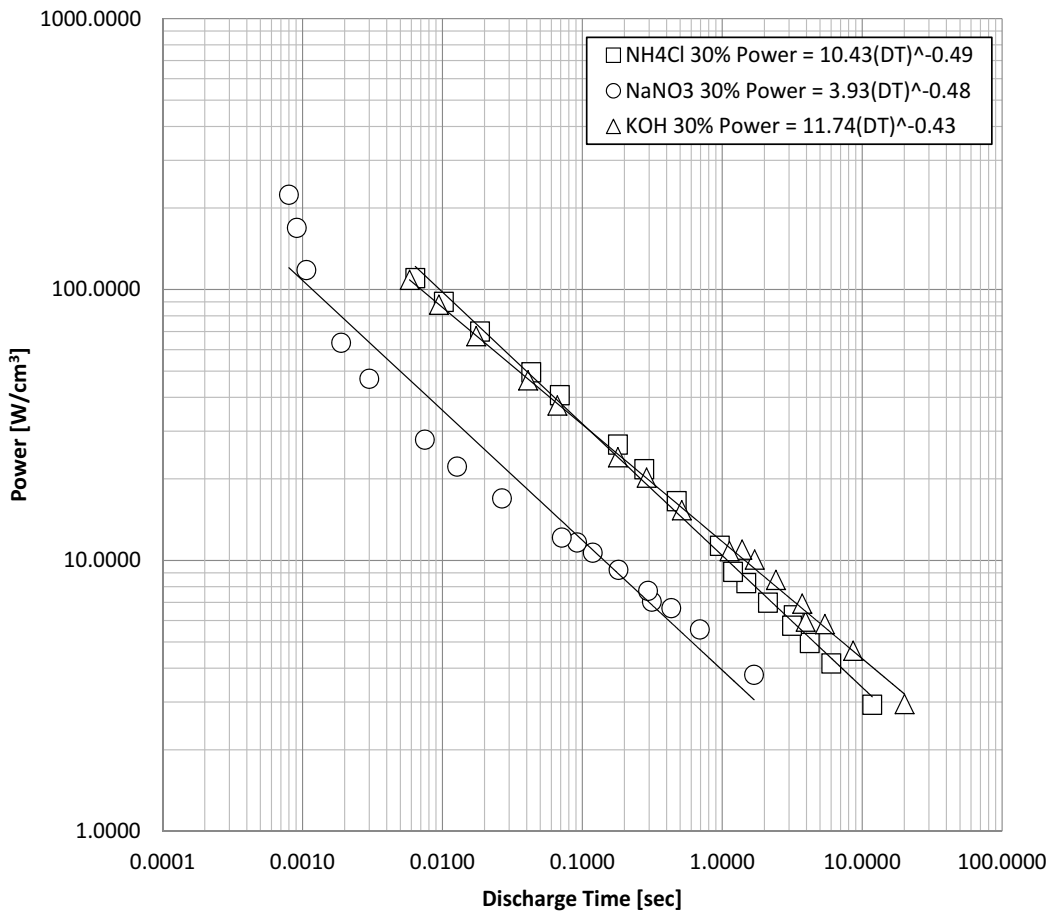


Figure 9. Power density comparisons. The power density for capacitors built with three different 30 wt% salt solutions is shown over more than three orders of magnitude of discharge time.

based on the similarity in the reported dielectric values over the full range of discharge times studied. It is also clear that the aqueous NaNO₃ capacitor yields the lowest power densities, by a factor of approximately three at all discharge times, as expected given the lower dielectric values reported. Although not shown here, the relative energy and power densities observed for the 30% solutions are exemplary of the relative values of these parameters at all concentrations.

4. Discussion

The following were observed for all nine ion capacitors containing dissolved ions: (i) All the capacitors displayed 'roll-off' of capacitance (<0.8 V), dielectric constant (<0.8 V), and energy density (0.1–2.3 V) as discharge time decreased. (ii) The roll-off, of all these parameters, is well described by simple power law expressions derived from data covering more than three orders of magnitude of discharge times. (iii) Power density is also well described by a simple power law, but in contrast to all other parameters of interest, increased in all

cases as the discharge time was reduced. (iv) The identity and concentrations of the solutes had a strong impact on the value of all capacitor performance parameters. (v) The value of all parameters was not a clear function of solute concentration, although the highest weight concentration, 30%, performed the best. (vi) In general, capacitors based on KOH and NH_4Cl were similar in behavior, but the NaNO_3 -based capacitors consistently showed the lowest values.

The data presented herein provide the first report on the behavior of T-SDM as a function of discharge time. This information is critical for assessing the value of any type of capacitor for application to 'pulsed power'. Indeed, the measured power densities, just greater than 100 W/cm^3 for both the aqueous KOH- and NH_4Cl -based capacitors, for discharges of 0.01 s , are exceptional. As shown in **Figure 10**, the KOH-based capacitor parameters fall above the 'range' of operation anticipated for EDLC-based supercapacitors and are far better than the performance determined using the identical methodology employed in this work to assess real commercial 'supercapacitors' [24] in our laboratory. Three supercapacitors were tested and the best passed through the bottom range of values anticipated by the plot shown (**Figure 10**), and the other two were completely below the 'bubble' of performance anticipated for 'double layer capacitors'.

It is also important to compare the data obtained in this study with earlier work on T-SDM. That earlier work was undertaken with a different objective: Study very slow discharges ($>1000 \text{ s}$) appropriate for determining their potential use of T-SDM as energy storage devices. The

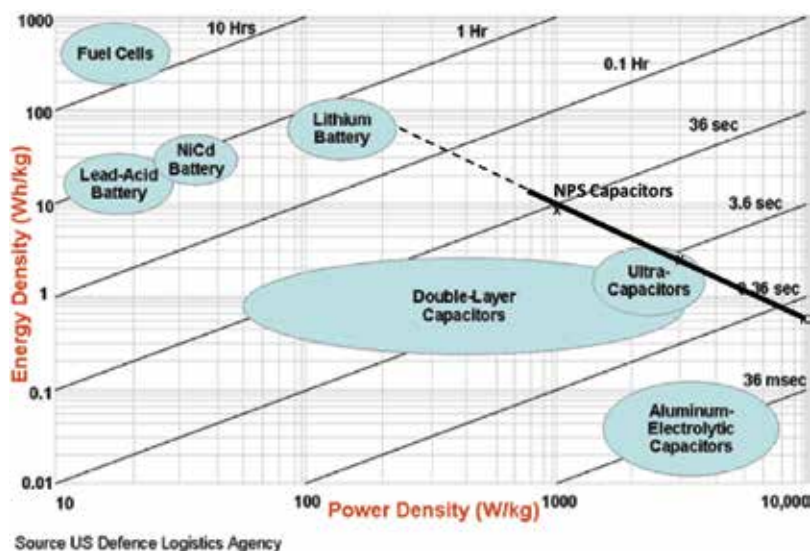


Figure 10. KOH 30 wt% NPS energy/power performance. On a modified US Defense Logistics Agency Ragone chart, it is clear that the 30 wt% KOH-based capacitor (solid line) is superior to that anticipated for EDLC or double layer capacitors. Also, the data fall on a line, which can reasonably be extrapolated using the power law fits (dashed curve). It was assumed that the dielectric is half salt water and half titania with density 2.6 g/cm^3 .

measured energy densities reported herein, for both KOH- and NH_4Cl -based capacitors, are comparable to the values obtained in prior studies. Those were obtained using a different solution, 30% NaCl, and a different measurement method, the traditional RC time constant method. In fact, using the simple power law dependencies obtained here and extrapolating to 1000 s, the energy density is a remarkable $\sim 600 \text{ J/cm}^3$. In the earlier RC time constant work a nearly identical titania matrix containing 30 wt% NaCl aqueous solution yielded nearly 400 J/cm^3 for similar discharge times. Given the different ionic solutions, the different measurement protocols and other minor differences, there is an excellent agreement between the two studies.

The basic model of T-SDM presented elsewhere [7, 8, 10] predicts high capacitance that decrease as the discharge time decreases. To understand both, a brief review of the static model of SDM and a qualitative review of the dynamics of SDM is required. Regarding the former: As illustrated by the cross-section model of an anodized titania filled with aqueous solution, **Figure 11**, dipoles created by the movement of ions in solution toward oppositely polarized electrodes create ‘giant dipoles’. These dipoles, opposite in polarization to the electrodes, reduce the field, everywhere, created by charges on the electrodes. As voltage is the line integral of field from ground to electrode, the lowering of field everywhere reduces the voltage. Thus, it takes more charge on the electrodes to reach the same voltage when these giant dipoles are fully (static conditions) aligned. More charge, at the same voltage, means a higher capacitance, by definition. In essence, dipole formation is the basis for capacitance enhancement for all types of dielectrics; however, for SDM the dipoles are orders of magnitude longer than in any solid so the field reduction, and consequently the increase in capacitance, is more dramatic. Next, it is necessary to reflect on the dynamics of dipole formation, that is the impact of frequency, or period, on dipole strength. Specifically, if the electrode polarization is switched too quickly for the ions in solution to ‘swim’ to the maximal (static) dipole positions, the net or effective, dipole length, and concomitantly the dielectric and capacitance values, are reduced. The

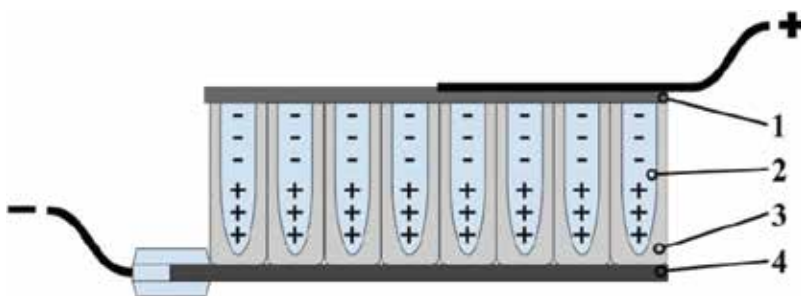


Figure 11. X-Section model of dipole formation in SDM. 1. Top electrode, Grafoil. 2. Tube filled with aqueous ion solution. 3. $90 \text{ nm} \times 8 \text{ }\mu\text{m}$ titania tubes formed by anodization. 4. Titanium metal electrode. Upon the application of a field, the ions in solution migrate to form dipoles oppositely polarized to the electrodes. The effective dipole strength in the dielectric is a function of time. Given sufficient time (static) dipoles of maximum length and charge separation form. The effective dipole length/strength is a function of net length and thus is discharge time/frequency dependent.

data suggest that effective dipole length follows a very simple pattern as a function of discharge time.

It is notable that this is only the second time [13] the constant current charge/discharge method has been employed to determine the power law relationship for 'supercapacitor' parameters, specifically capacitance, dielectric constant, and energy and power density, over orders of magnitude of discharge times. This method arguably provides higher fidelity, more reliable, insight into 'frequency' dependence of this type of capacitor than other measurement protocols.

5. Conclusions

This study establishes, empirically, that T-SDM capacitors, based on dielectrics created by filling micron scale titania tubes that form during titanium ionization with aqueous salt solutions, are superior to all other energy storage capacitors, relative to standard metrics. Using a recently developed constant current protocol, it was demonstrated that the capacitance, dielectric constant, and energy and power density as a function of discharge time follow power law relationships. Plotted on a Ragone chart, the power vs. energy density data is linear. All data lie above the values recorded for supercapacitors, ultra capacitors, and electrolytic capacitors on standard Ragone charts. Furthermore, the consistency of the data, that it resulted in power law relationships for capacitors derived from nine different salt solutions, indicates that the data and the fitted power laws are precise and are probably accurate. Notably, dielectric constants of more than 10^8 were recorded, and even for very short discharges for all capacitors, the dielectric constant was $>10^5$, establishing that the dielectrics are SDM over a broad range of discharge times (ca. 10^{-3} – >10 s). Finally, it should be noted that the measured power delivery increases as the discharge time decreases. For three of the capacitors, the measured power delivery was greater than 70 W/cm^3 for a 10 ms discharge, a time frame and a power delivery value consistent with the needs of pulsed power systems.

Author details

Steven M. Lombardo and Jonathan Phillips*

*Address all correspondence to: jphillip@nps.edu

Naval Postgraduate School, Monterey, CA, USA

References

- [1] Christen T, Carlen W. Theory of Ragone plots. *Journal of Power Sources*. 2000;**91**:210

- [2] Ragone D. Review of battery systems for electrically powered vehicles. SAE Technical Paper 680453. 1968. DOI: 10.4271/680453
- [3] Simon P, Gogotsi Y. Materials for electrochemical capacitors. *Nature Materials*. 2008;7:845
- [4] Dato A, Radmilovic V, Lee Z, Phillips J, Frenklach M. Substrate-free gas-phase synthesis of graphene sheets. *Nano Letters*. 2008;8:2012-2016
- [5] El-Kady MF, Strong V, Dubin S, Kaner RB. Laser scribing of high-performance and flexible graphene-based electrochemical capacitors. *Science*. 2012;335:1326
- [6] Shao Y, El-Kady MF, Wang LJ, Zhang Q, Li Y, Wang H, Mousavi MF, Kaner RB. Graphene-based materials for flexible supercapacitors. *Chemical Society Reviews*. 2015;44:3639
- [7] Yang X, Zhuang X, Huang Y, Jiang J, Tian H, Wu D, Zhang F, Mai Y, Feng X. Nitrogen-enriched hierarchically porous carbon materials fabricated by graphene aerogel templated Schiff-base chemistry for high performance electrochemical capacitors. *Polymer Chemistry*. 2015;6:1088-1095
- [8] Gandy J, Quintero F, Phillips J'. Testing the tube super dielectric material hypothesis: Increased energy density using NaCl. *Journal of Electronic Materials*. 2016;45:5499
- [9] Quintero F, Phillips J. Tube-super dielectric materials: Electrostatic capacitors with energy density greater than 200 J·cm⁻³. *Materials*. 2015;8:6208-6227
- [10] Fromille S, Phillips J. Super dielectric materials. *Materials*. 2014;7:8197-8212
- [11] Quintero F, Phillips J. Super dielectrics composed of NaCl and H₂O and porous alumina. *Journal of Electronic Materials*. 2015;44:1367
- [12] Jenkins N, Petty C, Phillips J. Investigation of fumed aqueous NaCl superdielectric material. *Materials*. 2016;9:118
- [13] Phillips J. Novel superdielectric materials: Aqueous salt solution saturated fabric. *Materials*. 2016;9:918
- [14] J Phillips, SS Fromille. Superdielectric materials US Patent 9,530,574 (2016)
- [15] Kao KC. *Dielectric Phenomena in Solids: With Emphasis on Physical Concepts of Electronic Processes*. Academic Press; New York, NY USA. 2004
- [16] Debye PJW. *Polar Molecules*. Chemical Catalog Company, Incorporated; New York, NY USA. 1929
- [17] Onsager L. Electric moments of molecules in liquids. *Journal of the American Chemical Society*. 1936;58:1486
- [18] Kim CH et al. Tailoring the pore structure of carbon nanofibers for achieving ultrahigh-energy-density supercapacitors using ionic liquids as electrolytes. *Journal of Materials Chemistry A*. 2016;4:4763

- [19] Xu Y, Lin Z, Zhong X, Huang X, Weiss NO, Huang Y, Duan X. Holey graphene frameworks for highly efficient capacitive energy storage. *Nature Communications*. 2014;**5**:4554. DOI: 10.1038/ncomms 5554
- [20] Sahu V et al. Ultrahigh performance supercapacitor from lacey reduced graphene oxide nanoribbons. *ACS Applied Materials and Interfaces*. 2015;**3110**(2015):7
- [21] Zwillling V, Darque-Ceretti E, Boutry-Forveille A, David D, Perrin MY, Aucouturier M'. Structure and physicochemistry of anodic oxide films on titanium and TA6V alloy. *Surface and Interface Analysis*. 1999;**27**:629
- [22] Roy P, Berger S, Schmuki P'. TiO₂ nanotubes: Synthesis and applications. *Angewandte Chemie, International Edition*. 2011;**50**:2904
- [23] Cortes FJQ, Arias-Monje PJ, Phillips J, Zea H. Empirical kinetics for the growth of titania nanotube arrays by potentiostatic anodization in ethylene glycol. *Materials & Design*. 2016;**96**:80-89
- [24] Lombardo SM. Characterization of Anodized Titanium-Based Novel Paradigm Supercapacitors: Impact of Salt Identity and Frequency on Dielectric Values, Power and Energy Densities. M.S. Thesis, Naval Postgraduate School; 2016
- [25] Phillips J, Clausen B, Dumesic JA. Iron pentacarbonyl decomposition over grafoil. Production of small metallic iron particles. *The Journal of Physical Chemistry*. 1980;**84**:1814
- [26] Phillips J, Dumesic JA. Iron pentacarbonyl decomposition over grafoil: II. Effect of sample outgassing on decomposition kinetics. *Applied Surface Science*. 1981;**7**:215-230
- [27] Barsoukov E, MacDonald JR. *Impedance Spectroscopy: Theory, Experimental and Applications*. 2nd ed. New York, NY, USA: John Wiley & Sons; 2005
- [28] MacDonald JR, Kenan WR. *Impedance Spectroscopy. Emphasizing Solid Materials and Systems*. New York, NY, USA: John Wiley & Sons; 1987
- [29] Kim Y, Kathaperumal M, Chen VW, Park Y, Fuentes-Hernandez C, Pan MJ, Kippelen B, Perry JW. Bilayer structure with ultrahigh energy/power density using hybrid sol-gel dielectric and charge-blocking monolayer. *Advanced Energy Materials*. 2015;**5**:1500767. DOI: 10.1002/aenm.201500767
- [30] Gogotski Y, Simon P. True performance metrics in electrochemical energy storage. *Science*. 2011;**334**:917
- [31] Conway BE. *Electrochemical Supercapacitors: Scientific Fundamentals and Technological Applications*. Springer Science and Business Media; New York, NY USA. 1999
- [32] Simon P, Burke AF. Nanostructured carbons: Double-layer capacitance and more. *Electrochemical Society Interface*. 2008:38-43
- [33] Ji H et al. Capacitance of carbon-based electrical double-layer capacitors. *Nature Communications*. 2014;**5**:3317
- [34] Reynolds GJ, Krutzer M, Dubs M, Felzer H, Mamazza R'. Electrical properties of thin-film capacitors fabricated using high temperature sputtered modified barium titanate. *Materials*. 2012;**5**:644

Enhancing Pseudocapacitive Process for Energy Storage Devices: Analyzing the Charge Transport Using Electro-kinetic Study and Numerical Modeling

Fenghua Guo, Nivedita Gupta and Xiaowei Teng

Additional information is available at the end of the chapter

<http://dx.doi.org/10.5772/intechopen.73680>

Abstract

Supercapacitors are a class of energy storage devices that store energy by either ionic adsorption via an electrochemical double layer capacitive process or fast surface redox reaction via a pseudocapacitive process. Supercapacitors display fast charging and discharging performance and excellent chemical stability, which fill the gap between high energy density batteries and high-power-density electrostatic capacitors. In this book chapter, the authors have presented the current studies on improving the capacitive storage capacity of various electrode materials for supercapacitors, mainly focusing on the metal oxide electrode materials. In particular, the approaches that mathematically simulate the behavior of interaction between electrode materials and charge carriers subject to potentiodynamic conditions (e.g., cyclic voltammetry) have been described. These include a general relationship between current and voltage to describe overall electrokinetics during the charge transfer process and a more comprehensive numerical modeling that studies ionic transport and electrokinetics within a spherical solid particle. The two aforementioned types of mathematical analyses can provide fundamental understanding of the parameters governing the electrode reaction and mass transfer in the electrode material, and thus shed light on how to improve the storage capacity of supercapacitors.

Keywords: pseudocapacitance, diffusion-limited redox process, electrode/electrolyte interface, electrokinetics

1. Introduction

Supercapacitors (SCs), also called electrochemical capacitors, are a class of energy storage devices that store electrical energy by either ionic adsorption via an electrochemical double layer capacitive process or fast surface redox reaction via a pseudocapacitive process. As shown in **Figure 1**, SCs bridge the performance gap between high energy density batteries and high-power-density capacitors (referring to electrostatic capacitors), the two leading electrical energy storage technologies [1]. Batteries technology, especially non-aqueous lithium-ion batteries (LIBs), has been successfully used in various applications in the past two decades especially in consumer electronics and electrical vehicles. On the other hand, capacitive storage technology offers a number of desirable properties hardly found in batteries, including fast charging and discharging process (usually achieved within seconds), long-term cycling life ($>10^6$ cycles), and high power performance (able to deliver at least 10 times more power than batteries). As a result, capacitive storage technology is very important for applications where a large amount of energy needs to be either stored or delivered quickly, including repetitive conversions between kinetic energy and electric energy (e.g., regenerative braking and forklifting), pulse power applications for laser or radar, power conditioning in the electrical grid to smooth the output of a full or half wave rectifier [2]. It is notable that both capacitive and battery storage technologies have promising applications in stationary storage. Renewable sun and wind energy sources generally have on-peak and off-peak load variations. To accelerate the adoption of renewable energy generation sources, chemical energy storage (e.g., batteries) and capacitive energy storage (e.g., capacitors) are required. Thus, electricity generated during off-peak hours can be stored efficiently and economically for use during peak demand [3].

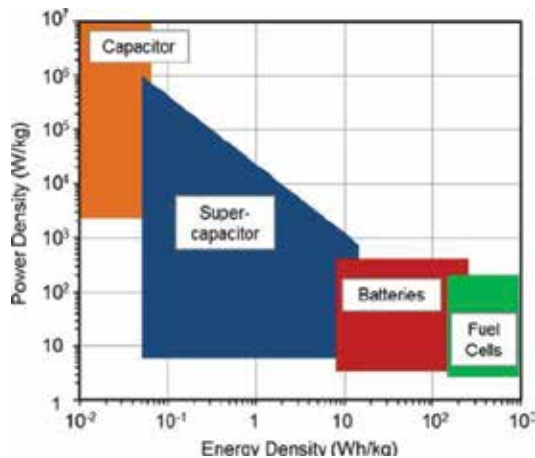


Figure 1. Ragone plot showing supercapacitors are intermediate energy storage devices filling the gap between batteries and conventional capacitors.

Although SCs offer complementary energy storage solution for many applications that are not suitable for batteries, the relatively low storage capacity and energy density limit SCs in more widespread usage. SCs usually contain three general classes of charge storage mechanisms:

- *Electrical double-layer (EDL) capacitive process* relies on the charge separation in a Helmholtz double layer at electrode/electrolyte interface by means of static charge (non-faradaic). The storage capacity of an EDL capacitor can be improved by a large surface area of the electrode/electrolyte interface (most EDL capacitors have a capacitance in a range from 10 to 20 $\mu\text{F}/\text{cm}^2$). EDL capacitors serve as the basis for the current technology in capacitive energy storage. Carbons are ideal EDL electrode materials for its high electrical conductivity, large surface area, and low density, delivering a storage capacity of up to 150 F g^{-1} in ionic liquid electrolytes [4].
- *Pseudocapacitive process* relies on the charge transfer process primarily happening at the interface between the electrode and the electrolyte. Three faradaic mechanisms have been identified to account for the capacitive electrochemical features that appear in pseudocapacitors, namely, underpotential deposition, redox pseudocapacitance, and intercalation pseudocapacitance [5]. Underpotential deposition typically involves hydrogen atom on the near surface on noble metal oxides (e.g., IrO_2 or RuO_2) [6]. Redox pseudocapacitance occurs at or near the surface of a material, accompanied by adsorption of ions [7]. Intercalation pseudocapacitance occurs when ions intercalate into the channels or layers of a redox-active material accompanied by a faradaic charge-transfer with no crystallographic phase change [8]. Metal oxides, metal carbides or nitrides are ideal pseudocapacitive electrode materials for their reversible redox activity, wide electrochemical potential and high chemical stability [9]. The storage capacity of a pseudocapacitive material is much higher than an EDL capacitive material (the former has a capacitance larger than 100 $\mu\text{F}/\text{cm}^2$, nearly one magnitude higher than the latter).
- *Diffusion-limited redox process* relies on the kinetically limited intercalation reactions as found in most standard battery materials, where ion intercalation and de-intercalation are intrinsically tied to the slow kinetics of solid phase transition between the intercalated and non-intercalated phases. It is notable that the difference between pseudocapacitive charge storage and battery-like diffusion-limited intercalation is rather vague, especially when the dimensions of an electrode material decreases from the micron-scale down to the nanoscale [10]. At the nanoscale, the specific surface area of a material (overall surface area per unit volume) increases inversely with the size, which results in a significant enhancement of redox pseudocapacitance and intercalation pseudocapacitance. Such enhancement of surface redox (pseudocapacitive) process may become the more dominant charge storage process traditional battery-like intercalation process as the sizes of materials progress from micro-scale to nanoscale. Thus, the materials may evolve from being a typical battery material to a pseudocapacitor material based on their size and/or nanoscale architecture, where phase transition is no longer a distinct structural feature of the electrode materials between the intercalated and non-intercalated states (**Figure 2**).

As discussed above, improving the storage capacity of SCs requires the enhancement of redox processes, such as redox pseudocapacitance, intercalation pseudocapacitance, as well as

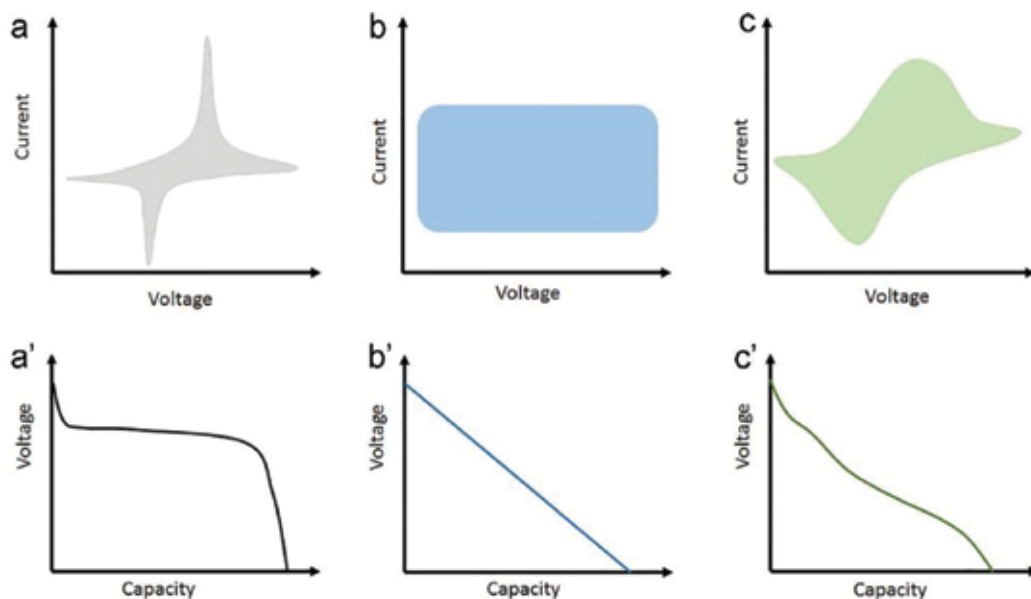


Figure 2. Schematics of charge transfer and storage processes observed in (a, a') large-sized battery-materials; (b, b') pseudocapacitive materials, and (c, c') nano-sized battery-materials.

diffusion-limited redox process. Therefore, the analysis of different charge storage mechanisms also becomes important. The goal of this chapter is thus to examine the parameters (e.g., size, morphology and structure) that will affect the evolution from battery-like behavior to pseudocapacitor behavior and to explore the interplay of these parameters to control redox kinetics.

2. Understanding electrochemical kinetics of charge transfer process by analyzing the electrochemical data during the cyclic voltammetry measurements

Redox reactions involve both surface adsorption/desorption and intercalation/deintercalation of electrolyte cations as shown in Eq. (1):



where MO is the transition metal oxide and C^+ is the charge carrier (e.g., Li^+ , Na^+ , or K^+). Upon the incorporation (via intercalation or adsorption) of C^+ , M cations will be reduced to balance the charges, and *vice versa*. Moreover, due to the dispersive nature of the electrode composites, separate percolation paths for ion and charge transport may be present, resulting in different paths for long range electronic and ionic conduction. Therefore, influences of the kinetic parameters (e.g., scan rate, potential window) and the structural parameters (e.g., size,

morphology, and crystalline structures) on the redox reactions are crucial to understand the charge-storage mechanism in electrode materials. All the kinetic and structural parameters need to be optimized in order to design cost-effective electrode materials that can store more energy while maintaining a stable electrode/electrolyte interface.

The understanding of the electrokinetics of charge storage inside the metal oxide nanomaterials can be obtained through analyzing the current-voltage curves at various scan rates obtained from CV measurements in the half-cell. The total charge stored in the electrode during SC operation is dependent on a relatively fast surface-controlled capacitive charge storage process and a relatively slow diffusion-controlled redox charge storage process. The latter is promoted by the battery-like intercalation/de-intercalation redox processes of the charge carriers (e.g., Li^+ , Na^+), while the former is attributed to the electrical double layer (i.e. EDL capacitance) and pseudocapacitance formed via the separation or adsorption and desorption of charge carriers at the near surface of the electrode.

For a strictly diffusion-limited redox reaction, the rate of charge transfer reactions, namely the current (i_d), is proportional to the square root of the scan rate (v) according to Eq. (2) [11].

$$i_d = 0.495FCA \left(\frac{D\alpha nFv}{RT} \right)^{\frac{1}{2}} \quad (2)$$

$$i_d = k_d v^{0.5} \quad (3)$$

where C is the concentration of charge carriers in the accumulation layer, α is the charge transfer coefficient, D is the diffusion coefficient of the charge carrier inside the electrode materials, n is the number of electrons involved in the Faradaic reaction, A is the surface area of the electrode materials, F is Faraday's constant, R is the molar gas constant, and T is the temperature. Eq. (2) can be further simplified to a form shown in Eq. (3) when all the reaction conditions are fixed except the scan rate.

On the other hand, the capacitive current (i_c) from EDL capacitance and pseudocapacitance has a linear dependence on the scan rate according to Eq. (4):

$$i_c = AC_c v \quad (4)$$

$$i_c = k_c v \quad (5)$$

where C_c is the capacitance from capacitive process and A is a constant. Eq. (4) can be further simplified to a form shown in Eq. (5) when all the reaction conditions are fixed except the scan rate.

Accordingly, the overall current at a given potential can be express as the sum of two separate charge storage mechanisms, that is capacitive current and kinetic current as shown in Eq. (6). Therefore, at higher scan rates, the overall current is dominated by capacitive current (i_c), due to its stronger linear dependence on scan rates shown in Eq. (6), whereas the overall current is dominated by diffusion-limited kinetic current (i_d) at lower scan rates. In this context, the overall current (i_{total}) is usually described by a simple power law as shown in Eq. (7).

$$i_{total} = i_c + i_d = k_c v + k_d v^{0.5} \quad (6)$$

$$i_{total} = a v^b \quad (7)$$

where a is an adjustable parameter and b is a variable heavily dependent on the relative contribution from i_c or i_d . It is apparent that the value of b is equal to either 0.5 or 1 when the overall currents are strictly dominated by capacitive (i_c) or kinetic (i_d) current, respectively.

Figure 3 shows the electrokinetic analysis of aqueous K-ion storage within vanadium oxide nanostructures using cyclic voltammetry (CV) measurements in a three-electrode half-cell with a 1 M KCl electrolyte, where the b -values of the peaks in all three of the color shadowed sections of the anodic and cathodic scans are plotted. In the potential range from -0.1 to 0.3 V (gray region in **Figure 3a**) the K-ion storage in the vanadium oxide is dominated by a diffusion-limited redox process as the b -values for the anodic and cathodic scans are close to 0.5 ($b_{anodic} = 0.44$, $b_{cathodic} = 0.69$). In the potential range from 0.7 to 0.9 V (red region in **Figure 3a**) the charge storage process is controlled by surface-related capacitive process because the b -values for the anodic and cathodic scans are very close to 1.0 ($b_{anodic} = 0.95$, $b_{cathodic} = 0.99$). While in the potential range from 0.3 to 0.7 V (blue region in **Figure 3a**) both the surface-controlled capacitive and diffusion-limited redox processes contribute to the charge storage as the b -values for the anodic and cathodic scans are between 0.5 and 1.0 ($b_{anodic} = 0.81$, $b_{cathodic} = 0.87$). The electrokinetic analysis suggests that charge storage of the vanadium oxide nanostructures benefits from both capacitive and diffusion-limited redox processes. The former process allows the high rate performance and the latter allows the high capacity performance of K-ion storage in the vanadium oxide nanostructures. The contribution of capacitive process (double-layer capacitance and/or pseudo-capacitance) and diffusion-limited redox process to the overall capacity can be quantified with the infinite sweep rate extrapolation, as shown in **Figure 3c**. For example, at a scan rate of 5 mV s^{-1} , 46% of the total capacity is attributed to capacitive process, whereas 93% of the total capacity is attributed to capacitive process at 200 mV s^{-1} .

Moreover, after rearranging Eq. (7) into Eq. (8), the values of k_c and k_d can be determined by the slope and intercepts of the resulting linear function via plotting $i/v^{0.5}$ as a function of $v^{0.5}$ at

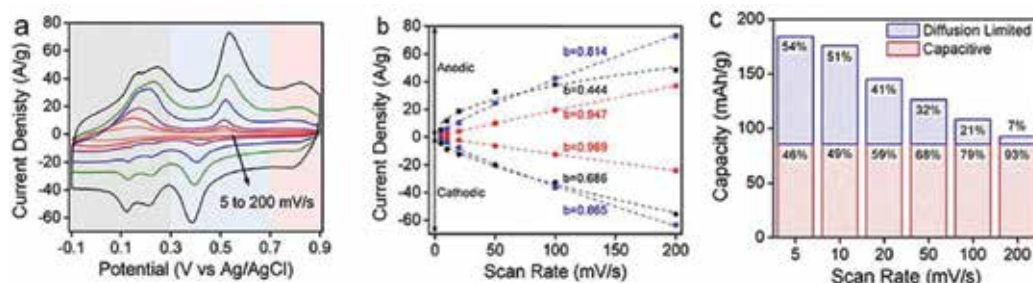


Figure 3. Electrokinetics analysis (b -values) of K-ion storage within the vanadium oxide nanostructures. (a) Cyclic voltammograms at various scan rates. (b) The calculated b values during the anodic and cathodic scans. (c) A stacked bar graph showing the percent of total capacitance coming from the diffusion limited and capacitive contributions.

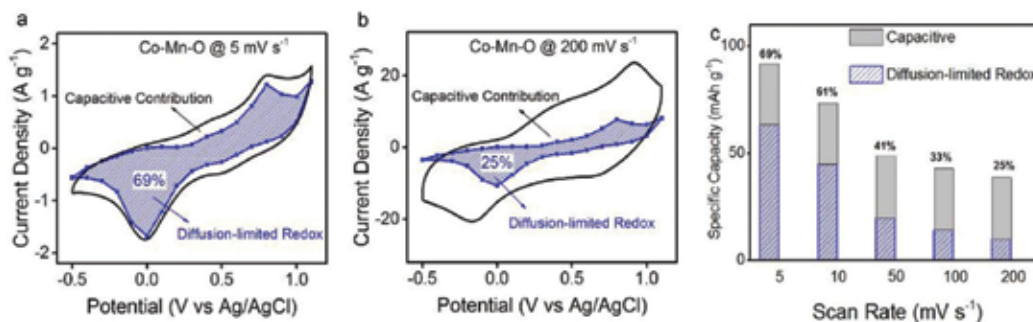


Figure 4. Electrokinetics analysis (k_c and k_d values) of Na-ion storage within the manganese oxide materials. CV current responses of the manganese oxide material are shown at the scan rates of (a) 5 mV s⁻¹ and (b) 200 mV s⁻¹. The total current (black line) is obtained experimentally and the diffusion-limited redox current (blue dot line with shadow) is calculated; (c) a stacked bar graph showing diffusion-limited redox capacity and capacitive capacity contribution of the manganese oxide material as a function of scan rate from 5 to 200 mV s⁻¹ (diffusion-limited redox capacity contributions are indexed).

various scan rates at a given potential. Therefore, the current attributed to diffusion-limited redox process ($i_d = k_d v^{0.5}$) and capacitive process ($i_c = k_c v$) at each scan rate can be obtained. And thus the potential- and scan rate-dependent charge storage mechanisms (e.g., capacitive or diffusion-controlled redox) during the CV scans can be revealed.

$$i_{total}/v^{0.5} = k_c v^{0.5} + k_d \quad (8)$$

Figure 4a and **b** show the typical CV curves of the manganese oxide material at scan rates of 5 mV s⁻¹ and 200 mV s⁻¹, where the distributions of diffusion-limited redox current and capacitive current are calculated and plotted. The complete results of diffusion-limited redox and capacitive contributions of manganese oxide from 5 to 200 mV s⁻¹ can be found in **Figure 4c**. It is clear that diffusion-limited redox contributions to the overall charge storage decreased with the increasing scan rate: at low scan rate of 5 mV s⁻¹, diffusion-limited redox process contributed nearly 69% of the overall current, while it only remained 25% at high scan rate of 200 mV s⁻¹. The enhanced capacitive contribution for Na-ion storage found in the manganese oxide material can be attributed to its layered MnO₂ component, where the large interlayer distance (~0.7 nm) facilitates the transport of Na-ion during charge and discharge processes.

3. Understanding electrochemical kinetics of charge transfer process using numerical analysis

Modeling electrodes or full-cells of batteries or supercapacitors has been extensively studied [12–15]. For example, Popov and coworkers have developed a one-dimensional model to analyze the performance of a hybrid system comprised of battery and supercapacitor (based on a Sony 18650 battery and a Maxwell's 10F supercapacitor) under pulse discharge currents

[15]. The proposed model has not only successfully predicted the power-energy relationship compared with the practical experimental conditions, but also reveals the capability of the hybrid system to deliver higher energy density than the battery-alone system while operating at high power density. However, little has been done on simulating the transition of the electrochemical behavior between the battery-type and capacitor-type charge storage mechanisms. In this book chapter, we present numerical solutions for a simple model of an electrode material and discuss in detail the interplay between redox reaction and diffusion of charge carriers, as well as the effect of dependence of open-circuit-voltage on chemical composition on the overall cyclic voltammetry behavior of the electrode in a half-cell setting. We are able to show the transition from a diffusion-limited charge transfer process (battery-like electrochemical behavior) to kinetic-limited charge transfer process (capacitor-like behavior) by changing the structural and experimental conditions.

3.1. The description of the mathematical model

Figure 5 shows a schematic of a single spherical electrode material model. The following assumptions are made during the analysis:

- i. The particle is a perfect solid sphere.
- ii. The transport of charge carriers (cations) within the solid particle is only limited by diffusion, and only radial diffusion has been considered. It is also assumed that the potential gradient within the particle is negligible, and thus migration of cations does not occur.
- iii. The charge-transfer reaction is governed by the Butler-Volmer electrokinetic expression.

Therefore, the flux of charge carriers (N) within the particle can be described using Eq. (9), and mass conservation of the charge carriers in the particle can be described using Eq. (10)

$$N = -D\nabla c \quad (9)$$

$$\frac{\partial c}{\partial t} = -\nabla \cdot N \quad (10)$$

where c is the concentration of charge carriers (such as Li^+ or Na^+), D is the diffusion coefficient during the ionic transport within the particle (assumed to be a constant).

Combining Eqs. (9) and (10) gives the conservation of the charge carriers in spherical coordinates:

$$\frac{\partial c}{\partial t} = D \left(\frac{\partial^2 c}{\partial r^2} + \frac{2}{r} \frac{\partial c}{\partial r} \right) \quad (11)$$

Starting from certain discharged state with a homogenous concentration of the charge carriers (c_0) in the particle, the electrokinetics during charging (oxidation or extraction of charge carriers out of the particle) and discharging (reduction or insertion of charge carriers into the

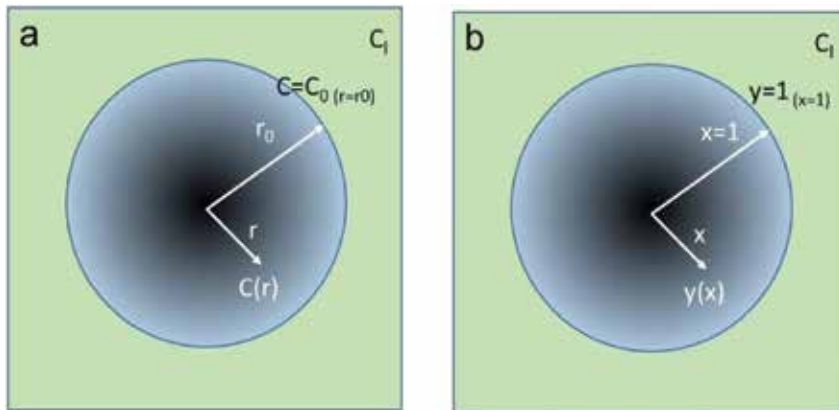


Figure 5. Schematic of a single spherical electrode material model in (a) a regular parameter denotation and (b) a dimensionless parameter denotation (when $c_0 = c_l$).

particle) processes can be described by a partial differential equation (Eq. (11)) with a set of initial condition (Eq. (12)) and boundary conditions at the surface of the particle (Eqs. (13) and (17)) and at the center of the particle (Eq. (14)):

$$c(r, t = 0) = c_0 \tag{12}$$

$$\frac{i}{F} = -D \left(\frac{\partial c}{\partial r} \Big|_{r=r_0} \right) \tag{13}$$

$$\frac{\partial c}{\partial r} \Big|_{r=0} = 0 \tag{14}$$

where i is the current density at the electrode surface and r_0 is the radius of the particle.

It is notable that the current density at the surface is also governed by the Butler-Volmer equation:

$$\frac{i}{F} = k(c_l)^{1-\beta}(c_\theta)^{1-\beta}(c_s)^\beta \left\{ \exp\left(\frac{(1-\beta)F\eta}{RT}\right) - \exp\left(-\frac{\beta F\eta}{RT}\right) \right\} \tag{15}$$

where k is a reaction rate constant, C_l is the concentration of the charge carrier in the liquid phase (assumed to be a constant in the calculation), c_θ is the surface concentration of vacant sites ready for cation intercalation, c_s is the concentration of cation on the surface of the electrode, and c_t is the concentration of total sites for seating cations ($c_\theta = c_t - c_s$). R is the gas constant, T is the temperature, and β is the symmetry factor, representing the fraction of the electrical potential used to promote the cathode reaction (β is usually considered to be 0.5). The overpotential η is defined as the difference between the applied potential (U_{app}) and the open-circuit potential of the particle (U) as shown in Eq. (16). It is assumed that U_{app} is uniform throughout the particle.

$$\eta = U_{app} - U \quad (16)$$

Combination of Eqs. (13) and (15) gives the following equation:

$$-D \left(\frac{\partial c}{\partial r} \Big|_{r=r_0} \right) = k(c_t)^{1-\beta} (c_\theta)^{1-\beta} (c_s)^\beta \left\{ \exp\left(\frac{(1-\beta)F\eta}{RT}\right) - \exp\left(-\frac{\beta F\eta}{RT}\right) \right\} \quad (17)$$

To facilitate the numerical analysis, the partial differential equation with its initial condition and boundary conditions as shown from Eqs. (11)–(17) can be transformed into dimensionless form with the following dimensionless variables:

- i. dimensionless time $\tau = \frac{tD}{r_0^2}$
- ii. dimensionless distance from the particle center $x = \frac{r}{r_0}$
- iii. dimensionless concentration $y = \frac{c}{c_t}$
- iv. dimensionless current density $j = \frac{ir_0}{FDc_t}$

Eqs. (11)–(14) then become following expressions accordingly:

$$\frac{\partial y}{\partial \tau} = \frac{\partial^2 y}{\partial x^2} + \frac{2}{x} \frac{\partial y}{\partial x} \quad (18)$$

$$y(x, 0) = 1 \text{ (when } c_0 = c_t) \quad (19)$$

$$j = - \left(\frac{\partial y}{\partial x} \Big|_{x=1} \right) \quad (20)$$

$$\frac{\partial y}{\partial x} \Big|_{x=0} = 0 \quad (21)$$

Eq. (19) is applicable only when ($c_0 = c_t$), while here we assume c_0 is lower but near c_t ($y < 1$) and the electrochemical process starts from the oxidation of the particles (extraction of charge carriers from the solid particles as shown in the forward direction in Eq. (1)), Eq. (17) then becomes:

$$\frac{\partial y}{\partial x} \Big|_{x=1} + a(y|_{x=1})^\beta (1 - y|_{x=1})^{1-\beta} \left\{ \exp\left(\frac{(1-\beta)F(U_{app} - U)}{RT}\right) - \exp\left(-\frac{\beta F(U_{app} - U)}{RT}\right) \right\} = 0 \quad (22)$$

where $y|_{x=1} = c_s/c_t$ and $a = \frac{kr_0c_t^{1-\beta}}{D}$.

Under potentiodynamic simulation, the applied potential changes linearly with time

$$U_{app} = U_0 + vt \quad (23)$$

where U_0 is the initial applied potential, v is the potential sweep rate.

Eqs. (18)–(23) can be solved with a partial differential equation solver PDE2D using the parameters listed in **Table 1**.

3.2. The influence of open-circuit voltage on the electrochemical behavior

From the numerical analysis, we have found that the value of the OCV of the particles at different concentration of the charge carriers strongly affects the shape of the CV, and therefore the entire charge storage mechanism. In this study, two different open-circuit voltage (OCV) expressions (as a function of the concentration of the charge carrier in the particle) are used as shown in **Figure 6**. They include (i) the simplified OCV of a capacitor material (**Figure 6a**), where the OCV linearly decreases with increasing concentration of charge carrier within the particle; (ii) the simplified OCV of a Li-ion battery material during phase transition (**Figure 6b**), where OCV of the particle is nearly independent of the charge carrier concentration within the particle for most of the composition range.

Considering one-electron transfer and the insertion of the charge carrier into the solid spherical particles occurs as shown in Eq. (24).



We assume that the conversion of MO_x into MCO_x is a one-phase reaction, where MO_x and MCO_x have a similar solid-solution type structure, analogous to proton intercalation into RuO_2 materials. The degrees of freedom can be calculated by the Gibbs phase rule:

$$F = C - P + 2 \quad (25)$$

where F is the degree of freedom, which is the number of thermodynamic parameters necessary for defining a system, C is the number of components, and P is the number of phases. For the reaction shown in Eq. (24), the system has two components ($C = 2$) including the charge carriers (C^+) and the host particle (MO_x), the degree of freedom is equal to 3 ($F = 2 - 1 + 2 = 3$). Beside the two intensive parameters, usually pressure and temperature, there is one additional degree of freedom that needs to be specified for the system. Thus, the chemical potential of the electrode (or OCV) has to be a function of temperature, pressure, and composition (the concentration of the charge carriers in the particle). Once composition changes (as the last degree

D ($\text{cm}^2 \text{s}^{-1}$)	10^{-9}
β	0.5
c_i (mol dm^3)	1.0
r_0 (cm)	5×10^{-4}
K ($\text{cm}^{5/2} \text{s}^{-1} \text{mol}^{-1/2}$)	6.3×10^{-5}
V (V s^{-1})	10^{-4}
a (dimensionless)	1

Table 1. Parameters set for the calculation.

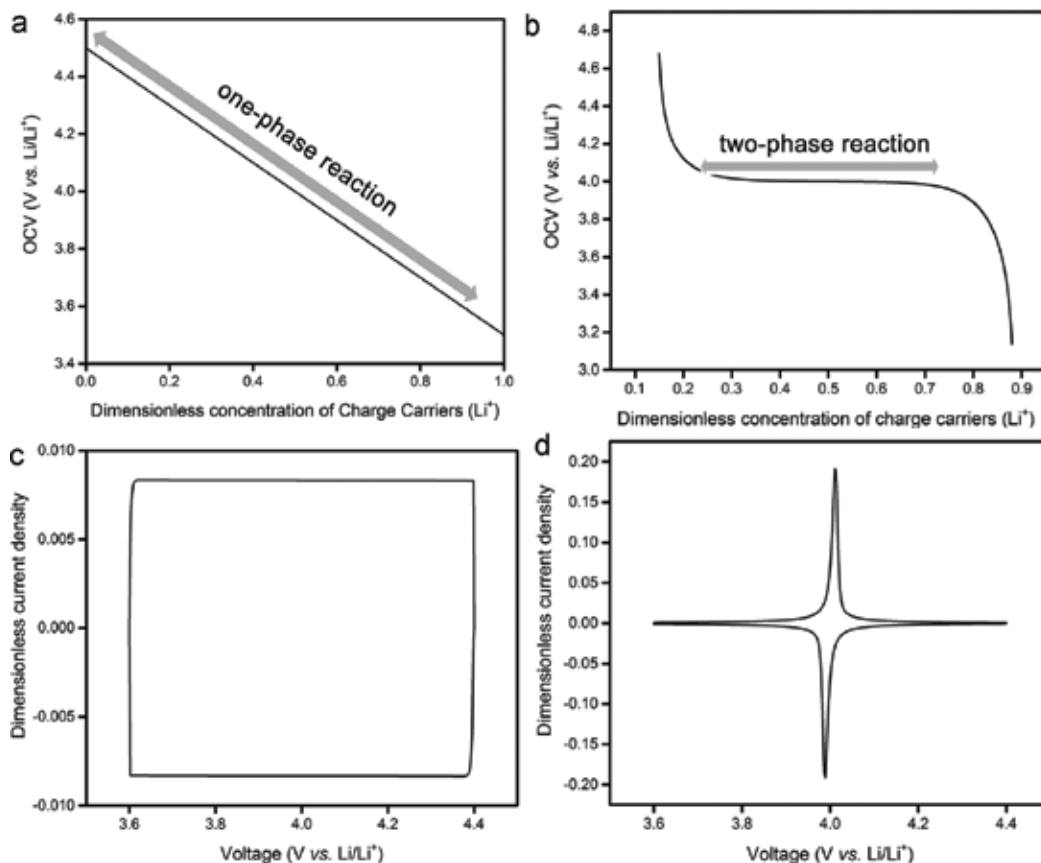


Figure 6. Simulated open-circuit-voltage (OCV) as a function of concentration of charge carrier (Li⁺) in (a) one-phase reaction and (b) two-phase reaction, and (c and d) their corresponding CVs curves.

of freedom), the OCV of the host particle changes accordingly at fixed temperature and pressure, as shown in **Figure 6b**. Therefore, in the one-phase discharge reaction (Eq. (24)), the voltage changes linearly with the concentration of the charge carriers.

As C⁺ continuously inserts into MCO_x, the further reduction of M cation eventually leads to the formation of new M-containing species (now it becomes a two-phase reaction), resulting in a new degree of freedom of 2 ($F = 2 - 2 + 2 = 2$). For a fixed pressure and temperature, there is no more independent degree of freedom left and all the thermodynamic functions including OCV should remain constant once the composition changes. Therefore, as shown in **Figure 6a** in the two-phase discharge reaction, the OCV is constant with the concentration of the charge carrier.

It is clear that in a two-phase reaction (**Figure 6d**), the CV curves show the distinct redox features that represent conventional battery material behavior. This is also congruent with the fact that a typical battery intercalation/deintercalation reaction is accompanied with a phase transition. On the other hand, in a one-phase reaction (**Figure 6c**), the CV curve shows a square-shaped current versus potential plot without distinct redox features. This unique CV

shape is often observed in classic EDL capacitor that uses carbon as electrode material or pseudocapacitor that uses RuO₂ as electrodes and H₂SO₄ as electrolyte. This simulation again highlights the fundamental difference between a battery material and a capacitor material: the former undergoes a phase transition upon the interaction with cation, while the latter can interact with cation without generation of a new crystalline phase.

3.3. The influence of interfacial reaction and diffusion of charge carriers on the electrochemical behavior

Parameter a is the dimensionless factor (shown in Eq. (22)) involving the concentration of the charge carriers in the liquid phase, and can be considered as the ratio of interfacial reaction rate ($kc_l^{2-\beta}$) to the diffusion rate of the charge carriers on the surface of the particle (Dc_l/r_0) as shown in Eq. (26).

$$a = \frac{kr_0c_l^{1-\beta}}{D} = \frac{kc_l^{2-\beta}}{Dc_l/r_0} \quad (26)$$

A large value of a indicates a faster interfacial charge-transfer kinetics and a slower diffusion of charge carrier, usually resulting from a large rate constant (k), a large particle radius (r_0) or a small diffusion coefficient (D). **Figure 7** shows the simulated CVs for various values of a at the scan rate of 0.1 mV/s, in which all the parameters described in the definition of a are fixed except the value of k . It is clear that the shapes of the CV are strongly dependent on the value of a . When the values of a increases, the peak potential of the anodic scan (oxidation reaction) shifts to lower potential values with a relatively narrower peak. Similarly, the peak potential of

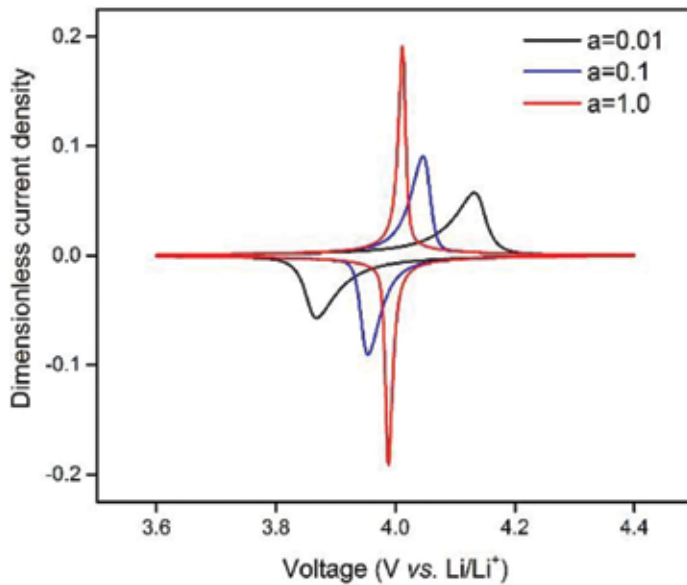


Figure 7. Simulated CV curves as a function of parameter a .

the cathodic scan (reduction reaction) shifts to higher potential values with a narrower peak. These changes strongly suggest that a large value of a reflects a fast interfacial reaction and/or a slow diffusion. Therefore, the extraction (anodic scan) and insertion (cathodic scan) of the charge carriers are limited by diffusion of charge carriers in the solid spherical particle, probably attributed to a relatively low diffusion coefficient (D) and/or a large particles size (r_0). Accordingly, at a large value of a , the solid particle behavior is closer to a battery electrode material, where diffusion-limited charge transport is the slowest step during the electrochemical process. In this context, to increase the capacitive charge transfer contribution, a smaller sized electrode and an electrolyte with cations having a higher diffusivity in the host electrode material is needed. The former points to the synthesis of nanostructured electrode material and the latter indicates Li-containing electrolyte. It is also notable that since the value of β is between 0 and 1, the value of $(1 - \beta)$ is always higher than zero. Therefore, it indicates that a low electrolyte concentration favors the contribution of capacitive process, though the overall charge storage might decrease.

Acknowledgements

This work was supported by the US Department of Energy (DOE), Office of Science, Basic Energy Sciences under Award # DE-SC0010286 (XT, FG). The work on synchrotron test is also supported by the National Science Foundation under Award #147791(FG).

Author details

Fenghua Guo, Nivedita Gupta and Xiaowei Teng*

*Address all correspondence to: xw.teng@unh.edu

Department of Chemical Engineering, University of New Hampshire, Durham, New Hampshire, USA

References

- [1] Conway BE. Transition from supercapacitor to battery behavior in electrochemical energy-storage. *Journal of the Electrochemical Society*. 1991;**138**:1539-1548
- [2] Burke A. Ultracapacitor technologies and application in hybrid and electric vehicles. *International Journal of Energy Research*. 2010;**34**:133-151
- [3] Turner JA. A realizable renewable energy future. *Science*. 1999;**285**:687-689
- [4] Simon P, Gogotsi Y. Materials for electrochemical capacitors. *Nature Materials*. 2008;**7**: 845-854

- [5] Conway BE, Birss V, Wojtowicz J. The role and utilization of pseudocapacitance for energy storage by supercapacitors. *Journal of Power Sources*. 1997;**66**:1-14
- [6] Zheng JP, Cygan PJ, Jow TR. Hydrous ruthenium oxide as an electrode material for electrochemical capacitors. *Journal of the Electrochemical Society*. 1995;**142**:2699-2703
- [7] Wei WF, Cui XW, Chen WX, Ivey DG. Manganese oxide-based materials as electrochemical supercapacitor electrodes. *Chemical Society Reviews*. 2011;**40**:1697-1721
- [8] Augustyn V et al. High-rate electrochemical energy storage through Li^+ intercalation pseudocapacitance. *Nature Materials*. 2013;**12**:518-522
- [9] Arico AS, Bruce P, Scrosati B, Tarascon JM, Van Schalkwijk W. Nanostructured materials for advanced energy conversion and storage devices. *Nature Materials*. 2005;**4**:366-377
- [10] Gogotsi Y, Simon P. True performance metrics in electrochemical energy storage. *Science*. 2011;**334**:917-918. DOI: 10.1126/science.1213003
- [11] Conway BE. *Electrochemical Supercapacitor: Scientific Fundamental and Technological Applications*. Kluwer Academic/Plenum Publisher; 1999
- [12] Zhang D, Popov BN, White RE. Modeling lithium intercalation of a single spinel particle under potentiodynamic control. *Journal of the Electrochemical Society*. 2000;**147**:831-838
- [13] Chandrasekaran R, Magasinski A, Yushin G, Fuller TF. Analysis of lithium insertion/deinsertion in a silicon electrode particle at room temperature. *Journal of the Electrochemical Society*. 2010;**157**:A1139-A1151
- [14] Doyle M, Newman J, Gozdz AS, Schmutz CN, Tarascon JM. Comparison of modeling predictions with experimental data from plastic lithium ion cells. *Journal of the Electrochemical Society*. 1996;**143**:1890-1902
- [15] Sikha G, White RE, Popov BN. A mathematical model for a lithium-ion battery/electrochemical capacitor hybrid system. *Journal of the Electrochemical Society*. 2005;**152**:A1682-A1693

Direct Laser Writing of Supercapacitors

Litty V. Thekkekara

Additional information is available at the end of the chapter

<http://dx.doi.org/10.5772/intechopen.73000>

Abstract

Direct laser writing is a single-step fabrication technique for the micro and nanostructures even below the sub-diffraction limits. In recent times, the technique is adapted to the fabrication of on-chip energy storages with additional features of flexibility and stretchability. The major category of the energy storages taken into consideration for laser writing belongs to the family of supercapacitors which is known for the high rate of charge transfer, longer life spans and lesser charging times in comparison with traditional batteries. The technology explores the possibilities of non-explosive all solid-state energy storage integration with portable and wearable applications. These features can enable the development of self-powered autonomous devices, vehicles and self-reliant infrastructures. In this chapter, we discuss the progress, challenges and perspectives of micro-supercapacitors fabricated using direct laser writing.

Keywords: direct laser writing, nanomaterials, on-chip supercapacitors, flexible

1. Introduction

The rapid technological advancements in this era demand the provision of electricity for the maintenance. In addition, the household requirements for the electricity are also in its peak of demand. The current energy resources like coal and oil are irreversible and depleting at a faster rate. On the other hand, the developments of renewable energy resources like solar and wind energies are limited by the intermittent nature and it demands the provision of energy storages to be accompanied which leads to the high cost of the resulting commercial energy modules resulting in a less attractiveness in the market. In addition, the disposal issues generated by the energy storages like traditional batteries are a major concern for the environment. On the other hand, green on-chip energy storages offer an efficient, cost-effective platform for integrated miniaturized devices, energy-harvesting, self-reliant residential and commercial buildings.

Micro-supercapacitors (MSCs) are a recent addition to the environmentally friendly energy storages with higher charge-discharge transfer rates on the contrary to traditional batteries [1]. The batteries whose lifetime is restricted due to the involvement of electrochemical redox reaction create the issues of additional storage and disposal space where MSCs which can be fabricated on any substrates utilize the electrostatic interactions of electrode-electrolyte materials.

The performance of MSC is determined by the available active electrode material and the voltage window of the electrolyte [2]. Based on the electrode-electrolyte interactions, the supercapacitors are divided into three major types: (i) electrochemical double layer capacitor (EDLC), (ii) pseudocapacitors and (iii) hybrid supercapacitors. EDLC works based on the electrostatic interaction between electrode and electrolyte ions where pseudocapacitors involve the redox reaction between electrodes and electrolyte ions similar to the batteries. A strong pseudocapacitance is not desirable in many applications due to the slow response time and high capacitance decay rate [3]. Hybrid supercapacitors combine the EDLC and pseudocapacitance effects in the performance which can be used to compensate the drawbacks of current commercial supercapacitors to become a replacement for the batteries.

Several methods are used for the fabrication of various kind of supercapacitors. The main categories are chemical techniques based on the nanomaterials [4] and electron beam lithography (EBL) [5]. The lesser integrability for flexible applications and cost involved in the fabrication of these techniques make them less desirable for industrial scale production of commercial applications. The recent reports on the use of direct laser writing (DLW) technique for the supercapacitor fabrication [6] is a fast and reliable single-step method with the possible integration of all substrates.

2. Direct laser writing

The DLW method mainly uses an ultrafast laser (femtosecond, fs or picosecond, ps lasers) [7] but recently continuous wave (cw) lasers are also used for specific materials [8]. The laser

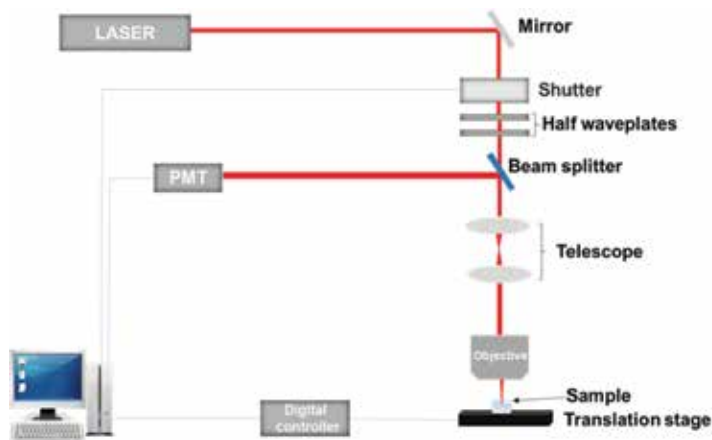


Figure 1. Schematic of direct laser writing setup.

source is tightly focused to a diffraction limited focal spot, using an objective made of different numerical apertures (NAs) forming a high intensity of laser beam. The transparency at the wavelength and spot size uniformity of the used laser beam as well as the sample uniformity is highly necessary to obtain good quality structures. However, due to the high-intensity generation from the tight focusing conditions, the non-linear process is triggered at the focal spot, which can lead to the photo-polymerization [9], microexplosion [10], photoreduction [11] and micro-machining process [12] in the material leaving remaining area unmodified. The sample moves with the help of three-dimensional (3D) translation stage according to the pre-programmed pattern design. The schematic of the DLW setup is given in **Figure 1**.

3. Direct laser writing of micro-supercapacitors

In the following sections, a detailed understanding of the DLW process on various electrode materials for MSCs is discussed.

3.1. Electrode materials

The electrodes of MSC require high active surface area, long-term stability, resistance to electrochemical oxidation or reduction, the capability of multiple cycling materials, optimum pore size distribution, minimized ohmic resistance with the contacts, sufficient electrode-electrolyte solution contact interface, mechanical integrity and less self-discharge [1].

3.1.1. Laser-scribed graphene and its derivatives

Materials such as carbon and its derivatives like porous activated carbon, carbon nanotubes, carbon aerogels or carbon-metal composites have a higher surface area of 100–220 m² g⁻¹ and they exhibit excellent stability but limited capacitance [4]. For activated carbons, only about 10–20% of the theoretical capacitance can be achieved due to the micropores that are inaccessible by the electrolyte [13]. The carbon nanotubes do not exhibit satisfactory capacitance unless a conducting polymer [14] is used to form a pseudocapacitance.

Graphene is a form of carbon with the high surface area up to 2675 m²/g and the intrinsic capacitance of 21 μF/cm², which sets the upper limit of EDLC capacitance of all carbon-based materials [15]. In addition, both faces of graphene sheets are readily accessible by the electrolyte. However, in practical applications, the surface area of graphene will be much reduced due to agglomeration.

Laser-scribed graphene (LSG), obtained from the DLW in graphene oxide (GO) material, is a cost-effective tunable alternative to graphene. The LSG films are used to fabricate MSC and other integrable applications and first reported from Ajayan's group with the use of carbon dioxide (CO₂) laser beam by adopting the design concept from capacitors [6] in 2011. This work is followed by the Kaner's group in 2012 through the production of high-performance LSG sandwich energy storages using a DVD burner [16].

Furthermore, two famous works came in the following years: The first work demonstrates the fabrication of all solid state MSCs using ionic gel electrolyte with interdigitated electrodes.

This kind of electrodes improves electrolyte ion transport that effectively improves the energy storage density and power density up to 10^{-3} Wh/cm³ and 10^1 W/cm³ (**Figure 2**) [17]. The next reported energy storage used the pre-patterned CO₂ laser irradiation on polyethylene terephthalate (PET) substrate to generate the high-quality graphene for the energy storage [18].

3.1.2. Oxides and polymers

The DLW method can be used for the fabrication of pseudocapacitors using different materials like ruthenium oxide (RuO₂) and manganese dioxide (MnO₂) and conductive polymers like polyaniline (PANI) with the LSG material becomes a direction of interest to achieve the high-performance MSCs in the given area [19]. For example, the hybrid of ultrathin MSCs made of MnO₂ sheets and graphene sheets using DLW offers an electrochemically active surface for fast absorption/desorption of electrolyte ions [20]. The contributions of additional interfaces at the hybridized interlayer areas to accelerate charge transport during charge/discharge process result in an energy density and power density of 2.4 mWh/cm³ and 298 mW/cm³, respectively.

3.1.3. Porous gold

The recent development of the well-connected nanoporous gold film using DLW is used in the fabrication of interdigital electrode materials for MSCs with high mechanical flexibility [21]. These MSCs exhibit a capacitance of 127 F cm⁻³ and energy density of 0.045 Wh cm⁻³. The gold metal is known for its high electrical conductivity and the concept adopted can be used efficiently to integrate with devices in lesser areal footprints (**Figure 3**).

The high-performance integrable MSCs fabricated using DLW which can be integrated with all platforms can be the future of energy storages.

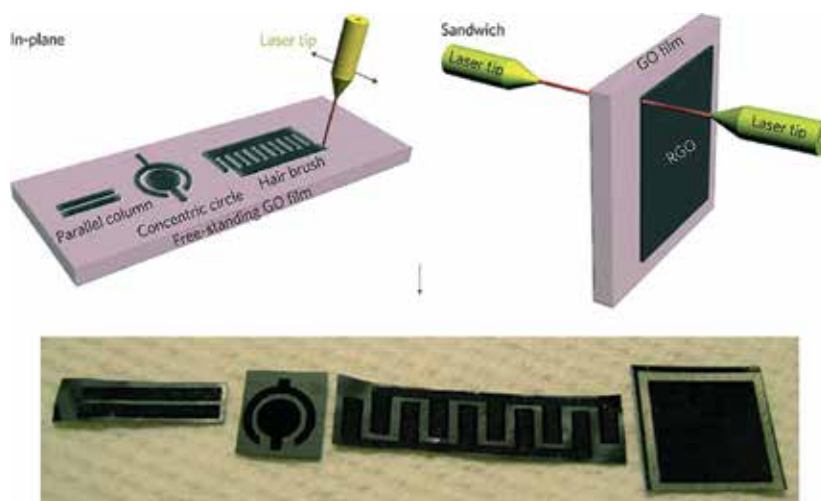


Figure 2. Direct laser writing of MSC. Reproduced with permission [6]. Copyright 2011, Nature Publishing Group.

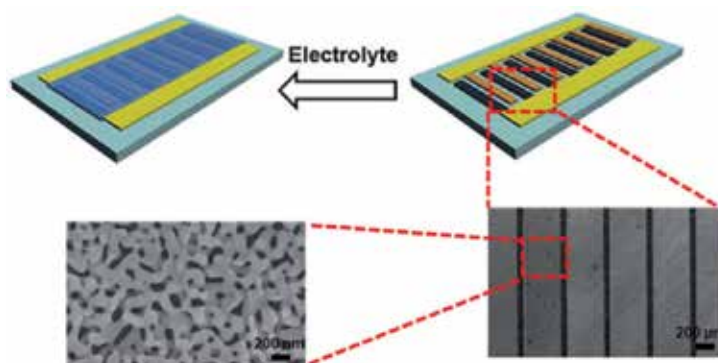


Figure 3. Direct laser writing for the fabrication of nanoporous gold film electrodes coated with MnO_2 [21]. Copyright 2016, Royal Society of Chemistry.

3.2. Matrix-assisted pulsed laser evaporation direct write (MAPLE-DW)

MAPLE-DW involves the laser forwarded transfer of liquid transfer matrix (transfer vehicle), which is composed of material to be deposited on the substrate below. A relatively flat and uniform film is achieved with the presence of liquid without the need for high temperature or post-processing involved in the lithographic techniques [22]. Pseudocapacitors from $\text{RuO}_2 \cdot 0.5 \text{H}_2\text{O}$ with the sulfuric acid as transfer vehicle result in an ideal capacitor behavior instead of the contamination generated from the transfer vehicles [23]. Moreover, the obtained specific (volumetric) capacitance of 720 F/g is comparable to the other laser-printed MSCs (**Figure 4**).

3.3. Parameter calculation

Generally, DLW-MS performance is calculated in specific (volumetric) and areal capacitance in metric quantity rather than the mass of the obtained electrodes due to the presence of significantly low volumes.

In brief, the specific capacitance was calculated from galvanostatic (CC) curves at different current densities by the formula:

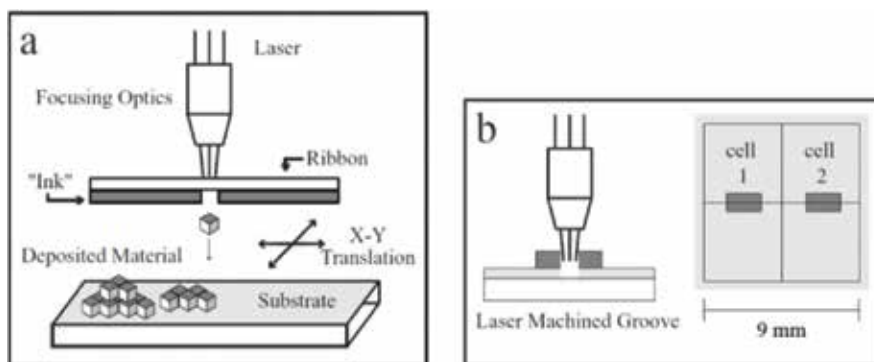


Figure 4. MAPLE-DW method for the fabrication of MSC. (a) Schematic of MAPLE-DW apparatus showing the method of forward laser transfer of an “ink” layer (b) Sample geometry: the two pseudocapacitors cells are 1 mm × 2 mm × 10 μm prior to laser machining [23]. Copyright 2002, SPIE Publishing Group.

$$C_{device} = i / \{-dV/dt\} \quad (1)$$

where i is the applied current (in amps, A) and dV/dt is the slope of the discharge curve (in volts per second, V/s).

Volumetric capacitance was given by

$$C_{vol} = C_{device} / V \quad (2)$$

where A and V refer to the area (cm^2) and volume (cm^3), respectively.

The power density of the device is calculated from galvanostatic curves at different charge/discharge densities and given by the formula:

$$P = (\Delta E)^2 / 4 R_{ESR} V \quad (3)$$

where P is the power in W/cm^3 , ΔE is the operating voltage window and R_{ESR} is the internal resistance of the device and can be given by the formula:

The energy density of the device can be calculated by the formula:

$$E = Cv * (\Delta E)^2 / (2 * 3600) \quad (4)$$

where E is the energy density in Wh/cm^3 , Cv is the volumetric capacitance and ΔE is the operating voltage window, V.

4. Challenges and perspectives

4.1. Electrode designs

The current energy storage devices are usually too heavy, rigid and bulky to match the requirements of flexible electronics [1]. Therefore, there is keen interest in the development of the light, elastic and mechanical properties with shape conformability in the next generation of energy storages. However, the bottleneck issues faced by the current MSCs are the lesser surface area of the electrode material and the more substantial mean ionic path of the electrolyte ions due to the diffraction-limited spatial resolution of the laser beam used for the preparation of electrode materials [24].

The first generation of MSCs is mainly involved in the 2D planar designs. However, these planar 2D electrodes are limited in the amount of energy storage capacities; on the other hand, increasing the thickness of the electrodes results in the low transportation of the electrolyte ions, which limits the rate transfer capabilities. The issue is initially addressed by Gao et al. where a variety of on-chip designs are tested to obtain an optimized design concept for the self-powering on-chip applications, and the interdigital electrode designs seem to be out-performing the other designs [6].

However, the fast growth of technologies like the flexible MEMS or self-reliant buildings demands the high-performance on-chip energy storages.

4.1.1. Fractal designs

New electrode designs can be a possible solution to improve the energy density of MSCs, and an example is the origami designs utilized in the flexible energy storages and electronics [25]. In the case of integrable energy storages using DLW, a better choice can be biomimetic designs [26]. The *Fern Leafs* is an efficient platform for energy storage in biological processes such as photosynthesis enabled by water transport on its vein density [27] as well as information compression [28]. The biomimetic structures inspired by the internal structure of *American Fern* (*Polystichum munitum*), which is also known as the *Barnsley fractals* [29], are a possible design for the enhancement of the active electrode material loading per unit area using DLW [30]. American fern leaves with self-repeating patterns of internal structure resemble the fractal design family known as *space-filling curves* [31].

From the comparison between the various designs of the space-filling fractal family, it is found that the Hilbert space-filling designs have the highest active surface area comparing to the other designs. The resulting MSCs have an energy density of $10^{-1} \text{ Whcm}^{-3}$ without compensating the rate of charge transfer (power density) and have a flexibility up to 60° [30]. The fractal designs offer a further chance to improve the performance of MSCs and still need a detailed investigation of various fractal families (**Figure 5**).

4.1.2. Three-dimensional micro-supercapacitors

Printing of high-performance MSCs in lesser footprints is possible with the development of three-dimensional (3D) MSCs. In 2015, Tour's group demonstrated the concept of the layer by layer stacking of individual laser-induced graphene (LIG) MSCs obtained from the PET sheets, which result in an areal capacitance of $>9 \text{ mF/cm}^2$ as shown in **Figure 6** [32] and can be considered for the ultra-portable and flexible application levels. In addition, reports of using multilayer structures made of rGO/Au particles [33] and LIG from polyamides using femto-second laser reduction with improved spatial resolution are promising directions for the 3D energy storages [34] (**Table 1**).

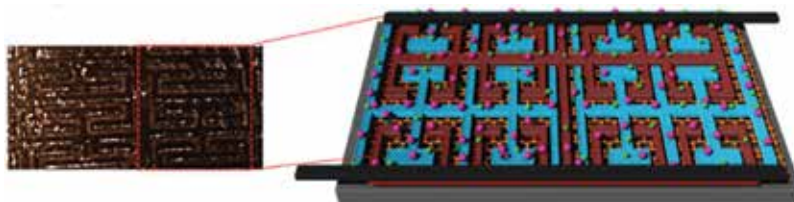


Figure 5. Fractal MSC [30]. Copyright 2017, Nature Publishing Group.

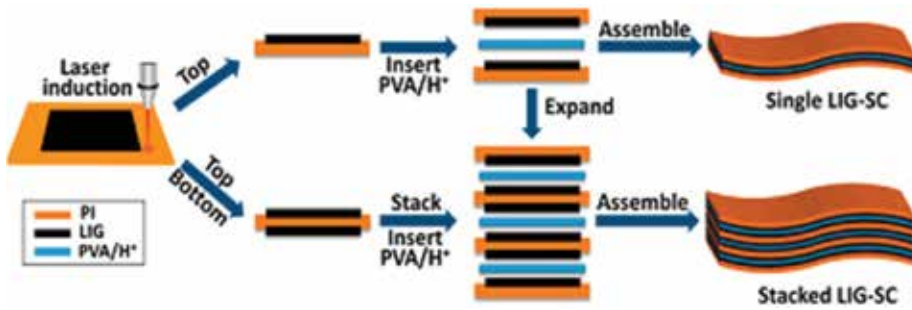


Figure 6. Stackable laser-scribed supercapacitors obtained using the direct laser writing in PET substrate [32]. Copyright 2015, ACS Publishing Group.

	Material	Methods	Properties
Ajayan [6]	Hydrated graphene oxide films	Direct laser writing (cw)	Specific capacitance of 5 mF/cm ² in water
Kaner [16]	Graphene oxide	Direct laser writing (cw)	Energy density- 10 ⁻² Whcm ⁻³
Kaner [17]	Graphene oxide	Direct laser writing (cw)	Power density of 200 W cm ⁻³ at 10,000 cycles in PVA-sulfuric acid
Tour [18]	Polymer	Direct laser writing (μ s)	BMIM-BF ₄ electrolyte with a specific capacitance of >4 mF cm ⁻² and power densities ~ 9 mWcm ⁻²
Hu [33]	Graphene oxide/gold nanoparticle	Direct laser writing (fs)	PVA/ H ₂ SO ₄ electrolyte with specific capacitance of 0.77 mFcm ⁻²
Gu [30]	Graphene oxide	Direct laser writing (cw)	with specific capacitance of 350 mFcm ⁻²
Hu [34]	Multilayer polymer	Direct laser writing (fs)	With a specific capacitance of 42 mFcm ⁻²

Table 1. Summary of the graphene supercapacitors fabricated using direct laser writing.

5. Electrolytes

The electrolyte has a significant role in determining other essential properties such as the energy density, power density, internal resistance, rate performance, operating temperature range, cycling lifetime, self-discharge, non-volatile nature and toxicity of the energy storage. The electrochemical range of an electrolyte decides the cell voltage window of the energy storages like the batteries and supercapacitors [9] as shown in the equation,

$$E = 1/2 CV \quad (5)$$

where E is the energy density, C is the specific capacitance and V is the cell voltage.

So far, the electrolytes used in an energy storage can be classified as liquid electrolytes and solid/quasi-solid state electrolytes [35]. Liquid electrolytes can be further grouped as aqueous electrolytes with a voltage range of 1.0–1.3 V, organic electrolytes within the voltage range of

1–2 V and ionic liquids (ILs) with a voltage range of 3.5–4.0 V. The solid or quasi-solid state electrolytes can be classified as organic and inorganic electrolytes with a voltage range of 2.5–2.7 V.

Among different electrolytes, aqueous ones possess high conductivity and capacitance but are limited by low cell voltage window, whereas organic and IL electrolytes can operate at higher cell voltage windows [36]. ILs are widely used in the energy storages owing to their attractive properties like the non-flammability, low vapor pressure and large operating potential window. Solid state electrolytes are devoid of leakage issues but are limited by the low conductivity.

6. Scale-up process of micro-supercapacitors

The considerable advantage of the DLW-MS is the possibility of large-scale production with the industrial grade. However, the scale-up process might introduce the difficulties of heat, enhancement of effective series resistance (ESR) and overcharge [1]. In addition, the cost of the process needs to be compatible to the existing battery technology. DLW technique due to its straight single-step process, which combines with the efficient tuning of nanomaterials, can provide an efficient solution to the issue in long term. The successful generation of high-performance MSCs will enable a step closer to the biocompatible light-weight portable and wearable devices as well as the replacement of large area spaces required for the energy storages.

7. Integration with applications

The self-powered autonomous systems will be the future direction with impact in large areas of technologies by the inclusion of additional features like portability, flexibility and stretchability. One of the integrated DLW-MS with existing renewable technology is discussed below.

7.1. Solar energy storages

Self-powered electronics and buildings, which utilize the renewable energy resources like solar energy, provide a green platform for the next-generation technology and find applications in skyscrapers, flexible, wearable, consumable and portable devices [37]. The primary issue faced by the renewable energies to be considered as the major electricity source such as the intermittent nature which limits the use of those energies during certain climatic conditions or in the remote areas which are isolated from the grid line electricity [38]. The current solar modules used to be accompanied by the energy storages in the commercial market are the traditional batteries, which intake almost 30% of the total cost of the solar module. In addition, the protective storage space for the energy storages becomes a significant issue when it comes to large-scale applications.

An integrated on-chip solar energy storages, which can be simultaneously charged using the solar electricity, can be a possible solution for the problem and energy stored can be used during the required times irrespective of the intermittent solar energy. However, the primary challenge for the integrated solar energy storage is to design the cell structure by incorporating both photoelectric and storage functions. The initial efforts are oriented around co-operating

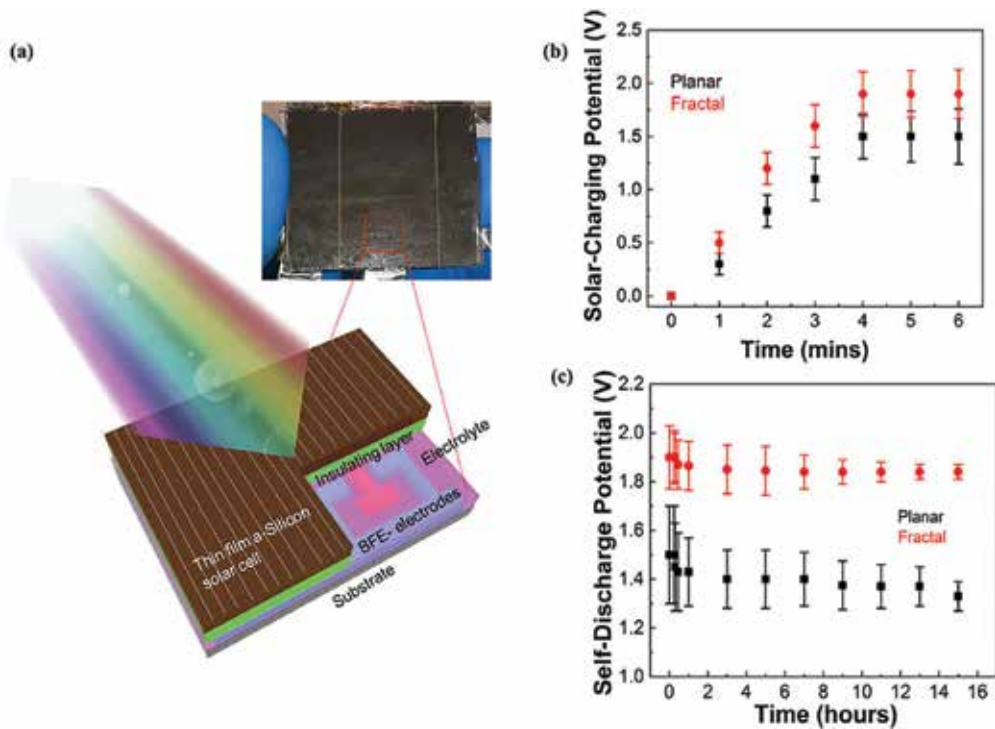


Figure 7. Solar energy storages using fractal electrodes on the reverse side of thin-film silicon solar cells [30]. Copyright 2017, Nature Publishing Group.

both photoelectric and storage functions in a single cell structure [39]. Due to the repeated oxidations and reductions shorten the lifetime of these batteries [1] and chemical storage functions in a single cell structure. The repeated oxidations and reductions shorten the lifetime of these batteries. The energy storages with storage mechanism free from electrochemical reactions as in batteries like capacitors can be a competent way of overcoming the problem.

In order to solve the issues, we developed solar energy storages using LSG electrodes in the interdigital form [40] as well as the fractal electrode designs (Figure 7) [30] and integrated on the reverse side of the silicon solar cells. The performance of the obtained solar energy storages is influenced by the efficiency of the solar cells and the discharge time for the output voltage is up to 22 days with excellent charge-discharge cycles of around 800.

8. Conclusions and future trends

Laser beam-material interactions induce the controlled changes in the physical and chemical properties of the electrode materials for MSCs. In addition, the smaller spatial resolution obtained using the tightly controlled focus spot can lead to the enhancement of specific volume load per unit area resulting in efficient storage of electrolyte ions within the layers of the electrodes. The desired electrode patterns fabricated using the writing process enable the supercapacitor features to be included in any substrates with the proper choice of electrolytes.

The improvement of further energy density obtained in laser-scribed supercapacitors using advanced techniques like super-resolution fabrication [41] along with the implementation of multifocal parallel array fabrication [42] can offer the fabrication in short period of time and deployment of self-powered autonomous systems in the next-generation technology like buildings, sensors, imaging, etc.

Acknowledgements

The author acknowledges the RMIT University for the financial support.

Conflict of interest

The author declares no conflict of interest.

Nomenclature

DLW	Direct laser writing
MSC	Micro-supercapacitors
fs	Femtosecond
ps	Picosecond
cw	Continuous wave
NA	Numerical aperture
EDLC	Electrochemical double layer capacitance

Author details

Litty V. Thekkekara

Address all correspondence to: littvarghese.thekkekara@rmit.edu.au

School of Science, RMIT University, Melbourne, Australia

References

- [1] Conway BE. Electrochemical supercapacitors: Scientific fundamentals and technological applications. Springer Science & Business Media. 2013. DOI: 10.1007/978-1-4757-3058-6

- [2] Winter M, Brod RJ. What are batteries, fuel cells, and supercapacitors? *Chemical Reviews*. 2004;**104**(10):4245-4270. DOI: 10.1021/cr020730k
- [3] Conway BE. Transition from “supercapacitor” to “battery” behavior in electrochemical energy storage. *Journal of the Electrochemical Society*. 1991;**138**(6):1539-1548. DOI: 10.1149/1.2085829
- [4] Wang G, Zhang L, Zhang J. A review of electrode materials for electrochemical supercapacitors. *Chemical Society Reviews*. 2012;**41**(2):797-828. DOI: 10.1039/C1CS15060J
- [5] Lobo DE, Banerjee PC, Easton CD, Majumder M. Miniaturized supercapacitors: Focused ion beam reduced graphene oxide supercapacitors with enhanced performance metrics. *Advanced Energy Materials*. 2015;**5**(19). DOI: 10.1002/aenm.201500665
- [6] Gao W, Singh N, Song L, Liu Z, Reddy ALM, Ci L, Vajtai R, Zhang Q, Wei B, Ajayan PM. Direct laser writing of micro-supercapacitors on hydrated graphite oxide films. *Nature Nanotechnology*. 2011;**6**(8):496-500. DOI: 10.1038/nnano.2011.110
- [7] Gamaly EG. *Femtosecond Laser-Matter Interaction: Theory, Experiments, and Applications*. Singapore: CRC Press; 2011
- [8] Do MT, Nguyen TTN, Li Q, Benisty H, Ledoux-Rak I, Lai ND. Submicrometer 3D structures fabrication enabled by one-photon absorption direct laser writing. *Optics Express*. 2013;**21**(18):20964-20973. DOI: 10.1364/OE.21.020964
- [9] Liska R, Ovsianikov A. *Multiphoton Lithography: Techniques, Materials, and Applications*. Weinheim: John Wiley & Sons, 2016
- [10] Misawa H, Juodkazis S. *3D Laser Microfabrication: Principles and Applications*. Weinheim: John Wiley & Sons; 2006
- [11] Zhang YL, Guo L, Xia H, Chen QD, Feng J, Sun HB. Photoreduction of graphene oxides: Methods, properties, and applications. *Advanced Optical Materials*. 2014;**2**(1):10-28. DOI: 10.1002/adom.201300317
- [12] Sugioka K, Cheng Y. *Ultrafast Laser Processing: From Micro-to Nanoscale*. Florida: CRC Press, 2013
- [13] Frackowiak E. Carbon materials for supercapacitor application. *Physical Chemistry Chemical Physics*. 2007;**9**(15):1774-1785. DOI: 10.1039/B618139M
- [14] Obreja VV. On the performance of supercapacitors with electrodes based on carbon nanotubes and carbon activated material—A review. *Physica E: Low-dimensional Systems and Nanostructures*. 2008;**40**(7):2596-2605. DOI: 10.1016/j.physe.2007.09.044
- [15] Wang Y, Shi Z, Huang Y, Ma Y, Wang C, Chen M, Chen Y. Supercapacitor devices based on graphene materials. *The Journal of Physical Chemistry C*. 2009;**113**(30):13103-13107. DOI: 10.1021/jp902214f
- [16] El-Kady MF, Strong V, Dubin S, Kaner RB. Laser scribing of high-performance and flexible graphene-based electrochemical capacitors. *Science*. 2012;**335**(6074):1326-1330. DOI: 10.1126/science.1216744

- [17] El-Kady MF, Kaner RB. Scalable fabrication of high-power graphene micro-supercapacitors for flexible and on-chip energy storage. *Nature Communications*. 2013;**4**:1475. DOI: 10.1038/ncomms2446
- [18] Lin J, Peng Z, Liu Y, Ruiz-Zepeda F, Ye R, Samuel EL, Yacaman MJ, Yakobson BI, Tour JM. Laser-induced porous graphene films from commercial polymers. *Nature Communications*. 2014;**5**:5714. DOI: 10.1038/ncomms6714
- [19] Hwang JY, El-Kady MF, Wang Y, Wang L, Shao Y, Marsh K, Ko JM, Kaner RB. 2015. Direct preparation and processing of graphene/RuO₂ nanocomposite electrodes for high-performance capacitive energy storage. *Nano Energy*. 2015;**18**:57-70. DOI: 10.1016/j.nanoen.2015.09.009
- [20] Li L, Zhang J, Peng Z, Li Y, Gao C, Ji Y, Ye R, Kim ND, Zhong Q, Yang Y, Fei H. High-performance Pseudocapacitive Microsupercapacitors from laser-induced Graphene. *Advanced Materials*. 2016;**28**(5):838-845. DOI: 10.1002/adma.201503333
- [21] Zhang C, Xiao J, Qian L, Yuan S, Wang S, Lei P. Planar integration of flexible micro-supercapacitors with ultrafast charge and discharge based on interdigital nanoporous gold electrodes on a chip. *Journal of Materials Chemistry A*. 2016;**4**(24):9502-9510. DOI: 10.1039/C6TA02219G
- [22] Morales M, Munoz-Martin D, Marquez A, Lauzurica S and Molpeceres C. *Laser-Induced Forward Transfer Techniques, and Applications. Advances in Laser Materials Processing (Second Edition)*, pp. 339-379, 2018. ISBN: 978-0-08-101252-9
- [23] Arnold C, Wartena R, Pratap B, Swider-Lyons K, Piqué A. Laser direct writing of hydrous ruthenium dioxide micro-Pseudocapacitors. *MRS Proceedings*. 2001;**698**. DOI: 10.1557/PROC-698-Q3.2.1
- [24] Stoller MD, Ruoff RS. Best practice methods for determining an electrode material's performance for ultracapacitors. *Energy & Environmental Science*. 2010;**3**:1294-1301. DOI: 10.1039/C0EE00074D
- [25] Nam I, Kim GP, Park S, Han JW, Yi J. All-solid-state, origami-type foldable supercapacitor chips with integrated series circuit analogues. *Energy & Environmental Science*. 2014;**7**(3):1095-1102. DOI: 10.1039/c3ee43175d
- [26] Bar-Cohen Y. *Biomimetics—Using nature to inspire human innovation. Bioinspiration & Biomimetics*. 2006;**1**(1):P1. DOI: 10.1088/1748-3182/1/1/P01
- [27] Zhang S-B, Sun M, Cao K-F, Hu H, Zhang J-L. Leaf photosynthetic rate of tropical ferns is evolutionarily linked to water transport capacity. *PLoS One*. 2014;**9**(1):e84682. DOI: 10.1371/journal.pone.0084682.t001
- [28] Barnsley MF, Hurd LP. *Fractal image compression*. A. K. Peters. Ltd; 1993
- [29] Barnsley MF. *Fractal everywhere*. Morgan Kaufmann Publications (1993)
- [30] Thekkekara LV, Gu M. Bioinspired fractal electrodes for solar energy storages. *Scientific Reports*. 2017;**7**:45585. DOI: 10.1038/srep45585

- [31] Jordan C. Cours d'analyse. pp. 587-594, Gauthier-Villars, Imprimeur-Libraire (1887)
- [32] Peng Z, Lin J, Ye R, Samuel EL, Tour JM. Flexible and stackable laser-induced graphene supercapacitors. *ACS Applied Materials & Interfaces*. 2015;7(5):3414-3419. DOI: 10.1021/am509065d
- [33] Li RZ, Peng R, Kihm KD, Bai S, Bridges D, Tumuluri U, Wu Z, Zhang T, Compagnini G, Feng Z and Hu A. 2016. High-rate in-plane micro-supercapacitors scribed onto photo paper using in situ femtolaser-reduced graphene oxide/Au nanoparticle microelectrodes. *Energy & Environmental Science*. 2016;9(4):1458-1467. DOI: 10.1039/C5EE03637B
- [34] Wang S, Yu Y, Ma D, Bridges D, Feng G and Hu A. High-performance hybrid supercapacitors on flexible polyimide sheets using femtosecond laser 3D writing. *Journal of Laser Applications*. 2017;29(2):022203. DOI: 10.2351/1.4983513
- [35] Zhong C, Deng Y, Hu W, Qiao J, Zhang L, Zhang J. A review of electrolyte materials and compositions for electrochemical supercapacitors. *Chemical Society Reviews*. 2015;44(21):7484-7539. DOI: 10.1039/C5CS00303B
- [36] Béguin F, Presser V, Balducci A, Frackowiak E. Carbons and electrolytes for advanced supercapacitors. *Advanced Materials*. 2014;26(14):2219-2251. DOI: 10.1002/adma.201304137
- [37] Kyeremateng NA, Brousse T, Pech D. Microsupercapacitors as miniaturized energy-storage components for on-chip electronics. *Nature Nanotechnology*. 2017;12(1):7-15
- [38] Parida B, Iniyar S, Goic R. A review of solar photovoltaic technologies. *Renewable and Sustainable Energy Reviews*. 2011;15(3):1625-1636. DOI: 10.1016/j.rser.2010.11.032
- [39] Miyasaka T, Murakami TN. The photocapacitor: An efficient self-charging capacitor for direct storage of solar energy. *Applied Physics Letters*. 2004;85(17):3932-3934. DOI: 10.1063/1.1810630
- [40] Thekkekara LV, Jia B, Zhang Y, Qiu L, Li D and Gu M. On-chip energy storage integrated with solar cells using a laser scribed graphene oxide film. *Applied Physics Letters*. 2015;107(3):031105. DOI: 10.1063/1.4927145
- [41] Ren H, Lin H, Li X, Gu M. Three-dimensional parallel recording with a Debye diffraction-limited and aberration-free volumetric multifocal array. *Optics Letters*. 2014;39(6):1621-1624. DOI: 10.1364/OL.39.001621
- [42] Gan Z, Cao Y, Evans RA, Gu M. Three-dimensional deep sub-diffraction optical beam lithography with 9 nm feature size. *Nature Communications*. 2013;4. DOI: 10.1038/ncomms3061

Toward High-Voltage/Energy Symmetric Supercapacitors via Interface Engineering

Yaqun Wang and Guoxin Zhang

Additional information is available at the end of the chapter

<http://dx.doi.org/10.5772/intechopen.73131>

Abstract

This chapter includes elaborately selected recent literatures on electrochemical energy storing in symmetric supercapacitors (SSCs) with high operating voltages (voltage >1.6 V) and high specific energy. SSCs are a typical sort of electrochemical capacitors with larger energy density than conventional capacitors; by involving electrode materials with stable interfaces (for instance, nitrogen-doped carbon materials) and electrolytes with wide safe potential window (for instance, ionic liquids), they can supply competitive energy relative to batteries. Fundamentals of SSCs are first introduced, aiming at clarifying some critical interfacial phenomena that are critical to enhance overall capacitive performance. State-of-the-art SSCs are included as demonstrations from the aspects of both enhanced capacitances and expanded voltages. We also provide a few feasible strategies for the design high-voltage/energy SSCs such as using inactive electrode materials.

Keywords: symmetric supercapacitor, electrode materials, electrochemical interface, high voltage, high energy

1. Introduction

The growing concerns over fossil fuels, in terms of global warming, pollution, and resource depletion, call for clean and renewable energy such as sunlight, wind, and hydrogen energy [1]. Consequently, great necessity has been urged regarding the development of rapid and efficient energy storage upon the generation of huge amount of the aforementioned types of energy. Supercapacitors (SCs), storing energy in or on the interfaces of electrode materials, are capable of fully charging/discharging within seconds or minutes, making them excellent candidates for the fast accumulation of these transient types of energy [2–4]. Also, taking advantage of the interfacial energy storage mechanism, unlike the deep-conversion mechanism in batteries, SCs

have excellent recyclability, typically >5000 times [5]. The past decade has witnessed significant progresses in SCs researches, many types of SCs have come to existence, including but not limited to electrochemical double-layer capacitors (EDLCs) and asymmetric supercapacitors (ASSCs), and they can be further sorted by applicable electrolytes (mainly three types electrolytes: aqueous, organic, and ionic liquid electrolytes) [2]. Still, they are not satisfactory enough from the perspectives of energy stored, which is mainly due to low capacitances or narrow potential windows especially in aqueous electrolytes [6, 7]. Coupling SCs with pseudo-capacitive electrode materials such as transition metal-based materials or electronically conductive polymers is feasible to enlarge the specific energy; however, the lifetime of pseudo-capacitors normally goes down quickly in a few hundred cycles [8, 9]. Currently, it is still very hard to simultaneously obtain large capacitance, high-operating voltage, and high-cycling stability.

Symmetric supercapacitors (SSCs), mainly including carbon-based EDLCs and a few SSCs with identical metallic component- or conductive polymer-based electrodes, supply much higher specific power and cycling stability than pseudo-capacitors, due to the interfacial charging/discharging mechanism [2, 10]. Their energy are given by the equation (1), in which E is the energy stored in capacitor cell, C_T is the total capacitance, and V is the operating voltage. E is proportional to total capacitance and square voltage, which means that specific energy E can be improved via two ways: increasing specific capacitance and expanding operating voltage [11]. Both of these aforementioned two aspects are highly related to the interfacial chemistry and phenomenon [5]. According to the electrochemical double-layer phenomenon established by Helmholtz, the electrochemical interface consists of electrode surface and thin layered electrolyte (containing ions or cations) adjacent to electrode surface. In the first place, this thin layer of electrolyte plays the fundamental roles of conducting ions and facilitating charge compensation on electrode interface; additionally, they can be decomposed or transformed to supply non-Faradaic current once charge transfer occurs when the electrons arrive in or depart from the conduction band of electrode [6]. Before that, electrolyte ions and molecules are forced to strongly absorb onto electrode surface to form a tightly packed stern layer [6, 7]. According to previous literatures, the efficiency and strength of absorption are highly depend on the surface properties of electrode materials, doping, defect, and functionality and can significantly alter the interactions between electrolyte and electrode interface [11–13]. Therefore, in order to achieve high operating voltage as well as high energy, it is critical to address the interface issues regarding both the surface properties of electrode materials and the applicable electrolytes.

$$E = 1/2C_T V^2 \quad (1)$$

In the past few decades, many review articles have discussed the investigations on materials selections and device fabrications for developing high-performance SCs, but few accounted for the interface designing and engineering. Also, research progresses from different angles (material synthesis, electrolyte selections, and device fabrications) have come to the point calling for a generic summary for improving the integrated performance of SCs on the clear understanding of electrode interfacial phenomenon. This chapter aims to present and discuss a number of relevant issues, including fundamentals of interfacial (mainly electric double layer (EDL)) capacitance, nanoscale charge transfer, discussions on a few benchmarked

SSCs with large operating voltage and specific energy, and last but not the least, feasibility of safely expanding operating voltage for the achievement of high-energy SSCs. In addition, the importance of carbonaceous electrode materials that are inactive for water splitting is highlighted, in which their specific energy can be significantly improved due to greatly expanded operating voltages. The prospects of SSCs developments are speculated based on the interface engineering on carbonaceous materials, highlighting the practical feasibilities of high-energy SSCs for the progressing smooth swing to renewable energy from traditional fossil fuels.

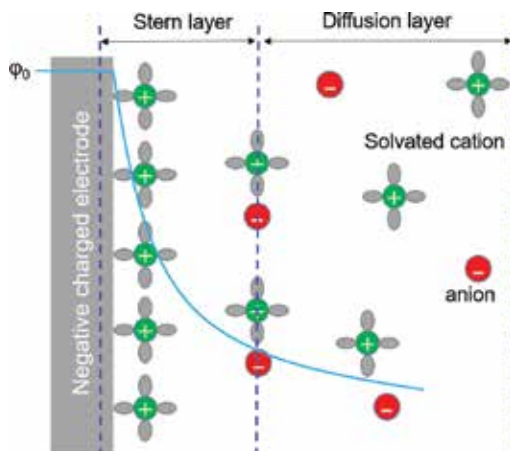
2. Basics of symmetric supercapacitors (SSCs)

Symmetric supercapacitors (SSCs) are mainly built on electrochemical double-layer configured identical positive and negative electrodes; most applicable electrode materials are carbon-based due to their high chemical stability of carbon materials [1, 14]. The electrochemical double-layer model, first established by Helmholtz, reveals that two oppositely charged ionic layers are formed at electrode-electrolyte interfaces under electrochemical forces driven. Afterward, Stern recognized that there are two regions of ion distribution at the electrode-electrolyte interfaces: one inner layer and one outer layer, as schematically depicted in **Scheme 1**. The inner region, where ions are strongly absorbed onto the electrode surface, is called the compact layer (or Stern layer); and the outer layer consists of a continuous distribution of ions in solution [10]. The capacitance at electrode-electrolyte interface (C_{EDL}) with electrochemical double-layer configuration can be divided into capacitance from the inner compact layer (C_H) and capacitance from the diffuse layer (C_{Diff}), as described in equation (2)

$$\frac{1}{C_{EDL}} = \frac{1}{C_H} + \frac{1}{C_{Diff}} \quad (2)$$

There are several critical factors that give significant impact on C_{EDL} , mainly including the conductivity of electrode material, the surface area of electrode materials, the accessibility to the inner electrochemical surface, the electric field across the electrode, and the electrolyte/solvent properties [15]. For instance, SCs with high-surface area porous carbon electrode materials (such as activated carbon) can store much more capacitances by several orders of magnitude. There are also a few other ways that are feasible to enlarge the capacitances including doping heteroatom elements and compositing stable metal oxides or conductive polymers [11, 16]. Heteroatom doping is able to break down the high symmetry of graphitic carbon, creating a large amount of defects, leading to the easy formation of compact inner absorption layer [16]. The advantages of using stable metal oxides or conductive polymers as electrochemical interfaces instead of carbon materials are obvious; they are capable of supplying much more capacitance through pseudo-capacitive absorption besides the EDL capacitance [17]. However, the greatly enlarged capacitances are often obtained on the basis of compromising the efficiency and cycling stability, and only a minor few metal oxides and conductive polymers are qualified due to conductivity and cost issues, which we will summarize later in Section 3.

Besides the electrode materials selection, it is also important to choose a proper electrolyte and solvent to form a robust electrode-electrolyte interface since energy stored in a SSCs



Scheme 1. Schematic representations of the cross-sectional EDL structure of electrode/electrolyte interface.

device is governed by the square of operating voltage multiplying capacitance, as described in equation (1). Relative to capacitance, operating voltage actually gives bigger impact on the specific energy of the whole SSCs device. Therefore, pushing the operating voltage to the limit by means of choosing proper electrolyte solution is of significant practical meanings, a robust electrode-electrolyte interface can efficiently prevent the nanoscale charge transfer at the interfaces, thus to largely expand the applicable operating voltage and to enhance the specific energy [6]. In general, electrode-electrolyte interfaces formed in ionic liquid are more stable than in organic solvents, and then in aqueous solution, which is governed by the chemical stable window of solvents [6]. Typically, the chemical stability of the abovementioned three types of electrolytes follows the sequence of ionic liquid > organic electrolyte > aqueous electrolyte. For instance, an ionic liquid electrolyte can deliver a potential window as wide as 4.0 V, while aqueous electrolyte can only supply a 1.23-V wide potential window due to water splitting at 1.23 V [18, 19]. However, in some aqueous cases, by suppressing the activity of water splitting such as in neutral electrolytes, the safe operating voltage can be largely expanded to 1.8 V [20, 21]. The operating voltage can be further enlarged by applying electrode material that has much less activity toward water splitting, leading to a 2.0-V safe operating voltage, which is clearly achieved by mediating the interface properties [22]. The discussion on interface engineering for safe voltage expansion is placed in Section 4.

3. High-capacitance electrode materials for SSCs

Symmetric supercapacitors (SSCs), as one typical sort of SCs, though are able to provide charging/discharging in several minutes, deliver incomparable capacitance as to secondary batteries (such as Li-ion battery) [23]. Therefore, it is crucial to enlarge the specific energy stored in each electrode by either optimizing existed electrode materials or developing new types of materials. For now, carbon-based materials contribute to most of electrode materials

used in SSCs due to their abundant sources, low costs, high porosity, excellent chemical stability, and conductivity [1, 13]. Considering the mechanism of energy stored in a SSC to be mainly dominated by electrical double-layer configurations, the overall performance of full SSCs is restricted below this value. Therefore, exploring high-performance electrode materials is urgent in order to achieve high-energy SSCs. There are mainly two types of commonly used materials: carbon-based materials and pseudo-capacitive materials, which we will separately describe in the following paragraphs.

3.1. Carbon-based materials

As mentioned in Section 2, EDL-configured SCs are mainly based on various kinds of carbon materials such as activated carbon (AC). In this specific part, the general ways of enlarging capacitance of carbon-based materials are first summarized via giving representative example. Generally speaking, three ways can be utilized to achieve these goals: (1) increasing the electrochemically accessible surface area (EASA), (2) creating more anchoring sites for charge carriers, and (3) involving few amounts of pseudo-capacitance on the basis of EDL capacitance [4, 15, 24]. As followed, we will give explanations on the latter two strategies; the foremost strategy of enlarging EASA is only for listing because it involves a very few interfacial chemistries, which is not our main topic here in this chapter.

The charming feature of carbon materials is mostly founded on the largely conjugated aromatic six-atom ringed carbon that create huge amount of delocalized electrons, for instance, graphene, one typical allotrope of carbon, have an ultrahigh charge carrier mobility of $200,000 \text{ cm}^2 \text{ v}^{-1} \text{ s}^{-1}$ [25]. Meanwhile, the large conjugation system of graphitized carbon intrinsically generates highly symmetric molecular structure. The superlarge conjugation system, on one hand, enables fast transportation of charge carriers and, on the other hand, leaves very few sites for ions to absorb. From this specific aspect, doping heteroatom species and creating defects in graphitic carbon lattice can significantly boost the apparent capacitance by providing more sites for ions anchoring, as depicted in **Scheme 2** [26]. In some cases, very strong chemical binding on heavily doped carbon sites can even generate charge transfer to achieve much larger capacitance [16, 27]. Therefore, if let a small proportion of conductivity sacrificed, desirably larger capacitances can be obtained via simply involving more heteroatom sites especially containing nitrogen species [11].

Activated carbons (AC) are the most commonly used electrode materials in SSCs because of their large surface areas and low costs. ACs are usually converted from carbon-rich chemicals and biomasses under the high-temperature activation of chemicals such as KOH, ZnCl_2 , and H_3PO_4 [28, 29]. Although, very high porosity is obtained, most of the heteroatom-containing functionalities and moieties are forced to be removed by the disturbance of high temperature [30]. The as-formed clean carbon surface may probably leave very limited sites that are readily to absorb ions, so the most obtainable capacitance using AC electrode materials are falling in $100\text{--}200 \text{ F g}^{-1}$. Thanks to the abundant chemistry of carbon species, most of inorganic elements can connect with carbon to break the symmetry of $\pi\text{-}\pi$ conjugation and also to include partial pseudo-capacitive sites for higher capacitance [11]. For instance, a nitrogen-doped porous carbon (N content $\sim 12 \text{ at.}\%$) reported by Huang et al. delivered an ultrahigh capacitance of 855 F g^{-1} and a high specific energy of 41 Wh kg^{-1} in aqueous electrolytes. The improvement



Scheme 2. Aromatic carbon lattices can embrace many types of heteroatom doping such as nitrogen (blue), oxygen (green), sulfur (pink), and so on. Defective carbon sites (red) that are unsaturated can also be treated as anchoring sites for ions.

mostly originates from robust redox reactions at electrochemically active nitrogen-containing sites that transform inert graphene-like layered carbon [16]. A nitrogen, sulfur-co-doped carbon fabricated by Sun et al. exhibited a very high specific capacitance of 427 F g^{-1} at 1.0 A g^{-1} and still showed an excellent capacitance of 270 F g^{-1} at superhigh current density of 100 A g^{-1} (**Figure 1**) [31]. However, the dopant content shall be controlled under an optimistic level; otherwise, the capacitance will not be increased because of severely damaged conductivity. For instance, Cheng et al. fabricated a high level of N, S, or B doping graphene, also called superdoping, achieving 29.82, 17.55, and 10.79 at% for N-, S-, and B-doping, respectively [32]. However, the 29.82 at%-N-doped graphene achieved a medium specific capacitance of 354 F g^{-1} while the pristine graphene without any doping obtained a specific capacitance of 213 F g^{-1} (taking 60% of heavily N-doped graphene).

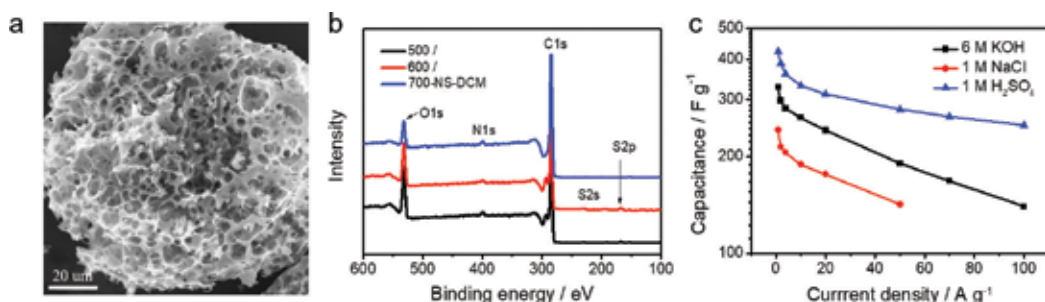


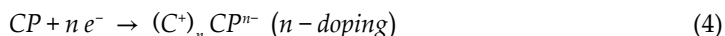
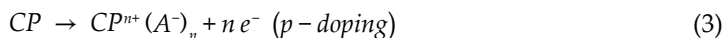
Figure 1. (a) SEM image and (b) XPS survey of NS-co-doped carbon materials. (c) Gravimetric capacitance of NS-co-doped carbon materials made SSCs in three aqueous electrolytes. Adapted with permission [31]. Copyright 2017, American Chemical Society.

3.2. Interfacial pseudo-capacitive materials

Pseudo-capacitance is achieved by Faradaic electron charge-transfer with redox reactions, intercalation or electro-sorption. Unlike electrochemical double-layer supercapacitor, pseudo-supercapacitor use electronically conducting polymers (ECPs) or stable metal oxides electrodes can achieve balanced capacitive performance of much enhanced capacitance and fairly good rate/cycling performance.

3.2.1. Electronically conducting polymers (ECPs)

ECPs are one typical sort of pseudo-capacitive materials that can engage electrochemical doping or redox reaction with anions and cations, many ECPs such as polyaniline (PANI), polypyrrole (PPy), and derivatives of polythiophene (PTh) have been widely applied in supercapacitors due to their large capacitances, flexibility, and low costs. The typical dopant level for these polymers as well as typical specific capacitances and applicable voltage ranges are given in **Table 1**. The mechanism of ECPs storing charges can be described by the following two formulas, *i.e.*, *p*-doping upon oxidization and *n*-doping upon reduction.



ECPs-made SSCs can be sorted into two categories: Type I-using the same *p*-doped ECPs for both electrodes and Type II-using the same ECPs but using different forms of ECPs as electrodes (*p*-doped form as positive electrode and *n*-doped form as negative electrode). When the Type I SSCs is charged, the positive electrode is completely oxidized while the negative electrode remains neutral, which supplies 0.5–0.75 V potential difference. When it is discharged, both electrodes are semi-oxidized, which makes only 50% of the *p*-doped capacitance can be used. In addition, the supplied potential of Type II SSCs is higher compared with Type I SSCs. This improvement would result in high specific energy due to much larger difference of square voltage (V^2).

Conducting polymer	Mw (g mol ⁻¹)	Conductivity (S cm ⁻¹)	Dopant level	Potential range (V)	Theoretical specific capacitance (F g ⁻¹)
PANI	93	0.01–5	0.5	0.7	750
PPy	67	0.3–100	0.33	0.8	620
PTh	84	2–150	0.33	0.8	485
PEDOT	142	300–500	0.33	1.2	210

Mw is molecular weight per unit monomer (g mol⁻¹) PANI is polyaniline, PPy is polypyrrole, PTh is polythiophene and PEDOT is poly (3,4-ethylenedioxythiophene).

Table 1. Theoretical specific capacitance of conducting polymers.

Many ECPs such as PANI and PPy can only be *p*-doped due to the very negative potentials required for *n*-doping, if compared with the reduction potential limit of molecular solvent-based electrolytes. For instance, Pan et al. synthesized PANI hydrogel with high surface area and three-dimensional porous nanostructures and demonstrated that the as-obtained PANI-based supercapacitor could supply a very large specific capacitance of 480 F g^{-1} , excellent rate capability, and very good cycling stability of 83% capacitance retention after 10,000 cycles but only provide a safe operating voltage of 0.8 V for SSCs. Unique three-dimensional (3D) microstructure by interconnected polymer (**Figure 2**) by Yu et al. exhibit good mechanical properties and high rate performance with specific capacitance of 400 F g^{-1} , excellent rate capability [33]. On the contrary, PTH and its derivatives can be used as *n*-doped ECPs; however, the conductivity of these ECPs after *n*-doping is not very high in the reduced state and thus leads to a low capacitance in the negative potential region [34]. For example, Stenger-smith et al. developed poly(3,4-propylenedioxythiophene) and poly(3,4-ethylenedioxythiophene) as electrode couples show good cycle life [35].

3.2.2. Transition metal oxides

Transition metal oxides show high pseudo-capacitive behavior with redox chemistry both on and in the interfaces, which have been extensively studied due to high specific capacitance. There are several commonly studied stable metal oxide materials such as RuO_2 (theoretical specific capacitance $\sim 1000 \text{ F g}^{-1}$) and MnO_2 (theoretical specific capacitance: $1100\text{--}1300 \text{ F g}^{-1}$) [36]. RuO_2 is one of the most explored electrode materials due to the high specific pseudo-capacitance,

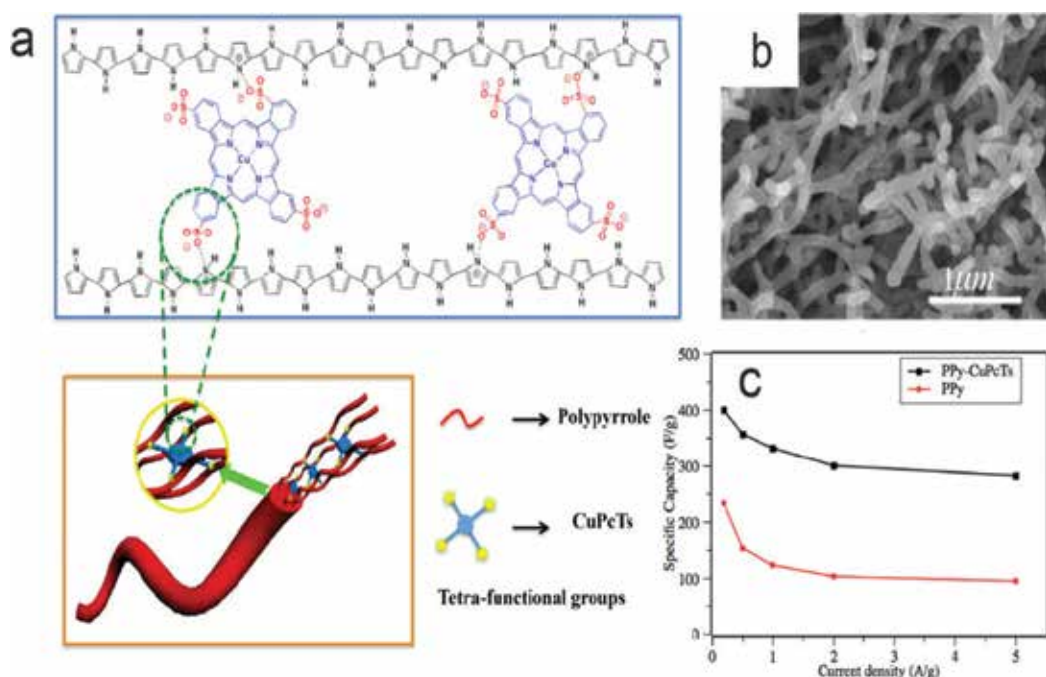


Figure 2. (a) Illustration depicting controlled synthesis of the CuPcTs doped PPy hydrogel. (b) SEM images of nanostructured PPy hydrogel. (c) Specific capacitance as a function of current density for CuPcTs-PPy and pristine PPy. Adapted with permission [31]. Copyright 2017, American Chemical Society.

reversible redox reaction, and long cycling life. For instance, RuO₂ can supply a safe operating voltage of 0.7 V in SSCs [37]. Due to the very high costs, RuO₂ is often limited in aerospace and military application. While MnO₂ is generally studied because of their low cost, low toxicity, environmental friendliness, and high theoretical capacitances (up to 1100–1300 F g⁻¹) [38–40]. The main mechanism of the pseudo-capacitive energy storage in MnO₂ is attributed to a reversible intercalation/de-intercalation of protons or an adsorption of cations such as Li⁺, Na⁺, K⁺ from electrolytes [39, 41]. These can be expressed by the following formula:



where X⁺ represents the protons and alkali metal cations (Li⁺, Na⁺, K⁺) in the electrolyte. Toupin and coworkers believed that the pseudo-capacitances are mainly occurring in the interfaces due to the difficulty of the protons or cations transportation into the bulk phase materials [38, 42–44].

3.2.3. Composites materials

Usually, the specific capacitance can be improved by tuning morphology, surface area, and porous structure of active material. The most common electrode materials are carbon materials, metal oxides, and ECPs. To maximize the advantages of these materials, composite materials are of great technological advantages due to the combination of the intrinsic properties of each component as well as the synergistic effect resulting from the hybrids. The composites of carbon materials with other materials such as ECPs and metal oxides, which often use carbon materials as substrate, for example, carbon nanotubes, carbon fibers, graphene materials, activated carbon, etc. As depicted in Section 3.2, ECPs and metal oxides are highly promising active electrode materials but these materials suffer from severe cycling stability problems because of the structure collapse caused by swelling and shrinking during charging/discharging. Hybridizing carbon materials with ECPs and/or metal oxides can synergistically boost nearly all the aspects of capacitive performance including conductivity, capacitance, and cycling stability. For instance, Peng et al. fabricated hollow fiber electrodes using reduced graphene oxide (RGO)/ECPs, simultaneously achieving large areal capacitance (304.5 mF cm⁻²), high flexibility, and high electrical conductivity [45].

4. Electrolyte-mediated operating voltage

Electrolyte is one of the key components of SCs, basically, conveying ionic current and leading the formation of electrical double layer, more importantly, under certain circumstances of matched electrode materials and electrolytes, and facilitating reversible redox processes for larger amount of charges stored in the interfaces. In general, electrolytes used in SSCs can be sorted into two main categories: liquid electrolytes and solid/quasi-solid state electrolytes. Liquid electrolytes can be further sorted into three groups: aqueous electrolytes, organic electrolytes, and ionic liquids (ILs), while solid/quasi-solid state electrolytes can be divided into organic electrolytes and inorganic electrolytes [7]. There is no once-for-all solution for electrolyte selection, each electrolyte has its own advantages and disadvantages. For

instance, in the group of liquid electrolytes, aqueous electrolytes exhibit very high ionic conductivity, low costs, and high safety, yet they can only deliver an operating potential window of about 1.0–1.3 V because the water splitting potential window is about 1.23 V. While the organic electrolytes and IL electrolytes can be operated at much higher voltages, typically organic electrolytes at 2.5–2.7 and IL electrolytes at 3.5–4.0 V. However, the expensive costs and potential risks for environment strongly hinder their practical applications. According to previous literatures, many aspects of electrolytes can have significant influence on the capacitive performance; here, in this short chapter, we focus on two main aspects: (a) the interaction between electrolyte and electrode materials and (b) the stable potential window. We will discuss the abovementioned two important aspects according to different types of liquid electrolytes (Table 2).

4.1. Aqueous electrolytes

There are many advantageous merits of aqueous electrolytes, for instance, high ionic conductivity (up to $\sim 1 \text{ S cm}^{-1}$) that can deliver very high power density, high safety that greatly simplifies the fabrication and assembly processes, and low costs that enables broad practical applications. Generally, aqueous electrolytes have three main classes: acidic electrolytes (H_2SO_4 , H_3PO_4 , etc.), basic electrolytes (KOH, NaOH, etc.), and neutral electrolytes (Li_2SO_4 , Na_2SO_4 , NaCl, etc.). Due to the narrow chemically stable window of water, the operable voltages for SSCs assembled using aqueous electrolytes are usually lying within 1 V. Consequently, the energy stored in single one SSCs is limited, which is far less competitive with organic and IL SSCs, not to mention batteries. Many efforts have been taken to broaden the safe working voltage of aqueous SSCs, which is mainly through the suppression of water splitting at electrode interfaces.

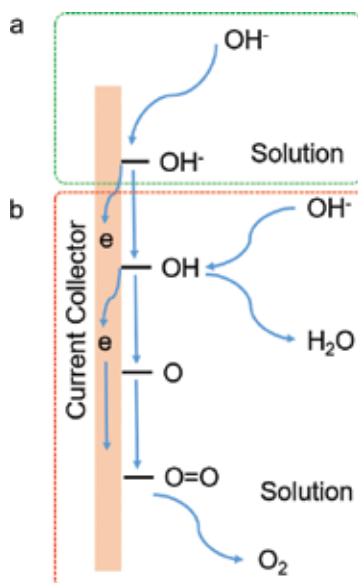
To understand the phenomenon occurring at the electrode/electrolyte interfaces, we need to look into the details of potential-driven water splitting at electrode interfaces. Water splitting basically requires three main steps: absorption, conversion, and desorption. Take water

	Aqueous electrolyte	Organic electrolyte	Ionic liquid
Operation voltage window (V)	≤ 1.2	2.5–2.8	2–6
Ionic conductivity, σ (ms cm^{-1})	High	Low	Very low
Viscosity, η	Low	Medium/high	High
Cost	Low	Medium/high	Very high
Work temperature	Narrow	Wide	Wide
Toxicity	Low	Medium/high	Low
Advantage	High conductivity	High voltage window	High thermal and chemical stability, wide voltage window
Disadvantage	Low voltage window	Large electrolyte ions, low conductivity,	High viscosity

Table 2. The comparative properties of different types of electrolytes.

oxidation as example, H_2O molecules and OH^- can both act as feeds for water oxidation while OH^- serve as charge carriers to provide capacitance. Initially, these oxygen-containing species are strongly absorbed on electrode surface to supply EDL capacitance. Once the binding force driven by applied potential was large enough the dielectric layer becomes conductive for electron, the excessive electron in OH^- would be readily transferred from OH^- to current collector. After complex processes of H^+ depletion, $\text{O}=\text{O}$ bond formation, and desorption of O_2 , the water splitting at cathode is completed, as schematically depicted in **Scheme 3**. There seems to be one threshold for the absorption mode turning from capacitive absorption to water splitting, and this threshold is highly related with the toughness of absorption and the capability of electrode materials catalyzing the complex processes for water splitting and also the potential applied.

In order to broaden the operating voltage window of SSCs, it is feasible through the suppression of splitting of electrolytes, for instance, in aqueous electrolytes, that can be done through the passivation of water splitting activity on the water splitting-inactive electrode surface. For instance, Zheng et al. developed a conductive polymer of poly(naphthalene four formyl ethylenediamine) (PNTE) and used them as anode materials for aqueous rechargeable Li-ion battery. The passivated hydrogen evolution activity of PNFE exhibited very large overpotential for HER and thus enabled a capacitor-like Li^+ storage kinetics in aqueous electrolytes [46]. Thereafter, Zhang et al. reported the fabrication of highly porous carbon materials with high carbon content (>93 at.%) and limited heteroatom doping. The as-synthesized carbon materials exhibited very sluggish water splitting performance, their stably operated voltage window for water splitting can be greatly broadened to 2.2 V or even higher on the carbon materials in neutral Li_2SO_4 electrolyte, as shown in **Figure 3** [47]. Normally, water molecules can be split into hydrogen and oxygen at 1.3–1.8 V, depending on the types of aqueous electrolytes applied.



Scheme 3. Schematic depictions of (a) capacitive absorption and (b) water oxidation.

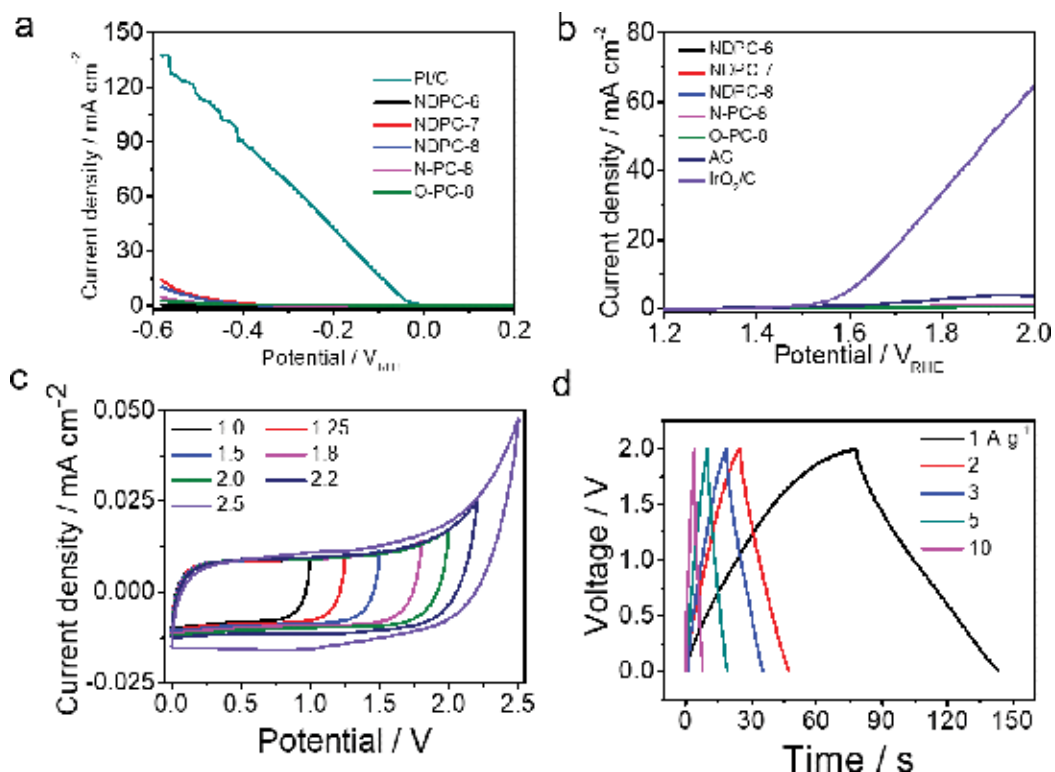


Figure 3. Hydrogen evolution and oxygen evolution reaction performance of non-doped porous carbon materials (NDPC-6/7/8) measured in (a) 0.5 M H₂SO₄ and (b) 0.1 M KOH, respectively. (c) CV profiles of NDPC-8 with different applied voltage windows, (d) GCD profiles of NDPC-8 with different current densities. Adapted with permission [47]. Copyright 2017, Royal Society of Chemistry.

Therefore, on the basis of large surface area, conductive electrode network, and proper electrolyte, the enlargement of operation voltage can be further realized through the application of electrode materials that have sluggish activity toward splitting of electrolytes. For example, it is feasible to use highly porous high-carbon content materials as electrode materials and Li₂SO₄ solution as electrolyte for the assembly of SSCs with wide operating voltage window.

4.2. Organic electrolytes

The specific energy of aqueous SSCs was mainly limited by the water splitting voltage at ~1.23 V. Therefore, organic electrolytes with high conductivity, wide electrochemical voltage window, excellent chemical stability and acceptable cost become the mainstream electrolytes in practical supercapacitor market. Organic electrolytes consist of organic solvents and salts, usually have an operating voltage up to 2.7 V or higher, which makes it highly attractive for high-energy SSCs [48]. Since the organic electrolytes contain two parts, we will give separate illustrations.

First, proper organic solvents can be chosen based on the following rules: high solubility for electrolyte salts, low viscosity to facilitate ionic transport, no side reaction with other parts of supercapacitor (including active materials, current collector, and separator), wide work temperature, and environmental friendliness. Among all organic electrolytes, the most widely used solvents are acetonitrile (AN) and propylene carbonate (PC). AN is capable of dissolving large quantities of salts but it is toxic and risky to environment. PC, a green solvent, has been widely used, meanwhile, it also has very wide stable working temperature and good conductivity. Also, other electrolytes such as γ -butyrolactone (GBL), N,N-dimethylformamide (DMF), N-methylpyrrolidone (NMP), N,N-dimethylacetamide (DMA) are applicable electrolytes that have been widely studied.

Second, the most common used electrolyte salts are chain-like quaternary ammonium salts such as tetraethylammonium tetrafluoroborate (TEA-BF₄) and triethylmethylammonium tetrafluoroborate (TEMA-BF₄) [49]. One feasible method to further enlarge the operating voltage window for organic electrolyte is through the increasing of electrolyte salts concentration. On one hand, one can find the optimized salt concentration that has the best solubility and chemical stability; on the other hand, it is one feasible way to thicken the layer of charge carriers instead of solvent molecule layer at the electrode/electrolyte interfaces. For instance, 1 mol L⁻¹ spiro-bipyrrolidinium tetrafluoroborate (SBP-BF₄) in PC solvent showed very high electrochemical stability on the interface due to its spiro rings molecular structure [50]. Yu et al. reported 1.5 mol L⁻¹ SBP-BF₄/PC shows higher conductivity of 17 mS cm⁻¹ than 1.5 mol L⁻¹ TEMA-BF₄/PC [51]. Other metal salt such as lithium/sodium salt are also applicable in carbon-based SSCs following the same rules for electrolyte picking up.

4.3. Ionic liquid electrolytes

Low-temperature ionic liquids (ILs) are pure organic salts containing no solvents with melting points below 100°C. If the liquid state can maintain at ambient temperature, they are called room temperature ionic liquids (RTILs). RTIL are the type of ILs of broad interests to supercapacitors especially SSCs due to their unique properties including non-volatility, poor combustibility and high resistance to heat. However, the ionic conductivity of ILs usually fall in 0.1–15 mS cm⁻¹, which is much lower than most of the commercial organic electrolytes. But ILs can show excellent conductivity at high temperature because of low viscosity. Many kinds of ILs have been widely used in supercapacitor; the two pairing ions of imidazole and pyrrole are most commonly studied. Generally speaking, the size and symmetry of cations strongly influence the melting points of ionic liquids. Normally, the imidazole possesses high conductivity with narrow potential window, alkylpyrrole shows wide operating voltage but high melting point. For instance, Chen et al. used a series of sponge-like carbon as electrode and 1-ethyl-3-methylimidazolium tetrafluoroborate (EMIM-BF₄) and 1-Butyl-3-methylimidazolium hexafluorophosphate (BMIM-PF₆) as electrolytes; the gravimetric capacitance of as-made SSCs can be improved to 445 F g⁻¹ with a high discharge voltage of 4 V, very good rate capability, and cycling stability [52].

5. Conclusions and perspectives

There have been many strategies proposed to pursue high-energy symmetric supercapacitors (SSCs), including two main parts: (1) the electrode materials' selection and design and (2) the electrolyte optimization. As described in Section 3, commonly, desirable electrode materials (mainly carbon-based materials) for SSCs can be obtained by meeting the following criterions: large specific surface area, hierarchical porosity, optimized heteroatom doping, and compositing with pseudo-capacitive materials such as electronically conductive polymers (ECPs) or stable metal oxides. Section 4 summarized the commonly used electrolytes and illustrated a few key principles of how to select a proper electrolyte for SSCs for different purposes. Three main types of liquid electrolytes: aqueous electrolytes, organic electrolytes, and ionic liquids (ILs) electrolytes hold different advantages, for instance, aqueous ones are low cost and highly ionic conductive while organic and IL ones can be operated at high voltages. However, there are also limits for each type of electrolytes, for example, the operating voltages of aqueous electrolytes are restricted in between 1.0 and 1.8 V and organic and ILs electrolytes are expensive and risky to environments. Based on the abovementioned advances in supercapacitors, we provided two feasible ways to further improve the capacitive performance of SSCs about the interface-related subjects, including (1) optimizing the types and contents of heteroatom dopants to involve pseudo-capacitance and expand the operating voltage by suppressing the activity of splitting electrolytes and (2) designing new types of electrolytes such as aqueous electrolytes containing neutral salts (Li_2SO_4 , Li-TFSI, etc.). In conclusion, on the basis of proper electrode/electrolyte's selection, we can achieve further development in SSCs through engineering the abovementioned two important aspects that are used for the construction of robust electrode/electrolyte interface.

Acknowledgements

This work was financially supported by the National Natural Science Foundation of China (21701101), the Shandong Scientific Research Awards Foundation for Outstanding Young Scientists (ZR201702180243), and the Program for Tsingtao AI-ion Power and Energy-storage Battery Research Team in the University.

Conflict of interest

All authors declare that they have no conflict of interests.

Appendices and Nomenclature

SSCs	symmetric supercapacitors
SCs	supercapacitors

EDLCs	electrochemical double-layer capacitors
ASSCs	asymmetric supercapacitors
AC	activated carbon
EASA	electrochemically accessible surface area
ECPs	electronically conducting polymers
PANI	polyaniline
PPy	polypyrrole
PTh	polythiophene
ILs	ionic liquids
PNTE	polynaphthalene four formyl ethylenediamine
NDPC	non-doped porous carbon materials
AN	acetonitrile
PC	propylene carbonate
GBL	γ -butyrolactone
DMF	N,N-dimethylformamide
NMP	N-methylpyrrolidone
DMA	N,N-dimethylacetamide
TEMA-BF ₄	triethylmethylammonium tetrafluoroborate
SBP-BF ₄	spiro-bipyrrolidinium tetrafluoroborate
EMIM-BF ₄	tetrafluoroborate

Author details

Yaqun Wang and Guoxin Zhang*

*Address all correspondence to: zhanggx@sdust.edu.cn

College of Electrical Engineering and Automation, Shandong University of Science and Technology, Tsingtao, China

References

- [1] Wu S, Zhu Y. Highly densified carbon electrode materials towards practical supercapacitor devices. *Science China Materials*. 2017;**60**:25-38. DOI: 10.1007/s40843-016-5109-4

- [2] Lu M. Supercapacitors: Materials, Systems and Applications. Weinheim: John Wiley & Sons; 2013. p. 450
- [3] Shukla A, Sampath S, Vijayamohanan K. Electrochemical supercapacitors: Energy storage beyond batteries. *Current Science*. 2000;**79**:1656-1661. DOI: 10.1016/j.elecom.2004.12.013
- [4] Simon P, Gogotsi Y. Materials for electrochemical capacitors. *Nature Materials*. 2008;**7**:845-854. DOI: 10.1038/nmat2297
- [5] Ohshima H. Electrical Phenomena at Interfaces and Biointerfaces: Fundamentals and Applications in Nano-, Bio-, and Environmental Sciences. Oxford: John Wiley & Sons; 2012. 850p
- [6] Béguin F, Presser V, Balducci A, Frackowiak E. Carbons and electrolytes for advanced supercapacitors. *Advanced Materials*. 2014;**26**:2219-2251. DOI: 10.1002/adma.201304137
- [7] Zhong C, Deng Y, Hu W, Qiao J, Zhang L, Zhang J. A review of electrolyte materials and compositions for electrochemical supercapacitors. *Chemical Society Reviews*. 2015;**44**:7484-7539. DOI: 10.1039/c5cs00303b
- [8] Hailiang W, Yongye L, Tisaphern M, Zhuo C, Hernan S. Advanced asymmetrical supercapacitors based on graphene hybrid materials. *Nano Research*. 2011;**4**:729-736. DOI: 10.1007/s12274-011-0129-6
- [9] Zhao C, Zheng W. A review for aqueous electrochemical supercapacitors. *Frontiers in Energy Research*. 2015;**3**:23. DOI: 10.3389/fenrg.2015.00023
- [10] Chen GZ. Supercapacitor and supercapattery as emerging electrochemical energy stores. *International Materials Review*. 2017;**62**:173-202. DOI: 10.1080/09506608.2016.1240914
- [11] Yang M, Zhou Z. Recent breakthroughs in supercapacitors boosted by nitrogen-rich porous carbon materials. *Advanced Science*. 2017;**4**:1600408. DOI: 10.1002/advs.201600408
- [12] Hao L, Li X, Zhi L. Carbonaceous electrode materials for supercapacitors. *Advanced Materials*. 2013;**25**:3899-3904. DOI: 10.1002/adma.201301204
- [13] Zhang LL, Zhao XS. Carbon-based materials as supercapacitor electrodes. *Chemical Society Reviews*. 2009;**38**:2520-2531. DOI: 10.1039/b813846j
- [14] Li X, Wei B. Supercapacitors based on nanostructured carbon. *Nano Energy*. 2013;**2**:159-173. DOI: 10.1016/j.nanoen.2012.09.008
- [15] Salanne M, Rotenberg B, Naoi K, Kaneko K, Taberna PL, Grey CP, Dunn B, Simon P. Efficient storage mechanisms for building better supercapacitors. *Nature Energy*. 2016;**1**:16070. DOI: 10.1038/nenergy.2016.70
- [16] Lin T, Chen IW, Liu F, Yang C, Bi H, Xu F, Huang F. Nitrogen-doped mesoporous carbon of extraordinary capacitance for electrochemical energy storage. *Science*. 2015;**350**:1508-1513. DOI: 10.1126/science.aab3798
- [17] Wang C, Zhan Y, Wu L, Li Y, Liu J. High-voltage and high-rate symmetric supercapacitor based on MnO₂-polypyrrole hybrid nanofilm. *Nanotechnology*. 2014;**25**:305401. DOI: 10.1088/0957-4484/25/30/305401

- [18] Xu Y, Lin Z, Zhong X, Huang X, Weiss NO, Huang Y, Duan X. Holey graphene frameworks for highly efficient capacitive energy storage. *Nature Communications*. 2014;**5**:4554. DOI: 10.1038/ncomms5554
- [19] Sun F, Wu H, Liu X, Liu F, Zhou H, Gao J, Lu Y. Nitrogen-rich carbon spheres made by a continuous spraying process for high-performance supercapacitors. *Nano Research*. 2016;**9**:3209-3221. DOI: 10.1007/s12274-016-1199-2
- [20] Demarconnay L, Raymundo-Piñero E, Béguin F. A symmetric carbon/carbon supercapacitor operating at 1.6 V by using a neutral aqueous solution. *Electrochemical Communication*. 2010;**12**:1275-1278. DOI: 10.1016/j.elecom.2010.06.036
- [21] Hsu YK, Chen YC, Lin YG, Chen LC, Chen KH. High-cell-voltage supercapacitor of carbon nanotube/carbon cloth operating in neutral aqueous solution. *Journal of Materials Chemistry*. 2012;**22**:3383-3387. DOI: 10.1039/c1jm14716a
- [22] Wang L, Zhang G, Han B, Chang Y, Li H, Wang J, Hu C, Chang Z, Huo Z, Sun X. A two-volt aqueous supercapacitor from porous dehalogenated carbon. *Journal of Materials Chemistry A*. 2017;**5**:6734-6739. DOI: 10.1039/C6TA10341C
- [23] Zhang C, Lv W, Tao Y, Yang QH. Towards superior volumetric performance: Design and preparation of novel carbon materials for energy storage. *Energy & Environmental Science*. 2015;**8**:1390-1403. DOI: 10.1039/c5ee00389j
- [24] Frackowiak E. Carbon materials for supercapacitor application. *Physical Chemistry Chemical Physics*. 2007;**9**:1774-1785. DOI: 10.1039/b618139m
- [25] Khan ZU, Kausar A, Ullah H, Badshah A, Khan WU. Graphene and graphene oxide: Synthesis, properties, and applications. *Advanced Materials*. 2010;**22**:3906-3924. DOI: 10.1002/adma.201001068
- [26] Borenstein A, Hanna O, Ran A, Luski S, Brousse T, Aurbach D. Carbon-based composite materials for supercapacitor electrodes: A review. *Journal of Materials Chemistry A*. 2017;**5**:12653-12672. DOI: 10.1039/C7TA00863E
- [27] Xu J, Xu F, Qian M, Xu F, Hong Z, Huang F. Conductive carbon nitride for excellent energy storage. *Advanced Materials*. 2017;**29**. DOI: 10.1002/adma.201701674
- [28] Zhang G, Wang L, Hao Y, Jin X, Xu Y, Kuang Y, Dai L, Sun X. Unconventional carbon: Alkaline dehalogenation of polymers yields N-doped carbon electrode for high-performance capacitive energy storage. *Advanced Functional Materials*. 2016;**26**:3340-3348. DOI: 10.1002/adfm.201505533
- [29] Zhang G, Luo H, Li H, Wang L, Han B, Zhang H, Li Y, Chang Z, Kuang Y, Sun X. ZnO-promoted dechlorination for hierarchically nanoporous carbon as superior oxygen reduction electrocatalyst. *Nano Energy*. 2016;**26**:241-247. DOI: 10.1016/j.nanoen.2016.05.029
- [30] Zhang G, Wang J, Qin B, Jin X, Wang L, Li Y, Sun X. Room-temperature rapid synthesis of metal-free doped carbon materials. *Carbon*. 2017;**115**:28-33. DOI: 10.1016/j.carbon.2016.12.093
- [31] Chang Y, Zhang G, Han B, Li H, Hu C, Pang Y, Chang Z, Sun X. Polymer dehalogenation-enabled fast fabrication of N, S-codoped carbon materials for superior supercapacitor and

- deionization applications. *ACS Applied Materials and Interfaces*. 2017;**9**:29753-29759. DOI: 10.1021/acsami.7b08181
- [32] Yuan L, Yuting S, Litao S, Jincheng L, Chang L, Wencai R, Feng L, Libo G, Jie C, Fuchi L. Elemental superdoping of graphene and carbon nanotubes. *Nature Communications*. 2016;**7**:10921. DOI: 10.1038/ncomms10921
- [33] Wang Y, Shi Y, Pan L, Ding Y, Zhao Y, Li Y, Shi Y, Yu G. Dopant-enabled supramolecular approach for controlled synthesis of nanostructured conductive polymer hydrogels. *Nano Letters*. 2015;**15**:7736-7741. DOI: 10.1021/acs.nanolett.5b03891
- [34] Bhat DK, Kumar MS. N and p-doped poly(3,4-ethylenedioxythiophene) electrode materials for symmetric redox supercapacitors. *Journal of Materials Science*. 2007;**42**:8158-8162. DOI: 10.1007/s10853-007-1704-9
- [35] Stenger-Smith JD, Webber CK, Anderson N, Chafin AP, Zong K, Reynolds JR. Poly(3,4-alkylenedioxythiophene)-based supercapacitors using ionic liquids as supporting electrolytes. *Journal of the Electrochemical Society*. 2002;**149**:A973-A977. DOI: 10.1149/1.1485773
- [36] Yu N, Yin H, Zhang W, Liu Y, Tang Z, Zhu MQ. High-performance fiber-shaped all-solid-state asymmetric supercapacitors based on ultrathin MnO₂ nanosheet/carbon fiber cathodes for wearable electronics. *Advanced Energy Materials*. 2016;**6**:1501458. DOI: 10.1002/aenm.201501458
- [37] Xia C, Chen W, Wang X, Hedhili MN, Wei N, Alshareef HN. Highly stable supercapacitors with conducting polymer core-shell electrodes for energy storage applications. *Advanced Energy Materials*. 2015;**5**:1401805. DOI: 10.1002/aenm.201401805
- [38] Toupin M, Brousse T, Bélanger D. Influence of microstructure on the charge storage properties of chemically synthesized manganese dioxide. *Chemical Materials*. 2002;**14**:3946-3952. DOI: 10.1021/cm020408q
- [39] Pang SC, Anderson MA. Novel electrode materials for thin-film ultracapacitors: Comparison of electrochemical properties of sol-gel-derived and electrodeposited manganese dioxide. *Journal of the Electrochemical Society*. 2000;**147**:444-450. DOI: 10.1149/1.1393216
- [40] Lee HY, Oh SM. Origin of cathodic degradation and new phase formation at the La_{0.9}Sr_{0.1}MnO₃/YSZ interface. *Solid State Ionics*. 1999;**90**:133-140. DOI: 10.1016/S0167-2738(96)00408-0
- [41] Owens BB, Passerini S, Smyrl WH. Lithium ion insertion in porous metal oxides. *Electrochimica Acta*. 1999;**45**:215-224. DOI: 10.1016/S0013-4686(99)00205-4
- [42] Chin SF, Pang SC, Anderson MA. Self-assembled manganese dioxide nanowires as electrode materials for electrochemical capacitors. *Materials Letters*. 2010;**64**:2670-2672. DOI: 10.1016/j.matlet.2010.09.020
- [43] Devaraj S, Munichandraiah N. Surfactant stabilized nanopetals morphology of α -MnO₂ prepared by microemulsion method. *Journal of Solid State Electrochemistry*. 2008;**12**:207-211. DOI: 10.1007/s10008-007-0364-7

- [44] Khomenko V, Raymundo-Piñero E, Béguin F. Optimisation of an asymmetric manganese oxide/activated carbon capacitor working at 2 V in aqueous medium. *Journal of Power Sources*. 2006;**153**:183-190. DOI: 10.1016/j.jpowsour.2005.03.210
- [45] Qu G, Cheng J, Li X, Yuan D, Chen P, Chen X, Wang B, Peng H. A fiber supercapacitor with high energy density based on hollow graphene/conducting polymer fiber electrode. *Advanced Materials*. 2016;**28**:3646-3652. DOI: 10.1002/adma.201600689
- [46] Wang Y, Cui X, Zhang Y, Zhang L, Gong X, Zheng G. Achieving high aqueous energy storage via hydrogen-generation passivation. *Advanced Materials*. 2016;**28**:7626-7632. DOI: 10.1002/adma.201602583
- [47] Wang L, Zhang G, Han B, Chang Y, Li H, Wang J, Hu C, Chang Z, Huo Z, Sun X. A two-volt aqueous supercapacitor from porous dehalogenated carbon. *Journal of Materials Chemistry A*. 2017;**5**:6734-6739. DOI: 10.1039/C6TA10341C
- [48] Rose MF, Johnson C, Owens T, Stephens B. Limiting factors for carbon-based capacitors chemical double-layer. *Journal of Power Sources*. 1994;**47**:303-312
- [49] Ue M, Ida K, Mori S. Electrochemical properties of organic liquid electrolytes based on quaternary onium salts for electrical double-layer capacitors. *Journal of the Electrochemical Society*. 1994;**141**:2989-2996. DOI: 10.1149/1.2059270
- [50] Nono Y, Kouzu M, Takei K, Chiba K, Sato Y. EDLC performance of various activated carbons in spiro-type quaternary ammonium salt electrolyte solutions. *Electrochemistry*. 2012;**78**:336-338. DOI: 10.5796/electrochemistry.78.336
- [51] Yu X, Ruan D, Wu C, Jing W, Shi Z. Spiro-(1,1')-bipyrrrolidinium tetrafluoroborate salt as high voltage electrolyte for electric double layer capacitors. *Journal of Power Sources*. 2014;**265**:309-316. DOI: 10.1016/j.jpowsour.2014.04.144
- [52] Wang X, Zhou H, Sheridan E, Walmsley JC, Ren D, Chen D. Geometrically confined favourable ion packing for high gravimetric capacitance in carbon-ionic liquid supercapacitor. *Energy & Environmental Science*. 2016;**9**:232-239. DOI: 10.1039/C5EE02702K

Classical Density Functional Theory Insights for Supercapacitors

Cheng Lian and Honglai Liu

Additional information is available at the end of the chapter

<http://dx.doi.org/10.5772/intechopen.76339>

Abstract

The most urgent issue for supercapacitor is to improve their energy density so that they can better compete with batteries. To design materials and interfaces for supercapacitor with higher energy density requires a deeper understanding of the factors and contributions affecting the total capacitance. In our recent works, the classical density functional theory (CDFT) was developed and applied to study the electrode/electrolyte interface behaviors, to understand capacitive energy storage. For porous electrode materials, we studied the pore size effect, curvature effect, and the surface modification of porous materials on the capacitance. Through CDFT, we have found that the curvature effects on convex and concave EDLs are drastically different and that materials with extensive convex surfaces will lead to maximized capacitance; CDFT also predicts oscillatory variation of capacitance with pore size, but the oscillatory behavior is magnified as the curvature increases; an increase in the ionophobicity of the nanopores leads to a higher capacity for energy storage, and a pore-like impurity can enter the pore, makes the pore ionophobic and storage more energy. We also find the mixture effect, which makes more counterions pack on and more co-ions leave from the electrode surface, leads to an increase of the counterion density within the EDL and thus a larger capacitance.

Keywords: supercapacitors, classical density functional theory, porous electrode, ionic liquid, electrical double layer

1. Introduction

Capacitive energy storage is the key component for sustainable energy systems, e.g. by storing the renewable but intermittent energy and making it accessible upon demand. The most commonly used energy storage devices are batteries and supercapacitors. A battery stores

energy by electrochemical reactions, while a supercapacitor stores energy through physicochemical adsorption, including formation of electric double layer and surface redox reactions. A battery has high energy density but low power density, while a supercapacitor boasts of high power density due to the fast surface physical and chemical processes. There are two types of supercapacitors: electric double-layer capacitors (EDLC) store electrical energy through formation of electric double layer at electrode/electrolyte interface, while pseudocapacitors store electrical energy by reversible redox reaction (including ion intercalation). Supercapacitors are becoming increasingly important for electrical energy storage due to their advantages on rapid charge/discharge rate, a virtually unlimited life, a wider range of working temperature, a very high efficiency, etc. However, the main drawback, a low energy density, has been limiting supercapacitors in the applications requiring many rapid charge/discharge cycles for short-term power needs. It is the most urgent issue to improve the energy density of supercapacitors [1]. The EDLC performance is strongly correlated with electroadsorption of ionic species at the inner surfaces of microporous electrode [2].

To design new materials and interfaces for EDLC with higher energy density, one requires a deeper understanding of the factors and contributions affecting the total capacitance of an EDLC. The most widely used electrode material for EDLC is porous carbon. Many types of carbon-based materials have been used for EDLC [3, 4], such as activated graphene oxide [5], activated carbon [6], carbide-derived carbon [7–9], carbon nanotube [10–12], onion-like carbon [13, 14] and graphene [15, 16]. The gravimetric capacitance of those carbon materials is quite sensitive to their structure, especially the porosity and specific surface area. The pore size can greatly affect the ion partitioning and packing inside the pore, which causes a large change on the capacitance. The relationship between the pore size and the capacitance of ionic liquids has been investigated by Simon and Gogotsi [1, 17, 18]. This important work reveals a clear physical insight into the pore size-dependent capacitance and suggests that the capacitance maximum can be achieved by optimally matching the pore size and ion size. Carbon nanotube has been reported as a novel EDLC electrode material [19, 20]. The reported capacitance of single-wall carbon nanotube is 180 F/g in aqueous electrolyte [11]. The onion-like carbon was also reported as a promising EDLC electrode and exhibit very large power density at discharging rate of up to 200 V/s [13, 21]. Moreover, graphene-based material also has been developed to be attractive EDLC material and its unique electronic structure could have large influence on the charge capacitive behavior [6, 15]. The pseudocapacitors and EDLC show distinctly different electrochemical behavior in cyclic voltammetry. Pseudocapacitance may contribute more capacitance than double-layer capacitance for the same surface area.

In general, the electrode-electrolyte interface is the most key issue of supercapacitors, fundamental understanding on this should be crucial. Experimental tools such as Atomic Force Microscopy (AFM) and X-ray reflectometry were applied to study the structural properties of EDLCs at the electrode surface [22–24]. However, it's difficult for experimental method to directly detect the nanoscale electrode-electrolyte interface. Computational methods, such as molecular dynamics (MD) simulations, were also used to investigate the distribution of ions near electrified interfaces [25–27]. Analytical methods [28–37] are computationally more efficient than MD simulations thereby suitable for a systematic investigation of the key parameters for relatively large systems. CDFT can be used to account for the ionic steric effects and electrostatic

correlations neglected in the Poisson-Nernst-Planck (PNP) or Poisson-Boltzmann (PB) equations, a conventional microscopic theory for EDLs. The non-mean-field effects are significant for room-temperature ionic liquids (RTILs) due to strong electrostatic interactions and high ion densities [38–40].

In this work, we discuss the impurity effect on the charging and capacitive behaviors based on the CDFT. CDFT had been successfully used in studying the EDL structure and the capacitance of ionic liquids and organic electrolytes systems [41–44]. It has been shown that the CDFT predictions are able to capture the essential results from earlier experimental and simulation studies and provides microscopic insights into the electrochemical behavior of ionic liquids as the working electrolytes for supercapacitors [45–47].

This paper is structured as follows. First, we describe our coarse-grained models of RTILs and porous materials and provide a brief introduction to the classical DFT method. Next, we discuss the pore structure of electrode and the electrolyte effect on the EDL structure and the capacitive performance of EDLCs. Finally, we summarize the main results and possible future work.

2. Classical density functional theory

We use a non-primitive model to represent the ionic species, impurities, and solvent molecules in the electrolyte solution [48]. The model system consists of charged hard spheres for ionic species and a hard-sphere dimer for solvent molecules. The pair potential between two arbitrary spheres/segments in the system, i and j , is given by

$$u_{ij}(r) = \begin{cases} \infty, & r < \frac{\sigma_i + \sigma_j}{2} \\ \frac{Z_i Z_j e^2}{4\pi\epsilon_0\epsilon r'}, & r \geq \frac{\sigma_i + \sigma_j}{2} \end{cases} \quad (1)$$

where r is the center-to-center distance, e is the elementary charge, ϵ_0 is the permittivity of free space, $\epsilon = 1$ is the local dielectric constant for the vacuum.

CDFT [44, 49–52] was used to obtain the EDL structure and capacitance for the carbon materials in contact with the electrolyte solution. The details of the CDFT calculations have been published before [42, 45, 47, 48, 53, 54]. Briefly, we obtained the surface charge densities at various electrical potentials. Given the number densities of ions and solvent molecules in the bulk and the system temperature, the pore size, the pore geometry, and the surface electrical potential, we solve for the density profiles of cations, anions and impurities, as well as the solvent segments inside the pore by minimization of the grand potential.

$$\begin{aligned} \beta\Omega[\rho_M(\mathbf{R}), \{\rho_a(\mathbf{r})\}] &= \beta F[\rho_M(\mathbf{R}), \{\rho_a(\mathbf{r})\}] + \int [\beta\Psi_M(\mathbf{R}) - \beta\mu_M] \rho_M(\mathbf{R}) d\mathbf{R} \\ &+ \sum_a \int [\beta\Psi_a(\mathbf{r}) - \beta\mu_a] \rho_a(\mathbf{r}) d\mathbf{r} \end{aligned} \quad (2)$$

where $\beta^{-1} = k_B T$, $R \equiv (\mathbf{r}_{\delta+}, \mathbf{r}_{\delta-})$ represents two coordinates specifying the positions of two segments in each solvent molecule, μ_α is the chemical potential of an ionic species, μ_M is the chemical potential of the solvent, $\Psi_a(\mathbf{r})$ stands for the external potential for ions, $\Psi_M(\mathbf{R})$ is the summation of the external potential for a solvent molecule, i.e. $\Psi_M(\mathbf{R}) = \sum_{i=\delta+, \delta-} \varphi_i(\mathbf{r}_i)$, and F is the total intrinsic Helmholtz energy. The number densities of the positive and negative segments of the solvent are calculated from

$$\rho_{\delta+}(\mathbf{r}_{\delta+}) = \int d\mathbf{R} \delta(\mathbf{r} - \mathbf{r}_{\delta+}) \rho_M(\mathbf{R}) \quad (3)$$

$$\rho_{\delta-}(\mathbf{r}_{\delta-}) = \int d\mathbf{R} \delta(\mathbf{r} - \mathbf{r}_{\delta-}) \rho_M(\mathbf{R}) \quad (4)$$

The intrinsic Helmholtz energy F includes an ideal-gas contribution and an excess contribution due to intermolecular interactions F^{ex} .

$$\beta F = \int [\ln \rho_M(\mathbf{R}) - 1] \rho_M(\mathbf{R}) d\mathbf{R} + \beta \int V_b(\mathbf{R}) \rho_M(\mathbf{R}) d\mathbf{R} + \sum_a \int [\ln \rho_a(\mathbf{r}) - 1] \rho_a(\mathbf{r}) d\mathbf{r} + \beta F^{ex} \quad (5)$$

Where V_b stands for the bonding potential of the solvent molecule. The detailed expression for each contribution and the numerical details can be retrieved from Ref. [45, 48]. In evaluation of the Coulomb energy, we calculate the mean electrostatic potential (MEP) from the density distributions of the ions by using the Poisson equation

$$\nabla^2 \psi(\mathbf{r}) = -\frac{4\pi e}{\epsilon} \rho_c(\mathbf{r}) \quad (6)$$

Eq. (9) can be integrated with the boundary conditions that defined by the operation potential. The surface charge density Q is obtained from the condition of overall charge neutrality. The differential capacitance C_d of the EDLs could be calculated by a derivative of the surface charge density Q with respect to the surface potential.

Time-dependent density functional theory (TDDFT) is an extension of the CDFT to describe dynamic or time-dependent processes based on the assumption of local thermodynamic equilibrium [54–62]. For ion diffusion in an electrolyte solution near electrodes, TDDFT asserts that the time evolution for the local density profiles of ionic species, $\rho_i(\mathbf{r}, t)$, follows the generalized diffusion equation

$$\frac{\partial \rho_i(\mathbf{r}, t)}{\partial t} = \nabla \cdot \{ D_i \rho_i(\mathbf{r}, t) \nabla [\beta \mu_i(\mathbf{r}, t) + \beta V_i(\mathbf{r})] \} \quad (7)$$

Where D_i stands for the self-diffusivity of ion i , $\beta = 1/(k_B T)$, k_B is the Boltzmann constant, T stands for the absolute temperature, $\mu_i(\mathbf{r}, t)$ is the local chemical potential and could be obtained by a derivative of the intrinsic Helmholtz energy F with respect to the density, and $V_i(\mathbf{r})$ denotes the external potential arising from the electrodes. With TDDFT, we could capture the ion dynamics inside the nanopores.

3. Electrode effect on the capacitive performance

3.1. Electrode geometry optimization

Whereas practical porous electrodes involve micropores with complicated morphology and pore size distributions [63, 64], theoretical modeling of EDLCs is mostly based on simplistic models to represent the pore geometry and the electrolyte-electrode interactions [65]. Specifically, three types of electrode structures are commonly used in theoretical investigations [66–68]: (i) planar surfaces (e.g., a flat surface or slit pores); (ii) cylindrical pores with their concave inner surfaces or cylindrical particles with their convex outer surfaces (e.g., carbon nanotubes); and (iii) spherical surfaces (e.g., onion-like carbons). The slit and cylindrical pore models are conventionally used for porous materials characterization [69]. Despite the fact that a great variety of porous carbons have been utilized in EDLCs, the effects of the pore size and geometry on the EDL structure remain poorly understood [70]. At the heart of the issue is the question: What is the microscopic structure of porous electrodes and how does the capacitance of EDLCs depend on the electrode pore geometry and electrolyte composition? Recent simulations and experiments indicate that both the pore size and geometry play an important role in determining the capacitance of EDLCs [25, 68, 71–73]. An important question is whether this behavior is generally valid, given the slit-pore model or solid particles used in theoretical calculations and the diversity of pore structure for realistic carbon electrodes. Specially, how does the pore structure and curvature affect the capacitance dependence on the pore size? To address these questions, we propose in this work a generic model to represent both pore size and curvature of carbon electrodes using the CDFT. CDFT is an ideal computational tool for examining the pore size and geometry effects, as it is computationally efficient and applicable over a wide range of pore sizes ranging from that below the ionic dimensionality to mesoscopic scales.

Figure 1 shows the integral capacitance as a function of pore width D at different inner core radii. In all cases, the surface electrical potential is fixed at $\psi_0 = 1.5$ V. As observed in a previous work for an ionic liquid in slit pores [41], the EDL capacitance exhibits the oscillatory dependence on the pore size. The distance between neighboring peaks (or valleys) is approximately equal twice the ion diameter. The oscillatory variation of the integral capacitance is closely affiliated with the layering structures of ion distributions inside the nanopores. The layer-by-layer distributions of cations and anions are evident near the charged surfaces [41].

As inner radius R decreases, the capacitance increases significantly. This is also expected from the increased EDL capacitance at both the inner and outer surfaces. The oscillatory dependence of the capacitance on the pore size is consistent with those corresponding to individual EDLs. Our results show that the EDLs have a smaller influence on the overall ion distributions inside the pore as the pore size falls, leading to a diminishing difference in average counterion and coion densities. On the other hand, a smaller inner core radius results in more counterions in the pore thus a larger capacitance.

This work illustrates the curvature and pore size effect of realistic porous electrodes and suggests the significant role of convex surfaces for the synthesis of new porous electrodes to

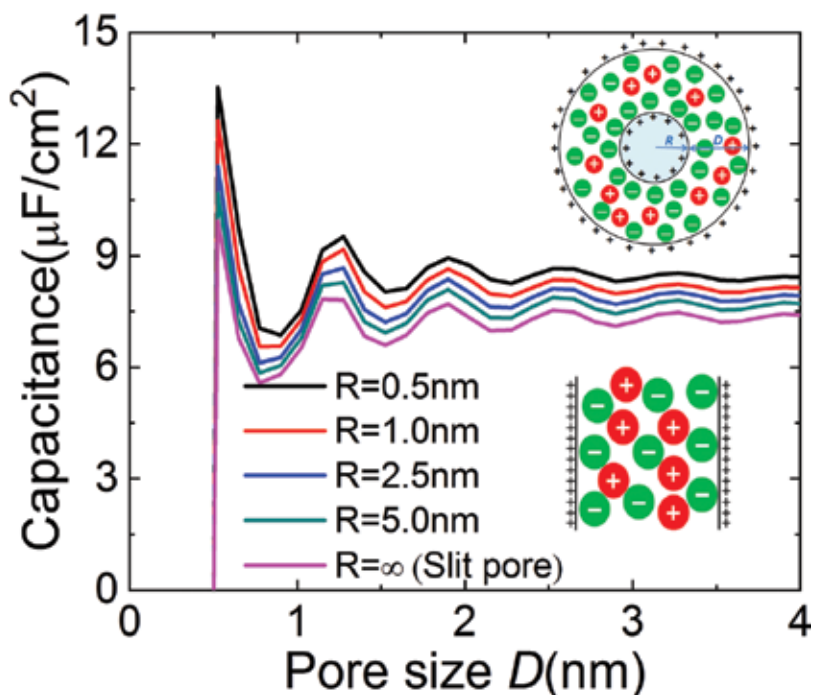


Figure 1. The overall integral capacitance versus the pore size for spherical shells of different inner radii. Reproduced from Ref. [41] with permission. Copyright 2016 American Chemical Society.

optimize EDLC performance. In particular, the spherical shell model provides a simple yet generic description of both pore size and curvature, opening up a new dimension to characterize nanoporous materials and quantify their performance for diverse applications including EDL capacitors.

3.2. Electrode surface modification

Energy storage via electrosorption depends not only on the electrical potential and the geometric compatibilities of the electrode pores and ionic species but also on specific interactions between mobile ions and the surface properties of electrode materials. While existing theoretical reports are mostly devoted to analyzing electrostatic interactions and confinement effects, relatively little is known on how specific ion-surface associations may influence the EDLC performance. Very recently, Kondrat and Kornyshev found that the capacitive performance is sensitive to the ion affinity with nanopores: their theoretical results show electrodes with ionophobic nanopores may have slightly lower, the same, or even higher energy storage capacity than the ionophilic ones, all depending on the electrode voltage [74–76]. The capacitance voltage curve is shifted to substantially higher voltages as the pore ionophobicity increases. Within an ionophobic pore, the stored energy could be higher than for ionophilic

pores when the electrodes are operated at sufficiently high voltages [74]. It has also been shown that the charging kinetics of an empty ionophobic nanopore is much faster than that of an ionophilic nanopore at similar conditions [75, 77]. Experimentally, the ionophobicity may be controlled by modifying the surface properties of nanoporous materials or by introducing special functional groups to the ionic species.

We discussed the effects of non-electrostatic ion-surface interactions based on the classical density functional theory (CDFT) [54, 78]. δE stands for the resolution energy, i.e. the energy cost to transfer an ion from the bulk to the slit pore. δE is used as an indication of the ionophobicity of nanopores: negative δE promotes adsorption of ions within the pore (viz., an

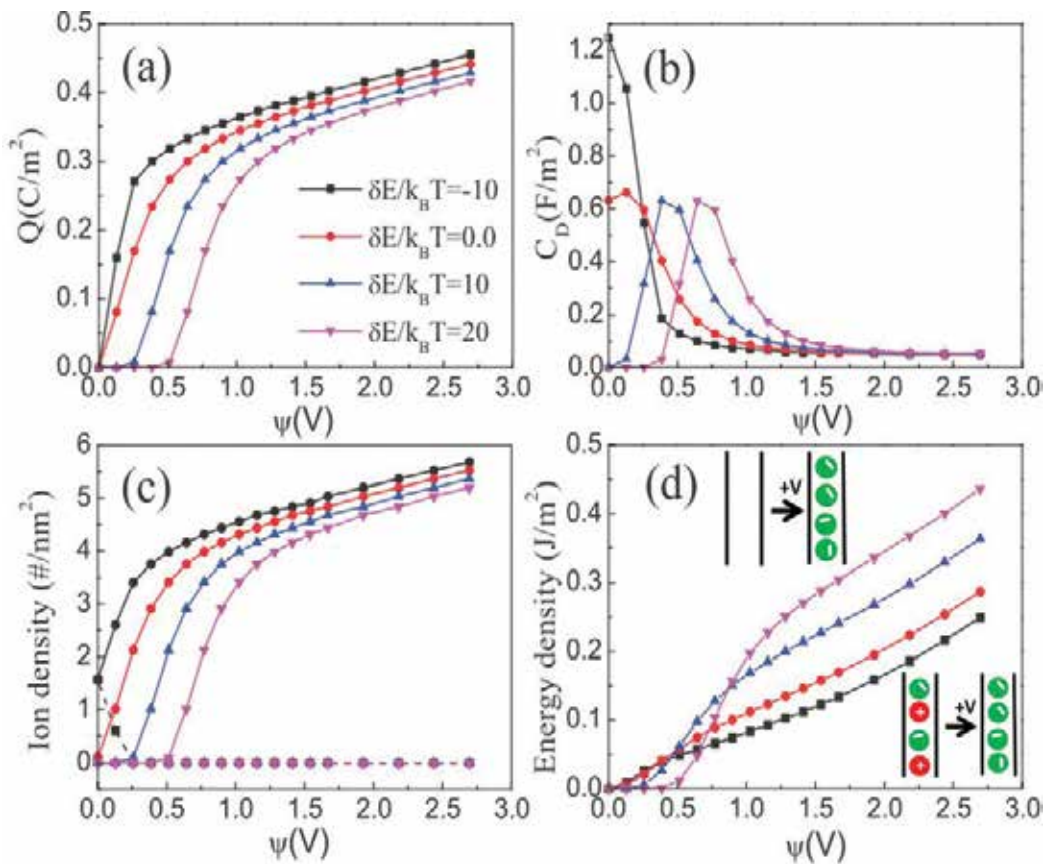


Figure 2. Theoretical predictions for the surface charge density (a), the differential capacitance (b), the average cation and anion densities inside the nanopore (c), and the energy stored per surface area (d) for an EDLC containing an organic electrolyte. Because of the system symmetry, the results are the same if the surface potential, ψ , is extended to the negative values. Here the concentration of the organic electrolyte is fixed at 1.0 M, the pore size is $D = 0.6$ nm. The ionophobicity of the nanopores is reflected in the ion resolution energy, δE , which represents the ion transfer energy from the bulk reservoir into the nanopore. In (c), the solid lines are average densities inside the pore for the counterions, and the dashed lines are for the coions. Because of their small values, the curves for the average coion densities collapse into the same zero line. Reproduced from Ref. [54] with permission. Copyright 2016 IOP Publishing.

ionophobic pore), while a positive δE means an ionophobic pore. For simplicity, we assume that δE is independent of the ion valence, the pore size, and the surface electrical potential.

In an ionophobic pore with a large ion resolution energy, both counterions and coions are nearly excluded from the nanopore at low surface electrical potential. In this case, counterions are inserted into the empty pore only when the electrical potential is sufficiently large to overcome the surface repulsion. The differential capacitance increases with the surface potential until it reaches a maximum. A further increase of the surface electrical potential leads to saturation of counter ions inside the pore and thus a decline of the capacitance. In both ionophobic cases shown in **Figure 2(b)**, the capacitance versus potential curve has a two-hump camel shape, and the capacitance value at the minimum is close to zero, in stark contrast to the maximum for an ionophilic pore. **Figure 2(b)** indicates that the peak capacitance shifts to a higher potential as the ionophobicity increases. In other words, we may find a bell shape to the two-hump camel shape transition in the capacitance-electrical potential curves by changing the surface ionophobicity. **Figure 2(d)** shows that, at low electrical potential, the energy density ($E(\psi) = \int_0^\psi C_D(x)x dx$) for an ionophilic pore is higher than that of an ionophobic pore, while the trend is opposite at high potentials. Because the peak of the camel shape differential capacitance shifts to higher potential, a more ionophobic pore offers higher storage energy. On the other hand, increasing ionophobicity prohibits counter ions from entering the pore, thus reduces the energy density at low potential. From the discussions above, we find that an ionophobic nanopore prevents counterion insertion and shifts the saturation point to a higher voltage. The energy stored in the EDLC can be promoted by the ionophobicity only when the electrode voltage is larger than a critical value [54].

4. Electrolyte effect on the capacitive performance

4.1. Solvent effect

Commercial EDLC devices mainly use the organic electrolyte in which a salt such as tetraethylammonium tetrafluoroborate is dissolved in an organic solvent such as acetonitrile (ACN) or propylene carbonate. It is very intriguing to unravel the role of the solvent during EDL charging inside small pores. By introducing a molecular dipole into our electrolyte, CDFT also allows us to examine the capacitance of an organic EDLC for different pore sizes and solvent polarity.

Our previous work illustrates the dependence of the capacitance on the pore size for the electrolyte/electrode models [45, 53]. For an ionic liquid EDLC, the capacitance oscillates with the pore size with a dampened magnitude around an average value of about $7.5 \mu\text{F}/\text{cm}^2$. The maximum capacitance occurs when the pore size is about the same as the ion diameter, which coincides with the anomalous increase of capacitance observed by Largeot et al. [17] Whereas a similar peak appears for the organic electrolyte, there is no significant oscillation as the pore size increases, and the capacitance at the first peak is less dramatic in comparison with the asymptotic value. The theoretical results thus offer a reconciliatory picture of the capacitance

dependence on the pore size for ionic liquid and organic electrolyte EDLCs. In the previous section, we discussed the capacitance dependence on pore size for an organic electrolyte with a moderate-polarity solvent (with a dipole moment of 3.4 Debye). But how would the solvent polarity affect the pore-size dependence of capacitance in a wide range of organic electrolyte EDLC?

Our CDFT calculations provide valuable insights into the effects of the dipole moment of the solvent in an organic electrolyte [43]. We found an optimal dipole moment that yields a maximum in the large-pore capacitance. These theoretical results further illustrate the rich behavior of the organic electrolytes inside porous electrodes. Moreover, it provides new considerations that can be taken into account when designing new experiments to select organic electrolytes for EDLCs.

4.2. Impurity or additive

RTIL has been used as electrolytes widely to increase the capacitive performance of electrochemical capacitors [82]. However, there are always some small amounts of impurity (e.g., water, alkali salts, and organic solvents) in RTIL, which may affect the electrochemical behavior of electrochemical devices. To understand the impurity effect, the RTIL with different impurities in the porous carbon electrodes is studied via CDFT. With a different type of binding energy with the surface or ionic species, the impurity shows a different influence on the EDL microstructures and contributes differently to the integral capacitance. It is noted that the impurity can be considered as either a contaminant or an additive to the ionic liquid, all depending on the interaction between the impurity and the electrode or ions [79, 80]. Meanwhile, the capacitance strongly oscillates with the variation of the pore size similar to that for the pure ionic liquid electrolyte. With strong binding of impurity to the ionic species, the RTIL/impurity mixture may lead to an enhanced capacitance oscillation. In certain pores, a significant increase in the capacitance can be obtained. The theoretical results provide insights for further investigation of supercapacitors aiming at rational design of porous electrode materials and charge carriers.

We also demonstrate that, under conditions favoring impurity accumulation in the nanopores of the electrode, impurity can change the EDL charging mechanism even at low bulk densities, shown in **Figure 3**. As the adhesion energy of impurity molecules with the electrode surface increases, the capacitance-potential curves can change from the bell shape to the two-hump camel shape, with the peak shifting toward a higher charging potential. Qualitatively the impurity effect on the charging behavior is similar to the solvent effect as studied by Rochester and coworkers [81]. Whereas the amount of impurity and solvent in the bulk is considerably different, the concentration effect can be compensated by the change in the transfer energy to yield a same charging behavior. As an ionophobic pore could be beneficiary for improving charge storage and charging dynamics, introduction of impurity molecules inside the pore makes it essentially more ionophobic thus enhances the energy storage. Our theoretical results suggest that special attention should be given to the nature of impurity and operation voltages when the surface properties nanoporous electrodes are modified to enhance the performance of EDLCs. It is worth noting that association between ions and impurity molecules, which

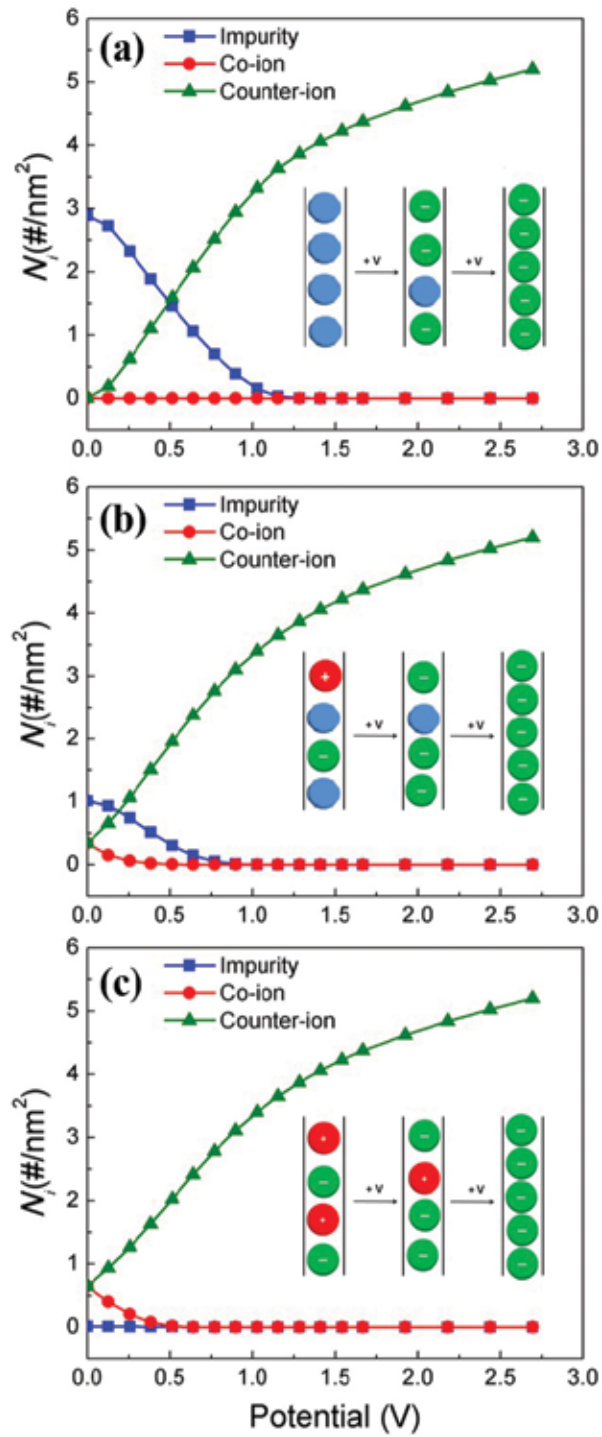


Figure 3. The number densities of ions and impurity molecules inside a nanopore of width $H = 0.6$ nm with different surface adhesion energies for the impurity molecules: (a) $\omega = -10k_B T$; (b) $\omega = -5k_B T$; (c) $\omega = 0.0k_B T$.

might happen for impurity molecules with large polarity, may give rise to different pictures of the charging behavior. For impurity molecules without affinity to ionic species, their accumulation inside the pore will increase the charge storage and capacitance, regardless of the polarity. The effects of ion binding with impurity molecules on the charging mechanism and energy density will be investigated in the future work. From a practical perspective, the impurity can be considered as either a contaminant (undesirable) or an additive (desirable) to room-temperature ionic liquids. Based on this study and our previous work [80], we suggest new experimental strategies to introduce additives into ionic liquids with specific surface binding affinity to the porous electrodes (e.g., by surface modifications). While significant efforts have been devoted to formulation of ionic liquid mixtures and selection of solvents [47], much less is known on how supercapacitor performance may be influenced by potent additives at a low concentration.

4.3. Ionic liquid mixture

Formulating RTIL mixed electrolytes was recently proposed as an effective and convenient strategy to increase the capacitive performance of electrochemical capacitors [82]. However, little is known about how the properties of EDLCs containing RTIL mixtures would be affected by the electrolyte composition [83–86]. Here, we investigate the EDL structure and the capacitance of two RTILs, 1-ethyl-3-methylimidazolium bis(trifluoromethylsulfonyl)imide (EMI-TFSI and 1-ethyl-3-methylimidazolium tetrafluoroborate (EMI-BF₄), and their mixtures with onion-like carbon electrodes using experiment and the CDFT. The principal difference between these ionic liquids is the smaller diameter of the BF₄⁻ anion relative to the TFSI⁻ anion and the EMI⁺ cation in **Figure 4**. We find that the capacitance versus the composition of the RTIL mixture exhibits a volcano-shaped trend; in other words, there exists a composition of the ionic mixture that yields a maximal integral capacitance [47]. The mixture effect, which makes more counterions pack on and more co-ions leave from the electrode surface, leads to an

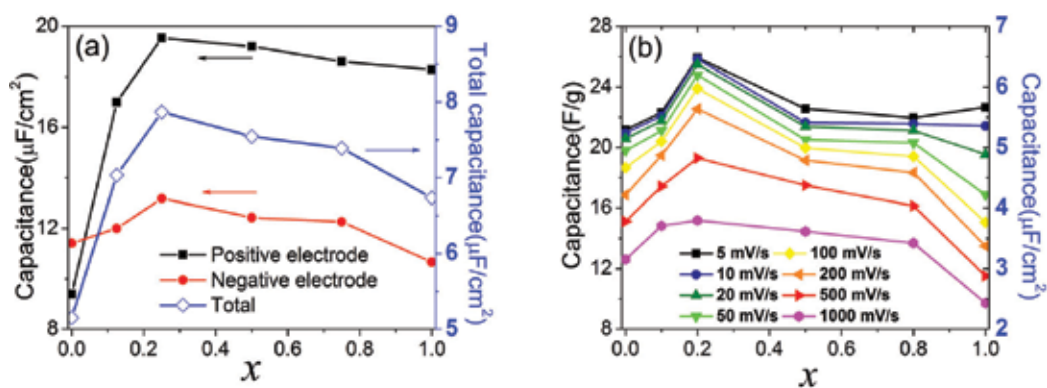


Figure 4. (a) Calculated integral capacitance for the positive, negative and total electrodes when the operating potential window (OPW) is fixed as 3.0 V. (b) Experimental results for a symmetric supercapacitor operating at 3.0 V. The electrode capacitance is shown as a function of the concentration of the RTIL mixture for different scan rates. Reproduced from Ref. [82] with permission. Copyright 2016 American Chemical Society.

increase of the counterion density within the EDL and thus a larger capacitance. These theoretical predictions are in good agreement with our experimental observations and offer guidance for designing RTIL mixtures for EDL supercapacitors with optimal performance [47].

4.4. Ion-ion interaction on the transport in nanopore

The charging kinetics of EDLs has a pivotal role in the performance of a wide variety of nanostructured devices. Despite the prevalent use of ionic liquids as the electrolyte, relatively little is known on the charging behavior from a microscopic perspective [33, 75, 77, 87–90]. Here, we study the charging kinetics of ionic liquid EDLs using the TDDFT that captures the molecular excluded volume effects and electrostatic correlations [39]. We found that the thermodynamic non-ideality plays a pivotal role in electrodiffusion and such effect cannot be captured by the lattice-gas model for the excluded volume effects. In particular, TDDFT predicts “wave-like” variation of the ionic density profiles that has not been identified in previous investigations [34]. This unusual charging behavior can be explained in terms of the oscillatory structure of ionic liquids near the electrodes. For ion transport in narrow pores with a high gating voltage, in **Figure 5**, the conductivity shows an oscillatory dependence on the pore size owing to the strong overlap of electric double layers [91].

Besides, our new TDDFT is able to account for the molecular excluded volume effects, electrostatic correlations, and the dispersion interactions. Our results show that the dispersion interaction between ions makes the surface charge be a non-monotonic function of time shown in **Figure 6**. However, the dispersion interaction between the electrode and ionic-liquid does not

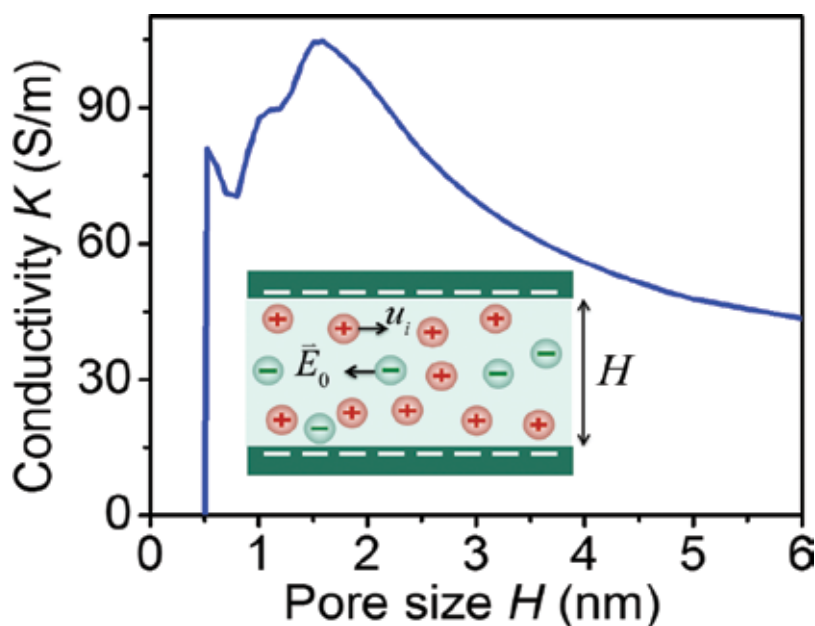


Figure 5. The conductivity shows an oscillatory dependence on the pore size [91]. Copyright 2017 Royal Society of Chemistry.

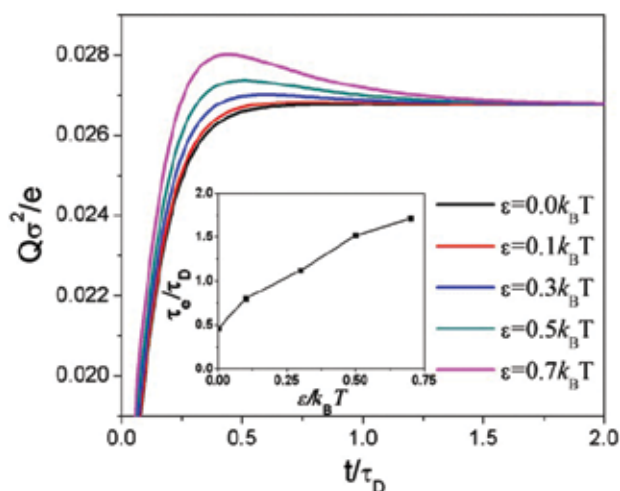


Figure 6. Evolution of surface charge density for different strengths of dispersion forces. (Inset) The time toward equilibrium as a function of the dispersion energy parameter ϵ . Reproduced from Ref. [92] with permission. Copyright 2016 American Physical Society.

change the monotonic evolution of surface charge density [92]. Both the ion-ion and the electrode-ion dispersion interactions increase the duration of the EDL charging process [92]. We also identified significant influence of the gating potential on the scaling behavior of the conductance with changes of pore size and the salt concentration. For ion transport in narrow pores with a high gating voltage, the conductivity shows an oscillatory dependence on the pore size owing to the strong overlap of electric double layers [91]. We hope these theoretical work enables a way to tune the charging behavior of electric double layer capacitors (EDLCs) by an appropriate choice of electrodes and ionic liquids.

5. Conclusion and perspective

In our recent works, the CDFT was developed and applied by us to study the electrode/electrolyte interface behaviors, to understand capacitive energy storage. As a statistical mechanical tool and an alternative to molecular dynamics or Monte Carlo simulation methods, CDFT offers a powerful and efficient mathematical framework to describe the equilibrium and dynamic properties of many-body systems in terms of the one-body density profiles. It allows one to precisely tune the parameters such as ion diameter, solvent dipole, and pore size over a large range and to focus on the most important physical problems to be addressed, using a computationally efficient coarse-grained approach to model real fluids. Through CDFT, we have found novel behaviors of electrolytes inside nanopores, such as capacitance oscillation, optimal dipole moment, and wave-like charging. Further development of CDFT for complex pore structures and charging kinetics would allow us to directly predict power density and energy density for supercapacitors.

Acknowledgements

This research was supported by the National Natural Science Foundation of China (No. 91334203), the 111 Project of China (No. B08021) and National Postdoctoral Program for Innovative Talents (BX201700076). Cheng Lian also thanks the financial support by China Postdoctoral Science Foundation (2017 M620137) and Shanghai Sailing Program (18YF1405400). We also thank Prof. Jianzhong Wu in UC Riverside for helpful guidance and discussion.

Conflict of interest

The authors declare no competing financial interest.

Author details

Cheng Lian and Honglai Liu*

*Address all correspondence to: hlliu@ecust.edu.cn

State Key Laboratory of Chemical Engineering and School of Chemistry and Molecular Engineering, East China University of Science and Technology, Shanghai, China

References

- [1] Chmiola J, Yushin G, Gogotsi Y, Portet C, Simon P, Taberna PL. Anomalous increase in carbon capacitance at pore sizes less than 1 nanometer. *Science*. 2006;**313**:1760-1763
- [2] Fedorov MV, Kornyshev AA. Ionic liquids at electrified interfaces. *Chemical Reviews*. 2014;**114**:2978-3036
- [3] Zhang LL, Zhao XS. Carbon-based materials as supercapacitor electrodes. *Chemical Society Reviews*. 2009;**38**:2520-2531
- [4] Zhai YP, Dou YQ, Zhao DY, Fulvio PF, Mayes RT, Dai S. Carbon materials for chemical capacitive energy storage. *Advanced Materials*. 2011;**23**:4828-4850
- [5] Wang DW, Li F, Liu M, Lu GQ, Cheng HM. 3D aperiodic hierarchical porous graphitic carbon material for high-rate electrochemical capacitive energy storage. *Angewandte Chemie, International Edition*. 2008;**47**:373-376
- [6] Zhu YW, Murali S, Stoller MD, Ganesh KJ, Cai WW, Ferreira PJ, Pirkle A, Wallace RM, Cychoz KA, Thommes M, Su D, Stach EA, Ruoff RS. Carbon-based supercapacitors produced by activation of graphene. *Science*. 2011;**332**:1537-1541

- [7] Chmiola J, Largeot C, Taberna PL, Simon P, Gogotsi Y. Monolithic carbide-derived carbon films for micro-supercapacitors. *Science*. 2010;**328**:480-483
- [8] Gogotsi Y, Nikitin A, Ye HH, Zhou W, Fischer JE, Yi B, Foley HC, Barsoum MW. Nanoporous carbide-derived carbon with tunable pore size. *Nature Materials*. 2003;**2**:591-594
- [9] Dash R, Chmiola J, Yushin G, Gogotsi Y, Laudisio G, Singer J, Fischer J, Kucheyev S. Titanium carbide derived nanoporous carbon for energy-related applications. *Carbon*. 2006;**44**:2489-2497
- [10] Hu S, Rajamani R, Yu X. Flexible solid-state paper based carbon nanotube supercapacitor. *Applied Physics Letters*. 2012;**100**:104103
- [11] An KH, Kim WS, Park YS, Moon JM, Bae DJ, Lim SC, Lee YS, Lee YH. Electrochemical properties of high-power supercapacitors using single-walled carbon nanotube electrodes. *Advanced Functional Materials*. 2001;**11**:387-392
- [12] Yu CJ, Masarapu C, Rong JP, Wei BQ, Jiang HQ. Stretchable supercapacitors based on buckled single-walled carbon nanotube macrofilms. *Advanced Materials*. 2009;**21**:4793-4797
- [13] Pech D, Brunet M, Durou H, Huang PH, Mochalin V, Gogotsi Y, Taberna PL, Simon P. Ultrahigh-power micrometre-sized supercapacitors based on onion-like carbon. *Nature Nanotechnology*. 2010;**5**:651-654
- [14] Portet C, Yushin G, Gogotsi Y. Electrochemical performance of carbon onions, nanodiamonds, carbon black and multiwalled nanotubes in electrical double layer capacitors. *Carbon*. 2007;**45**:2511-2518
- [15] Stoller MD, Park SJ, Zhu YW, An JH, Ruoff RS. Graphene-based ultracapacitors. *Nano Letters*. 2008;**8**:3498-3502
- [16] Liu CG, Yu ZN, Neff D, Zhamu A, Jang BZ. Graphene-based supercapacitor with an ultrahigh energy density. *Nano Letters*. 2010;**10**:4863-4868
- [17] Largeot C, Portet C, Chmiola J, Taberna PL, Gogotsi Y, Simon P. Relation between the ion size and pore size for an electric double-layer capacitor. *Journal of the American Chemical Society*. 2008;**130**:2730-2731
- [18] Chmiola J, Largeot C, Taberna PL, Simon P, Gogotsi Y. Desolvation of ions in subnanometer pores and its effect on capacitance and double-layer theory. *Angewandte Chemie, International Edition*. 2008;**47**:3392-3395
- [19] Collins PG, Bradley K, Ishigami M, Zettl A. Extreme oxygen sensitivity of electronic properties of carbon nanotubes. *Science*. 2000;**287**:1801-1804
- [20] Baughman RH, Zakhidov AA, de Heer WA. Carbon nanotubes—The route toward applications. *Science*. 2002;**297**:787-792
- [21] Gao Y, Zhou YS, Qian M, He XN, Redepenning J, Goodman P, Li HM, Jiang L, Lu YF. Chemical activation of carbon nano-onions for high-rate supercapacitor electrodes. *Carbon*. 2013;**51**:52-58

- [22] Lauw Y, Horne MD, Rodopoulos T, Webster NAS, Minofar B, Nelson A. X-ray reflectometry studies on the effect of water on the surface structure of [C4mpyr][NTf2] ionic liquid. *Physical Chemistry Chemical Physics*. 2009;**11**:11507-11514
- [23] Hayes R, Borisenko N, Corr B, Webber GB, Endres F, Atkin R. Effect of dissolved LiCl on the ionic liquid–Au(111) electrical double layer structure. *Chemical Communications*. 2012;**48**:10246-10248
- [24] Tamura K, Nishihata Y. Study on the behavior of halide ions on the Au(111) electrode surface in ionic liquids using surface X-ray scattering. *Journal of Physical Chemistry C*. 2016;**120**:15691-15697
- [25] Feng G, Huang J, Sumpter BG, Meunier V, Qiao R. Structure and dynamics of electrical double layers in organic electrolytes. *Physical Chemistry Chemical Physics*. 2010;**12**:5468-5479
- [26] Feng G, Jiang X, Qiao R, Kornyshev AA. Water in ionic liquids at electrified interfaces: The anatomy of electrosorption. *ACS Nano*. 2014;**8**:11685-11694
- [27] Porter AR, Liem SY, Popelier PLA. Room temperature ionic liquids containing low water concentrations—a molecular dynamics study. *Physical Chemistry Chemical Physics*. 2008;**10**:4240-4248
- [28] Lee AA, Kondrat S, Vella D, Goriely A. Dynamics of ion transport in ionic liquids. *Physical Review Letters*. 2015;**115**:106101
- [29] Gavish N, Yochelis A. Theory of phase separation and polarization for pure ionic liquids. *The Journal of Physical Chemistry Letters*. 2016;**7**:1121-1126
- [30] Kilic MS, Bazant MZ, Ajdari A. Steric effects in the dynamics of electrolytes at large applied voltages. I. Double-layer charging. *Physical Review E*. 2007;**75**:021502
- [31] Bazant MZ, Kilic MS, Storey BD, Ajdari A. Towards an understanding of induced-charge electrokinetics at large applied voltages in concentrated solutions. *Advances in Colloid and Interface Science*. 2009;**152**:48-88
- [32] Yochelis A. Transition from non-monotonic to monotonic electrical diffuse layers: Impact of confinement on ionic liquids. *Physical Chemistry Chemical Physics*. 2014;**16**:2836-2841
- [33] Yochelis A. Spatial structure of electrical diffuse layers in highly concentrated electrolytes: A modified Poisson–Nernst–Planck approach. *The Journal of Physical Chemistry C*. 2014;**118**:5716-5724
- [34] Jiang J, Cao D, Jiang D-e, Wu J. Kinetic charging inversion in ionic liquid electric double layers. *The Journal of Physical Chemistry Letters*. 2014;**5**:2195-2200
- [35] Qiao Y, Tu B, Lu B. Ionic size effects to molecular solvation energy and to ion current across a channel resulted from the nonuniform size-modified PNP equations. *The Journal of Chemical Physics*. 2014;**140**:174102

- [36] Lu B, Zhou Y, Holst M, McCammon J. Recent progress in numerical methods for the Poisson-Boltzmann equation in biophysical applications. *Communications in Computational Physics*. 2008;**3**:973-1009
- [37] Xu Z, Ma M, Liu P. Self-energy-modified Poisson-Nernst-Planck equations: WKB approximation and finite-difference approaches. *Physical Review E*. 2014;**90**:013307
- [38] Alij6 PH, Tavares FW, Biscaia EC Jr, Secchi AR. Effects of electrostatic correlations on ion dynamics in alternating current voltages. *Electrochimica Acta*. 2015;**152**:84-92
- [39] Jiang J, Cao D, Jiang D-E, Wu J. Time-dependent density functional theory for ion diffusion in electrochemical systems. *Journal of Physics: Condensed Matter*. 2014;**26**:284102
- [40] Alij6 PH, Tavares FW, Biscaia E, Secchi AR. Steric effects on ion dynamics near charged electrodes. *Fluid Phase Equilibria*. 2014;**362**:177-186
- [41] Jiang D-e, Jin Z, Wu J. Oscillation of capacitance inside nanopores. *Nano Letters*. 2011;**11**:5373-5377
- [42] Lian C, Jiang D-E, Liu H, Wu J. A generic model for electric double layers in porous electrodes. *The Journal of Physical Chemistry C*. 2016;**120**:8704-8710
- [43] Jiang D-E, Wu J. Unusual effects of solvent polarity on capacitance for organic electrolytes in a nanoporous electrode. *Nanoscale*. 2014;**6**:5545-5550
- [44] Wu J, Li Z. Density-functional theory for complex fluids. *Annual Review of Physical Chemistry*. 2007;**58**:85-112
- [45] Jiang D-E, Jin Z, Henderson D, Wu J. Solvent effect on the pore-size dependence of an organic electrolyte supercapacitor. *The Journal of Physical Chemistry Letters*. 2012;**3**:1727-1731
- [46] Wu J, Jiang T, Jiang D-E, Jin Z, Henderson D. A classical density functional theory for interfacial layering of ionic liquids. *Soft Matter*. 2011;**7**:11222-11231
- [47] Lian C, Liu K, Van Aken KL, Gogotsi Y, Wesolowski DJ, Liu HL, Jiang DE, Wu JZ. Enhancing the capacitive performance of electric double-layer capacitors with ionic liquid mixtures. *ACS Energy Letters*. 2016;**1**:21-26
- [48] Henderson D, Jiang D-E, Jin Z, Wu J. Application of density functional theory to study the double layer of an electrolyte with an explicit dimer model for the solvent. *The Journal of Physical Chemistry B*. 2012;**116**:11356-11361
- [49] Evans R. The nature of the liquid-vapour interface and other topics in the statistical mechanics of non-uniform, classical fluids. *Advances in Physics*. 1979;**28**:143-200
- [50] Robert E, Martin O, Roland R, Gerhard K. New developments in classical density functional theory. *Journal of Physics: Condensed Matter*. 2016;**28**:240401
- [51] Amin H, Le W, Walter GC. A density functional theory for colloids with two multiple bonding associating sites. *Journal of Physics: Condensed Matter*. 2016;**28**:244009

- [52] Lian C, Chen X, Zhao S, Lv W, Han X, Wang H, Liu H. Substrate effect on the phase behavior of polymer brushes with lattice density functional theory. *Macromolecular Theory and Simulations*. 2014;**23**:575-582
- [53] Jiang D-e, Wu J. Microscopic insights into the electrochemical behavior of nonaqueous electrolytes in electric double-layer capacitors. *The Journal of Physical Chemistry Letters*. 2013;**4**:1260-1267
- [54] Lian C, Liu H, Henderson D, Wu J. Can ionophobic nanopores enhance the energy storage capacity of electric-double-layer capacitors containing nonaqueous electrolytes? *Journal of Physics: Condensed Matter*. 2016;**28**:414005
- [55] Archer AJ. Dynamical density functional theory for molecular and colloidal fluids: A microscopic approach to fluid mechanics. *Journal of Chemical Physics*. 2009;**130**: Artn 014509
- [56] Zhao SL, Wu JZ. Self-consistent equations governing the dynamics of nonequilibrium colloidal systems. *Journal of Chemical Physics*. 2011;**134**: Artn 054514
- [57] Lian C, Wang L, Chen X, Han X, Zhao S, Liu H, Hu Y. Modeling swelling behavior of thermoresponsive polymer brush with lattice density functional theory. *Langmuir*. 2014;**30**:4040-4048
- [58] Stopper D, Roth R, Hansen-Goos H. Communication: Dynamical density functional theory for dense suspensions of colloidal hard spheres. *The Journal of Chemical Physics*. 2015;**143**:181105
- [59] Archer AJ. Dynamical density functional theory for molecular and colloidal fluids: A microscopic approach to fluid mechanics. *The Journal of Chemical Physics*. 2009;**130**: 014509
- [60] Marconi UMB, Melchionna S. Kinetic theory of correlated fluids: From dynamic density functional to lattice Boltzmann methods. *The Journal of Chemical Physics*. 2009;**131**: 014105
- [61] Archer AJ, Rauscher M. Dynamical density functional theory for interacting Brownian particles: Stochastic or deterministic? *Journal of Physics A: Mathematical and General*. 2004;**37**:9325
- [62] Dzubiella J, Likos CN. Mean-field dynamical density functional theory. *Journal of Physics: Condensed Matter*. 2003;**15**:L147
- [63] Merlet C, Rotenberg B, Madden PA, Taberna PL, Simon P, Gogotsi Y, Salanne M. On the molecular origin of supercapacitance in nanoporous carbon electrodes. *Nature Materials*. 2012;**11**:306-310
- [64] Palmer JC, Llobet A, Yeon SH, Fischer JE, Shi Y, Gogotsi Y, Gubbins KE. Modeling the structural evolution of carbide-derived carbons using quenched molecular dynamics. *Carbon*. 2010;**48**:1116-1123

- [65] Meunier V, Huang JS, Feng G, Qiao R, Sumpter BG. Modern theories of carbon-based electrochemical capacitors: A short review. In: Proceedings of the ASME International Mechanical Engineering Congress and Exposition 2010; Vol. 11. 2012. pp. 21-30
- [66] Huang J, Sumpter BG, Meunier V. Theoretical model for nanoporous carbon supercapacitors. *Angewandte Chemie International Edition*. 2008;**47**:520-524
- [67] Huang J, Sumpter BG, Meunier V, Yushin G, Portet C, Gogotsi Y. Curvature effects in carbon nanomaterials: Exohedral versus endohedral supercapacitors. *Journal of Materials Research*. 2010;**25**:1525-1531
- [68] Feng G, Li S, Presser V, Cummings PT. Molecular insights into carbon supercapacitors based on room-temperature ionic liquids. *The Journal of Physical Chemistry Letters*. 2013; **4**:3367-3376
- [69] Landers J, Gor GY, Neimark AV. Density functional theory methods for characterization of porous materials. *Colloids and Surfaces A—Physicochemical and Engineering Aspects*. 2013;**437**:3-32
- [70] Vatamanu J, Bedrov D. Capacitive energy storage: Current and future challenges. *The Journal of Physical Chemistry Letters*. 2015;**6**(18):3594-3609
- [71] Li S, Han KS, Feng G, Hagaman EW, Vlcek L, Cummings PT. Dynamic and structural properties of room-temperature ionic liquids near silica and carbon surfaces. *Langmuir*. 2013;**29**:9744-9749
- [72] Van Aken KL, McDonough JK, Li S, Feng G, Chathoth SM, Mamontov E, Fulvio PF, Cummings PT, Dai S, Gogotsi Y. Effect of cation on diffusion coefficient of ionic liquids at onion-like carbon electrodes. *Journal of Physics: Condensed Matter*. 2014;**26**:284104
- [73] Wang H, Pilon L. Mesoscale modeling of electric double layer capacitors with three-dimensional ordered structures. *Journal of Power Sources*. 2013;**221**:252-260
- [74] Kondrat S, Kornyshev AA. Pressing a spring: What does it take to maximize the energy storage in nanoporous supercapacitors? *Nanoscale Horizons*. 2016;**1**:45-52
- [75] Kondrat S, Kornyshev A. Charging dynamics and optimization of nanoporous supercapacitors. *The Journal of Physical Chemistry C*. 2013;**117**:12399-12406
- [76] Lee AA, Kondrat S, Kornyshev AA. Single-file charge storage in conducting nanopores. *Physical Review Letters*. 2014;**113**:048701
- [77] Kondrat S, Wu P, Qiao R, Kornyshev AA. Accelerating charging dynamics in subnanometre pores. *Nature Materials*. 2014;**13**:387-393
- [78] Cheng L, Xian K, Honglai L, Jianzhong W. On the hydrophilicity of electrodes for capacitive energy extraction. *Journal of Physics: Condensed Matter*. 2016;**28**:464008
- [79] Liu K, Lian C, Henderson D, Wu J. Impurity effects on ionic-liquid-based supercapacitors. *Molecular Physics*. 2017;**115**:454-464

- [80] Liu K, Wu J. Boosting the performance of ionic-liquid-based supercapacitors with polar additives. *The Journal of Physical Chemistry C*. 2016;**120**:24041-24047
- [81] Rochester CC, Kondrat S, Pruessner G, Kornyshev AA. Charging ultrananoporous electrodes with size-asymmetric ions assisted by apolar solvent. *Journal of Physical Chemistry C*. 2016;**120**:16042-16050
- [82] Van Aken KL, Beidaghi M, Gogotsi Y. Formulation of ionic-liquid electrolyte to expand the voltage window of supercapacitors. *Angewandte Chemie International Edition*. 2015;**54**:4806-4809
- [83] Costa R, Pereira CM, Silva AF. Structural ordering transitions in ionic liquids mixtures. *Electrochemistry Communications*. 2015;**57**:10-13
- [84] dos Santos DJ, Cordeiro MND. Effect of replacing [NTf₂] by [PF₆] anion on the [BMIm][NTf₂] ionic liquid confined by gold. *Molecular Simulation*. 2015;**41**:455-462
- [85] Siimenson C, Siinor L, Lust K, Lust E. Electrochemical characterization of iodide ions adsorption kinetics at Bi(111) electrode from three-component ionic liquids mixtures. *ECS Electrochemistry Letters*. 2015;**4**:H62-H65
- [86] Lall-Ramnarine S, Suarez S, Zmich N, Ewko D, Ramati S, Cuffari D, Sahin M, Adam Y, Rosario E, Paterno D. Binary ionic liquid mixtures for supercapacitor applications. *ECS Transactions*. 2014;**64**:57-69
- [87] Kondrat S, Oshanin G, Kornyshev AA. Charging dynamics of supercapacitors with narrow cylindrical nanopores. *Nanotechnology*. 2014;**25**:315401
- [88] Péan C, Merlet C, Rotenberg B, Madden PA, Taberna P-L, Daffos B, Salanne M, Simon P. On the dynamics of charging in nanoporous carbon-based supercapacitors. *ACS Nano*. 2014;**8**:1576-1583
- [89] Pean C, Rotenberg B, Simon P, Salanne M. Understanding the different (dis)charging steps of supercapacitors: Influence of potential and solvation. *Electrochimica Acta*. 2016;**206**:504-512
- [90] He Y, Huang J, Sumpter BG, Kornyshev AA, Qiao R. Dynamic charge storage in ionic liquids-filled nanopores: Insight from a computational cyclic voltammetry study. *The journal of Physical Chemistry Letters*. 2015;**6**:22-30
- [91] Lian C, Gallegos A, Liu H, Wu J. Non-scaling behavior of electroosmotic flow in voltage-gated nanopores. *Physical Chemistry Chemical Physics*. 2017;**19**:450-457
- [92] Lian C, Zhao S, Liu H, Wu J. Time-dependent density functional theory for the charging kinetics of electric double layer containing room-temperature ionic liquids. *The Journal of Chemical Physics*. 2016;**145**:204707

Edited by Lionginas Liudvinavičius

This edited volume *Supercapacitors - Theoretical and Practical Solutions* is a collection of reviewed and relevant research chapters, offering a comprehensive overview of recent developments in the field of electronic devices and materials. The book comprises single chapters authored by various researchers and is edited by a group of experts. Each chapter is complete in itself but united under a common research study topic. This publication aims at providing a thorough overview of the latest research efforts by international authors on electronic devices and materials and opens new possible research paths for further novel developments.

Published in London, UK

© 2018 IntechOpen

© EasternLightcraft / iStock

IntechOpen

